Characterisation and use of innovative sorbents for metal/metalloid stabilisation in contaminated soils

PhD thesis

Thesis supervisor: **doc. Mgr. Martina Vítková, Ph.D.**

Thesis reviewers: **prof. RNDr. Edgar Hiller, Ph.D.**
(Comenius University Bratislava)

Dr. Ivan Carabante
(Luleå University of Technology)

Mgr. Jan Filip, Ph.D.
(Regional Centre of Advanced Technologies and
Material, Palacký University, Olomouc, Czech Republic)

Czech University of Life Sciences Prague
Faculty of Environmental Sciences
Department of Environmental Geosciences

Prague, 2024

Characterisation and use of innovative sorbents for metal/metalloid stabilisation in contaminated soils

Aikaterini Mitzia

Characterisation and use of innovative sorbents for metal/metalloid stabilisation in contaminated soils

Aikaterini Mitzia

Czech University of Life Sciences Prague (2024)

Acknowledgement

Abstract

The main objective of the present thesis was to evaluate the efficiency of various soil amendments intended for metal(loid) immobilisation in contaminated soils. The two main studied materials, biochar (BC) and nano zero-valent iron (nZVI), were investigated individually or combined, modified, and originated from alternative sources. Although their metal(loid) retention efficiency has been well-established in laboratory solutions, knowledge gaps regarding their behaviour under various environmental conditions remained. Therefore, one of the aims of the current work was to answer questions about metal(loid) immobilisation efficiency and material functionality changes under relevant environmental conditions, i.e. different moisture content, flood, changing redox conditions, and increasing time. Keeping up with the current research trend concerning sustainability and circular economy, waste-derived amendments were also included in the presented experiments. Firstly, the efficiency of BC, nZVI, and a mixture of the two for the immobilisation of Zn, Pb, and Cd in contaminated soil was assessed under 60 and 100% of soil's water holding capacity. Then, BC, nZVI and an nZVI-BC composite, were incubated from 1 up to 15 months in contaminated soil and their efficiency for Zn, Pb, Cd, and As retention over time was investigated. From these studies it occurred that nZVI was efficient for rapid but rather short-term immobilisation of Pb and As while BC seemed to be capable for long-term immobilisation of Zn and Cd along with soil pH retention. The promising behaviour of BC and the need for more sustainable remediation solutions lead to the use of sewage sludge as the source material for amendment production (sludgechar). Five sludgechars with variable compositions were pyrolysed and tested for their removal efficiency towards Cd, Co, Cu, Ni, Pb, Zn, As, Cr and Sb. Upon their efficiency for metal removal, the sludgechars were applied in five contrasting soils with different level and origin of contamination, variable soil use and properties. It was concluded that the efficiency of the studied sludgechars depends on all these factors. Redox fluctuations which typically occur in the field during flood events were simulated in the laboratory scale to investigate the amendment efficiency and metal(loid) mobility under such conditions. Our preliminary results highlight the effect of Eh and pH as the main factors controlling metal(loid) mobility followed by amendment efficiency. The presence of Fe and Mn oxides was considered as the most important immobilisation mechanism in all of the presented studies.

Abstrakt

Hlavním cílem této práce bylo zhodnotit účinnost různých půdních ošetření zaměřených na imobilizaci kovů/metaloidů v kontaminovaných půdách. Dva stěžejní studované materiály, biochar (BC) a nanočástice nulamocného železa (nZVI), byly zkoumány samostatně nebo v kombinaci, v modifikované verzi či za použití odlišných materiálových zdrojů. Ačkoliv se tyto materiály úspěšně osvědčily pro retenci kovů/metaloidů v laboratorních podmínkách, jejich chování v různých podmínkách životního prostředí nebylo doposud dostatečně prozkoumáno. Jedním z cílů této práce bylo tedy odpovědět na otázky týkající se účinnosti imobilizace kovů/metaloidů a změn ve funkčnosti materiálů v rozdílných podmínkách prostředí, tj. v závislosti na odlišném obsahu vlhkosti, zaplavení, redoxních podmínkách a v závislosti na čase. V souladu se současným trendem výzkumu v oblasti udržitelnosti a oběhového hospodářství byly do experimentů zahrnuty také materiály vyprodukované z odpadu. Nejprve byla vyhodnocena účinnost BC, nZVI a kombinace těchto dvou materiálů pro imobilizaci Zn, Pb a Cd v kontaminované půdě za stavu 60% a 100% maximální retenční vodní kapacity půdy. Následně byly BC, nZVI a kompozit nZVI-BC inkubovány po dobu 1 až 15 měsíců v kontaminované půdě, přičemž byla zkoumána jejich účinnost pro záchyt Zn, Pb, Cd a As v průběhu času. Z těchto studií vyplynulo, že nZVI je účinné pro rychlou, nicméně spíše krátkodobou imobilizaci Pb a As, zatímco BC se zdá být schopen dlouhodobě imobilizovat Zn a Cd a zároveň udržet pH půdy. Slibné chování BC a nezbytnost aplikovat nová remediační opatření z hlediska udržitelného rozvoje vedla k použití čistírenských kalů jako vstupního materiálu pro výrobu materiálu zde nazvaného sludgechar. Pět sludgecharů s odlišným složením bylo pyrolyzováno a testováno pro jejich účinnost v odstraňovaní Cd, Co, Cu, Ni, Pb, Zn, As, Cr a Sb. Na základě toho byly sludgechary aplikovány do pěti odlišných půd s různým původem a množstvím kontaminace, rozdílným využitím půdy a odlišnými vlastnostmi. Z výsledků vyplynulo, že účinnost studovaných kalů závisí na všech těchto faktorech. Dále byly simulovány výkyvy redoxního potenciálu v laboratorním měřítku, které v terénu typicky nastávají během povodní, se záměrem zjistit mobilitu kovů/metaloidů za těchto podmínek v závislosti na použitém materiálu. Naše předběžné výsledky zdůrazňují vliv Eh a pH jakožto hlavních činitelů ovlivňujících mobilitu prvků, která je dále ovlivněna i samotnou účinností jednotlivých materiálů. Přítomnost oxidů Fe a Mn byla ve všech prezentovaných studiích považována za nejdůležitější imobilizační mechanismus.

Table of contents

Chapter I

General Introduction

Content

Problem outline

Soil pollution is currently a major topic of global concern with multiple implications; 15 (!) out of the 17 sustainable development goals set by the United Nations to be achieved by 2030 are hindered by soil pollution. Possibly the biggest challenge when dealing with polluted soils is to manage contaminants that do not degrade but persistently stay in the environment while translocating. This is the case of inorganic contaminants, i.e. metals and metalloids. For this reason, immobilisation is a promising method to tackle metal(loid) pollution in soils. Materials which are analogues of compounds that naturally occur in the soils (e.g. Fe oxides and carbon-based sorbents) with known efficiency of scavenging risk metal(loid)s have already been used for soil remediation with encouraging results. However, questions regarding the behaviour of such materials in the long-term and under variable environmental conditions still remain and served as the motivation for the research presented in the current PhD thesis.

1.1. Metals and metalloids in the environment

Metals have been so important for the human kind that certain eras are named after them, i.e. Copper Age (3500 – 2300 BCE), Bronze Age (3300 – 1200 BCE), Iron Age (1200 – 550 BCE). Gold and silver have been used as early as the Copper Age while mixing of Cu and Sn to create an alloy (known as bronze) led to the beginning of the Bronze Age. In total, eight metals (Cu, Au, Ag, Fe, Sn, Pb, Zn and Hg) are believed to have been utilised by ancient civilisations. Impressively, knowledge regarding the toxicity of metals already existed in the ancient times when Hippocrates described the symptoms of Pb poisoning (Murr, 2015).

Metals and metalloids are naturally occurring in the environment in variable concentrations among the different geographical regions. Some of the metal(loid)s are essential for living organisms as micronutrients (B, Co, Cr, Cu, Fe, I, Mn, Mo, Se, and Zn) while others have no biological functions and thus considered toxic (As, Cd, Pb, and Hg) (Alloway, 2013). However, even the elements of the first group can be toxic if present in higher concentrations than needed. Therefore, they are called **potentially toxic** or **risk** elements. Potentially toxic elements exist in the earth crust and may be released into the environment when bedrock weathering takes place. This is a source of **natural contamination**. However, risk elements existing in the bedrock are mostly unavailable to biota and their release into environment is a timely geological procedure. On the contrary, metal(loid) release due to **anthropogenic activities** is higher, and metal(loid)s are more **available**, and therefore more toxic (Adriano, 2001). Atmospheric pollution is mainly owed to combustion processes and smelting but also natural sources such as volcanic eruptions share a part of the blame. Water pollution has its origins in mining, manufacturing, and municipal wastewater disposal. Although risk elements settle in the sediments after entering the aquatic ecosystems, volatilisation keeps some of them to the surface where they can evaporate. In addition, water cycling promotes the translocation of risk elements. Eventually, contaminants both from airborne and aquatic origin, are ending up in the soil (Kabata-Pendias, 2011). In total, the presence of risk metal(loid)s in soils has an impact on the environment and human health especially because the risk elements accumulate and eventually being transferred in the food chain. Metal(loid) toxicity has severe impacts on all living organisms because it

interferes with most metabolic and physiological processes. Some of the effects of toxic metal(loid)s on living organisms are mentioned later in this section. However, it is important to mention here that the total load of risk elements present in the soil is not an environmental hazard *per se*, but it depends on the actual availability of a risk element.

1.1.1 Metal(loid) availability and speciation

According to EPA (2007), the (environmental) **availability** refers to the total amount of a risk element available for physical, chemical and biological processes while **bioavailability** is the level of absorption of a bioaccessible metal into, onto or across the biological membranes of an organism. **Bioaccessible** are the amounts of available metal(loid)s that actually interact with an organism (EPA, 2007). Understanding the differences between total and bioavailable concentrations is of particular importance to effectively address metal(loid) contamination risks. Ultimately, what defines the fate, mobility, bioavailability, and toxicity of metal(loid)s in the environment is their **speciation** (Alloway, 2013). For instance, organic As and especially arsenobetaine is not considered carcinogenic to humans, while inorganic species such as trivalent and pentavalent As are (IARC, 2012). The term speciation is used to describe the amounts and kinds of the different forms in which an element exists. Different forms of the same element might have a completely different toxicity impact. In the solid state, the term "fractionation" (or "solid speciation") describes the different forms or solid phase group in which a metal(loid) occurs, while in the dissolved state it is called "solution speciation" (Young, 2013). Three forms of metal(loid)s can be summarised based on their involvement in soil interactions: 1) inert metal(loid)s which interact in long periods (of years) usually by mineral weathering, organic decomposition or redox changes, 2) non-labile metal(loid)s that are bound strongly but not irreversibly to soil constituents and interacting slowly (in days to months), and 3) labile metal(loid)s which may interact instantly and reversibly with soil components being susceptible to changes in solution equilibrium (Young, 2013). The last form is the most crucial because the partitioning of a metal(loid) between the solid and solution phases is crucial for its bioavailability and mobility in soils (Rieuwerts et al., 1998).

1.1.2 Factors affecting metal(loid) availability and speciation in soils

As it appears from the previous section, metal(loid) availability is key to estimating the toxicity of metal(loid)s in soil. Few factors can influence the availability and mobility of metal(loid)s in soil with **pH** being the most impactful. The main effect once **pH rises** is that the surface charge on sorption sites (e.g. soil Fe oxides) becomes more negative, thus promoting the adsorption of **cationic** metals. The competition for adsorption sites between metal cations and for H^+ will decrease as there will be less H^+ in the less acidic conditions. In addition, changes in metal(loid) speciation may occur due to the new formation of metal complexes and OH^-, which can be less soluble (Young, 2013). On the other hand, the opposite effect is expected for metal(loid) **anions**: increased pH values, result in a decrease of positively charged soil surfaces to which metal(loid) anions are bound (e.g. Beesley et al., 2015). In addition, competition of OH^- with metal(loid)s for sorption sites and the prevailing negative surface charges provoke anion release in the soil solution (Kumarathilaka et al., 2018).

Although the **redox potential (Eh)** received less research attention than pH in the past, it is in fact one of the factors governing the pH and consequently metal(loid) availability in soils (Husson, 2013). The redox potential is a measurement of the tendency of a chemical species to be reduced (gain electrons) or oxidised (lose electrons). A typical example of redox fluctuation is soil flooding which impedes oxygen diffusion causing anaerobic conditions and thus causes Eh values to decrease (Frohne et al., 2011; Rinklebe et al., 2016 and references therein). Subsequently, pH values increase in acidic soils due to the consumption of H^+ by most reduction reactions (negative Eh-pH correlation) and the opposite phenomenon occurs when soil re-drying follows (Young, 2013). In terms of metal(loid) availability in the environment, redox plays a key role by affecting metal(loid) speciation. In the case of As, which is a redox sensitive element, its speciation is key to its toxicity: under oxidising conditions and pH<2, the H_3AsO_4 form is the main As species and at higher pH values $H_2AsO_4^-$ and $HAsO_4^{2-}$ prevail. In reduced conditions, H_3AsO_3 is the main form and is converted into $H_2AsO_3^-$ at lower pH and $HAsO_3^{2-}$ at higher pH (>12) (Kumarathilaka et al., 2018). As presented in Fig. 1.1, water safety with regards to As content, is strongly influenced by As speciation. Overall, As^{3+} species are more toxic than As^{5+} and anions such as AsO^{2-}, AsO_4^{3-}, and $H_2AsO_4^-$ are the

most mobile in soils (Kabata-Pendias, 2011). In general, the availability of redox-sensitive elements in the environment is highly dependent on their redox state (Rinklebe, 2020).
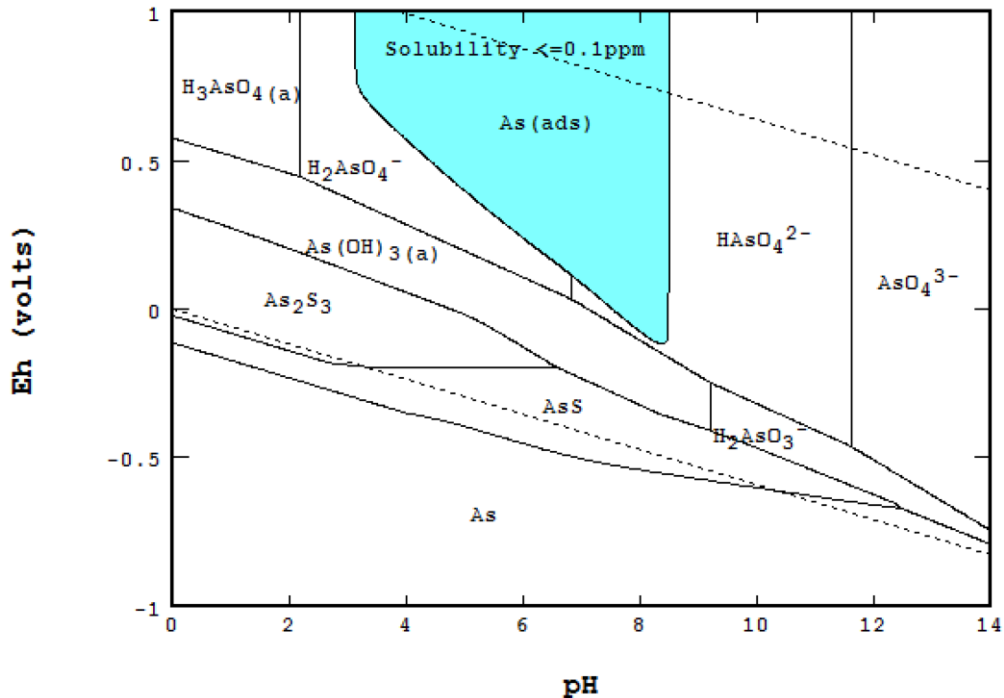
Figure: 1.1: *Eh-pH diagram of As speciation in As-Fe-S-water system. ΣAs = 37.5 mg/L, mole ratio Fe/As =10. Blue part (<0.01 ppm of soluble As) represents the limit of As in potable water according to WHO (2022). Image reproduced from Huang (2016) under the licence CC BY 4.0 (https://creativecommons.org/licenses/by/4.0/).*

Besides these major soil properties, **soil components** such as Fe/Mn oxides, organic matter, and layered silicates such as clays can strongly affect metal(loid) availability in soils (Rieuwerts et al., 1998).

Fe and Mn hydr(oxides)

The presence of Fe, Mn, and Al hydr(oxides) in soils is very common and they play a crucial role in metal(loid) availability. They are naturally occurring in soils in various shapes and sizes and occasionally found on the surface of clay minerals, in soil pores or as concretions and nodules. Their presence in oxidising conditions can strongly affect metal(loid) solubility (Rieuwerts et al.,

6

1998). Their high specific surface area and negative charge are the main reasons for their increased efficiency in metal(loid) retention (Adriano, 2001).

Iron oxides and hydroxides are products of weathering in soils and they are characterised by their mineral structure. Examples of distinct structure of different Fe oxides are presented in Fig. 1.2. In particular, ferrihydrite and schwertmannite are the ones considered poorly-crystalline while the rest, i.e. goethite, haematite, lepidocrocite, maghemite, magnetite, and wüstite are crystalline (Cornell & Schwertmann, 2003). The crystallinity and ageing of Fe oxides play a key role in their capacity for metal(loid) retention because different Fe oxides have different specific surface area. When used in soil remediation, Fe is applied in soils in the form of Fe^0 or Fe precursors which are eventually oxidised to other Fe forms. The oxidation reactions of Fe^0 in soils include (Komárek et al., 2013):

$$Fe^0 + 2H_2O + O_2 \rightarrow Fe(II) + 4OH^- \qquad (1)$$

$$Fe(II) + 2H_2O + O_2 \rightarrow Fe(III) + 4OH^- \qquad (2)$$

$$Fe(III) + 2H_2O \rightarrow FeOOH + 3H^+ \qquad (3)$$
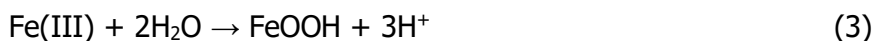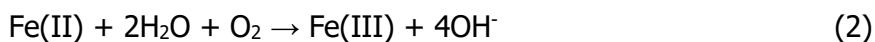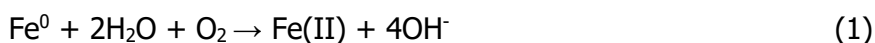
In general, the crystallisation of Fe oxides increases with time unless specific conditions hinder the process (e.g. pH). Iron oxides and hydroxides are excellent scavengers of both metals and metalloids which makes Fe-based amendments favourable tools for environmental remediation (Kumpiene et al., 2019). The main mechanisms for metal(loid) retention by Fe oxides are: 1) surface adsorption, 2) solid-state diffusion and 3) binding and fixation inside the mineral particles (Kabata-Pendias, 2011). The efficiency of Fe oxides for metal(loid) binding is governed by redox reactions which control Fe speciation.
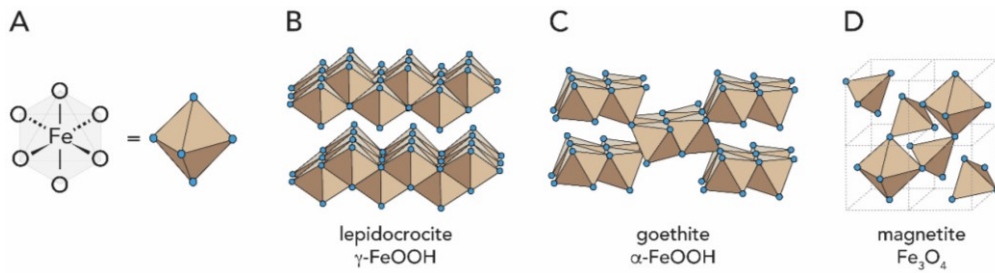
Figure 1.2: *Octahedra of Fe (A) and crystal structure of different Fe oxides (B-D). Image reproduced from Moura and Unterlass (2020) under the license CC BY 4.0 (https://creativecommons.org/licenses/by/4.0/).*

The **hydr(oxides) of Mn** are also secondary minerals important for metal(loid) retention in soils present in the wide range between $Mn^{II}O$ and $Mn^{IV}O_2$. Like Fe oxides, they show distinct crystal structure which can be layered-like or tunnel-like (Fig. 1.3). Birnessite is the most common oxide of Mn in soils (Alloway, 2013; Komárek et al., 2013). The vast variety of minerals including Mn oxides existing in nature is partially owed to the multiple oxidation states that Mn can be found (Grangeon et al., 2020). The oxidation of Mn^{2+} is, by large, a product of bacterial or fungi reactions in soils (Sposito, 2008). Often, Mn oxides are associated with Fe oxides but they have been reported to be more efficient than Fe in the immobilisation of some metals and especially Pb (Rieuwerts et al., 1998). Also, Mn is reported to be more mobile than Fe and thus easily redistributed between different soil horizons during weathering (Grangeon et al., 2020). Yet, Fe oxides are considered more important metal(loid) scavengers in soil due to their increased occurrence compared to Mn (Komárek et al., 2013). Manganese oxides are susceptible to dissolution under reducing conditions (Alloway, 2013) which may provoke the release of previously retained metal(loids)s (Kumpiene et al., 2008). Except for the sorption, Mn oxides have the ability to change the speciation of redox sensitive elements (As, Co, Cr) and thus affect their availability. In the case of As, As(III) oxidation to As(V) decreases its toxicity but the opposite effect occurs for Cr (Kumpiene et al., 2008).
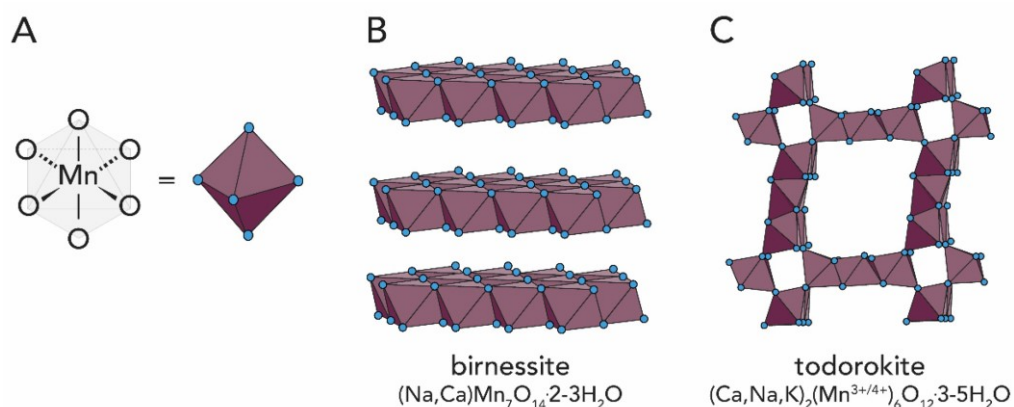
Figure 1.3: *Octahedra of Mn (A), layered-like (B) and tunnel-like (C) Mn oxides. Image reproduced from Moura and Unterlass (2020) under the license CC BY 4.0 (https://creativecommons.org/licenses/by/4.0/).*

Organic matter

Organic matter comprises of (mainly) plant products in variable stages of decay. Its content can significantly vary from 1% (sandy soils) to 90% (peat) depending on the soil type (Young, 2013). Organic matter plays a critical role in metal(loid) retention especially of airborne depositions. In addition to the retention of organic matter itself, the biota that is likely present on the surface of the soils can also accumulate metal(loid)s and thus increase the overall retention by organic matter (Rieuwerts et al., 1998). By the term "organic matter" mostly **humus** -the top 20 cm layer of soils- is implied although non-humic substances also exist. Humus is comprised by C (50-60%), O (30-40%) and H and N in about 5% and represents the part of organic matter that has reached its maximum decomposition and resists to further decay (Alloway, 2013). Humus is the most important fraction of organic matter contributing to soil fertility and, although not directly, in metal(loid) contaminated soils can also improve contaminant retention by e.g. decreasing bulk density of the soil, increasing water retention and more (Havlin, 2005). During humification process, the negatively charged phenol-, carboxyl and amino- functional groups are providing sites for binding. Thus metal(loid)s are bound to a variety of sites on humus by two or three bonds. The main components of humus that control metal(loid) binding are humic and fulvic acids. Those are strongly adsorbed on surfaces of Fe/Mn/Al oxides and in this way affect the metal(loid) mobility in soils in variable ways. In one hand, the formation of stable metal precipitates with soil colloids promotes metal(loid) retention. On the other hand, the

competition of anionic metal(loid)s with humic and fulvic acids for binding sites on Fe/Mn/Al oxides may result in metal(loid) release (Alloway, 2013). Finally, due to their mobility in soils, humic and fulvic acids can also influence the metal(loid) solubility and translocation in the soil profile (Kabata-Pendias, 2011).

Clay minerals

Clay minerals are layered aluminosilicates having a sandwich shape made of Si tetrahedra and Al octahedra sheets (Fig. 1.4). The ratio of tetrahedra and octahedra sheets is defining clay minerals into three layer types (i.e. 1:1, 2:1, and 2:1:1). Clay minerals are abundant in soils and can be divided into five groups based on the isomorphic substitutions in the layer: kaolinite, illite, smectite, vermiculite, and chlorite (Sposito, 2008). Due to their natural occurrence and efficiency in metal(loid) retention of both anions and cations they have been used as a sorbents in contaminated water and soils (Otunola & Ololade, 2020). Their efficiency is strongly influenced by their layered structure, their high specific surface area, high cation exchange capacity and chemical and mechanical stability (Uddin, 2017). The most common clays used in remediation of metal(loids) are bentonite, montmorillonite and attapulgite. Particularly for Zn^{2+}, the presence of muscovite along with clay minerals, was found to significantly affect its immobilisation in soil (Otunola & Ololade, 2020).
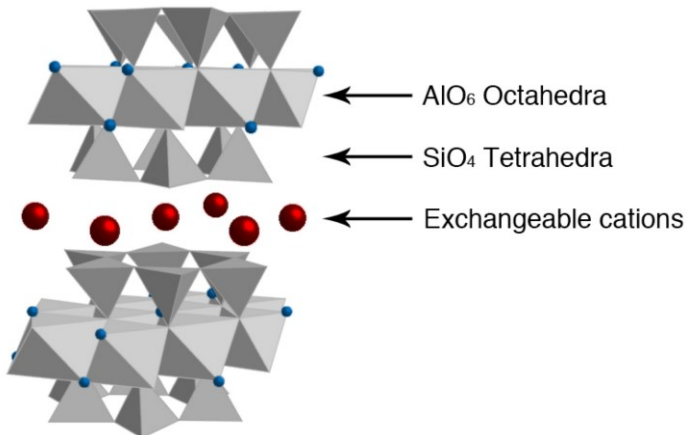
Figure 1.4: *Mineral structure of clay mineral according to the 2:1 layer type. Image adapted from Nakato & Miyamoto (2009) under the license CC BY 4.0 (https://creativecommons.org/licenses/by/4.0/).*

1.2 Soil contamination as a global issue

According the European Soil Data Center "**soil contamination"** is the occurrence of pollutants in soil above a certain level causing a deterioration or loss of one or more soil functions and also the presence of man-made chemicals or other alteration in the natural soil environment" (ESDAC). **Soil pollution**, describes the presence of chemicals and other substances out of place and /or above certain limits which has adverse effects on non-targeted organisms (FAO & ITPS, 2015). Soil pollution is considered a "silent" threat because it is invisible and odourless unlike air and water contamination which are easy to spot. Yet, soil pollution is considered more dangerous than other soil threats (e.g. soil erosion) because it is causing serious hazards to the environment and humans (FAO and UNEP, 2021). As mentioned in the very first paragraph of this thesis, soil pollution is currently affecting directly or indirectly 15 of the 17 United Nations **sustainable development goals (SDG)**. The goals SDG 1 (zero poverty), SDG 2 (zero hunger), and good health and wellbeing (SDG 3) are hindered because soil contamination decreases the crop yield and quality and affects human health. The SDG 7 about clean energy and SDG 8 about decent work and economic growth are strongly linked to soil contamination because industrial activities releasing hazardous contaminants into soil account for a great part of world-wide soil contamination. The goals for sustainable cities and communities (SDG 10) and responsible consumption and production (SDG 11) are closely linked to contamination because the current thoughtless product consumption lead to the exploitation of natural resources (including metal(loid) extraction) and the generation of dangerous waste. Goal 12 for climate action is interlinked with soil contamination mainly regarding unsustainable agriculture strategies. Goal 6 about clean water and sanitation as well as life below water and life on land (SDGs 14 and 15) are severely affected by soil contamination due to the high mobility of contaminants in the environment and the continuous hazardous impacts of contamination. Even societal goals SDG 5 (gender equality), SDG 9 (reducing inequalities), SDG 16 (peace and justice) and SDG 17 (partnership to achieve the goals) are hindered because soil contamination is affecting the global population unequally (FAO and UNEP, 2021). It is apparent from the above that soil contamination and soil pollution are bilaterally connected with key issues of global concern. Acting against soil contamination can directly assist the implementation of all SDGs.

1.2.1 Hazardous effects of meta(loid)s

Effects on living organisms

Risk metals and metalloids are harmful for the environment and all living organisms. Since they do not degrade, toxic elements accumulate in environmental compartments, translocate to other media, or enter the food chain and thus deplete all organisms. Depending on the metal(loid) type, the concentration and the affected organism, the effects of risk elements can vary. Nevertheless, a common hazardous effect of risk element accumulation is the generation of reactive oxygen species (ROS) which lead to oxidative stress in plants, animals and human cells (Okereafor et al., 2020). Oxidative stress in turn, depletes the biological molecules of organisms such as proteins and enzymes (Alengebawy et al., 2021). Risk elements can have poisonous effects on the soil microorganisms by disrupting the composition, size and enzymatic activities of soil biota (Alengebawy et al., 2021) while they inhibit (among others) the functions of growth, seed germination, and metabolism to plant species (Sall et al., 2020). They can cause chlorosis, root deformation, decrease in biomass, DNA damage and alter enzymatic activity in plants (Alengebawy et al., 2021). In aquatic organisms, toxic metal(loid)s can cause growth inhibition, tissue damage, respiratory problems, and death (Kakade et al., 2023). Humans accumulate toxic metal(loid)s by consumption of contaminated crops (90%) and inhalation of atmospheric particles (10%). Toxic metal(loid)s negatively influence cell organelles such as lysosomes, mitochondria and cell membrane and can alter the cell modulation (Das et al., 2023). They can damage the DNA structure and intervene in its functions and thus cause mutations or carcinogenesis (Tchounwou et al., 2012). Specific health effects to humans include cardiovascular disease, diabetes, neurological problems (caused by As), itai-itai disease and osteoporosis (from Cd), anaemia, renal dysfunction, stroke (from Pb) (Parida & Patel, 2023), nausea, metabolic syndrome, and increased chances of heart disease (from Zn) (Alengebawy et al., 2021). Exposure to toxic metal(loid)s can also increase the chances of infertility for women (J. Lin et al., 2023) while death caused by toxicity is not unlikely.

Effects on soil

Soil contamination by toxic metal(loid)s depletes key properties of soils (e.g. buffering, filtration and retention mechanisms, microorganism hosting, pH and more) which in turn might make soil unsuitable for agriculture, pasture, and

infrastructure (FAO, 2018; Rodríguez Eugenio et al., 2018) leading to decrease in crop production with detrimental economic effects. Increased concentrations of potentially toxic elements can affect the nutrient availability in soils especially when competing elements co-exist (e.g. Cu and Zn) (Alengebawy et al., 2021). Soil fertility and rate of organic matter decomposition are delayed in the presence of toxic metal(loid)s. Overall, soil contamination is a multifaceted threat affecting water, air, food, and eventually human health, but at the same time soil is the sink of other types of hazardous depositions from air and water. This could be called a soil contamination vicious cycle and it is schematically presented in Fig. 1.5.
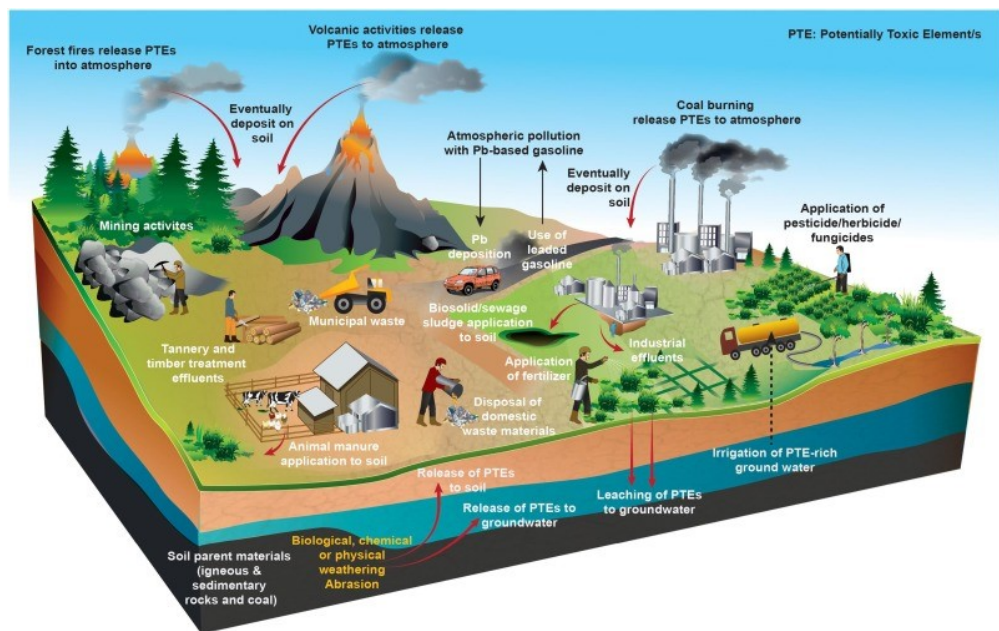
Figure 1.5: *Representation of contaminant fluxes resulting/originating in soil contamination. Image reproduced from Palansooriya et al. (2020) (https://doi.org/10.1016/j.envint.2019.105046) under the licence CC BY-NC-ND 4.0 (https://creativecommons.org/licenses/by-nc-nd/4.0/).*

In 2014, 340,000 contaminated sites existed in EU-39 but the estimation of potentially contaminated sites was 2.5 million (EEA, 2014). The updated but modest estimation for the potentially contaminated sites is 2.8 million (EEA, 2022; Payá Pérez & Rodríguez Eugenio, 2018). Even within EU, estimation of the extent of urban soil contamination is challenging due to heterogeneity and

data bias implying that there is a need for universal guidelines regarding contaminant thresholds, soil assessment methods and protocols for sampling, analysing and monitoring of soils (Binner et al., 2023).

The main and most impactful human activities that contribute to soil contamination are mining and smelting of metal(loid)s (Carvalho, 2017; Palansooriya et al., 2020; Rodríguez Eugenio et al., 2018). Mining and smelting of ores have been taking place since ancient times due to the need for metal resources. The increased monetary value earned by metal(loid) exploitation as compared to other activities and the subsequent increase of the world GDP led to a financial dependency on mining industry with detrimental effects on the environment (Carvalho, 2017; Ericsson & Löf, 2019).

1.3 Mining and smelting of metal(loid)s

Metal(loid)s are useful in numerous applications: from agricultural tools to mobile phones, metal(loid)s are widely used in the industry and everyday life. For this reason, humans have been exploiting the natural metal(loid) resources by **mining** economically important ores since prehistoric times (Murr, 2015). According to the Mineralogical Society of America, mining an ore deposit is economically sustainable when the desired element concentrations in the ore are hundreds to thousands of times higher than their crustal abundance. Some elements in low concentrations are associated with minerals that are mined for other elements, but the material process results in a valuable byproduct (i.e. elements associated with Cu, Pb, and Zn ores). Elements such as Au, Ag, and the platinum group are so valuable that almost any mineral containing that element in sufficient grades can be mined. There are two major concerns resulting from mining: 1) the production of tailings which are waste possibly including toxic elements and 2) the exposure of ores to weathering, which might further mobilise the toxic metal(loid)s they contain (Carvalho, 2017; Punia & Bharti, 2023). **Smelting** is the procedure of obtaining a metal in its elemental form or as simple compound by heating its ore beyond the melting point usually with the presence of oxidising factors. The pollution pathways occurring from smelting are 1) the production of toxic waste including slags, tailings and combustion residues and 2) the atmospheric deposition of metal-

rich particles to the adjacent soils (Xu et al., 2021). Today, even though the negative impacts of mining and smelting are generally known, the effects of the past activities are still present due to the long-lasting dissolution of smelter wastes into soils and the **persistent** nature of metal(loid)s (Ettler, 2016). Nonetheless, the wide variety of applications in which metal(loid)s are needed contributed to the steady increase of the mining and smelting operations with occasional peaks throughout time. Figure 1.6 represents in a comparable way the amounts of economically important ores that were mined in 2021.
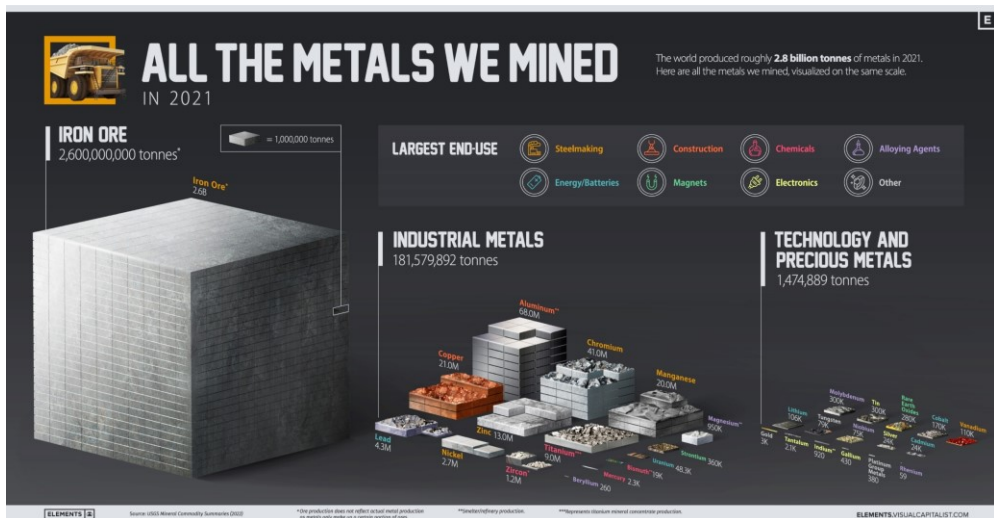
Figure 1.6: *Graphical illustration of the amount of metals extracted by mining of ores in year 2021. Source of image:* https://elements.visualcapitalist.com/all-the-metals-mined-in-2021/. *Source of data: USGS, Mineral Commodity Summaries (2022).*

1.3.1 Impacts of mining; an example from the Czech Republic

A local example of severe soil contamination owed to post-mining activities is the district of Příbram in the Czech Republic. The area of Příbram has a long legacy of mining and smelting activities dating back to the 1311 (Dostál et al., 2006). The main products were Ag and Pb which were mined from 1786 until 2006, while in 1972 smelting gave its place to recycling old car batteries and other secondary Pb products (Ettler et al., 2004). In 1990s, the smelter company of Příbram was criticised for the environmental impact of its operations and after several improvements in the used technologies now it represents an exemplary company of recycling Pb waste using environmentally sustainable techniques (Dostál et al., 2006; Ettler et al., 2005). Yet, the long-

lasting mining and smelting activities in the district of Příbram have caused severe water and soil contamination in the vicinity of the old smelter which is still evident today (Ettler et al., 2001, 2006, 2009). The concentrations of main contaminants are alarming: Zn up to 4100 mg/kg, Pb up to 4230, Cd up to 42 and As up to 330 mg/kg (Vítková et al., 2018).

Experimental site

Due to the severe metal(loid) contamination that is evident in the district of Příbram, the Department of Environmental Geosciences of the Czech University of Life Sciences Prague has set up an experimental site at the alluvium of the Litavka River (downstream from the Příbram smelter; see Fig. 1.7).The experimental site has been in operation since 2014 ensuring automatic measurements of meteorological and hydrological data. A fully equipped weather station takes measurements regarding air temperature, precipitation, global radiation, soil heat flux, wind velocity, soil moisture content, soil suction pressure, groundwater level, and pan evaporation. The data is collected every 10 or 20 minutes and wireless transmission is enabled. From 2015, 9 soil microplots (1 m^2 each) with different treatments (biochar and nZVI) were established. Finally, from 2019, two lysimeters; one filled with untreated soil and one with BC-treated soil were installed. A long-standing and complex research and many detailed investigations have been performed on this site not only regarding metal(loid) immobilisation (Hudcová et al., 2019, 2021; Jačka et al., 2018; Michálková et al., 2016; Teodoro et al., 2020a; 2020b; Trakal et al., 2011; Vaňková et al., 2021; Vítková et al., 2017, 2018; Wu et al., 2019) but also regarding soil hydraulic properties (Jačka et al., 2018; Seyedsadr et al., 2022; Šípek et al., 2019). Therefore, this thesis represents a piece in the mosaic of this research. The soil samples that were used in many of the experiments conducted during my PhD studies primarily originated from the alluvium of the Litavka River (Chapters I, II, & V).
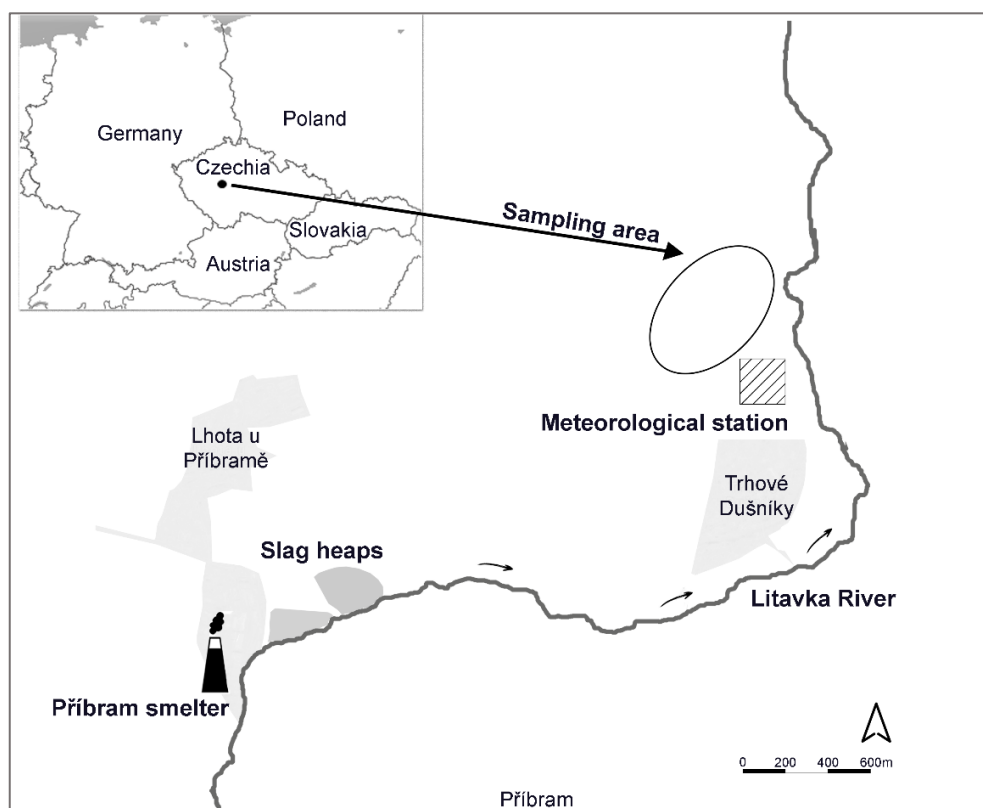
Figure 1.7: *Map of the experimental site at the alluvium of the Litavka River, presenting the soil sampling area in the vicinity of the smelter at the Příbram District. Adapted from (Mitzia et al., 2020), Copyright Elsevier (2020).*

1.4 Instrumental approaches for investigating metal(loid)s in soil

For some metals, their solid phase appearance (e.g. lustre of gold) or some of their properties (e.g. magnetism of iron) are reasons for their high economic value. When an ore contains precious or other important metals, it is vital to be able to distinguish them among other compounds and estimate potential impurities (Fig. 1.8). A powerful tool that can be used for this purpose is the **electron microscope** (together with specific detectors). In gold mining industry for instance, an electron microscope (especially if combined with automated analysis software) can assist in ore characterisation, provide

accurate chemical analyses, grain size analyses, spatial distribution of Au, provision of statistical data, and eventually minimise the time and financial risk of the operation (Burke et al., 2017; Costa et al., 2022; Lund & Lamberg, 2014). In the past century, different electron microscopes were developed aiming to investigate solid materials using high resolution imaging. Due to the property of metals to be conductive and thus promote the interaction with the electron beam, the electron microscopes were initially tested for metallurgical applications. Later on, electron microscopy was used in many other applications with the help of conductive materials attached to the specimen (Pansu & Gautheyrou, 2006). Today, SEM and EPMA are considered traditional methods used in mineral characterisation and ore processing (Lottermoser, 2017). Apart from mining and metallurgical industry electron microscopes are used in geology, mineralogy, material science, soil science, biology and more fields. Because the microstructure influences the macroscopic properties of a material, it is important to investigate it in order to manufacture a material with desirable properties (Borrajo-Pelaez & Hedström, 2018).

In the 1930s, the call for an instrument with a high resolution enabling the observation of details in the atomic level led to the development of first transmission electron microscope (TEM) by Knoll and Ruska in 1931. However, the poor resolution of the initial product urged the scientists into continuing the efforts for the development of a more powerful microscope. These efforts led Knoll to built the first scanning microscope in 1935 while von Ardenne improved the resolution of TEM and thus became responsible for the first scanning transmission electron microscope (STEM) in 1938. The first modern **scanning electron microscope (SEM)** *with 50nm resolution and up to 8000x magnification was developed by Zworykin, Hillier and Snyder in 1942. After continuous developments, finally in 1965, the first commercial SEM was manufactured according to the prototype system built by Pease and Nixon. Another electron microscope, the* **electron probe micro analyser (EPMA)** *was patented in the 1940s. In 1949 Castaing described and built the first EPMA instrument which was later commercially introduced in the market (in 1956). Although historically the SEM and the EPMA were developed separately and they were considered as separate instruments, in fact they share similar technology (Goldstein et al., 2003; Schmitt, 2014).*

The basic principle of all electron microscopes lies in the interaction of an **electron beam** with the specimen that is being investigated (Pansu & Gautheyrou, 2006). In the case of SEM, the electron beam is focused by the help of electromagnetic lenses on a small spot on the surface of the specimen. The beam scans the sample using raster analysis. The measured spot can be

as low as **1 nm** (Schmitt, 2014). The products of such interaction i.e. the **backscattered electrons (BSE)**, the **secondary electrons (SE)**, **X-rays**, and cathodoluminescence are recognised by the relevant detectors. For the creation of an image, the BSE mode uses the material contrast to reflect the **atomic weights** of the elements detected (the heavier the atomic weight the brighter the area) while in the SE mode, the **topography** of the sample is reflected thus areas closer to the detector are brighter and those further are darker (Schmitt, 2014). In Figure 1.8a for example, the heavier metal particles (i.e. Au) are clearly indicated in BSE mode by their brighter appearance while quartz is darker.
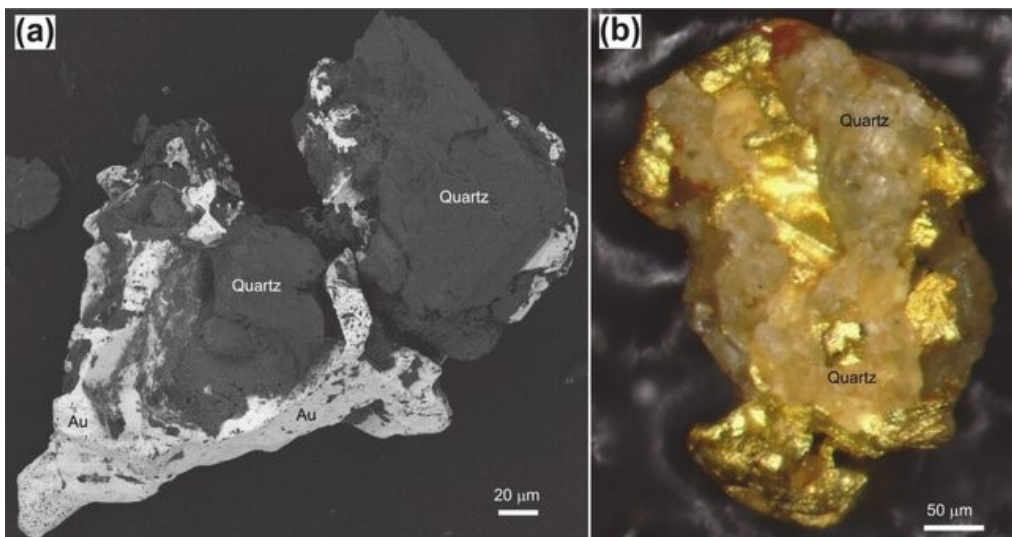
Figure 1.8: *Example of the usefulness of SEM/EDS in metallurgy: a) SEM image of particles containing Au and quartz and b) appearance of particle containing Au and quartz. Figure was reproduced from Craw et al. (2016) with the permission from the authors.*

In order to investigate the chemical composition of a specimen, SEM devices are equipped with **energy dispersive X-ray spectrometer (EDS)** detectors. The characteristic X-rays that are emitted by the beam $\times$ specimen interaction, can be used to define the **composition** of the specimen because every chemical element has its characteristic X-ray spectrum. Except for qualitative analysis, the EDS offers the advantage of quantitative analysis as well (Goldstein et al., 2003; Pansu & Gautheyrou, 2006; Schmitt, 2014).

1.4.1 Solid-state analyses in metal(loid) investigation

Coupling of SEM with EDS is a robust method for the detection and quantification of chemical elements in soil specimens in a non-disruptive way. The combination of visual and chemical information can facilitate the detailed investigation of contaminated soil samples (Fig. 1.9) and give an insight regarding the possible mechanisms of metal(loid) binding in soil components. The structure and chemical composition of compounds present in the soil can be detected with a high level of precision in close related to the method of sample preparation (polished surface is required for highly precise results). However, for increased accuracy and quantitative analysis that will lead to a specific mineral phase identification and metal(loid) substitution determinations in their structure, EPMA is preferable.
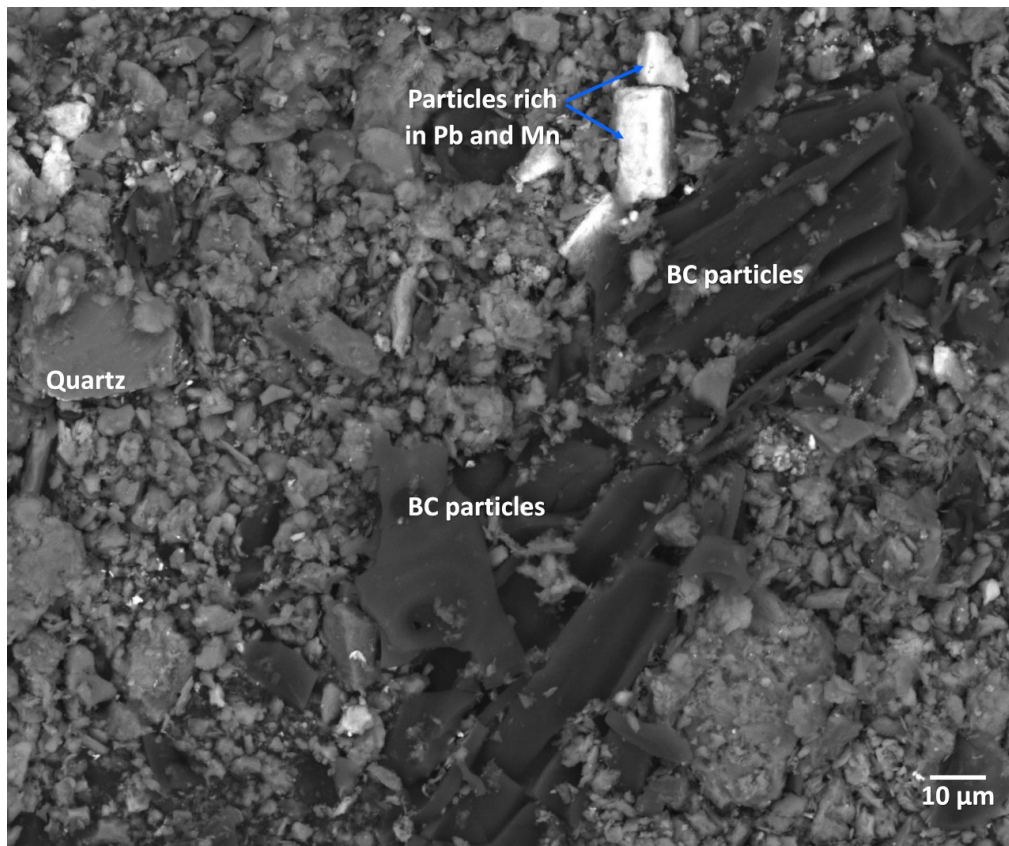
Figure 1.9: *Image from SEM/EDS analysis of soil sample presenting BC particles, quartz and particles with high content in Pb and Mn. The particles show distinct brightness in the BSE mode*.

Unlike SEM, the EPMA can perform sample analyses in the size of even **1 μm** as implied by the name of the instrument. The detection limit of EPMA can be as low as 200 ppm (Berry et al., 2017). These specifications make EPMA a powerful tool for accurate quantitative analyses of samples and mineral mapping (Pownceby et al., 2007). Not only the chemical composition but also the structure can be estimated precisely with the help of EPMA, making the determination of **mineral phases** feasible (Pansu & Gautheyrou, 2006; Schmitt, 2014).

Another method that is widely used for the determination of mineral phases in bulk sample is the **X-ray diffractometry (XRD).** The elastic scattering of XRD radiation enables the identification of the parameters of the crystal lattice and the geometrical distribution of the atoms in the crystal structure (Pansu & Gautheyrou, 2006). Unlike electron microscopes, XRD has the ability to distinguish the different phases of the same material and can perform qualitative and quantitative analyses (Schmitt, 2014). It can be used as a basic tool to determine major minerals in a solid sample however, XRD is not recommended for the investigation of non-crystalline solids (i.e. non-diffractive matrices) (Pansu & Gautheyrou, 2006).

The common use of X-ray absorption spectra **(XAS)** in the field of geochemistry is based on the method's ability to provide information about the oxidation state and geometry of a specimen tested in gas, liquid or solid forms (Zimmermann et al., 2020). In fact, XAS combines two interconnected methods: the X-ray absorption near-edge structure (XANES) in which after the absorption of a photon, an electron is excited from a core state to an empty state, and the X-ray absorption fine structure (EXAFS) which is found at higher energies than the XANES region. The XANES spectra can give insight into the oxidation state, the geometrical structure of the central atom examined, and its magnetic properties, while EXAFS may report quantitative results such as coordination number, distance of bonds, and local structure around the absorbed atom (Henderson et al., 2014; Yano & Yachandra, 2009). The methods are relatively common in the field of soil remediation in the last years as they can provide important information about elemental speciation and much more.

1.5 Solutions to the problem of metal(loid) contamination

1.5.1 Soil remediation methods

There are variable methods (Fig.1.10) to tackle metal(loid) contamination, all of which aim at the mitigation of their toxicity since metal(loid) degradation is unlikely. This is achieved either by decreasing the **concentration** of risk metal(loid)s or by decreasing their **availability** in soils. There are two large categories of remediation techniques: *ex-situ* and *in-situ* (Rehman et al., 2023). ***Ex-situ*** techniques are based on the extraction of the contaminated soil and its transfer to specialised facilities for remediation. Three categories of *ex-situ* techniques can be summarised: thermal, chemical and physical. **Thermal** methods aim at the vitrification of soils with toxic metal(loid)s in glasslike materials by the use of high temperatures. **Chemical** methods include 1) the solidification by the use of binding chemical substances and 2) soil washing which involves the use of chemicals that can remove toxic metal(loid)s from the soil. In the latter, the soil is replaced by clean sand and gravel while the extractant solution is treated as dangerous waste. **Physical** methods are the most commonly used method for soil remediation and involve the excavation of contaminated soil and its safe disposal and subsequent replacement with healthy soil. ***In-situ*** techniques are applied directly at the contaminated site and usually include physical, chemical, electrical, and biological techniques. **Physical** methods mostly implement covering of contaminated soils to separate them from the surrounding environment and groundwater. **Chemical** methods such as immobilisation involve the solidification and chemical stabilisation of metal(loid)s by the application of soil amendments. Chemical methods inhibit the mobility of metal(loid)s by changing their solid speciation and make them unavailable to biota while still present in the soil. **Electrical** methods target the electrokinetic behaviour of risk metal(loid)s; the anions and cations are separated by polarisation and then removed from the soil by electroplating or ion exchange. **Biological** methods make use of bacteria or plant species that are known to accumulate toxic metal(loid)s. Phytoremediation is a technique in which specific plant species accumulate toxic elements from the soil and then they are either removed by removing the plant leaves (phytoextraction) or they are immobilised in the vadose zone by

root accumulation or by immobilisation within the rhizosphere (phytostabilisation) (Bolan et. al, 2011).
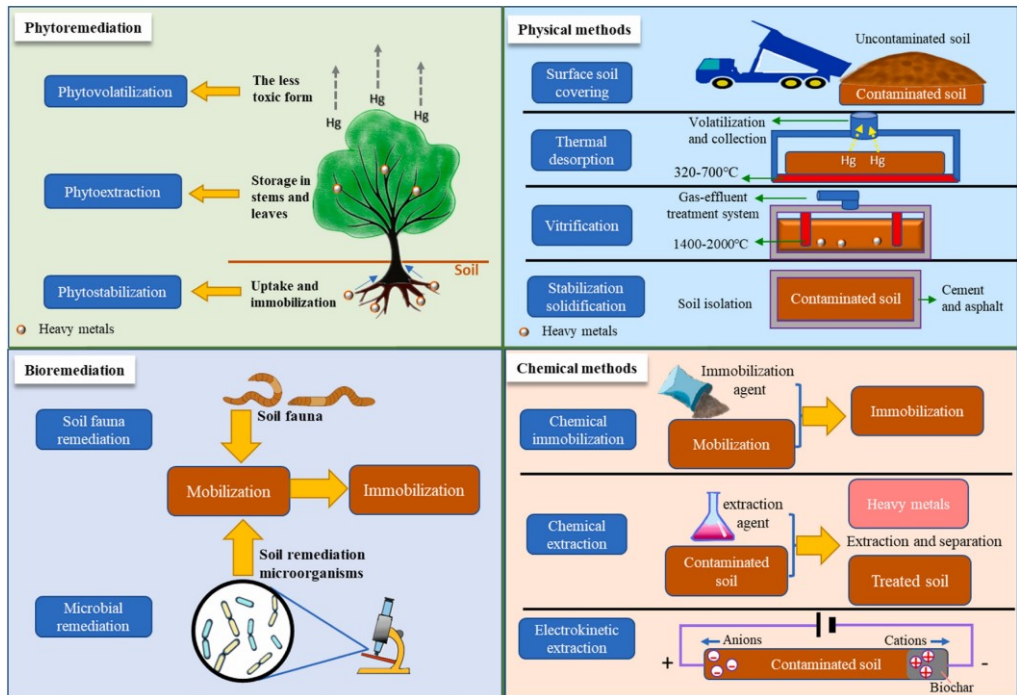
Figure 1.10: *Different categories of soil remediation methods. Image reproduced from Gao et al. (2022) Copyright Elsevier (2022).*

The apparent variety of remediation methods implies that there are advantages and disadvantages of each method and also more and less appropriate methods for a specific site (Khalid et al., 2017). For instance, soil replacement is one of the most common methods for soil remediation from risk metal(loid)s until today (Ding et al., 2024; Rehman et al., 2023). The advantages of this method are the simple implementation, the immediate remediation effect, and the significant decrease in pollutant concentrations. However, replacement method severely disturbs the environment and generates a huge volume of waste which needs to be transferred, making it a costly operation. This approach is appropriate for rather small areas exhibiting heavy pollution and requires monitoring of the remediated land to avoid secondary pollution (Dhaliwal et al., 2020; Lima et al., 2017; Rajendran et al., 2022; Rehman et al., 2023; Song, Xu, et al., 2022). Hence, soil replacement is a conventional remediation method that works but is probably inappropriate in the large scale.

Over the last 20 years, **chemical stabilisation or immobilisation** has evolved as an alternative to soil excavation and refill (Kumpiene et al., 2019). Immobilisation is a remediation method based on rendering metal(loid)s less available/mobile usually by changing their chemical form or speciation although they are still present in the soil (W. Cui et al., 2023). Typically, the introduction of immobilising agents to the contaminated soil changes the most available fractions of metal(loid)s (i.e. exchangeable fraction) to more geochemically stable forms (i.e. stable minerals or precipitates) (L. Liu et al., 2018; Lwin et al., 2018). Additionally, in some cases, immobilising materials can alter the speciation of a metal(loid) from a more mobile and toxic form to a less harmful (e.g. Cr(VI) is reduced to Cr(III) by various reducing agents). The above mechanisms rely on the processes of adsorption, precipitation, ion exchange, complexation, and redox reactions (W. Cui et al., 2023; Lwin et al., 2018). Figure 1.11 schematically presents the mechanisms involved in immobilisation. Immobilisation has been extensively studied and even employed as a remediation method because of the critical advantages it offers (e.g. compared to landfilling) and also because of the plethora of stabilising agents already developed (W. Cui et al., 2023; Palansooriya et al., 2020). Unlike landfilling, immobilisation involves less mechanical disturbances to the environment and thus eliminates the cost of remediation while it can be the method of choice in large contaminated areas (W. Cui et al., 2023) and it is a method with a long-term perspective (Rehman et al., 2023). Additionally, immobilisation is rather simple and rapid to implement (compared to invasive excavation methods), it is efficient for a wide range of contaminants, it may supply nutrients to the soil, and shows good social acceptance (Lwin et al., 2018). Except for the retention of metal(loid)s, soil amendments usually have other positive impacts to the soil properties with the most common and important being pH increase or water retention improvement. Furthermore, depending on the specific amendment, other properties such as Fe/Mn/Al oxides content, soil organic matter content, nutrient content, soil porosity, water holding capacity, cation exchange capacity, soil fertility and more, can be improved (W. Cui et al., 2023). It is not a coincidence, that traditional carbon-based fertilisers are among the most popular immobilising agents for soil remediation. Due to the advantages of immobilisation, and the variety of immobilising materials with encouraging results for soil remediation, this method was studied in the current PhD thesis.
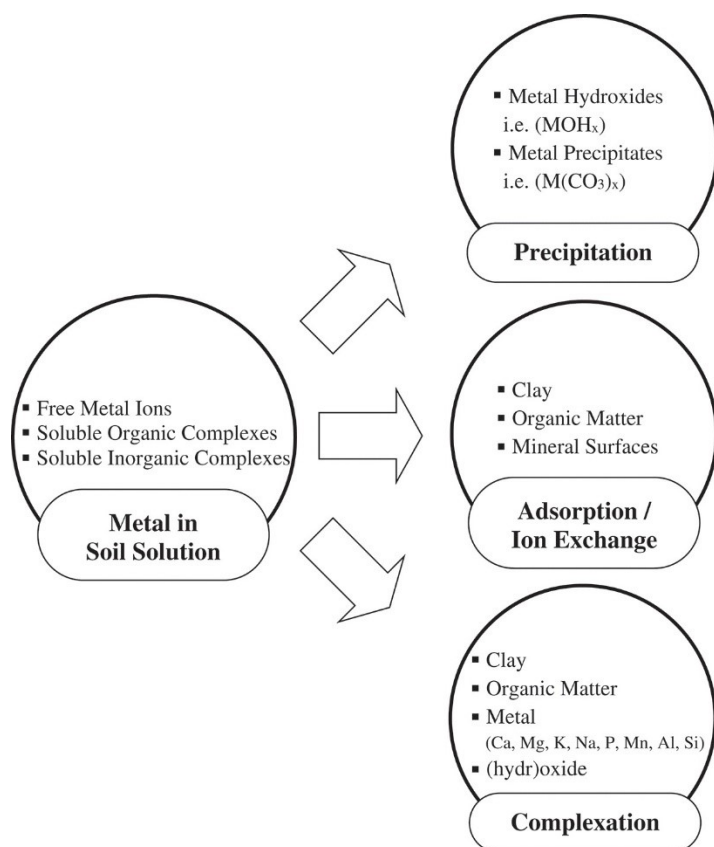
Figure 1.11: *Mechanisms employed during immobilisation for metal(loid) retention. Figure reprinted by (Lwin et al., 2018), © Copyright 2018, Informa UK Limited, trading as Taylor & Taylor & Francis Group, https://www.tandfonline.com.*

1.5.2   Amendments used for metal(loid) immobilisation in soils

The use of various substances as immobilising amendments is based on their natural presence in soils. Currently, one of the most popular amendments for water and soil remediation is **nano zero-valent Fe (nZVI)** (H. Chen & Qian, 2024; Rajendran et al., 2022) while the use of **Fe oxides** is overall quite common (Komárek et al., 2013; Kumpiene et al., 2019). A traditional soil improver used for hundreds of years is organic matter which makes **carbon-based** materials and primarily **biochar** quite popular for soil remediation (P. Wu et al., 2023; Y. Wu et al., 2024). The key detail in both categories of amendments is that they naturally occur in the soils. Therefore, synthetic Fe oxides, nZVI, biochar, and combined materials of those, represent **natural analogues** of the substances that metal(loid)s are binding on. The application

of soil amendments that are not "alien" to the soils, implies a guaranteed efficiency (up to a certain extent), eliminates the environmental risks that can occur upon the substance introduction and is a more socially-accepted approach compared to the use of new and artificial compounds. For these reasons, the current PhD study emphasizes on the application of nZVI, biochar and modified materials based on those two products along with other pyrolysed organic materials.

Nano zero-valent iron (nZVI) and Fe oxides

Nano zero-valent iron (nZVI; nano Fe^0) is nothing but metallic Fe particles of nano size (i.e. <100 nm). The increased efficiency of nZVI for environmental remediation along with its relative affordability made it a very popular treatment (Phenrat and Lowry, 2019 and references therein). Particles of nZVI have a strongly **reducing** nature that can alter the speciation (and thus toxicity) of some metal(loid)s. At the same time, nZVI exhibits high **sorption** capacity induced by both ZVI nanoparticles and the **newly-formed Fe oxides** that are produced by Fe^0 oxidation (Filip et al., 2019). A key advantage of nZVI is the small size of its particles offering **high specific surface area** which makes nZVI 1) a great sorbent for both organic and inorganic pollutants with flexibility for use in **multi-element contaminated** sites and 2) eases its **mobility** in the soil (Grieger et al., 2019; Stefaniuk et al., 2016). Additionally, nZVI synthesis can occur in almost any laboratory therefore regarded simple and cost-efficient (depending on the synthesis method; see later in this section) (Mackenzie & Georgi, 2019). At last, nZVI application is considered to be **low cost** compared to conventional remediation methods both in terms of labour and energy (Grieger et al., 2019). It is evident from the above that nZVI is an efficient and versatile tool for soil remediation and especially valuable for the soils that are contaminated with variable risk metal(loid)s. On top of that, Czech Republic is one of the first countries in Europe to have used nZVI in field application (Mueller et al., 2012) and participated in the European project NANOREM (2013-2017). Commercial production of nZVI that has been used in numerous studies, takes place in the Czech Republic by NANOIRON, Ltd. Notably, until 2018 (i.e. commence of my PhD studies) most of the research implementing nZVI for metal(loid) remediation concerned mostly water and rarely soils (e.g. Galdames et al., 2017; Gil-Díaz et al., 2014; Vítková et al., 2017). The behaviour of nZVI particles in the soil including potential interactions with soil compounds and **long-term** efficiency were still unclear.

Therefore, nZVI and certain modified nZVI products have been further investigated in the current PhD study. Application of the amendments in soils and for relatively long periods of time with the perspective to reveal the actual nZVI remediation potential is presented in Chapter III while the behaviour of nZVI products over time under changing moisture regime is presented in Chapters II & V.

Synthesis methods of nZVI

Although commercially available products were employed in the thesis, the nZVI synthesis is described below. Briefly, the synthesis of nZVI can be categorised in: bottom-up and top-down processes. Bottom-up synthesis, which is the most commonly used method for bare nZVI production, starts either from nano-sized Fe oxides, Fe-containing salts or other Fe-containing compounds and is based on the attachment of molecules or atoms of Fe^0 together. On the contrary, the top-down approach, implements larger scale particles and eventually transforms them to nano-scale particles by milling, etching and/or machining (Mackenzie & Georgi, 2019). Both of these methods are physical but chemical synthesis of nZVI can be also performed (e.g. reduction of dissolved Fe oxides by borohydride (BH_4^-) or by H_2 at high temperatures) (Stefaniuk et al., 2016). It is worth mentioning the evolving methods of obtaining ZVI from microorganisms, fungi, or various plant extracts (e.g. leaves, flowers, seeds) which have the ability to reduce iron ions to a lower valence state (Ying et al., 2022). This method shows promising potential for the production of nZVI at low-cost since it requires no energy and no reducing reagents and is therefore called "green nZVI synthesis". Except for the bare nZVI multiple other products such as bimetallic nZVI materials or other modified products have been developed (Mackenzie & Georgi, 2019).

nZVI activation

For the purposes of this PhD study mainly bare nZVI was used however, due to its high reactivity, **air-stable** products were chosen (i.e. NANOFER STAR powder; Fig. 1.12a). In general, nZVI particles can be extremely flammable and reactive and thus unsafe. For these reasons, 1) the handling of nZVI in the form of a water slurry and 2) passivation of nZVI so that it is not immediately reactive have been developed (Ribas et al., 2017). NANOFER STAR is a product developed by NANOIRON Ltd. (CZ) which consists of an Fe^0 core surrounded by a shield of Fe oxides (see Fig. 1.12c) resulting from the induced oxidation

of nZVI particles (passivation). According to the manufacturing company, the air-stable product offers convenient handling, cheaper transportation and less packaging since it is not pyrophoric while storage of a sealed container is practically for unlimited time (NANOIRON, Ltd., CZ). Although passivation guarantees the safety of the nZVI product, it introduces a new challenge which is the decrease of Fe^0 **reactivity** and thus decreased efficiency for metal(loid) retention (Ribas et al., 2017). To overcome this obstacle, an **activation** procedure has been investigated by Ribas et al. (2017) and suggested as a solution to regain nZVI reactivity before application while Kašlík et al. (2018) suggested that the appropriate size of passivated nZVI layer can actually serve both the reactivity safety and offer immediate activation upon use without waiting for activation (typically 48h). However, the latter study concerned application in aqueous solutions where the interactions between Fe oxides and H_2O can induce faster destruction of the Fe oxide shield. For the experiments conducted in this PhD study, the activation procedure as recommended by the manufacturer (NANOIRON, Ltd., CZ) and by Ribas et al., (2017) has been implemented prior to nZVI application in soils (for details see: Mitzia et al., 2020, 2023).
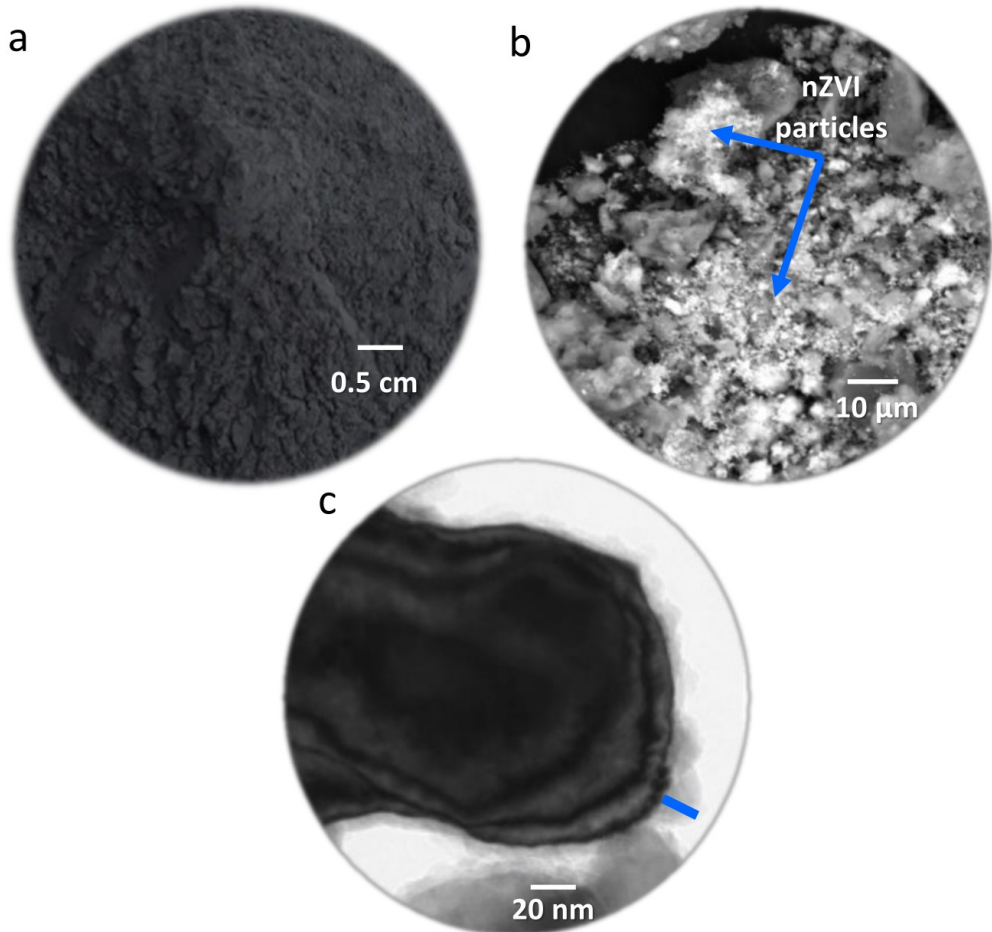
Figure 1.12: *Different representations of nZVI. a) NANOFER STAR nZVI powder, b) NANOFER STAR in soil as seen by SEM; BSE mode and C) NANOFER STAR as seen by TEM; nZVI particle with Fe oxide shield (image c adapted from Vítková et al., (2017), Copyright Elsevier (2017)).*

Mechanisms of metal(loid) retention

The mechanisms that are used by nZVI for metal(loid) retention are mainly adsorption, (co)-precipitation, and redox reactions but the actual mechanisms employed in each case depend on the specific metal(loid) (Fig. 1.13). In particular, the Fe oxide shield of passivated nZVI particles comprises amorphous or poorly-crystalline oxides which provide perfect space for ion **adsorption**. Additionally, the Fe^0 core is strongly reducing and thus three immobilisation scenarios can be derived based on the standard redox potential of the metal(loid) *vs.* nZVI. The first, includes metal(loid)s with E^0 much more

positive than nZVI (incl. As and Cu) for which **reduction** and **precipitation** on or close to the nZVI surface are the most commonly implemented mechanisms. For the second, metal(loid)s with E^0 slightly more positive than the E^0 nZVI (incl. Pb) can be reduced and adsorbed. Finally, metal(loid)s with E^0 similar or more negative than that of nZVI (inlc. Cd and Zn) can be mainly adsorbed by the Fe oxides on the nZVI surface or precipitate in the form of hydroxides (K. Li et al., 2023; O'Carroll et al., 2013). In addition, for anionic metal(loid)s such as Cr, the reduction of Cr(VI) to Cr(III), which is much less toxic, and its subsequent precipitation are a combined reduction – **co-precipitation** mechanism (K. Li et al., 2023). In the case of As, whose speciation is the opposite of Cr in terms of toxicity, the reduction if As (V) to As (III) might be partially followed by: further reduction to As (0), by adsorption of As (III) on the nZVI surface, or **oxidation** of As (III) to As (V) while As (V) might also directly be adsorbed by the nZVI surface (K. Li et al., 2023). Additionally, the application of nZVI usually induces a pH increase which favours the adsorption of positively charged ions on the negatively charged nZVI surface (Filip et al., 2019). Since the soil studied in the present PhD study is an example of contamination by both cationic metals (Zn, Pb, Cd) and anionic metalloids (As), the use of nZVI for immobilisation was targeted.
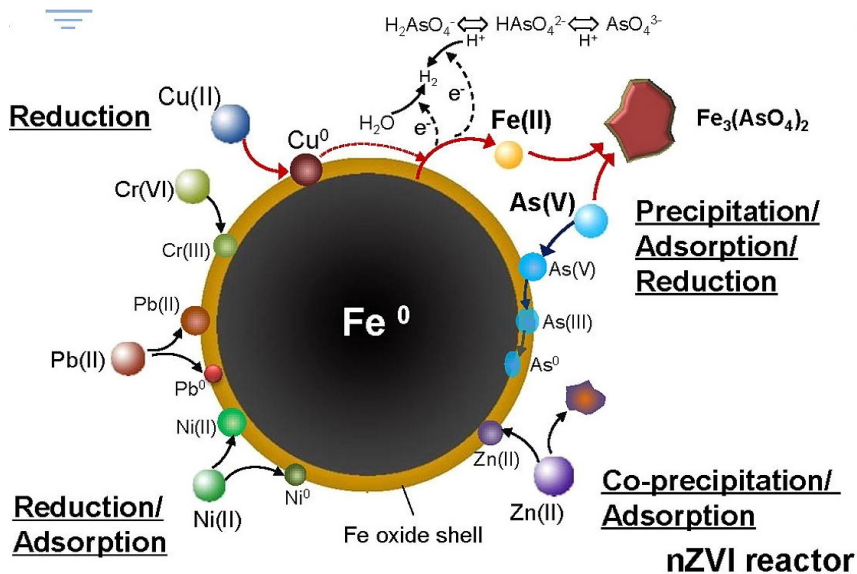
Figure 1.13: Immobilisation mechanisms employed by nZVI. Image adapted from Li et al., (2014) Copyright Elsevier (2014).

nZVI oxidation

When nZVI is in contact with oxygen or water, naturally, corrosion occurs and thus the Fe^0 is oxidised to other Fe forms, i.e. **Fe oxides**. In this case nZVI is acting as an Fe precursor to produce Fe oxides which are known to be great metal(loid) scavengers (e.g. Komárek et al., 2013; Kumpiene et al., 2019). The oxidation of nZVI is spontaneous, can happen in steps or directly and as shown in our study it is not necessarily proportional to time (Mitzia et al., 2023). Nevertheless, this exact transformation (i.e. oxidation) is the key to the efficiency of nZVI for metal(loid) immobilisation in soils (Komárek et al., 2013). Of course, the activation of nZVI particles prior to application (discussed earlier in this section) enhances the reactivity of the sorbent and speeds-up the oxidation procedure, yet the oxidation in soil happens in much slower pace than in water solutions. Different Fe (hydr)oxides have different structure and different properties. For instance, goethite ($α-Fe^{3+}O(OH)$) is the most common stable Fe oxide in soils. Haematite ($a-Fe_2O_3$) is another stable Fe oxide which is often the end member of oxidation processes. Other common Fe (hydr)oxides include lepidocrocite, ferrihydrite, magnetite and maghemite. Lepidocrocite ($γ-FeOOH$) is a polymorph of goethite. Ferrihydrite ($Fe_2O_3•nH_2O$) is a poorly-crystalline Fe oxide with variable composition (with respect to H_2O). Magnetite (Fe_3O_4) which has both Fe(II) and Fe(III) oxides in its composition ($Fe^{II}Fe_2^{III}O_4$), owes its name to its magnetic properties. Maghemite ($γ-Fe_2O_3$) is a product of magnetite oxidation also with magnetic properties (Cornell & Schwertmann, 2003; Sposito, 2008). Goethite (Baragaño et al., 2020; Cui et al., 2017), maghemite and magnetite (Michálková et al., 2014; Michálková, Komárek, Veselská, et al., 2016), ferrihydrite and lepidocrocite (as products of Fe^0 oxidation) (Kumpiene et al., 2021) have all been efficient in metal(loid) retention. Usually, the oxidation of Fe starts from poorly-crystalline and gradually evolves to more crystalline (i.e. stable) Fe oxides. In fact, the crystallinity of Fe oxides is a key parameter affecting the metal(loid) retention by Fe oxides and thus different Fe oxides can show different metal(loid) retention efficiency (e.g. Komárek et al., 2018). Consequently, the oxidation of nZVI in the soil is a crucial procedure which controls its ability for metal(loid) retention and is intended to occur. However, a careful assessment of the immobilisation state needs to be conducted in order to realise potential release of risk metal(loid)s in the long-term. The long-term immobilisation efficiency of nZVI products and the effect of time on Fe oxidation was one of the purposes

of my PhD study and was deeply investigated by Mitzia et al. (2023) which is presented in Chapter III.

nZVI modifications

Nano zero-valent iron has been extensively studied over the last years for its great potentials for metal(loid) immobilisation (Baragaño et al., 2020; Gil-Díaz et al., 2014, 2019; He et al., 2022; Hiller et al., 2021; K. Li et al., 2023; Teodoro et al., 2020; Vítková et al., 2018); yet, it has some functional drawbacks. The nano particles of Fe^0 are strongly magnetic which results in their self-attraction. This leads to the formation of agglomerates of nZVI particles (Fig. 1.12b) and is the greatest limitation of nZVI because it limits its mobility in soils (Ken & Sinha, 2020; Phenrat et al., 2019). In addition, when nZVI particles are not passivated with a protective shield, the strong reactivity of nZVI can cause vivid reactions which are unfavourable. For these reasons, **modifications** of nZVI have emerged increasingly during the last years to create more stable and effective products (Phenrat & Lowry, 2019 and references therein; Trakal et al., 2019). Those include: coating of nZVI particles with other compounds (usually polymers), combining nZVI with other metals (bimetallic nZVI), impregnating nZVI on other compounds or support it on their structure, sulfidation, emulsion and more (Petala et al., 2022). Variable compounds from natural minerals such as bentonite and kaolinite to synthesised materials such as resins or carbon-based materials have been used to support nZVI (Ken & Sinha, 2020). Among them, biochar (BC) holds a special place because it is a low-cost material, non-toxic, allows combinations with other materials, and shows immobilisation efficiency for both organic and inorganic pollutants (S. Wang et al., 2019a). Therefore, the modification of nZVI with biochar can combine the advantages of both materials, limit the aggregation of nZVI and promote its mobility in soil. Encouraging results on nZVI-BC immobilisation for metals and metalloids were published before 2018 but the studies concerning soil remediation were scarce: Su et al. (2016) and Zhang et al. (2018) reported successful remediation of Cr(VI) contaminated soils, using a BC-nZVI composites. In addition, studies where nZVI and BC were co-applied in soil were also rare (Oleszczuk & Kołtowski, 2017; N. Zhang et al., 2017). Based on those, nZVI combined with BC (Mitzia et al., 2020) and supported by BC (Mitzia et al., 2023) were studied during my PhD for metal(loid) immobilisation in soil. Consequently, BC was also tested alone.

Biochar and organic amendments

According to the International Biochar Initiative, "biochar is a solid material obtained from the thermochemical conversion of biomass in an oxygen-limited environment" (IBI). The use of biochar (BC) as a soil improver is linked to the *Terra Preta* (i.e. Amazonian Dark Earths; ADE), lands with increased fertility, high content of nutrients and organic matter (Lehmann, 2009). Although BC is not exactly an analogue of *Terra Preta*, research on BC production and utilisation was mainly initiated by the improved properties that ADE showed (Lehmann & Joseph, 2015). Based on this, BC can be considered a traditional **fertiliser** with proven efficiency to improve various soil properties as displayed in Fig. 1.14. Biochar application can influence soil properties such as fertility, water retention, cation exchange capacity (CEC), bulk density, soil pH, crop growth, NPK content, organic matter content, and microbiological activity (Beesley et al., 2010; Jien, 2019; Y. Zhang et al., 2021).
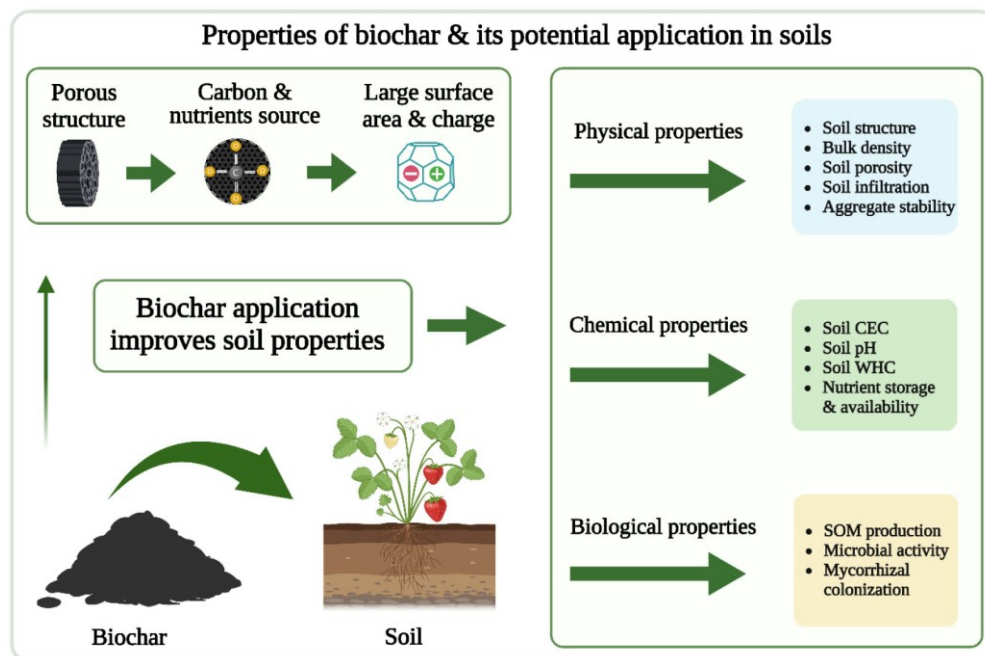
Figure 1.14: *Benefits of biochar use in soils. Image reproduced from Zulfiqar et al. (2022) under the licence CC BY-NC-ND 4.0 (https://creativecommons.org/licenses/by-nc-nd/4.0/).*

Additionally, in the last decades, BC has been also applied as a **sorbent** for contaminant immobilisation in water and soils (e.g. Ok et al., 2019; Y. Wu et al., 2024). Biochar has a variety of desirable properties including **stable**

organic matter content (resistant in mineralisation compared to natural organic matter), large **specific surface area**, increased **cation exchange capacity**, number of **oxygen containing functional groups**, high **porosity**, increased **mineral** content, and usually strongly alkaline **pH**, which make it a great sorbent for risk metal(loid)s in soils (Duwiejuah et al., 2020; Almatrafi, et al., 2022; Tack & Egene, 2019a; Y. Zhang et al., 2021)., Moreover, BC can be a low-cost material (depending on the feedstock), easily available and manageable (i.e. light-weight powder; Fig. 1.15a, no chemical reactivity) and with high social acceptance for use in environmental remediation projects (H. Lin et al., 2022). On top of those, the hospitable structure of BC (Fig. 1.15b,c) make it an ideal candidate for impregnation with other materials. There are two ways in which BC can be an effective tool for risk metal(loid) immobilisation in soils: directly, by retention of contaminants (e.g. adsorption), and indirectly, by altering physico-chemical properties (mainly pH increase) that control metal(loid) availability in soils (Taraqqi-A-Kamal et al., 2021). Although the efficiency of BC for risk metal(loid) immobilisation is known and was well-documented until 2018 (Abbas et al., 2018; Ahmad et al., 2014, 2017; Anawar et al., 2015; Trakal et al., 2011), long-time studies investigating the efficiency and overall behaviour of BC in the soil were scarce (O'Connor et al., 2018). Therefore, one of the objectives of the current PhD study, was to investigate the changes in BC efficiency over time and especially under changing conditions as presented in Chapters II, III & V.
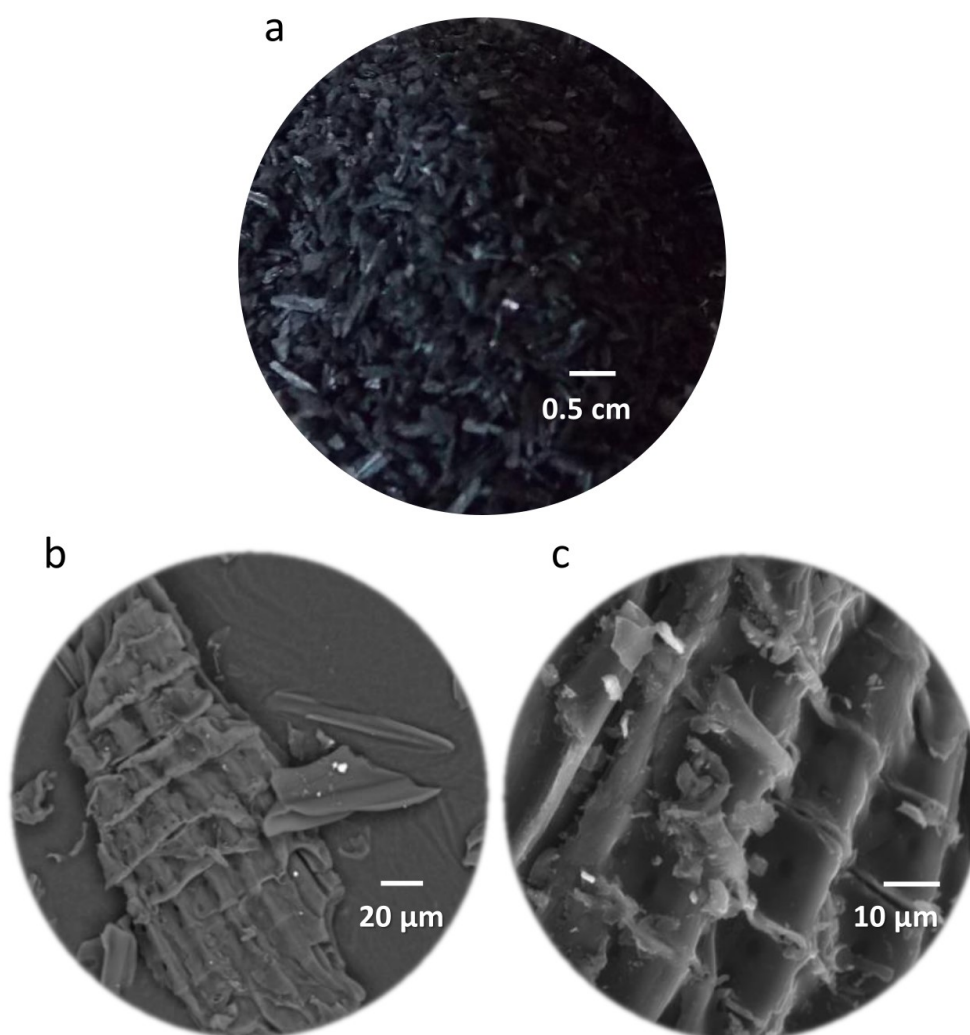
Figure 1.15: *Different representations of biochar. a) woody BC powder, b) BC structure as seen by SEM in BSE mode, and c) in SE mode.*

Pyrolysis conditions and feedstock

Biochar can be produced from any sort of organic mater (wood, crop waste, manure, municipal waste and more) either by **pyrolysis** (i.e. thermochemical conversion in inert conditions) or by hydrothermal carbonisation (conversion of wet biomass to biochar) (Lee et al., 2019). During the production of BC, volatile gases and hydrocarbons (bio-oils) are also produced. Pyrolysis is the most common method of the two and is characterised by the temperature, the heating rate and the residence time. Thus, fast pyrolysis occurs at 400-600 °C,

with a rate of 300 °C/min and residence time between 0.5 to 10 sec. This kind of pyrolysis mostly produces bio-oil and a smaller load of BC. Slow pyrolysis on the other hand, occurs in temperatures from 300 °C to 800 °C, with heating rate between 5 and 10 °C and residence time ranging from minutes to hours. Slow pyrolysis produces around 35-50 wt. % BC (Lee et al., 2019). Hydrothermal carbonisation occurs in much lower temperatures compared to pyrolysis, namely 180-260 °C for 5 min to 6 h, and it is an ideal method for the conversion of wet biomass without the need to pre-dry it and shows high conversion efficiency (Lee et al., 2019). For metal(loid) immobilisation, two main factors of BC production play an important role in the properties of the final product: the **pyrolysis conditions** and the **feedstock** (Ahmad et al., 2014). According to Zhao et al. (2013), BC's surface area and pH are mostly influenced by pyrolysis temperature, while CEC, organic carbon, and mineral contents, and carbon sequestration capacity of biochar are primarily influenced by the origin of raw material. In particular, higher pyrolysis temperatures (i.e. >500 °C) usually result in BCs with more stable C content, higher specific surface area, higher ash content, and higher pH, all of which can promote cationic metal(loid) immobilisation in soils (Ippolito et al., 2020; Jin et al., 2016; Almatrafi, et al., 2022; Palansooriya et al., 2020; Tack & Egene, 2019b). However, for anionic metal(loid)s, higher pH values have the opposite effect and this may lead to BCs eventually causing mobilisation (e.g. Beesley et al., 2015). Both mineral content (Ca, Mg, K, P, Fe, Mn) and the risk metal(loid) content (e.g. Cu, Zn, Pb, Sb) of BCs tend to increase at higher pyrolysis temperatures due to their content "magnification" after the removal of volatile compounds (T. Chen et al., 2014). Also, potential leaching of risk metal(loid)s contained in the BC feedstock, decreases with increasing pyrolysis temperature (X. Zhang et al., 2022). The CEC and the content of surface functional groups are lower at higher pyrolysis temperatures although some studies reported higher CEC at higher temperatures (Tomczyk et al., 2020). The surface groups on BC are of particular importance because they could either accept or donate electrons which makes a BC acidic or alkaline and hydrophilic or hydrophobic (Amonette, & Joseph, 2012). In terms of feedstock, woody BC might have lower pH than other materials likely due to the presence of P- and Ca-containing salts in the non-woody biomasses. Nevertheless, the presence of oxygen groups also plays a crucial part in the final pH with carboxyl ones, resulting in higher pH values (Tomczyk et al., 2020). Biochar produced from wood was reported to have higher specific surface area compared to BCs from

other raw materials, thus showing increased metal(loid) adsorption efficiency (Ippolito et al., 2020). Although higher specific surface area does not guarantee higher adsorption (Hudcová et al., 2022; Trakal et al., 2014), a higher surface area results in higher pore volume which promotes the mass transfer of metal(loid)s into BC pores and provides more active sites for binding (Agrafioti et al., 2014). Biochars produced from manures, crop-waste or sewage sludge, on the other hand, may have higher ash content and CECs and higher pH values compared to woody BCs but they exhibit lower specific surface area and less district porous structure (Ippolito et al., 2020). This is due to the higher ash content, which can result in blocking or clogging of the biochar pores and reduce the surface area and hinder the metal(loid) retention on their surface (Rangabhashiyam et al., 2022; Tomczyk et al., 2020). The mineral content of the final material is not only a significant factor in metal(loid) adsorption (Shen et al., 2018; P. Wu et al., 2023) but also for nutrient enrichment of soil (Ippolito et al., 2020).

Biochar retention mechanisms

Biochar induces metal(loid) retention through six main mechanisms (Abbas et al., 2018; Gao et al., 2022; Y. Wu et al., 2024): surface sorption, electrostatic interactions, ion exchange, precipitation, complexation and redox reactions (Fig. 1.16). Surface **sorption** occurs due to diffusion of metal(loid) ions on the biochar pores or due to *van der Waals* forces which lead to the formation of chemical bonds. **Electrostatic interaction** is governed by the point of zero charge (PZC) of the BC and the pH of the contaminant solution. Both the BC and the contaminants are charged and therefore electrostatic interactions occur between them. Based on this principle, when the pH of the surroundings is higher than the pH_{PZC} of the BC, then BC surface gets negatively charged and thus attracting cations while when the pH of the surroundings is lower than the pH_{PZC} of the BC, then anions are attracted. Especially for anionic species, electrostatic interaction is the main mechanism of their retention by BC. For **ion exchange** the differentiation between cationic and anionic species is crucial because this mechanism is based on the exchange of target contaminants with similarly charged ions located on the BC surface. Hence, the cationic species (usually metals) are exchanged by cations or protons on the BC surface and thus are immobilised. On the contrary, anionic species (e.g. As) cannot be exchanged. This is the main reason why BCs are generally not efficient for anion retention. The CEC of a biochar is a measurable property

that can show the potential of a BC for metal retention. Attention should be given to ion exchange because it can be reversible and thus result in contaminant release. The mechanism of **precipitation** is based on the formation of solids either on the surface or in the soil solution during the sorption process. The precipitates can be insoluble forms of a metal (since metals are usually immobilised in this way), thus presenting great stability. The mineral components of BC play a key role in the precipitates' formation. **Complexation** involves the binding of metal(loid)s with specific ligands resulting in the formation of stable complexes. The complexation ability of a BC may increase over time due to the formation of more carboxyl groups on BC surface after BC oxidation. Due to the presence of redox active moieties on the surface of BC, **redox reactions** can also be initiated. Biochar can both receive and donate electrons and thus act as a "geobattery" (Klüpfel et al., 2014; J. Yuan et al., 2022). This mechanism can be employed for the immobilisation of As and Cr; however, potential reversibility of the redox reaction can result in contaminant release.
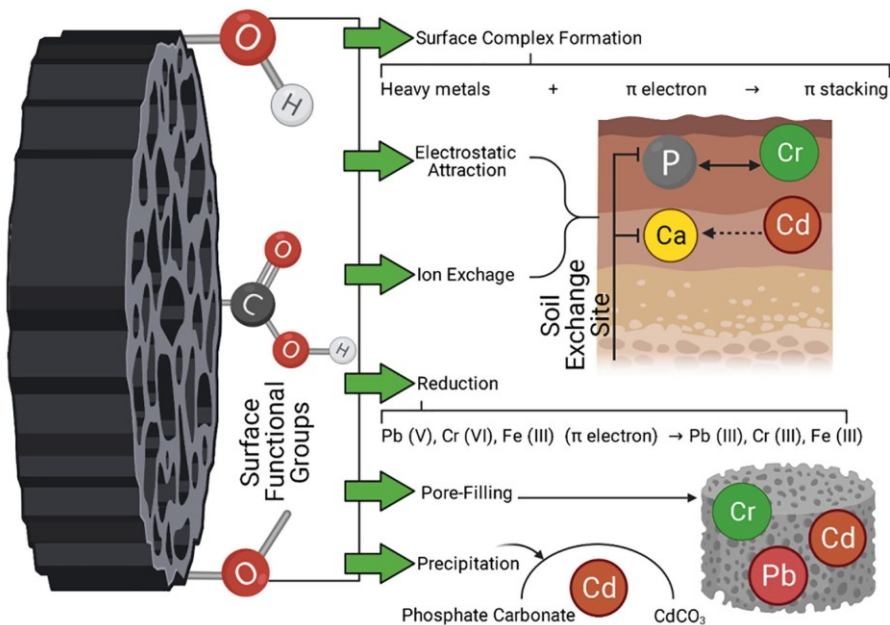
Figure 1.16: *Metal(loid) immobilisation mechanisms employed by biochar. Image reproduced from Ahmed et al. (2021) under the licence CC BY-NC-ND 4.0 (https://creativecommons.org/licenses/by-nc-nd/4.0/).*

As mentioned earlier, biochar can indirectly affect the metal(loid) availability in soils by enhancing key soil properties. Among these factors, pH is universally acknowledged as the most significant because it controls metal(loid) availability (e.g. Ok et al., 2019). The pH increase that is usually an outcome of BC application in a contaminated soil, results in a decrease in metal mobility. On the contrary, an increase in pH values might (and usually does) have an adverse effect of the mobility of anionic metal(loid)s (such as As and Sb), which are more mobile at higher (>5) pH values mainly due to the decrease of positively charged binding surfaces (Beesley & Marmiroli, 2011). Although BC has been sometimes efficiently used for **As immobilisation** in soils (Kumar & Bhattacharya, 2022; Shaheen et al., 2019; J. Wu et al., 2020), more studies found that BC promotes or does not decrease As mobility in soils (Gao et al., 2022; Vithanage et al., 2017; Zarzsevszkij et al., 2023; Y. Zhang et al., 2022). This finding calls for caution when taking decisions about the remediation of multi-element contaminated soils. In order to tackle the limited efficiency of BC for As immobilisation, modifications of BC products have been suggested (Trakal et al., 2019; Vithanage et al., 2017; Y. Wu et al., 2024). Among them, **modification** of BC with the incorporation of Fe oxides or nZVI (Fig. 1.17) has received positive feedback. A composite of nZVI and BC can have the advantages of both materials (e.g. high reduction ability, high CEC ability, pH increase) and at the same time, it minimises the negative effect of BC on metalloid mobilisation and the agglomeration tendency of nZVI as described before (Trakal et al., 2019; Y. Zhang et al., 2022). In general, nZVI-BC composites have been suggested as promising materials for metal and metalloid immobilisation in soils for the following reasons. They are non-toxic, with increased number of oxygen functional groups and surface sites and enhanced pore properties compared to BC alone. The Fe^0 nanoparticles can be easily dispersed onto the BC matrix (Fig. 1.17b) which improves nZVI stability. At last, local BC sources can be utilised for their production thus promoting cost-efficiency (Trakal et al., 2019). As previously discussed, a combination of BC and nZVI has been tested in the current PhD study (Chapters II, III & V). The BC products used in our experiments were commercially available by Carbon Terra (GmbH, DE) and LAC (Ltd., CZ). More details regarding their properties can be found in Mitzia et al. (2020, 2023).
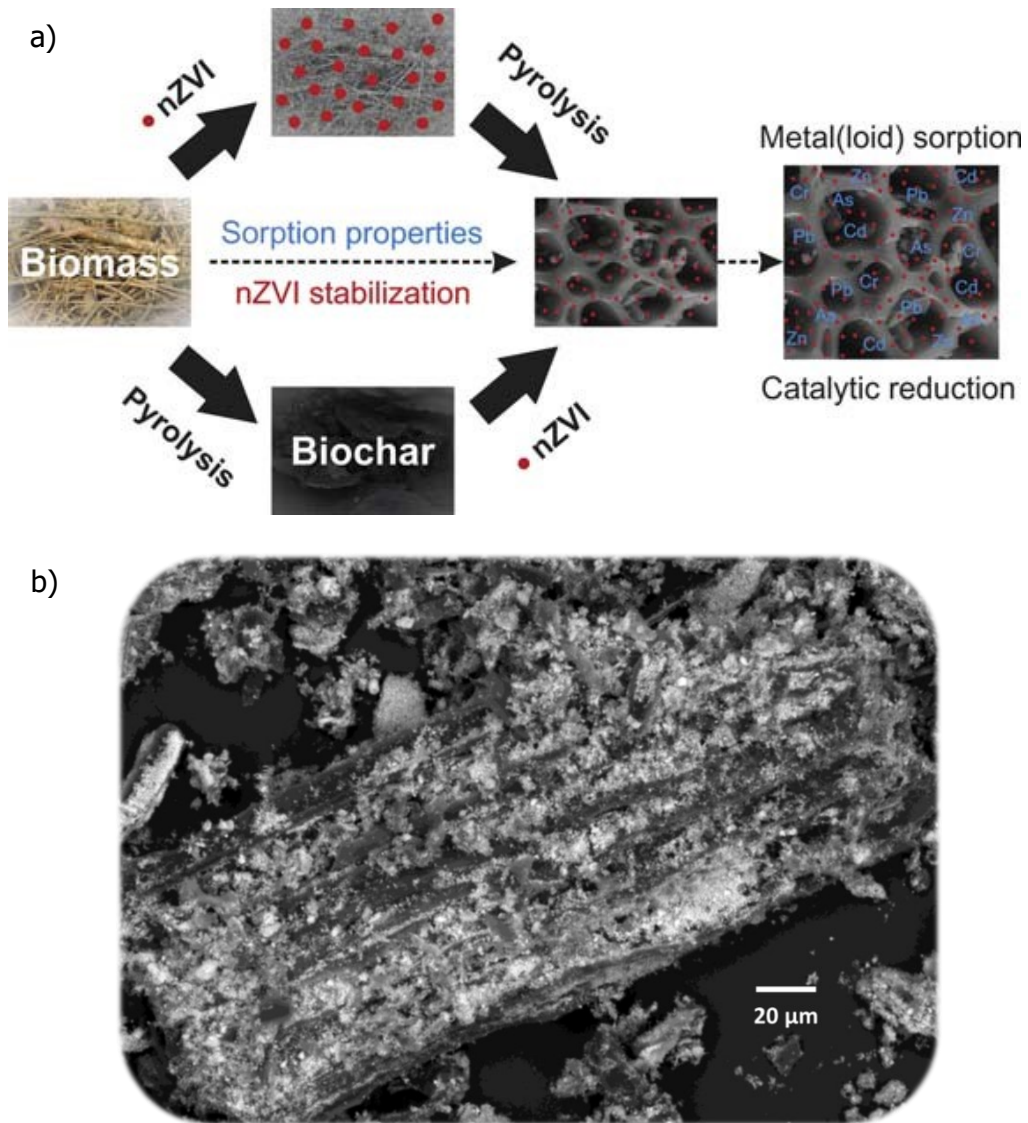
Figure 1.17: *a) Production of nZVI-modified BC and b) SEM image of nZVI-BC particle. Image a) is reproduced from Trakal et al. (2019), Copyright Elsevier (2019).*

Waste-derived biochar

Biochar can be a great cost-effective solution for metal(loid) immobilisation since, by default, **waste** materials are used for its production. This feature makes BC a sustainable product in terms of waste reuse and provides a plethora of options regarding feedstock. Sewage sludge-derived BC is a bright example of waste reuse with multiple environmental benefits. **Sewage sludge** is "any

solid, semisolid, or liquid residue generated during the municipal wastewater and sewage treatment process" (Wijesekara et al., 2016). The generation of sewage sludge is unavoidable and calls for immediate management to reduce the volume and sanitise the sludge, at least by removing the water (Fig. 1.18a). Ultimately, sewage sludge needs to be safely disposed which is a high-cost operation mainly due to necessary treatment, storage, transportation, and final disposal (Kacprzak et al., 2017). Furthermore, management of sludge is challenging due to the high loads that are produced and the variable composition sewage sludge can have depending on the original waste material (T. Liu et al., 2014). Sludge is rich in **organic matter** and typically contains increased amounts of nutrients such as Ca, K, N, Na, and P, but might also contain inorganic and organic pollutants and pathogens (Christodoulou & Stamatelatou, 2016). It is evident that appropriate treatment of sewage sludge is necessary as described in the European Regulation (EU, 1986). **Pyrolysis**, has been proved to decrease the available fraction of metal(loid)s (Agrafioti et al., 2013; Z. Cui et al., 2022; D. Li et al., 2022; X. Zhang et al., 2022) and minimise or completely remove the content of organic pollutants in sludge (Buss, 2021; L. Wang et al., 2020). On top of that, it can minimise the water content and thus the volume of sewage sludge. Therefore, the emerging idea of using sewage sludge as a feedstock for BC production can be considered a win-win situation in which sewage sludge is safely managed and a soil amendment is produced (Singh et al., 2020). Based on those, pyrolysed sludge (Fig. 1.18b) can be considered a sustainable soil improver with the ability to increase the organic matter, nutrient content (e.g. Fe enrichment; Fig. 1.18c), and the pH of the soil. For these reasons, sewage sludge has been implemented for soil remediation (Álvarez-Rogel et al., 2018; Chagas et al., 2021; Figueiredo et al., 2019; Grobelak & Jaskulak, 2019; L. Wang et al., 2020; Zhao et al., 2023). From this perspective, sewage sludge is not only a waste but a potential resource for material recovery (Christodoulou & Stamatelatou, 2016) and circular economy (Khan et al., 2023). Lately, due to the benefits of the use of pyrolysed sludge, increasing research regarding the sustainable and safe use of sewage sludge-derived biochar (**sludgechar**) has been increasingly popular (Hušek et al., 2022; Khan et al., 2023; Mayilswamy et al., 2023; Rangabhashiyam et al., 2022). Due to the multiple environmental benefits of the reuse of sewage sludge, sludgechars have also been investigated for metal(loid) remediation in water and soils (Chapter IV).

a

b

c

Fe sulphates
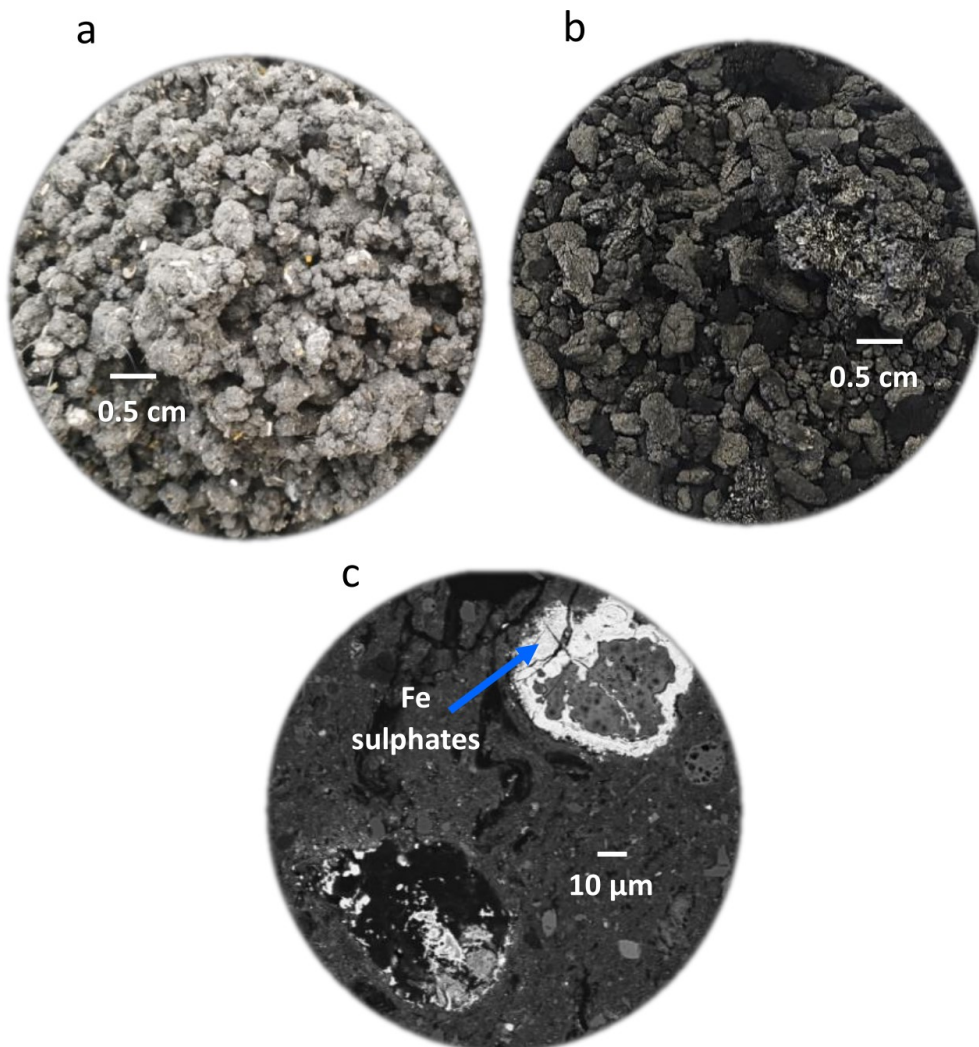
Figure 1.18: *Images of sludge and sludge-derived materials: a) dewatered sludge without further treatment, b) pyrolysed sludge (sludgechar) and c) sludgechar as seen by SEM in BSE mode, polished thin sections. Image c) is adapted from Mitzia et al., 2024, Copyright Elsevier (2024).*

Chapter II

Assessment of biochar and/or nano zero-valent iron for the stabilisation of Zn, Pb and Cd: A temporal study of solid phase geochemistry under changing soil conditions

Aikaterini Mitzia, Martina Vítková, Michael Komárek

Content

Abstract

The remediation of a soil contaminated with Zn, Pb and Cd was tested by using biochar (BC), nano zerovalent iron (nZVI) and a combination of these two (BC þ nZVI). Each amendment was individually applied to the soil at 2 wt%. We tested the influence of 1) the used amendments, 2) time, and 3) soil moisture conditions on the metal availability and soil physico-chemical parameters using various extraction methods, as well as soil pore water samplings. We found that metal availability was mainly affected by pH under the influence of time and water content. Among the tested treatments, BC was the most successful, resulting in the lowest amounts of the target metals in the pore water and the smallest temporal changes in metal concentrations and pH in the soil. The use of nZVI efficiently decreased water-extractable Pb in the short- and long-term. The BC þ nZVI treatment also yielded promising results regarding the immobilisation of the studied metals. Time provoked a general decrease in pH, which occasionally increased the available metal concentrations. Raising the soil water content increased the pH and subsequently lowered the available metal concentrations in the pore water. The mechanisms of metal stabilisation were further investigated by SEM/EDS. The results indicated that the used soil amendments enhanced the binding of Zn, Pb, and Cd on Fe/Mn/Al oxides/hydroxides, which in turn resulted in the stabilisation of the target metals.

2.1   Introduction

Biochar (BC) and nano zerovalent iron (nZVI) have become increasingly popular for environmental remediation. In particular, BC (i.e. a solid material resulting from the pyrolysis of organic matter), which has been traditionally used as a soil fertiliser, has recently been used for the remediation of soil from organic and inorganic contaminants (O'Connor et al., 2018). Remediation using nZVI has primarily been applied for groundwater remediation (Lefevre et al., 2016), but its use in soils remains scarce. The main mechanisms that are employed by these sorbents for pollutant decontamination are surface sorption, ion exchange, (co)-precipitation (Abbas et al., 2018; Kumar et al., 2018), and redox reactions (provided by nZVI as an electron donor) (Yirsaw et al. 2016). However, the application of such sorbents is not solely aimed at remediating contaminated soils, but also at enhancing soil functionality (Lwin et al., 2018), e.g. by promoting soil fertility (Ahmad et al., 2014) or by altering the pH, which is one of the key factors affecting metal mobility in soils (Houben et al., 2013; Pérez-Esteban et al., 2014). Moreover, the presence of soil organic matter, as well as Fe-, Mn-, and Al- oxides/hydroxides, plays an important role in metal sorption in soils (Neubauer et al., 2002; Sipos et al., 2018; Vítková et al., 2017, 2018).

Apart from the positive influence of the studied sorbents in soils, some drawbacks, such as the agglomeration of nZVI, calls for modified or combined materials (Trakal et al., 2019). Kaolinite, bentonite, mesoporous silica, activated carbon and biochar are some of the materials used to support nZVI particles (Dong et al., 2017). Biochar is cheap, simple to synthesise, non-toxic, and has the ability to make nZVI less unstable and more mobile in soils due to the distribution of nanoparticles in its structure (which prevents aggregation) (Tan et al., 2016). Therefore, BC has already been used for nZVI modification, yielding promising results for metal(loid) removal (Zhou et al., 2014; Yang et al.; 2018). However, most studies focus only on water or laboratory solutions. The co-application of BC and nZVI has rarely been tested in soils for the remediation of organic (Oleszczuk & Kołtowski, 2017) and inorganic (Zhang et al., 2017; Frick et al., 2019) contaminants.

In this study, we applied commercial products of BC or nZVI and their combination in multi-contaminated soil samples and conducted various types of laboratory experiments and solid phase analysis. The sampling of pore

water, in addition to extraction results, was selected because it is non-disruptive to the soil matrix and can estimate the concentrations of risk elements directly available for potential plant uptake (Moreno-Jiménez et al., 2011). The objectives of the current work were mainly to assess the availability of metals in each soil treatment as a response to time and actual water content, and secondarily to investigate the mineral transformations in the soil after the amendment application. Studies dealing with the functionality of soil amendments as influenced by time and water conditions are scarce. However, these parameters can significantly affect the metal stabilisation efficiency of the amendments. Hence, research on this topic is highly important and we provide such information in this paper.

2.2 Materials and methods

2.2.1 Soil samples and soil amendments

The soil that was used for this research was obtained from the alluvium of the Litavka River (Příbram District, Czech Republic, Fig. S2.1). The average annual temperature in the area is 7 °C and the average annual precipitation is 650–750 mm (Šípek et al., 2019). The sampling site is in the close vicinity of the Příbram smelter (Fig. S2.1). Although Ag and Pb smelting ceased in 1972, the past industrial activity produced large amounts of slag and other waste material, which were dumped in the near-by areas (Fig. S2.1), raising concerns about water and soil contamination (Ettler et al., 2001). Basic characteristics of the studied soil can be found in Table 2.1. Available concentrations of Zn in the soil have been reported in our previous studies and vary from about 10 to 25 mg kg^{-1} in water extracts and between 360 and 480 mg kg^{-1} in CaCl$_2$, Pb was found in much lower amounts, yielding up to 70 µg kg^{-1} in water leachates and 2 mg kg^{-1} in CaCl$_2$, while average Cd concentration in water and CaCl$_2$ leachates is 0.17 mg kg^{-1} and 10 mg kg^{-1}, respectively (Hudcová et al., 2019; Michálková et al., 2016; Vítková et al., 2018). Various amendments (and their modifications) i.e. BC (along with phytoremediation) (Břendová et al., 2015), nZVI (Vítková et al., 2017, 2018), amorphous manganese oxides (Michálková et al., 2016), and layered-double hydroxides (Hudcová et al., 2019) have been successful in metal(loid) stabilisation in samples of this soil under specific laboratory conditions. Nevertheless, further research on novel sorbents and their

modifications that are (cost-)efficient in multi-contaminated areas under various soil moisture conditions, are required.

Table 2.1. *Basic characteristics of the studied soil (n = 3).*

Soil characteristic	Value
pH_{H2O}[a]	5.98
pH_{KCl}[a]	5.27
Particle size distribution[b]	**Percentage**
Sand	75
Slit	20
Clay	5
***Aqua regia* extracted**	**mg/kg**
Al	9100±219
As	385±11
Ca	1436±26
Cd	31.6±1
Fe	32974±629
K	1529±43
Mn	4695±99
Pb	3854±121
Zn	3082±83

a According to ISO10390:2005
b According to Vítková et al. (2017)

The soil was sampled from the surface layer (0-25 cm), air-dried and sieved to <2 mm. The pseudo-total amount of metals/metalloids in the soil matrix was determined by microwave-assisted *aqua regia* extraction using the Multiwave PRO microwave reaction system SOLV (Anton Paar, Germany): about 0.25 g of each sample was digested, according to EPA 3051A (2007). In addition to the original protocol, 1 mL of H_2O_2 was added to the acid mixture (9 ml HNO_3 + 3 ml HCl) in order to enhance the soil organic matter decomposition. The samples were left to react overnight before being placed in the microwave oven. Prior to ICP OES analysis, the samples were diluted with deionised water to 50 mL, followed by filtration using 0.45 µm pore nitro-cellulose syringe filters.

As amendments we used the following commercial products: 1) a certified biochar (Carbon Terra product; GmbH, Germany) made of 80% coniferous and 20% deciduous wood chip pyrolysed at 700 °C for 36 h and 2) an air-stable nano zero-valent iron product (NANOFER STAR, NANO IRON, Ltd., Czech Republic). Both products were sieved to <0.5mm particle size. For the

activation of Fe^0 nanoparticles, (i.e. removal of the Fe-oxide layer), vigorous mixing was conducted in 1) demineralised water (following the manufacturer's recommendations) and 2) 0.02 M ammonium oxalate solution (for its ability to dissolve iron oxides), both in a 1:4 solid/liquid ratio. Mixing of BC in demineralised water was performed for uniformity. The BC-nZVI treatment was prepared by the addition of BC powder to the nZVI-water suspension (1:1 w/w) during mixing. The BC particles were occasionally covered or filled with nZVI particles (Fig. S2.2). A fresh suspension of each sorbent (i.e. nZVI in water, nZVI in ammonium oxalate, BC and BC+nZVI) was prepared immediately before its application to the soil.

2.2.2. Initial incubation

The soil was individually amended with each sorbent (2 wt.%) in the form of a suspension. The portion was chosen based on several aspects: 1) stabilisation efficiency, 2) overall cost of future full-scale application, and 3) potential negative effects of nZVI on biota. Various amounts from 0.01 wt.% (Wang et al., 2016) to 10 wt.% of nZVI (Fajardo et al., 2018) have been reported and applied in soils. Vítková et al. (2017, 2018) used 1 wt.% of nZVI with a positive effect on Zn stabilisation and plant growth, but still with toxic levels of available Zn. However, negative or even toxic effects on microbial/fungal community and plants have been reported for nZVI-treated soil (Wu et al., 2018; Xue et al., 2018). Therefore, 2 wt.% of nZVI was assumed as a balance between remediation efficiency, potential toxicity and cost. The rest of the amendments were applied in the same ratio for uniformity. A non-treated soil sample (i.e. control) was used for comparison. A total mass of 2 kg (including the amendment) was thoroughly homogenised, watered, and maintained at 60% of the soil water holding capacity (WHC) for 1 month to reach *pseudo*-equilibrium conditions after the application of the amendments. The samples were kept in 6-L polypropylene containers, which were partly open to allow the air come inside, stored at ambient temperature (22−25 °C) and protected against direct sunlight. The soil samples were regularly manually mixed and watered so as to maintain 60% of WHC. After the incubation period, the soil was dried at 40 °C and sieved again. An aliquot of each soil sample was kept for subsequent analyses to evaluate the efficiency of the 1-month incubated treatments with regards to the immobilisation of the target metals (i.e. Zn, Pb and Cd).

2.2.3 Pot experiment

A 60-day pot experiment was conducted in order to assess 1) the actual available concentration of metals and 2) the changes in metal concentrations as a function of time and water content. Approximately 270 g of incubated soil and a soil pore water sampler (Rhizon sampler, Rhizosphere Research Products, Netherlands) were placed in each pot (polypropylene, 0.42 L volume, conical frustum shape, r_1=5 cm, r_2=6.35 cm, h=7.5 cm). In total, 25 pots were prepared, i.e. 5 replicates of each treatment and 5 control samples. The pots were kept at ambient temperature (22–25 °C), regularly watered (without mixing and aeration), and pore water was collected after 10, 50 and 60 days from the re-equilibrated soil. The pots were initially maintained at 60% of the soil WHC. After day 50, watering was increased to reach 100% of WHC in order to simulate rainy events and waterlogging during floods in the area. Soil pore water was sampled using the rhizons and was immediately subjected to pH, Eh, and electric conductivity (EC) measurements and prepared for subsequent analyses. The soil from each pot was air-dried and further subjected to a set of extractions to compare the changes in metal concentrations before and after the pot experiment.

2.2.4   Chemical extractions

In order to investigate temporal changes (before and after the pot experiment) in the stabilisation efficiency and the key soil parameters between the different soil treatments, single and sequential extractions were performed.

Single extractions

Soil samples (4 g, n = 3) were shaken for 3 h in suspensions of 1) deionised water and 2) 0.01 M $CaCl_2$ (liquid to solid ratio of 10 mL g^{-1}). The leachates were centrifuged (9000 rpm, 10 min), filtered (0.45-µm nitrocellulose syringe filters), measured for pH, Eh, and EC and prepared for further analyses (Quevauviller, 1998).

Sequential extraction

A mass of 1 g of each soil sample (n = 3) was subjected to sequential extraction according to Rauret et al. (2000) and analysed for metal concentrations. At the third step of the procedure, after the initial addition of 10 mL of 30% H_2O_2

(according to the protocol) no additional H_2O_2 was needed (in contrast with the protocol) based on our previous experiments. The final solid residues were dried and subjected to microwave-assisted digestion as described previously.

Extraction of iron and aluminium oxides/hydroxides

In order to better understand and describe the changes of metal binding mechanisms, the amount of amorphous and crystalline Fe oxides/hydroxides and Al oxides/hydroxides was assessed following the ISO 12782 (2012) group of standards. A mass of 2 g of each soil sample ($n = 3$) was used for each extraction.

A solution of ascorbic acid (adjusted to pH 8) was prepared according to ISO12782-1. Forty mL of the final solution were added to each soil sample, after which the samples were shaken for 24 h at ambient temperature. Centrifugation (9000 rpm, 10 min), filtration (0.22-µm nitrocellulose syringe filters) and dilution of the samples for subsequent ICP OES analysis were conducted immediately after.

Crystalline Fe oxides and hydroxides were extracted with dithionite (adjusted to pH 4.8) according to ISO 12782-2. Forty mL of this solution were added to the samples prior to shaking in an orbital shaker (60 °C, 210 min). After cooling down for 30 minutes, the samples were centrifuged, filtered, diluted and preserved for further ICP OES analysis (as previously discussed).

Aluminium oxides/hydroxides extraction was conducted according to ISO 12782-3, using 40 mL of ammonium oxalate/oxalic acid at pH 3 for each soil sample. The samples were shaken in a horizontal shaker for 4 hours and then centrifuged (5000 rpm 30 min). Approximately 10 mL of the supernatant were filtered using 0.22 µm nitrocellulose syringe filters after discarding the first 3 mL. The final extractant was refrigerated until subsequent analysis.

2.2.5 Instrumental analytical methods

The concentrations of major and trace elements in all the tested solutions (acidified to a final concentration of 2% HNO_3 before analyses) were determined by ICP OES (Agilent 730, Agilent Technologies, USA). Carbon contents were determined using a carbon analyser (TOC-L CPH, Shimadzu, Japan). The concentrations of anions (F^-, Cl^-, NO_3^-, PO_4^{3-}, SO_4^{2-}) in the water

extracts and pore water samples were determined by ionic chromatography (Dionex ICS-5000+, Thermo Fischer Scientific). For the solid-state analysis, polished thin sections of the amended (incubated) soil samples were prepared and carbon-coated before analysis. A TESCAN VEGA3XMU scanning electron microscope (SEM) (TESCAN Ltd., Czech Republic) equipped with a Bruker QUANTAX200 energy dispersive X-ray spectrometer (EDS) were used for microscopic investigations. The actual voltage was set to 15 kV, and occasionally to 20 kV.

2.2.6 Data treatment

The results were statistically tested using the software Statistica (version 13.4.0.14, Tibco Software Inc.). The non-parametric Mann-Whitney U test was used to test the statistical significance ($p<0.05$) of the results after determining that the data did not have a normal distribution. Possible correlations were also determined using Pearson coefficient ($p<0.05$).

As a complementary method to the analytical results, the PHREEQC-3 geochemical code (Parkhurst & Appelo, 2013) was used to determine the speciation of metals and predict the potential solubility-controlling phases. The T_H database was used for all the calculations. See also Hudcová et al. (2019) for input details.

2.3   Results and Discussion

2.3.1 Soil pore water changes - pot experiment results

The interpretation of the pore water results indicates that apart from the used sorbents themselves their indirect effects (i.e. pH buffering, promotion of metal sorption on soil minerals) also played an important role in metal availability. The BC-treated soil samples yielded the highest pore water pH values among all the treatments in all the samplings, while also yielding the lowest metal concentrations for all 3 target metals (Fig. 2.1). Significant ($p<0.05$) negative correlations were observed between pH values and metal concentrations in pore water: pH–Zn ($r=-0.79$), pH–Pb (up to $r=-0.82$) and pH–Cd ($r=-0.76$). Similar correlations were reported by Vítková et al. (2018) with results from the same soil. Consequently, pH was suggested as the key factor affecting metal

availability in soil pore water (i.e. the highest pH values were connected to the lowest metal concentrations). On the 10th day of the pot experiment, the treatment efficiency with regards to the stabilisation of Zn and Cd was as follows: BC > Control > BC+nZVI > $nZVI_{oxal}$ > nZVI, whereas on the 50th and 60th days: BC > BC+nZVI > nZVI > Control > $nZVI_{oxal}$ (Fig. 2.1). It is important to note that the insufficient stabilisation of Zn and Cd by nZVI (observed on the 10th day) was only temporary. Lead, on the other hand, was stabilised by nZVI even during the first 10 days, while in general, the BC–bearing treatments were the most efficient in terms of Pb immobilisation (Fig. 2.1). However, Pb was generally detected in very low amounts compared to the other metals because of its limited availability. This was clear from the sequential extraction results (Fig. S2.3). Furthermore, according to the PHREEQC calculations, Pb in pore water was suggested to be in its most mobile form (free Pb^{2+} ion), in percentages ranging from 44–53% on the 10th day of the pot experiment to 73–78% on the 50th day and 65–76% on the 60th day, which was significantly ($p < 0.05$) lower compared to 83–95% for Cd^{2+} and 86–96% for Zn^{2+} (Table S2.1). Consequently, Pb was the least available among the 3 studied metals as expected.
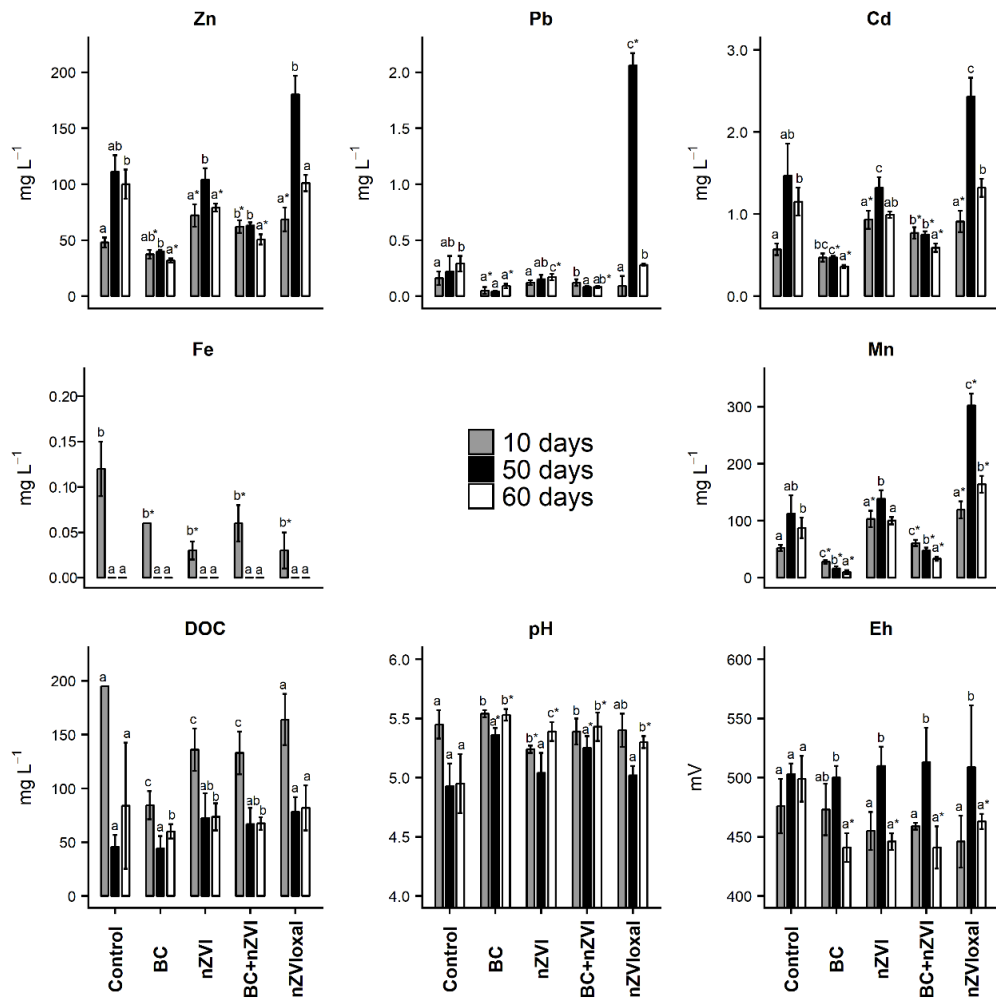
Figure 2.1: *Changes in selected soil pore water parameters as a function of time and soil moisture conditions (the water content was 60% of WHC during the first 50 days, followed by an increase to 100% of WHC until the 60th day, n = 5). Bars with the same letters indicate non-significant differences; asterisks indicate significant (p<0.05) differences from the control soil.*

The decrease in pore water pH observed on the 50th day of the pot experiment in all the samples (Fig. 2.1) is believed to be the main reason behind the increased availability of all the studied metals (Rieuwerts et al., 1998). The PHREEQC results indicated that, on the 50th day of the pot experiment, all 3 target metals were found in their free ionic form (i.e. Zn^{2+}, Pb^{2+} and Cd^{2+}, respectively) at higher rates than those of the 10th day (Table S2.1). Moreover, close-to-zero saturation indices of smithsonite ($ZnCO_3$) and otavite ($CdCO_3$) indicated that metal carbonates were the principle solubility-controlling phases

on the 10th day of the pot experiment (Table S2.2). The drop of pH on the 50th day resulted in the dissolution of metal-bearing phases, such as smithsonite, similar to what was suggested by Van Damme et al. (2010).

The significant ($p < 0.05$) differences in Zn and Cd concentrations induced by the increased water content (60th day) that were observed in all the treatments except the control (Fig. 2.1), suggest that the actual moisture conditions are crucial when assessing the sorbent functionality. However, the speciation of Cd and Zn remained the same independently of the actual soil water content (Table S2.1). When it comes to Pb, the percentages of Pb^{2+} dropped from 73–78% to 65–67% for the amended samples after the moisture content was increased, while no particular change in Pb speciation was determined in the control (Table S2.1). The higher portions of Pb^{2+} in the control soil pore water samples (44% on day 10 compared to 75–76 % on days 50–60) corresponded to a progressive increase in the available Pb concentration (Fig. 2.1). This behaviour was related to the decrease in pore water pH from 5.45 on the 10th day to 4.93 and 4.95 on the 50th and 60th days, respectively (pH–Pb $r = -0.72$ on the 50th and $r = -0.82$ on the 60th days). In contrast, the pH values of all the amended soil samples increased again after reaching full saturation (day 60; Fig. 2.1). Consequently, due to the strong correlations of metal mobility with pH, the water-content related effects on the amendment buffering activity are essential for the metal immobilisation process.

The time- and pH-dependent availability of Cd and Zn in soil pore water has been previously reported for amended and non-amended soils (Beesley et al., 2010; Tye et al., 2003). However, studies related to temporal fluctuations in soil water content are scarce (Yang et al., 2019), and even so, interactions between water content and sorbents in soils are rarely investigated. Recently, Salam et al. (2019) reported that soils, amended with several types of BC and incubated at different moisture conditions, yielded a higher pH increase at higher water contents (compared to lower water contents). Changes in soil water content may have a strong impact on redox reactions in soil, which in turn affect 1) metal mobility and 2) the behaviour of functional groups on the surface of BC (Yuan et al., 2017; El-Naggar et al., 2018). Moreover, Yang et al. (2008) found that the decrease of Cr(VI) in nZVI-amended soils was higher when the water/soil ratio was higher. The same effect can be observed for the reaction between nZVI and soil, which induces an Eh decrease followed by a

pH increase (Shi et al., 2011). Higher water contents in soils may decrease Eh and subsequently increase pH (Salam et al., 2019) due to the well-known negative correlation between pH and Eh (Rinklebe et al., 2016a, 2016b). In our study, pH was negatively correlated with Eh (r=−0.72), however, no strong correlations between Eh (Fig. 2.1) and metal concentrations were determined in pore water.

Both the experimental and modelling results indicated significant temporal changes. In particular, the dissolution/precipitation of Fe/Mn phases was the most critical factor affecting metal sorption. The absence of Fe in the pore water samples of all the treatments on the 50th and 60th days (Fig. 2.1) could be a result of enhanced precipitation of new Fe phases. Ferrihydrite was predicted to be the most probable (Table S2.2), and Fe(III) species prevailed in the tested solutions (Table S2.1) according to PHREEQC. At the same time, the sorption of metals on Fe–oxides was confirmed by SEM/EDS (Fig. 2.3) and is discussed below. Moreover, the observed Mn release (Fig. 2.1) from the nZVI- and nZVI$_{oxal}$-treated samples was proportional to the low stabilisation efficiency of these treatments. In contrast, BC-containing samples yielded the lowest values of dissolved Mn and the lowest risk metal concentrations in pore water. Correlations between the amount of available Mn and the 3 studied risk metals in pore water were determined as follows: Mn–Zn r=0.94, Mn–Pb r=0.84 and Mn–Cd r=0.96, indicating that the dissolution/precipitation of Mn played an important role in terms of metal stabilisation. Iron and Mn form important mineral phases in soils, represented by a small particle size, low solubility and a high surface reactivity (Sposito, 2008), making them great scavengers of risk elements (Komárek et al; 2013; Kumpiene et al., 2008). No Mn oxides were predicted as solubility-controlling phases in the pore water, except for rhodochrosite ($MnCO_3$) (Table S2.2). The role of rhodochrosite in the remediation of a metal-contaminated soil has been discussed previously (Michálková et al., 2016).

Dissolved organic carbon (DOC) concentrations generally decreased over time (Fig. 2.1), while a significant pH–DOC correlation was determined (r=−0.85, p<0.05), indicating that pH was also the main driver of carbon release. The soil treated with BC, a material known for its ability to sequestrate organic carbon (Anawar et al., 2015), had the lowest amounts of DOC in the pore water. The organic matter content of soils correlated with a lower risk-metal availability

(e.g. Kwiatkowska-Malina, 2018), further supporting the role of BC in metal-stabilisation.

2.3.2 Extractability of metals in H_2O and $CaCl_2$

The availability of target elements in soil was assessed using extractions in H_2O and $CaCl_2$ before the pot experiment, i.e. using soil incubated for 1 month, and after the pot experiment, i.e. after exposure to additional watering and different moisture contents over time. Thus, the temporal changes in the elemental composition and physico-chemical parameters in soil were determined (Fig. 2.2). The results indicated that not only the applied sorbents, but also the time-dependent incubation conditions played an important role in the metal immobilisation processes.

Regarding the different soil treatments, Zn_{H2O} was significantly ($p<0.05$) stabilised by nZVI and $nZVI_{oxal}$ before the pot experiment (Fig. 2.2A), probably due to the significant correlation of pH_{H2O}−Zn ($r=−0.76$, $p<0.05$). In contrast, BC and BC+nZVI yielded the lowest amounts of Zn (Fig. 2.2I) in the $CaCl_2$ extraction, but no correlations with pH were determined in that case. After the pot experiment, Zn concentrations were significantly ($p<0.05$) stabilised by all the treatments in both extractions, but BC yielded the lowest values (Fig. 2.2A, I). Significant correlations of pH_{H2O}−Zn ($r=−0.86$ to $r=−0.96$ at $p<0.05$) indicated the key role of pH on metal availability in soils. Cadmium concentrations in water were generally low (up to 0.7 mg kg^{-1}), and they were lower in the soil treated with nZVI and $nZVI_{oxal}$, but only temporarily (before the pot experiment), while BC and BC+nZVI treatments yielded minimal concentrations of Cd after the pot experiment (Fig. 2.2C). The lowest amount of Cd_{CaCl2} was noticed in BC-treated soil, followed by BC+nZVI-treated soil, both before and after the pot experiment (Fig. 2.2K). Again, pH seemed to be an important driver of Cd availability, yielding pH−Cd correlations between $r=−0.75$ and $r=−0.87$. Water-extracted Pb was significantly ($p<0.05$) lower than that of the control in the samples treated with $nZVI_{oxal}$, BC and BC+nZVI, while no stabilisation was noted for $CaCl_2$-extracted Pb before the pot experiment (Fig. 2.2B, J). After the pot experiment, almost all of the used treatments in both extractions yielded significantly ($p<0.05$) lower amounts of Pb, except for BC in the H_2O extraction (Fig. 2.2B, J). Although the total percentages of Pb^{2+} generally increased over time according to PHREEQC, the

control samples consistently had significantly ($p < 0.05$) higher amounts compared to the treated ones (Table S2.3). It should be noted that, despite the nZVI treatment yielding higher amounts of Pb_{H2O} than the control soil before the pot experiment, this amount decreased over time (Fig. 2.2B). The fluctuations in Pb availability are believed to be due to the DOC–Pb correlation ($r=0.63$, $p<0.05$), which points out the well-known affinity of Pb for soil organic matter (Jensen et al., 2006; Kennou et al., 2015; Vodyanitskii et al., 2014).

It is known that nZVI is oxidised upon contact with water in soil, and as a result the potential contaminants are reduced to achieve an oxidation–reduction equilibrium (Galdames et al., 2017). Therefore, the strongly reducing nature of nZVI, which is one of the main mechanisms of its efficiency (Stefaniuk et al., 2016), might cause the dissolution of soil organic matter. As a result, Pb may become more available due to its complexation nature. This was clearly observed in the results of the BCR extraction, where a higher portion of exchangeable Pb and a lower % of Pb bound to organic matter were found in the nZVI-treated samples compared to the control and BC-treated samples (Fig. S2.3). Although the samples treated with nZVI yielded the highest DOC_{H2O} values before the pot experiment, this effect was mitigated over time (i.e. after the pot experiment; Fig. 2.2F). Concerning the $nZVI_{oxal}$ treatment, the results indicated that nZVI was efficiently activated as the oxide layer was dissolved by stirring with ammonium oxalate solution and the stabilisation of metals was fast (Fig. 2.2A, C). At the same time, the presence of oxalates seems to limit the extensive leaching of DOC in the $nZVI_{oxal}$-treated soil (Fig. 2.2F).
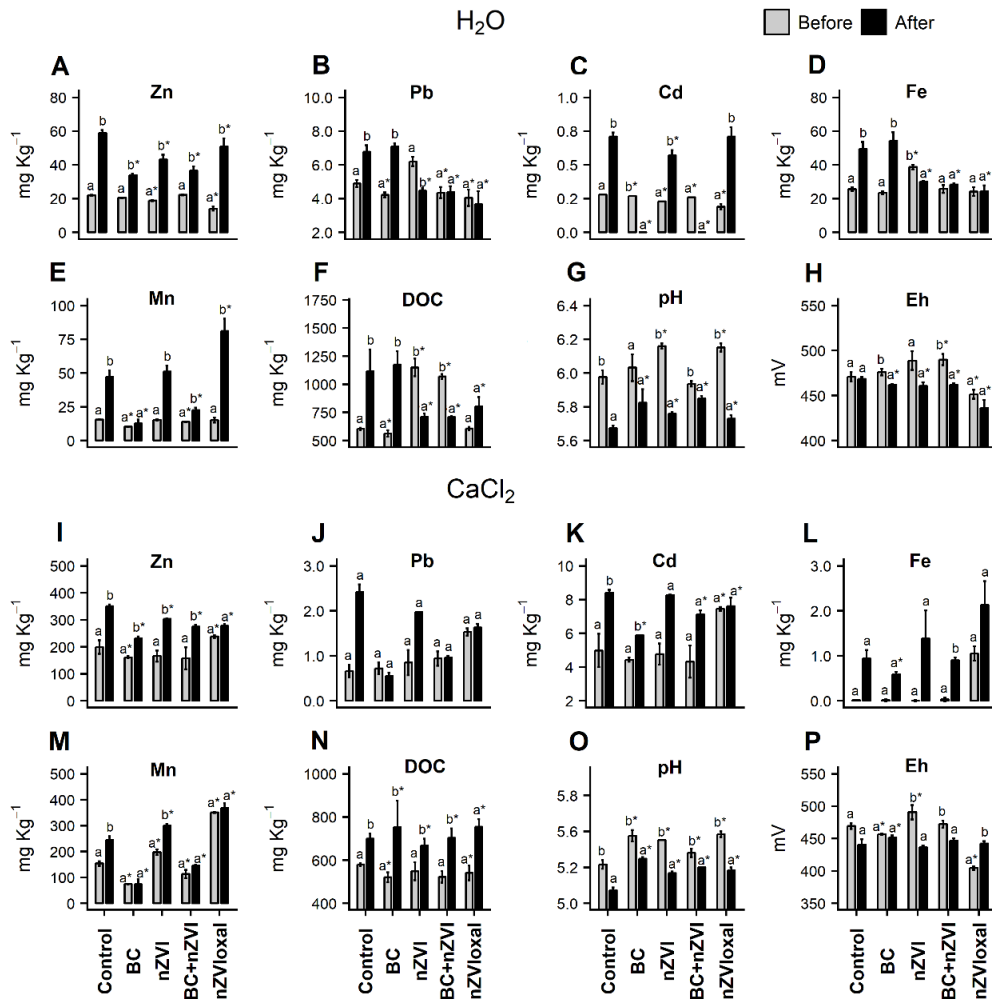
Figure 2.2: *Changes in metal availability, pH, Eh and DOC before and after the pot experiment, expressed using H2O and CaCl2 single extractions (n = 3). Bars with the same letter indicate non-significant differences; asterisks indicate significant (p<0.05) differences from the control.*

It can be assumed that the functionality of the amendments was highly dependent on temporal changes in soil water content. Time-dependent solid phase changes (aging) and metal availability changes in soils are affected by temperature, pH, moisture content, drying-rewetting cycles and the total metal concentrations (Lock & Janssen 2003). Yet, pH is the most crucial factor determining how profound the effect of aging would be on metal availability (Lock & Janssen 2003). Several studies have reported that aging of

contaminated soils (amended or not) results in contaminant decrease (e.g. Lacalle et al., 2018; Venegas et al., 2016), which is generally related to a pH increase. However, the pH in our study decreased significantly ($p < 0.05$) over time. Particularly, the range of pH values was 5.27–6.20 before and 5.09–5.81 after the pot experiment (Fig. 2.2G, O). However, the BC-treated samples had the most stable pH values over time. In addition, significant ($p < 0.05$) correlations between metals and pH were determined both before ($r = -0.75$ to $r = -0.76$) and after ($r = -0.82$ to $r = -0.96$) the pot experiment. The Eh values ranged from 404 to 491 mV before and from 436 to 468 mV after the pot experiment, yielding occasionally significant ($p < 0.05$) differences (Fig. 2.2H, P). Negative correlations of Eh with the studied metals were present in the soil extracts ($r = -0.61$ to $r = -0.77$), both before and after the pot experiment. It is known that variations in Eh can influence the release of metals in soils (Frohne et al., 2011).

The interactions between soil redox potential and metal concentrations are not single-directional though; Eh and pH are also affected by redox active elements in soils or elements occurring in high concentrations (Husson, 2013). Metal concentration variations are strongly related to soil solid phase–solution interactions (Rieuwerts et al., 1998; Roberts et al., 2005). The solubility of metals in soils is on one hand controlled by the mineral source and the potential for metal adsorption on soil constituents and on the other hand by dynamic soil properties such as pH and redox potential, soil water content and soil-metal interaction duration (Young, 2013). Consequently, the efficiency of soil treatments over time may be affected by multiple interactions in the soil matrix and by changes in the water content, which in turn can provoke an Eh-pH fluctuation (as already discussed), and finally, pH is expected to define metal availability.

The role of major elements in metal behaviour cannot be neglected. In particular, the significant ($p < 0.05$) correlations that were observed between the studied metals and Mn before and after the pot experiment (Mn–Zn, $r = 0.70$–0.86, Mn–Cd, $r = 0.76$–0.94 and Mn–Pb, $r = 0.73$–0.87) imply that Mn dissolution was connected with metal availability. Moreover, although Mn_{H2O} levels were similar in all the soil samples before the pot experiment, BC and BC+nZVI were the only treatments that retained the same Mn levels afterwards (Fig. 2.2E). Additionally, significant sorption on Mn oxides was observed in the

BC–based samples by SEM/EDS (Fig. 2.3), although no Mn oxide precipitation was suggested by PHREEQC (Table S2.4). In contrast, the nZVI–containing samples yielded the highest amounts of dissolved Mn (Fig. 2.2E, M) similarly to the pore water results (Fig. 2.1), where rhodochrosite was the main solubility-controlling phase (Table S2.4). Vítková et al. (2018) also reported excessive Mn release in nZVI treated soil samples. Iron solubility in H_2O was also higher in the nZVI-treated samples than in the rest of the treatments, which did not occur in the case of the $nZVI_{oxal}$ samples (Fig. 2.2D). The PHREEQC calculations showed that Fe(III) was the prevailing form for all the treatments and suggested the precipitation of secondary Fe^{3+}-bearing phases (Tables S2.4, S2.5). A temporal increase in the values of DOC_{CaCl2} was observed (Fig. 2.2N) without any correlations between DOC and pH or the studied metals. However, an explanation could be found in the significant DOC_{H2O}–Fe correlation ($r=0.81$, $p<0.05$), confirming the well-known affinity of Fe for organic matter (Lindsay, 1991).

2.3.3 Mineralogical investigations

The solid-state analysis of the amended soil samples (after 1 month of incubation) showed that Mn and Fe oxides and oxyhydroxides were the major scavengers of metals in the studied soil. In particular, BC often occurred as a particle covered by Mn oxides containing up to 30 wt. % Pb (Fig. 2.3A) or as stand-alone BC particles with adhering soil particles. Up to 0.5 wt. % Zn and Pb were detected on the BC surface. This observation clearly corresponds to the sequential extraction results of the BC–containing soil samples, yielding higher percentages of Pb bound to oxides compared to the nZVI–treated samples (fraction B, Fig. S2.3). In addition, various soil Fe, Mn or Fe-Mn oxides containing Pb and Zn were observed by SEM/EDS within all the amended samples (Fig. 2.3). The sorption of target metals on Mn-oxides was often observed in the soil that was treated with BC (with or without nZVI) (Fig. 2.3A, C); however, no precipitation of common Mn oxides/hydroxides was predicted by PHREEQC (Table S2.2), which showed strongly negative saturation indices values. On the other hand, Nelson et al. (1999) highlighted the importance of amorphous biogenic Mn oxides in controlling Pb adsorption, compared to common crystalline Mn oxides and even to Fe oxides. Various soil Fe-oxides, with up to 10 wt. % Zn, were detected in the nZVI-treated soil sample (Fig.

2.3B) and numerous Mn-oxides containing up to 20-30 wt. % Pb and up to 4 wt. % Zn were also found.

From these results, we can assume that the presence of nZVI in soils had a strong indirect effect on metal behaviour based on the reduction of Mn from primary Mn or Fe-Mn phases (observed by SEM), followed by the formation of secondary Mn and Fe oxides, which was further responsible for metal sorption. Vítková et al. (2018) studied the same soil and concluded that the main mechanisms of metal stabilisation using nZVI were sorption on Fe-oxides and on primary or secondary Mn-phases. However, nZVI often forms aggregates, which limit its functionality for sorption. Indeed, no target metals were detected on the surface of the nZVI aggregate (Fig. 2.3B). The agglomeration of nZVI is one of its major and well-known disadvantages, causing lower mobility of the product in soils and possible clogging of soil pores (Stefaniuk et al., 2016; Xue et al., 2018). Consequently, pure nZVI may initiate attenuation processes in soils rather than work as an actual sorbent.
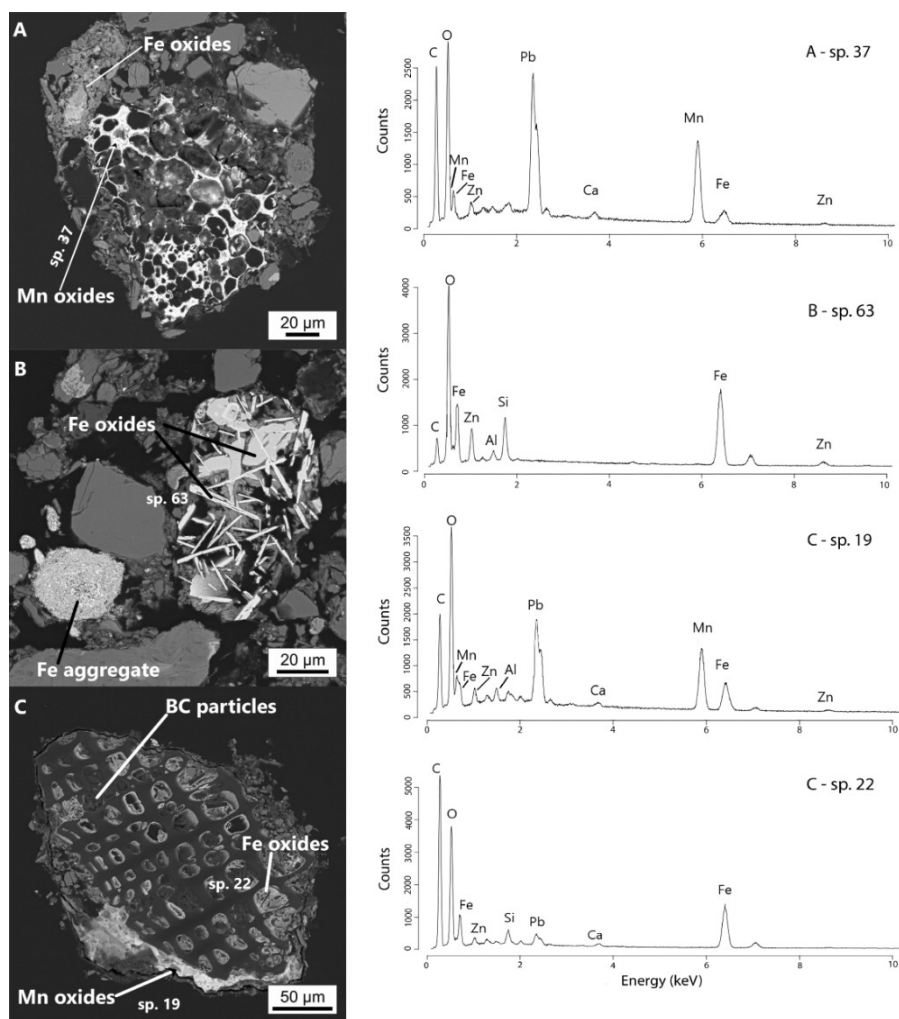
Figure 2.3: *Backscattered electron images (SEM analysis) of the amendments incubated in the studied soil with their corresponding EDS spectra. A) BC-treated soil, up to 3 wt.% Zn and 5 wt.% Pb found on Fe oxides, up to 30 wt.% Pb found on Mn oxides; B) nZVI-treated soil, Fe oxides with up to 10 wt.% Zn, no target metals were found on the Fe aggregates; C) BC+nZVI-treated soil, Fe-Mn oxides with up to 2 wt.% Zn and 20 wt.% Pb.*

Silicates containing up to 11 wt. % of Zn and up to 9.5 wt. % of Pb were detected in the amended samples. Moreover, the occasional sorption of up to 2.5 wt. % of Cd on Al–oxides was observed by SEM/EDS (data not shown). The concentration of dissolved Al resulting from ISO extraction 12782 (Fig. S2.4) is indicative of the amount of Al oxides/hydroxides in the soils, and furthermore, Al(OH)$_3$ was predicted by PHREEQC to precipitate and thus might be partly

responsible for metal sorption under the given conditions (Table S2.4). The main retention mechanism after the BC+nZVI treatment was sorption on soil Fe, Mn or Fe-Mn oxides (Fig. 2.3C). Manganese oxides containing up to 28 wt.% Pb and up to 4 wt.% Zn were observed. Aggregates of nZVI with partly formed secondary Fe-oxides were noticed, but aggregation was limited compared to the nZVI-only treated sample.

Recent studies confirmed that a synthesised nZVI-BC composite improves the functionality of nZVI and prevents the formation of Fe aggregates (Han et al., 2015; Deng et al., 2018). Biochar-supported nZVI products have been reported as having successfully remediated Cr(VI) in soils (Su et al., 2016; Zhang et al., 2018), however, most studies implementing nZVI-BC products concern (laboratory) aqueous solutions, which does not have to be representative of natural conditions in the field. The use of BC to support Fe^0 particles has the potential to enhance the functionality of nZVI, yet this strongly depends on the actual characteristics of the BC that is used (Wang et al., 2019). Moreover, the synthesis of the nZVI-BC composite is cost-efficient if biomass is pre-treated with nZVI particles before pyrolysis and the thermal conversion is performed together (Trakal et al., 2019). Experiments using different types of BC composites are currently being performed in our laboratories.

2.4 Conclusion

Although the efficiency of commercial products such as BC and nZVI for remediation is well documented, their behaviour under changing soil conditions has been scarcely studied. Moreover, our results show that the combination of different methods and approaches (chemical analysis, solid phase analysis, geochemical modelling) is crucial in predicting the behaviour of metals in amended soils to avoid any misleading interpretations of contaminant immobilisation.

In general, BC-containing treatments were the most efficient with regards to metal stabilisation and pH conservation. Their immobilisation efficiency was more pronounced over time, showing a more stable response compared to the other amendments. In contrast, nZVI treatments were more rapid; showing short-term metal stabilisation in the soil. In this regard, a combination of these two amendments may ensure the functionality and applicability for both short-

or long-term soil remediation. Therefore, testing of nZVI composite materials or easily available modified nZVI products is strongly recommended.

Temporal changes imposed by constant watering and by an increase in soil water content provoked shifts in the pH values, which influenced metal availability, amendment functionality and mineral phase transformations. Based on the mineralogical analyses, the main stabilisation mechanisms were different for each of the target metals, i.e. sorption on Fe oxides for Zn, sorption on Mn oxides for Pb, and sorption on Al oxides for Cd. It was thus assumed that sorbent application may enhance weathering and the transformations of the primary Fe/Mn/Al phases present in the soil, followed by the immobilisation of risk metals through sorption on the newly formed (hydr)oxides. The presence of various scavenging mechanisms may further ensure efficient stabilisation of metals under a wide range of environmental conditions (e.g. soil moisture content).

2.5 Supplementary Information

Materials and Methods
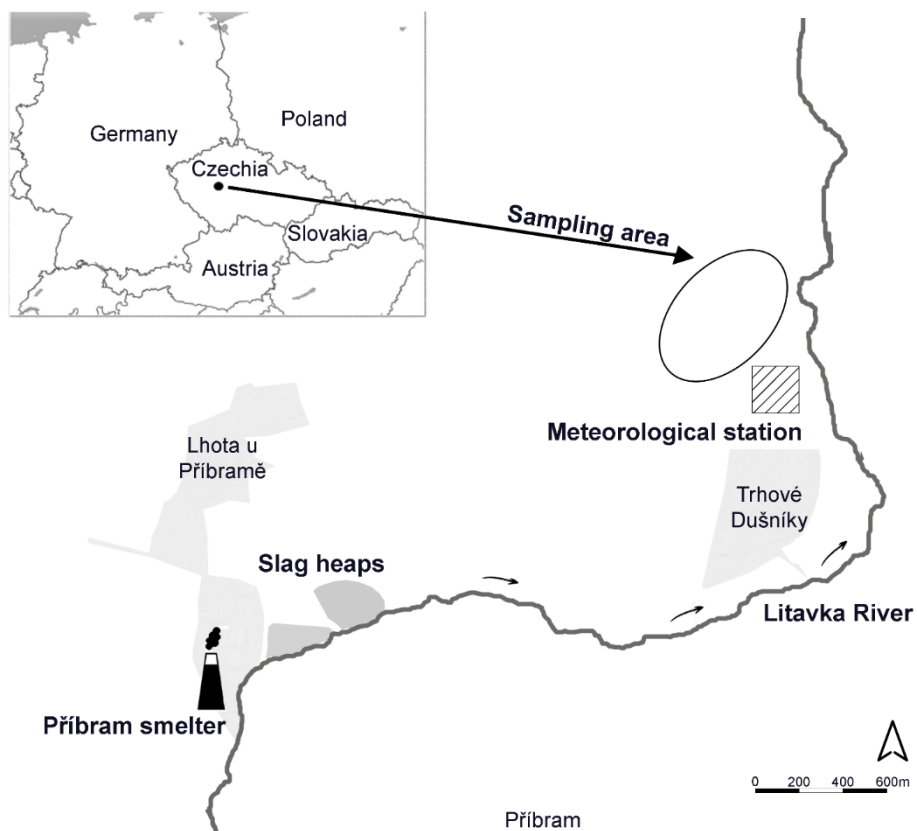
Figure S2.1: *Map of the studied area indicating the main sources of pollution*.
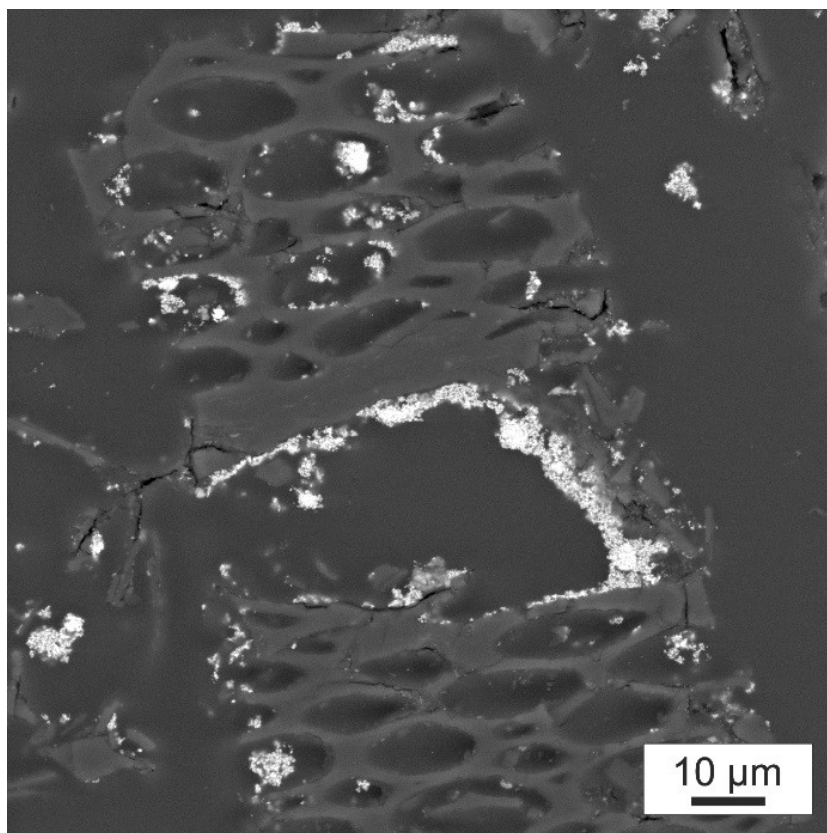
Figure S2.2: *Picture of biochar particle combined with nano zero-valent iron (BC+nZVI) obtained from SEM/EDS analysis*

Results and discussion
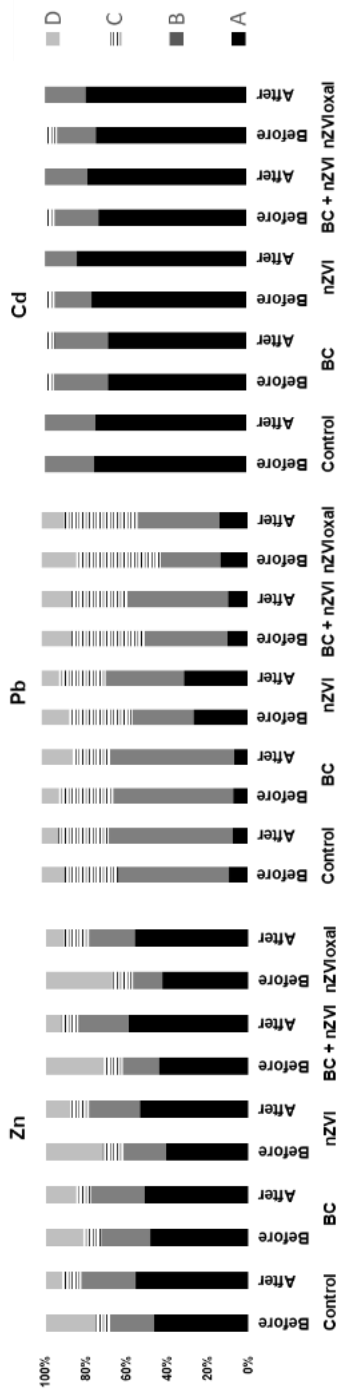
Figure S2.3 *Results from the sequential extraction (according to Rauret et al., 2000) for the incubated soil before and after the pot experiment. A: exchangeable metal fraction, B: fraction bound to oxides, C: fraction bound to organic matter, D: residual fraction*

69

Table S2.1 Speciation of target risk metals, Mn, and Fe in the soil pore water as calculated by the PHREEQC-3 geochemical code (part1/2).

Speciation	10 days					50 days					60 days				
	nZVI$_{oxal.}$	BC+nZVI	nZVI	BC	Control	nZVI$_{oxal.}$	BC+nZVI	nZVI	BC	Control	nZVI$_{oxal.}$	BC+nZVI	nZVI	BC	Control
Cd^{2+}	88%	85%	87%	87%	83%	95%	93%	93%	94%	93%	92%	94%	94%	94%	94%
$CdSO_4^0$	4%	4%	2%	4%	6%	0%	1%	0%	1%	0%	0%	1%	1%	1%	1%
$CdNO_3^+$	5%	9%	9%	6%	6%	5%	5%	6%	5%	5%	7%	4%	5%	4%	4%
$CdCl^+$	3%	2%	2%	2%	4%	0%	1%	1%	1%	1%	0%	1%	1%	1%	1%
Fe^{2+}	30%	24%	41%	7%	9%	–	–	–	–	–	–	–	–	–	–
$Fe(OH)_2^+$	70%	76%	59%	93%	91%	–	–	–	–	–	–	–	–	–	–
Mn^{2+}	94%	93%	94%	93%	92%	98%	97%	97%	97%	97%	97%	97%	97%	97%	98%
$MnSO_4^0$	3%	2%	1%	3%	4%	0%	1%	0%	1%	0%	0%	1%	0%	1%	0%
$MnNO_3^+$	2%	4%	4%	3%	3%	2%	2%	2%	2%	2%	3%	2%	2%	2%	2%

70

Table S2.1 Speciation of target risk metals, Mn, and Fe in the soil pore water as calculated by the PHREEQC-3 geochemical code (part2/2).

Speciation	60 days					50 days					10 days				
	nZVIoxal.	BC+nZVI	nZVI	BC	Control	nZVIoxal.	BC+nZVI	nZVI	BC	Control	nZVIoxal.	BC+nZVI	nZVI	BC	Control
$MnHCO_3^+$	0%	0%	0%	1%	0%	0%	0%	0%	0%	0%	1%	1%	1%	1%	1%
Pb^{2+}	65%	67%	67%	67%	76%	78%	73%	74%	76%	75%	48%	47%	53%	50%	44%
$PbHCO_3^+$	12%	15%	14%	18%	7%	4%	7%	4%	5%	4%	32%	23%	18%	27%	33%
$PbNO_3^+$	22%	15%	17%	12%	16%	18%	19%	22%	17%	20%	13%	24%	26%	17%	14%
$PbSO_4^0$	1%	2%	1%	2%	1%	0%	2%	1%	2%	1%	5%	5%	3%	5%	7%
$PbCO_3^0$	0%	1%	1%	1%	0%	0%	0%	0%	0%	0%	1%	1%	0%	1%	1%
Zn^{2+}	94%	94%	94%	95%	96%	96%	95%	95%	95%	95%	89%	87%	89%	89%	86%
$ZnSO_4^0$	0%	1%	1%	1%	1%	0%	1%	0%	1%	0%	4%	4%	2%	4%	6%
$ZnHCO_3^+$	1%	1%	1%	1%	0%	0%	0%	0%	0%	0%	3%	2%	1%	2%	3%
$ZnNO_3^+$	5%	3%	4%	3%	3%	4%	4%	5%	4%	4%	4%	8%	7%	5%	5%

Table S2.2 *Saturation indices of selected phases found in the pore water solution as calculated by the PHREEQC-3 geochemical code.*

Phase	Formula	10 days					50 days					60 days				
		$nZVI_{oxal}$	$BC{+}nZVI$	$nZVI$	BC	Control	$nZVI_{oxal}$	$BC{+}nZVI$	$nZVI$	BC	Control	$nZVI_{oxal}$	$BC{+}nZVI$	$nZVI$	BC	Control
Ferrihydrite		**1.36**	**0.62**	**0.05**	**0.87**	**1.07**[a]	–	–	–	–	–	–	–	–	–	–
Goethite	$\alpha\text{-}FeOOH$	**4.06**	**3.32**	**2.75**	**3.57**	**3.77**	–	–	–	–	–	–	–	–	–	–
Manganite	$MnOOH$	-4.71	-4.89	-5.16	-4.44	-4.40	-4.46	-4.38	-4.64	-4.72	-5.17	-4.60	-5.16	-4.78	-5.35	-5.23
Rhodochrosite	$MnCO_3$	-0.30	-0.78	-0.84	-0.87	-0.54	-1.45	-1.64	-1.72	-2.13	-1.92	-0.82	-1.21	-0.83	-1.55	-1.69
Otavite	$CdCO_3$	-1.24	-1.48	-1.69	-1.48	-1.34	-2.30	-2.27	-2.54	-2.50	-2.62	-1.72	-1.80	-1.65	-1.83	-2.40
Cerussite	$PbCO_3$	-1.64	-1.69	-1.94	-1.83	-1.31	-1.60	-2.49	-2.73	-2.80	-2.68	-1.68	-1.95	-1.71	-1.72	-2.23
Smithsonite	$ZnCO_3$	-1.11	-1.33	-1.55	-1.33	-1.17	-2.19	-2.10	-2.40	-2.33	-2.59	-1.59	-1.63	-1.51	-1.65	-2.22
	$ZnCO_3{\cdot}1H_2O$	-0.85	-1.07	-1.29	-1.07	-0.91	-1.93	-1.84	-2.14	-2.07	-2.33	-1.33	-1.37	-1.25	-1.39	-1.96

[a] Saturation indices in the interval <-1.5;1.5> are highlighted with grey background, values >0 are given in bold.

Table S2.3 Speciation of target metals available in the H2O extracts as calculated by the PHREEQC-3 geochemical code.

After the pot experiment					Before the pot experiment					Speciation
nZVI$_{oxal}$	BC+nZVI	nZVI	BC	Control	nZVI$_{oxal}$	BC+nZVI	nZVI	BC	Control	
99%	99%	99%	0%	99%	95%	95%	95%	94%	95%	Cd^{2+}
1%	1%	1%	0%	1%	5%	5%	5%	6%	5%	$CdSO_4^0$
9%	2%	3%	2%	4%	1%	0%	0%	0%	1%	Fe^{2+}
91%	98%	97%	98%	96%	99%	100%	100%	100%	99%	$Fe(OH)_2^+$
98%	97%	98%	98%	98%	93%	94%	93%	94%	94%	Mn^{2+}
1%	1%	1%	1%	1%	4%	4%	4%	4%	4%	$MnSO_4^0$
0%	0%	0%	0%	0%	1%	1%	0%	1%	0%	$MnNO_3^+$
1%	2%	2%	1%	1%	2%	2%	3%	2%	2%	$MnHCO_3^+$
63%	55%	58%	64%	72%	45%	49%	35%	51%	52%	Pb^{2+}
33%	39%	38%	31%	26%	39%	39%	48%	36%	36%	$PbHCO_3^+$
1%	1%	1%	1%	1%	5%	6%	4%	6%	6%	$PbSO_4^0$
3%	5%	3%	3%	2%	11%	6%	13%	7%	6%	$PbCO_3$
97%	96%	96%	97%	97%	91%	91%	90%	91%	92%	Zn^{2+}
1%	1%	1%	1%	1%	5%	5%	4%	5%	5%	$ZnSO_4^0$
2%	3%	3%	2%	1%	3%	3%	5%	3%	3%	$ZnHCO_3^+$
1%	0%	0%	0%	0%	1%	1%	1%	1%	1%	$ZnNO_3^+$

Table S2.4 *Saturation indices of selected phases found in the water extracts as calculated by the PHREEQC-3 geochemical code.*

		Before the pot experiment					After the pot experiment				
	Formula	Control	BC	nZVI	BC+nZVI	$nZVI_{oxal}$	Control	BC	nZVI	BC+nZVI	$nZVI_{oxal}$
Al(OH)₃	$Al(OH)_3$	**-0.05**[a]	**0.26**	**0.46**	**0.13**	-0.02	**0.48**	**0.85**	**0.29**	**0.41**	**0.12**
Ferrihydrite		**3.00**	**3.03**	**3.40**	**2.95**	**3.18**	**2.90**	**3.14**	**2.79**	**2.88**	**2.63**
Hydronium-jarosite	$(H_3O)Fe^{3+}_3(SO_4)_2(OH)_6$	-0.19	-0.34	**0.03**	-0.16	-0.48	-0.75	-0.61	-1.61	-1.58	-1.82
Natrojarosite	$NaFe_3(SO_4)_2(OH)_6$	**0.00**	**0.02**	**0.49**	**0.00**	-0.16	-0.80	-0.36	-1.60	-1.34	-1.81
Rhodochrosite	$MnCO_3$	-1.44	-1.54	-0.91	-1.47	-1.14	-1.58	-1.83	-1.18	-1.39	-1.13
Otavite	$CdCO_3$	-2.04	-1.96	-1.67	-2.02	-1.90	-2.30	–	-1.99	-2.32	-2.07
Cerussite	$PbCO_3$	-0.22	-0.23	**0.24**	-0.29	-0.05	-0.59	-0.30	-0.49	-0.37	-0.68
Smithsonite	$ZnCO_3$	-1.94	-1.90	-1.48	-1.93	-1.82	-2.14	-2.06	-1.91	-1.83	-1.98

[a] Saturation indices in the interval <-1.5;1.5> are highlighted with grey background, values >0 are given in bold.
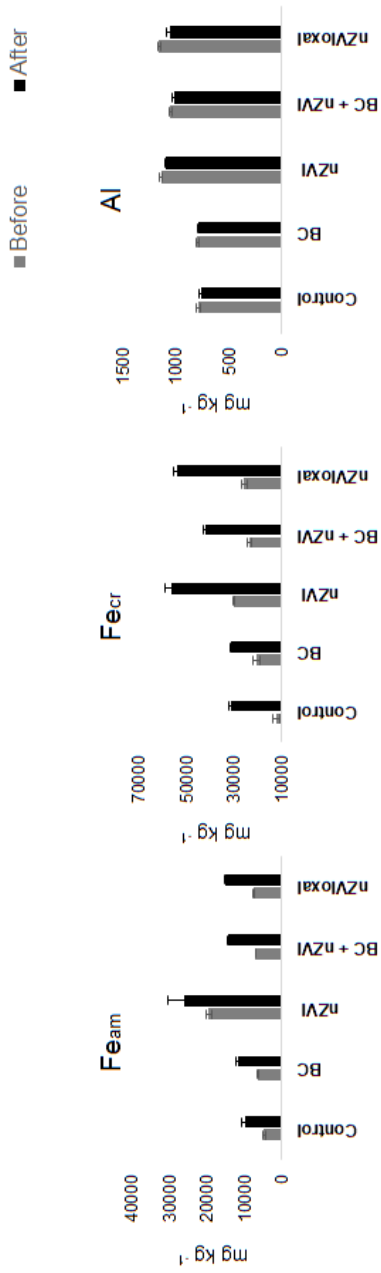
Figure S2.4 *Dissolved Fe (indicating the presence of amorphous and crystalline iron oxides/hydroxides) and Al (indicating the presence of aluminium oxides/hydroxides) resulting from the ISO 12782 (2012) extractions.*

Chapter III

Revealing the long-term behaviour of nZVI and biochar in metal(loid)-contaminated soil: focus on Fe transformations

Aikaterini Mitzia, Martina Vítková, Gildas Ratié, Rostislav Chotěborský, Delphine Vantelon, Alexander Neaman, Michael Komárek

Content

Abstract

The long-term behaviour of stabilising amendments for soil remediation is rarely being tested. Therefore, we conducted time-dependent experiments using contaminated soil from a post-mining area. The soil was individually incubated for 1, 3, 12 and 15 months with 1) biochar (BC), 2) nano zero-valent iron (nZVI) and 3) a composite of nZVI and BC (nZVI-BC). Two experimental designs were realised: 1) mixing of the soil with the amendments and 2) applying the amendments as a layer between the soil and silica sand. With this dual approach, both the immobilisation efficiency and the solid phase transformations of the amendments were investigated under the effect of time. Solid-state (SEM/EDS, XAS, XRD) and liquid phase (pore water sampling, soil extractions) analyses were employed for a holistic assessment of the amendments. The three tested amendments demonstrated different efficiencies for metal(loid) immobilisation in this soil. Biochar and nZVI-BC were mostly efficient for long-term immobilisation, especially for Zn and Cd, while the efficiency of nZVI was instant but rather short-term and preferably towards Pb and As. The oxidation of nZVI was not directly proportional to time, and the nZVI products, such as lepidocrocite, ferrihydrite, and magnetite, were identified in the same proportions regardless of Fe^0 oxidation. Implications of natural attenuation were also noticed in the control soil. However, enhancement of the contaminated soil with amendments is still recommended since the important metal(loid) scavengers (Fe and/or Mn oxides) in the soil occurred at least 2 times more often after the amendment application.

Environmental significance statement

The efficiency of amendments for immobilisation of metal(loid)s in soil may change over time, resulting in release of contaminants, and recent studies have focused mainly on short-term laboratory experiments. Therefore, the long-term behaviour of soil amendments needs to be assessed, especially when using nano zero-valent iron (nZVI), which inevitably oxidises and transforms to various Fe phases. We found that the immobilisation of Zn, Pb, Cd and As fluctuated over time. The transformation of nZVI (i.e. oxidation) was not directly proportional with time. Our results provide a wider view of the amendment performance in reasonable time steps and environmental conditions. This study is useful for understanding the long-term behaviour of amendments and their actual perspectives for soil remediation.

3.1 Introduction

Chemical stabilisation or immobilisation is a widespread remediation method in which the amendments immobilise inorganic contaminants, e.g. metals and metalloids, in soils (Derakhshan Nejad et al., 2018). It is therefore necessary to study the long-term behaviour of such amendments and ensure not only their remediation efficiency but also their environmental safety (Tauqeer et al., 2021). Currently, nano zero-valent iron (nZVI) and biochar (BC) are the most common materials used for metal(loid) immobilisation in water and soil (Lefevre et al., 2016; Almatrafi, et al., 2022; Wang, et al., 2022; Y. Wang et al., 2020). However, a considerable number of studies have addressed the potential toxic effects of nZVI on living organisms (Anza et al., 2019; Castaño et al., 2021; Tang et al., 2021; Vanzetto & Thomé, 2022; Xie et al., 2017), while some researchers have recently focused on the possible negative impacts of BC (e.g. desorption of potentially toxic elements from BC) (Godlewska et al., 2021; Sun et al., 2021; Taraqqi-A-Kamal et al., 2021). Due to the tendency of nZVI to agglomerate, modifications (including nZVI supported by BC) have been proposed (Ken & Sinha, 2020; Trakal et al., 2016a; S. Wang et al., 2019b) to mitigate this tendency and enhance the product's remediation efficiency. Most importantly, the long-term behaviour of soil amendments is rarely studied, although there may be release of inorganic contaminants previously retained by BC (J. Wang et al., 2021a) and nZVI (Calderon & Fullana, 2015; Danila et al., 2020). In addition, studying Fe solid speciation after nZVI and nZVI composites application is of key importance in terms of immobilisation efficiency because the large range of Fe oxyhydroxides that can be produced (depending on chemical conditions) (Bae et al., 2018) may influence and change the availability and partitioning of inorganic contaminants (Shi et al., 2021).

To solve the gap in the knowledge concerning the behaviour of nZVI, BC and nZVI-BC in the long term, we performed experiments of more than 1 year duration using an interdisciplinary approach. We combined X-ray diffraction (XRD) to determine the existing crystalline Fe phases and X-ray absorption near edge structure (XANES) to quantify the solid speciation of Fe. Scanning electron microscopy was used to observe the potential visual changes of the amendments and to better understand the metal(loid) distribution and affinity to mineral phases. Finally, the chemical composition of the soil and solution

enabled us to understand the metal(loid) immobilisation/release dynamics. The objective of this study was to investigate both the metal(loid) immobilisation efficiency of BC, nZVI and nZVI-BC and the time-induced changes in the solid and liquid phases. Our main hypotheses were that 1) a longer incubation time results in more efficient metal(loid) immobilisation and 2) a longer incubation time increases the transformation rate of nZVI through the oxidation process and the formation of secondary Fe (oxyhydr)oxides. This study provides information about the long-term behaviour of amendments, especially nZVI, and highlights the importance of amendment-supported natural attenuation.

3.2 Materials and Methods

3.2.1 Studied soil and amendments

The soil used in the present study originated from the alluvium of the Litavka River (Příbram District, Czech Republic). Detailed information about the contaminated area has been extensively reported (Ettler et al., 2001; Mitzia et al., 2020; Vaněk et al., 2008). The soil is sandy and heavily contaminated by Zn, Pb, Cd and As due to former long-lasting mining and smelting activities (Mitzia et al., 2020; Vítková et al., 2017, 2018). Concentrations of specific elements and other basic characteristics of the studied soil can be found in Table 3.1. The soil was collected from 0 to 25 cm, air-dried and sieved (< 2 mm) before further manipulation.

Three different soil amendments were applied (Table 3.1): 1) an air-stable powder product of nZVI (NANOFER STAR, Nano Iron, Ltd., Czech Republic), 2) a woody BC (a mixture of pine and spruce wood saw-dust pyrolysed at 700 °C), and 3) a composite of nZVI-BC containing 33 wt.% Fe and 67 wt.% C. The nZVI-BC composite was prepared by pyrolysis (700 °C) of mixed pine and spruce saw-dust biochar pre-treated with an Fe precursor (haematite powder, α-Fe_2O_3) (Semerád et al., 2021). Both BC and nZVI-BC were purchased from LAC, Ltd., Czech Republic. The activation of the used amendments was necessary before their application to soil. For details about the activation procedure see the Supplementary Information (SI).

.

Table 3.1 *Characteristics of the studied soil and amendments (tested in triplicate).*

Soil samples			Sorbents		
pH_{H2O}[a]	5.98				
pH_{KCl}[a]	5.27		**nZVI**	**BC**	**nZVI-BC**
Element concentrations[b] (mg kg^{-1})		pH_{H2O}[a]	6.86	10.0	11.3
As	385±11	**CEC[c]**			
Cd	31.6±1	**(cmol kg^{-1})**	2.91	4.63	14.5
Fe	32974±629				
Mn	4695±99				
Pb	3854±121	**S$_{BET}$[d]**			
Zn	3082±83	**(m^2 g^{-1})**	25	351	203

[a] According to ISO 10390 (2005)[29]

[b] According to EPA 3051A (2007)[30].

[c] Cation exchange capacity [31].

[d] Specific surface area (BET method).

3.2.2 Acid neutralisation capacity

To evaluate the potential for pH buffering of each amendment, the acid neutralisation capacity (ANC) was determined according to protocol EN 14997. The procedure was conducted for i) pure BC, nZVI and nZVI-BC and ii) bulk control soil to compare the ANC of amendments versus the ANC of the contaminated soil. A mass of 5 g in duplicate was placed in a 100 mL polyethylene (PE) bottle, and 45 mL of demineralised water was added to ensure the maximum solid-to-liquid ratio (S/L) ratio of 1 g/10 mL. The suspensions were continuously agitated. Solutions of HNO3 (14 M and 1 M) of analytical grade were used to manually decrease the pH value from the starting pH (i.e. natural pH of the material) to pH ≤4 according to the protocol.

3.2.3 Pot experiment – experimental setup

The studied amendments were individually applied at a ratio of 2 wt.% to a total of 200 g of soil. Two different experimental designs were realised: 1) the mixed design and 2) the layered design (Fig. 3.1).

In the mixed design, 2 wt.% of each amendment was individually mixed with the soil and placed in a plastic pot (Fig.3.1A). This design was intended to simulate a real-world scenario where intensive and continuous soil–sorbent interactions occur.

The layered design was realised by embodying a reactive barrier of the amendment directly into the soil without any separating media. As the sorbent represented an even layer between the contaminated soil (on the top) and silica sand (at the bottom), additional checking of any potential leaching through the sorbent layer was feasible by analysing the bottom-placed sand layer (Fig. 3.1B). A mass of 100 g of pure silica sand (ST 03/08 PH50, Sklopísek Střeleč, JSC, Czech Republic; 0.55-mm grain size, pH 7.2) was used in this case. The layered design aimed to elucidate the time-dependent mineral transformations of the solid-state by investigating the sorbent particles separately from the soil. In addition, we aimed to see the efficiency of a layer as a real reactive barrier that can potentially be removed from the soil. Therefore, another objective of using two designs was to define whether mixing the amendments with soil or applying them as a layer is more efficient for metal(loid) immobilisation.

In both designs, four incubation time periods existed: 1, 3, 12 and 15 months. A pot with unamended soil (control) was included in each group. During the incubation time, the pots were regularly watered to maintain 70% of the soil's water holding capacity (WHC). A common gardening geotextile was placed on the soil surface in every pot to protect it from dust deposits, prevent rapid water evaporation and ensure even soil moisture conditions during watering. In addition, for the pots of the mixed design of 3- and 15-month incubation, a rhizon sampler (Rhizosphere Research Products, Netherlands) was installed in the soil to collect pore water (Fig. 3.1A).
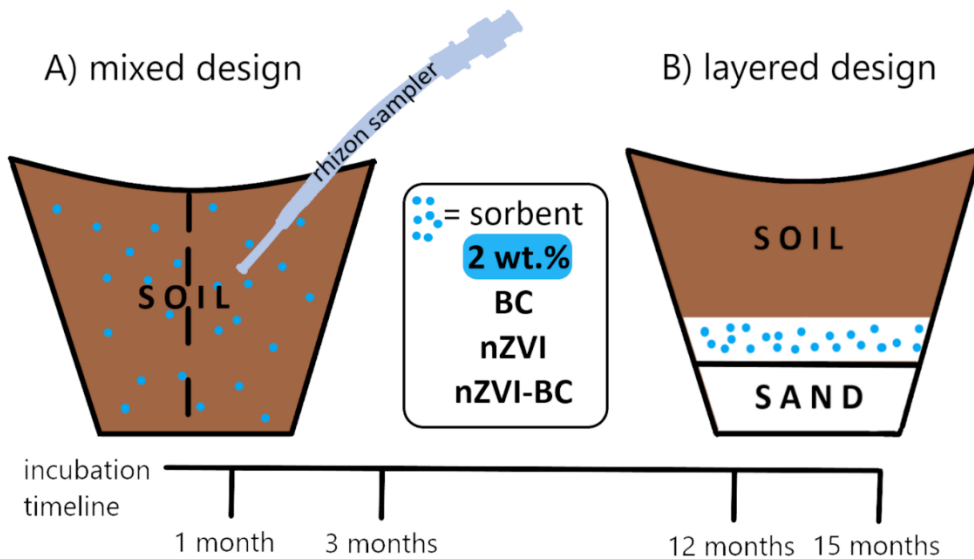
Figure 3.1: *Setup of the pot experiment including the two designs with the same incubation time steps and soil amendments.*

3.2.4 Pore water sampling

At the end of the 3- and 15-month incubation periods, pore water was collected using the rhizons from the mixed soil variants, and pH, Eh and conductivity were immediately measured. An aliquot was prepared for subsequent analyses (i.e. ICP–OES and/or ICP–MS, ion chromatography and carbon content analyses). For detailed information about the calculation of the concentrations see later in the text and in the SI. After pore water sampling, the pots were watered again and incubated for one more week to be ready for the wet soil extraction.

3.2.5 Wet soil extraction

Soil samples (in triplicate) from every pot of the mixed soil variant were subjected to single extractions using demineralised water according to Quevauviller (1998). The soil was sampled and extracted in a wet state (i.e. at 70% WHC) without prior drying to better depict the available element concentrations that correspond to real (i.e. wet) conditions. It has been reported that drying and rewetting of soils can significantly affect C and N fluxes (Unger et al., 2010), microbial activity (Birch, 1958) and available element

concentrations (Paranaíba et al., 2020). To maintain a specific S/L for the extraction, the water volume that was already contained in the wet soil was included in the total liquid amount (i.e. amount of reagent + water).

The amount of water in the soil samples was individually calculated based on the exact wet mass of each sample and the known WHC%. Therefore, demineralised water was added to the soil samples at a S/L ratio of 1 g/10 mL, including the soil water, and agitated for 3 h. After this, the sample suspensions were centrifuged at 9000 rpm for 10 minutes, and the supernatant was filtered using 0.45 µm nitrocellulose syringe filters. Immediately after filtration, the pH, Eh and conductivity were measured, and an aliquot was prepared for subsequent analyses.

3.2.6 Total digestion of sand

Samples of sand from the bottom of each layered pot were carefully separated from the sorbent layer. The sand samples were subjected to total digestion according to the EPA 3051a method (2007). In brief, 0.25 g of silica sand reacted with a mixture of 9 mL of HNO_3, 3 mL of HCl and 1 mL of HF concentrated acids for approximately 30 minutes before being placed in a microwave unit (Multiwave PRO microwave reaction system SOLV, Anton Paar, Germany). After microwave digestion, the samples were cooled for 30 minutes and then poured into 60 mL Savillex digestion vessels. The vessels were placed on a hot plate for approximately 3 h at 150 °C for complete evaporation. The residues were then dissolved in 20 mL of 2% HNO_3, filtered at 0.45 µm, and subjected to further analyses. All of the samples were tested in triplicate with procedural blanks.

3.2.7 Instrumental analytical methods – solid-state analyses

Scanning electron microscopy (SEM) coupled with energy dispersive X-ray spectroscopy (EDS)

Scanning electron microscopy was applied to visualise the incubated amendment particles and to determine the elemental changes after the soil–amendment interactions. A TESCAN VEGA3XMU scanning electron microscope (TESCAN Ltd., Czech Republic) equipped with a Bruker QUANTAX200 EDS unit was used. Both the samples of mixed soil-sorbent and samples of the sorbent layer were prepared for microscopic investigations, i.e. placed on an adhesive

carbon sticker on SEM pins and were carbon-coated right before the analysis. The voltage was set to 15 kV and occasionally to 20 kV. To evaluate the long-term effects of the incubation with the tested amendments in detail, the soil samples from the 15-month incubation period were subjected to a full-frame SEM using a TESCAN MIRA3 GMU microscope (TESCAN Ltd., Czech Republic) with an Oxford Aztec X-MaxN 50 instruments EDS unit (see the details in the SI).

XRD analysis

For the determination of the crystallinity of the used amendments and their potential mineral transformations or secondary mineral formations during the incubation time, samples from the sorbent layer were collected and analysed using XRD. An XRD unit (D2 PHASER, Bruker, Germany) equipped with a LYNXEYE XE-T detector (CuKα radiation, 10 kV, 30 mA) was used. In the case of nZVI samples, a step of $0.02°$ s^{-1} in the 2θ range of $3°-90°$ was used. For the structural determination of nZVI-BC samples, the measuring step was set to $0.08°$ s^{-1} in the 2θ range of $3°-90°$. The amorphous nature of BC samples was checked using a step of $0.1°$ s^{-1} in the 2θ range of $3°-90°$. For the identification of existing phases, the DIFRAC. EVA V4 software and the ICDD PDF-2 database (2018) were used.

X-ray absorption spectroscopy (XAS)

The Fe solid speciation was determined using the Fe K-edge X-ray Absorption Near Edge Structure (XANES) spectra collected on the LUCIA beamline in the SOLEIL synchrotron facility (Paris, France) (Vantelon et al., 2016). The selection of reference compounds (i.e. Fe-bearing phases) was based on XRD results performed on the soil and layer samples and on expected Fe (oxyhydr)oxides during nZVI transformation (S. Wu et al., 2019). Therefore, a set of Fe (oxyhydr)oxides, such as ferrihydrite, lepidocrocite, goethite and magnetite, and Fe-phyllosilicates, such as muscovite and montmorillonite, were used as reference compounds. Samples and reference materials were prepared as pellets of finely ground and homogenised powder with cellulose. Additionally, the original Fe materials, i.e. nZVI and nZVI-BC amendments, were activated in slurry form just before their measurement. They were also used as references. The data were collected under primary vacuum (10^{-2} mbar) using a Si (311) double-crystal monochromator with a $2*$ $2mm^2$ beam size. An Fe metallic foil was used for the calibration of the monochromator by setting

the first inflexion point of XANES to 7112 eV. Spectra were collected in transmission (using a Si diode) and fluorescence modes (using a Bruker SDD mono-element 60 mm^2) over an energy range of 7050 to 7300 eV.

3.2.8 Instrumental analytical methods – liquid state analyses

The concentrations of major and trace elements in pore water, extracts and digests were determined using an ICP OES unit (Agilent 730, Agilent Technologies, USA) and ICP MS (iCAP Q Thermo Fischer Scientific). Dissolved organic carbon contents (DOC) in the soil extracts and pore water were determined by a carbon analyser (TOC-L CPH, Shimadzu, Japan). The concentrations of anions (F$^-$, Cl$^-$, NO$_3^-$, PO$_4^{3-}$, SO$_4^{2-}$) in the water extracts and pore water were determined by ionic chromatography (Dionex ICS-5000+, Thermo Fischer Scientific).

3.2.9 Data treatment

For the statistical treatment of results, the software Statistica (version 13.4.0.14, Tibco Software Inc.) was used. In order to investigate the significance of the differences among the soil treatments, the nature of the data was first determined followed by adequate tests such as ANOVA (for parametric data) or Kruskal–Wallis test (for non-parametric data). Afterwards, t-test and Mann–Whitney U test (adjusted with Bonferroni correction) were used, respectively, to find the significant changes between different time-steps of the same soil treatment. The level of significance was set to $p<0.05$ for all these tests. To explore the potential correlations between different factors, the Pearson coefficient was used with a significance level of $p<0.05$.

The Fe XANES spectra were extracted and treated using ATHENA software (Ravel & Newville, 2005). All the spectra (*n*=3) from each sample were merged and normalised by fitting the pre-edge with a linear function and the post-edge with a quadratic polynomial function. In addition, for the samples of control soil only, the average of the samples (*n*=10) was performed and used as "control soil" due to the significant similarity between the samples over time. The relative Fe solid speciation was obtained by linear combination fits (LCFs) using model compounds over the XANES spectra ranging from 7108 to 7158 eV without forcing the weights to sum up to 1. The quality of the fit was

characterised using the R factor. The accuracy of this LCF procedure was calculated to be±10%.

To supplement the analytical results, the PHREEQC-3 geochemical code by Parkhurst & Appelo (2013) was used which enabled projections of metal speciation and solubility-controlling phases in the solutions of water extracts and pore water. The results were calculated using the T_H database. More information can be found in the SI.

3.3 Results and discussion

3.3.1 Investigations by SEM/EDS

Samples from every time step of 1) the control soil, 2) the soil mixed with BC, nZVI and nZVI-BC, 2) the soil-sorbent interface from the layered pot design and 4) the separated sorbent layer from the layered pot design were investigated. The images from the control and the mixed variant were intended to visualise the risk element distribution and accumulation in the studied soil, while the images from the soil-sorbent interface and the sorbent layer were mostly indicators of the time-induced changes of the used amendments. In particular, solid phase changes of the Fe-based treatments (in which Fe^0 oxidation was expected) were better visualised.

Control soil

In control samples, Fe and Mn oxides containing Zn and Pb were usually present as stand-alone particles in the soil matrix or covering other soil particles (Fig. S3.1). Zinc was mostly accumulated on Fe oxides, while Pb was preferably accumulated on Mn oxides (Fig. S3.1A). However, Fe oxides also contained Pb in many cases, or mixed Fe and Mn oxides containing both metals were detected (Fig. S3.1F). Cadmium and As were also observed accumulating on Fe and/or Mn oxides, although not as often as Zn and Pb because of the low concentrations. During the SEM/EDS analysis of the control soil, a mineral formation with the composition of sphalerite (ZnS) was detected and captured (Fig. S3.2). Sphalerite is considered one of the primary minerals containing Zn in this soil, while galena (PbS) represents the primary Pb mineral, both originating from former mining activities (Ettler et al., 2006).

BC-treated samples

Particles of BC were often detected inside the soil matrix (Figs. 3.2 and S3.3) in every incubation step. Numerous Fe and/or Mn oxides containing target metal(loid)s were found either covering the surface of soil or BC particles (Figs. 3.2B, D and S3.3F) or as stand-alone particles adhering to BC (Figs. 3.2A, C and S3.3I) or dispersed in the soil matrix (Figs. 3.2D and S3.3E, G, H). Zinc was mostly related to Fe-Mn oxides. Lead was preferably accumulated on Mn oxides or alternatively on Fe-Mn oxides and was rarely found exclusively on Fe oxides (Fig. 3.2C). Arsenic was rarely detected (due to the generally low concentrations), and if so, it was related to Fe-Mn oxides (Figs. 3.2B, C and S3.3H). Notably, the SEM/EDS analyses revealed the elemental distribution of the studied elements and suggested a potential binding mechanism of Pb and As in the BC-treated samples. In particular, Figs. 3.2B, C and S3.3H show that the presence of Mn-Fe oxides, often covering the BC particles, was crucial for the accumulation of Pb and As. The increased affinity of Pb (Covelo et al., 2007; Negra et al., 2005) and As (Hiller et al., 2021) to Mn oxides in soil have been reported earlier. Complexation with functional groups on the BC surface, cation-π interactions, precipitation with BC minerals and ion exchange have been suggested to be the main mechanisms of cationic metal immobilisation by BC(Gong et al., 2022; Soria et al., 2020). The accumulation of metal(loid)s on Mn oxides might be due to specific adsorption on the Mn oxide surfaces or the negative charges that prevail (Negra et al., 2005). The pH increase induced by the BC application in soil was reported to enhance cationic metal binding on Fe-Mn oxides due to less competition for H^+ (F. Yang et al., 2021a) but might provoke anionic metal(loid) release (Abdelhafez et al., 2014).
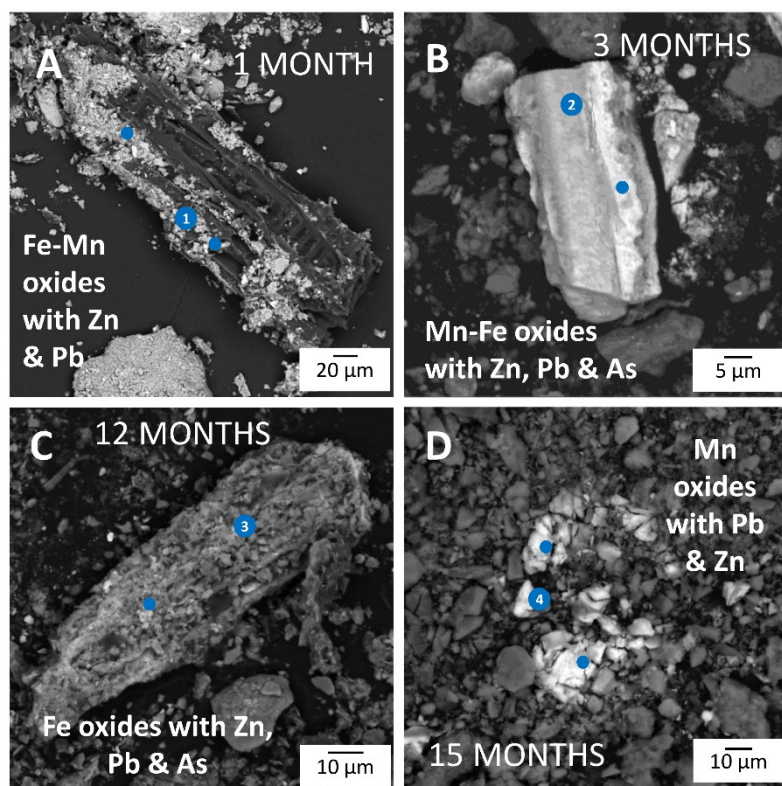
Figure 3.2: *Selected BSE images of BC-treated soil. The corresponding EDS spectra are indicated by number(s) (Fig. S3.7). Images A and D are taken from the mixed soil, images B and C are from the soil-BC interface. A) Fe-Mn oxides with up to 8.2 wt.% Zn and 9.1 wt.% Pb. B) Mn-Fe oxides (up to 1.7, 24 and 1 wt.% Zn, Pb and As, respectively). C) Fe oxides adhering to BC particle with up to 5 wt.% Zn, 10 wt.% Pb and 1.2 wt.% As. D) Fragments of Fe-Mn oxide particle (up to 3 and 12.5 wt. % Zn and Pb, respectively).*

nZVI-treated samples

Regardless of the experimental design (mixed or layered) in the nZVI-treated samples, the presence of Fe oxides was dominant either as nZVI particles forming aggregates (Figs. 3.3A, B, C, E and S3.4F, I), covering the surface of soil particles (Figs. 3.3D, E and S3.4G, H), or as stand-alone particles (Figs. 3.3A and S3.4H). As previously observed, Zn was preferably accumulating on Fe oxides and Pb on Mn-Fe oxides. Adsorption and co-precipitation of Zn and Pb on newly-formed Fe- and Al- (oxyhydr)oxides was previously confirmed for this soil amended with nZVI (Vítková et al., 2017). For metal(loid)s with E^0 more negative than nZVI (such as Zn) sorption and complexation are the most likely immobilisation mechanisms by nZVI while for those with much more positive

E^0 than nZVI (such as As) reduction and precipitation are more probable. For Pb, which has slightly more positive E^0 than nZVI, sorption, precipitation and partial chemical reduction are preferred mechanisms (Gil-Díaz et al., 2014; Vítková et al., 2017).

In the layered samples, nZVI remained intact in most of the cases, and visual signs of oxidation were noticed only at the soil-sorbent interface. According to the SEM images from the soil-sorbent interface (Figs. 3.3A and S3.4I) and the sorbent layer (Fig. S3.4F), the observed nZVI particles were bright (i.e. atomically heavier, containing >80 wt.% of Fe and < 20 wt. % O_2) and contained either none or <1 wt.% of the target contaminants, although in some cases, Fe oxides with higher amounts of Zn, Pb and As were detected in the soil-sorbent interface (Fig. S3.4H). Gil-Díaz et al. (2014) and Hiller et al. (2021) also reported the presence of nZVI aggregates with high contents of Fe and occasional Pb and Zn contents. In contrast, in the mixed samples, the nZVI particles observed after 12 and 15 months of incubation (Figs. 3.3C, D) were less bright and contained increased amounts of Zn (up to 4 wt.%), Pb (up to 9 wt.%) and As (up to 1.2 wt.%), indicating the scavenger role of the newly formed Fe oxides. In addition, various mixed Fe and/or Mn oxides containing variable amounts of Zn, Pb or As were commonly observed during SEM/EDS in the mixed samples (Figs. 3.3D, E, S3.4G). These findings imply that nZVI is getting oxidised over time (although the oxidation was found not to be directly proportional to time in the layered design (see earlier in text), and the oxidation products are responsible for risk element immobilisation (Hiller et al., 2021; Shi et al., 2021; S. Wu et al., 2019).
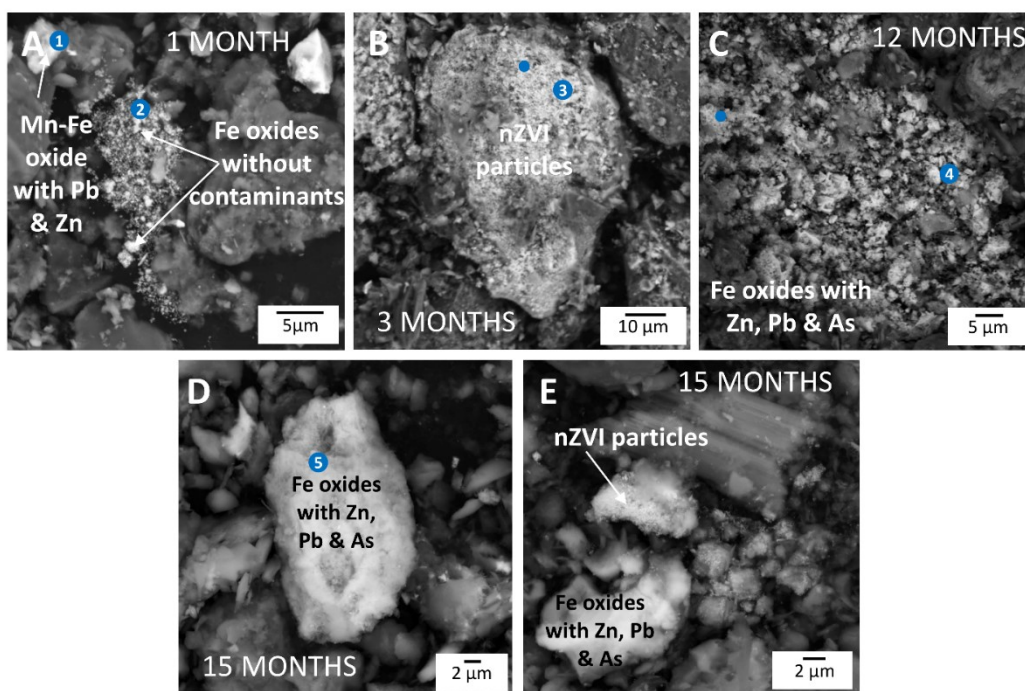
Figure 3.3: *SEM images of the nZVI treatment with numbered EDS spectra (Fig. S3.8). Image A is taken from the soil-nZVI interface and images B–E are from the mixed soil. A) Mn-Fe oxides (3.8 and 16.2 wt.% Zn and Pb, respectively) and nZVI particles with no contaminants. B) Particles of nZVI with < 1 wt. % risk metals). C) Oxidised nZVI particles with 4, 9 and 1.2 wt.% Zn, Pb and As, respectively. D) Fe oxides with 1.2, 4.6 and 1 wt.% Zn, Pb and As, respectively. E) Fe oxides (1.1 wt.% Zn, 4.2 wt.% Pb and 1 wt.% As) and nZVI agglomerate without contaminants.*

nZVI-BC-treated samples

In the mixed samples treated with nZVI-BC, Fe and Fe-Mn oxides with target contaminants were often detected. These oxides either covered the surface of soil particles (Figs. 3.4A and S3.5G) or existed as stand-alone particles (Figs. 3.4C, D) or on top of nZVI-BC particles (Figs. 3.4B, D, E and S3.5H, I). Elemental mapping of the mixed soil sample proved the presence of Fe on the surface of a BC particle after 15 months of incubation (Fig. S3.10). In the images from the sorbent layer and the soil–sorbent interface, the particles of BC were usually covered/filled partially (Figs. S3.5F, I) or completely (Fig. 3.4C) with nano Fe^0 particles. These nZVI particles were bright and contained no contaminants (discussed previously in this section). In other cases, soil components adhering to the nZVI-BC particles were observed and often included Fe oxides and risk elements (Figs. 3.4D, S3.5H). Stand-alone soil

particles with Zn and Pb were also detected (Fig. 3.4C). In total, similar to what we observed in the nZVI-treated samples, the nZVI particles in the nZVI-BC-mixed soil samples were less bright, more oxidised and usually contained higher concentrations of contaminants (Figs. 3.4B, D, E) than the particles observed in the sorbent layer (Fig. 3.4C) or the soil-sorbent interface. In addition, increased amounts of Zn (up to 19.7 wt.%) were detected in the mixed nZVI-BC samples compared to the other treatments (up to 10 wt.% in control, 8.2 wt.% in BC and 4 wt.% in nZVI), while Pb was found in concentrations up to 16.3 wt. % and As up to 0.6 wt.%. Increased efficiency in Pb immobilisation by a composite of nZVI-BC compared to original BC and nZVI products was reported by Mandal et al.(2020). Except for the mechanisms of complexation and electrostatic adsorption that are employed for immobilisation by pure BC, the amendment of BC with Fe can promote reduction, chelation and co-precipitation of risk elements (Gong et al., 2022). At last, based on the EDS results from the nZVI-BC- and nZVI-treated samples, we suggest that mixing the amendments with the soil is more efficient for metal(loid) immobilisation than applying them as a layer.
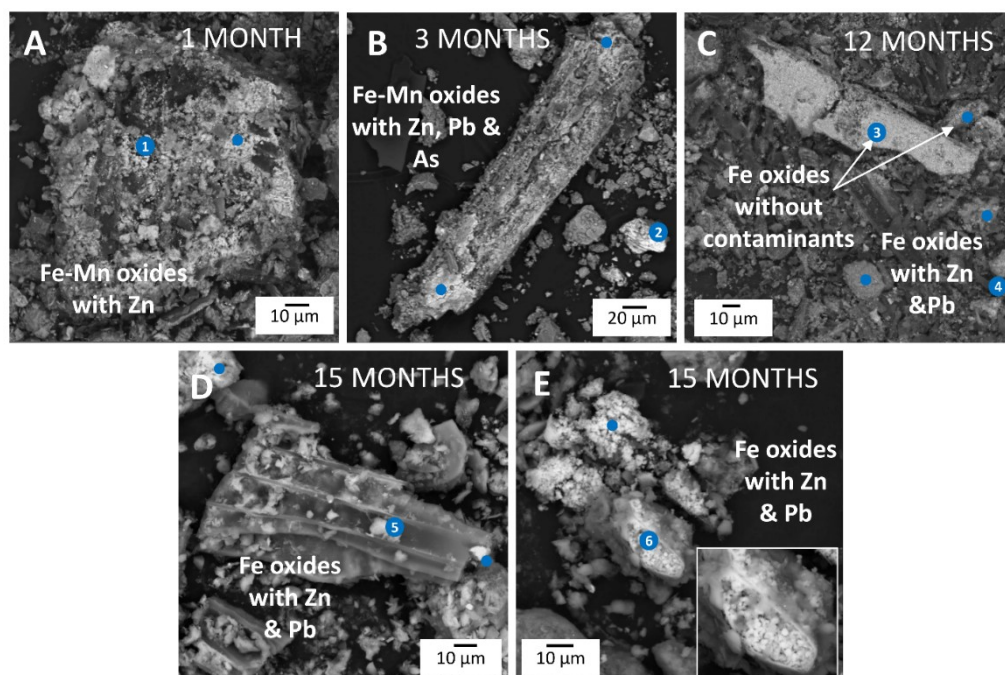
Figure 3.4: *SEM images from the nZVI-BC treatment with numbered EDS spectra (Fig. S3.9). Images A, B, D and E are captured from the mixed soil and image C is from the sorbent layer. A) Fe-Mn oxides with up to 11 wt.% Zn. B) Fe-Mn oxides with up to 2.4, 16.3 and 0.6 wt.% Zn, Pb and As, respectively. C) nZVI particles without contaminants and Fe oxides with up to 3.8 wt.% Zn and 1.7 wt.% Pb. D) Fe oxides with up to 1.1 wt. % Zn and 1.6 wt.% Pb on a BC particle. E) Fe oxides on BC with up to 1.8 wt.% Zn and 3.7 wt.% Pb. The inset presents a magnified image of the particle formation around point 6.*

The importance of Fe and Mn oxides for metal(loid) immobilisation in soil is known and well documented (Komárek et al., 2013) and was highlighted by the EDS results in this and our previous studies (Mitzia et al., 2020; Vítková et al., 2018). Based on the detailed SEM/EDS analysis of the 15-month incubated soil samples, we statistically verified that Zn is mostly accumulating on Fe oxides and Pb on Mn oxides (Figs. S3.11–14). In addition, the affinity of Pb to Mn phases was detected two times more often in the BC-treated soil samples (Fig. S3.12) than in the control soil (Fig. S3.11). This phenomenon can be explained by enhanced dissolution of existing Mn oxides as a response to BC-induced pH-Eh conditions and (co)precipitation of secondary Mn oxides with Pb. Reductive dissolution of Mn oxides in BC-amended soils under dynamic redox conditions was reported by Beiyuan et al. (2020). In the nZVI-treated samples (Fig. S3.13), the affinity of Zn to Fe phases and the combined affinity

of Zn and Pb to Fe phases were detected six times more often than in the control (Fig. S3.11). As expected, arsenic was mostly detected in combination with Fe phases in the control samples (Fig. S3.11). More importantly, the risk metal(loid) affinity to Fe phases was observed at least two times more often in the treated soil samples (especially nZVI) than in the control soil. Based on these observations and our previous study with the same soil in which the fraction of Zn, Pb and Cd bound to oxides increased after the application of similar amendments (Mitzia et al., 2020), it can be assumed that the immobilisation was mainly achieved by binding of metal(loid)s on Fe and/or Mn oxides. It is noteworthy, that even though the soil used in this study has a high Fe content (Table 3.1), the addition of nZVI significantly enhanced the accumulation of metal(loid)s on Fe phases. Therefore, studying the newly formed Fe phases of each incubation time step was critical to understand the contaminant immobilisation process.

3.3.2 Fe solid speciation using XAS

Based on XRD findings (Figs. S3.15A, B), ferrihydrite, lepidocrocite, goethite and magnetite were used along with the pure sorbents (i.e. NANOFER STAR and nZVI-BC composite) to quantify the Fe speciation in the sorbent layers.

The XANES Fe K-edge spectra of control soil presented a pre-edge with two maxima at 7109 eV and 7115 eV, a white line with a wide peak from 7132 to 7133 eV and a first broad oscillation centred at 7160 eV (Fig. 3.5A). The Fe K-edge spectra of the pure nZVI and pure nZVI-BC (Fig. 3.5B) presented similar spectra to metallic Fe (Schlegel et al., 2008). In comparison with Fig. 3.5A, the pre-edges of the pure sorbents were not distinguishable from the white line which expressed a maximum between 7130 and 7131 eV (Fig. 3.5B). The oscillations for both nZVI and nZVI-BC were broad with smaller amplitude than those of Fig. 3.5A. The detailed LCFs demonstrated that the Fe speciation of the Příbram soil is dominated by goethite, haematite, magnetite and Fe in phyllosilicates (Fig. 3.5C).

The XANES Fe K-edge spectra of the treated soil (mixed with nZVI and nZVI-BC) were similar to that of the control soil, with an error rate of ±10% (LCF accuracy). Indeed, bulk mixed soil expressed an Fe solid speciation similar to the control soil (from 90% to 98% Figs. 3.5C, D). Therefore, the addition of nZVI to the soil (i.e. 2 wt.%) did not significantly change the total bulk Fe

speciation in the mixed samples (Fig. 3.5). For this reason, the sorbent layer from the layered design was investigated by XAS measurements to observe the transformation products of nZVI and nZVI-BC without the native Fe components from the soil. (Fig. 3.6).
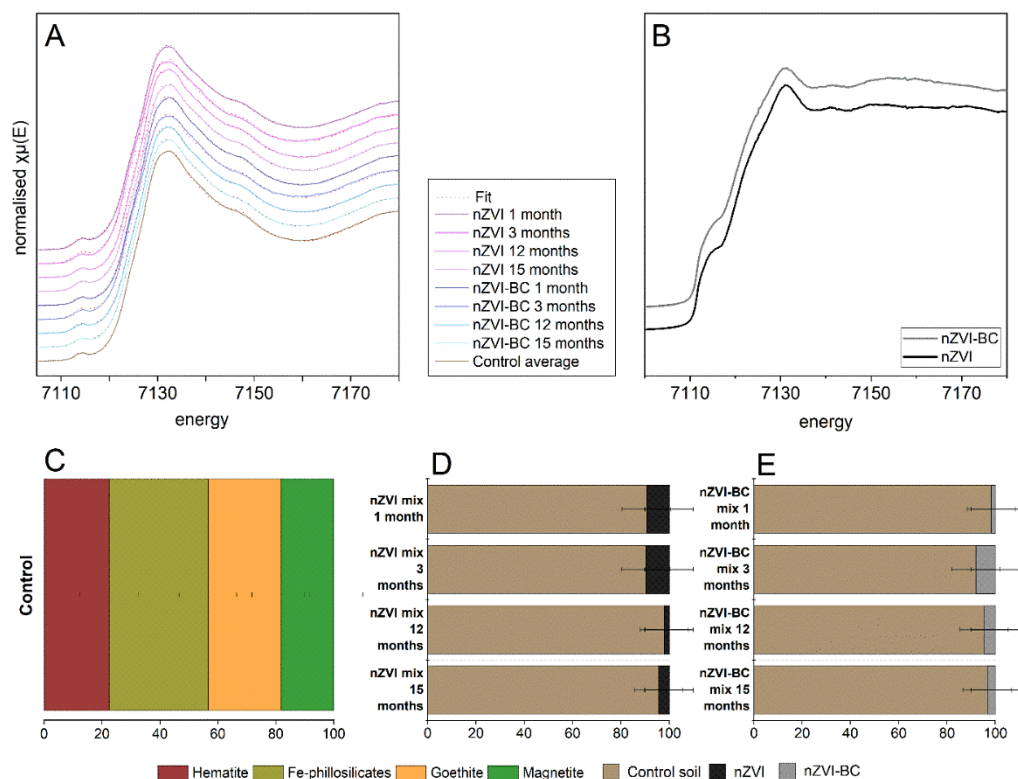
Figure 3.5: *Fe K-edge XANES spectra for A) all the mixed soil samples and B) for the original sorbents followed by the Fe speciation in C) control soil, D: nZVI-treated soil and E) nZVI-BC-treated soil for all the incubation time steps (expressed in % distribution, normalised to 100%).*

The nZVI and nZVI-BC sorbent layer samples showed different XANES Fe K-edge spectra over time exposure. For the nZVI samples, the spectra exhibited a pre-edge with a maximum from 7115 to 7116 eV, a white line from 7130-7132 eV and a first sharp oscillation point between 7159 and 7162 eV (Fig. 3.6A). For the nZVI-BC samples, the pre-edge of the Fe K-edge spectra had a maximum from 7114 to 7119 eV, the white line was between 7130 and 7132 eV, and the first broad oscillation was at 7160-7162 eV (Fig. 3.6B). Based on the comparison with the spectra of the original nZVI and nZVI-BC sorbent layers (Fig. 3.5B), the transformation process was observed with the

modification of the pre-edge between the samples of different time steps. The decrease of the amplitude of the pre-edge in this case, indicated a decrease in the contribution of Fe^0 in the total Fe speciation. This is interpreted as an oxidation process of the amendments leading to the formation of Fe (oxyhydr)oxides. In particular, the amplitude of the pre-edge of pure nZVI was larger than nZVI 15-month incubated sample > nZVI 1- and 12-month incubated sample and finally by nZVI 3-month incubated sample (Fig. 3.6A). The same sequence, from the least oxidised to the most, was observed in the pre-edge amplitude for nZVI-BC sorbent layer samples: pure nZVI-BC >15 months > 1 month > 12 months > 3 months (Fig. 3.6B).
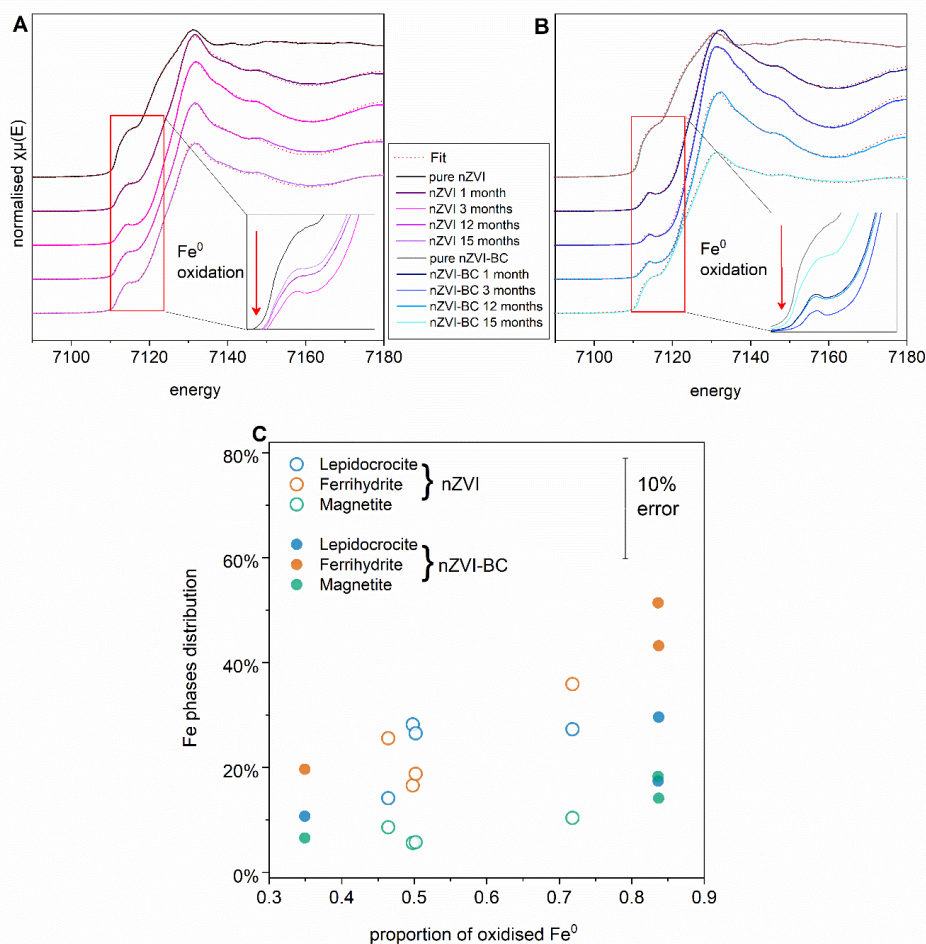
Figure 3.6: *Fe K-edge XANES spectra for the sorbent layers of A) nZVI and B) nZVI-BC from the different incubation time steps (expressed in % distribution, normalised to 100%). A zoom expressed the pre-edge of the spectra without increment to assist the comparison with each other. The arrow is showing the direction to the most oxidised sample. C) The distribution of Fe phases in relation to the proportion of oxidised Fe0. The proportion of oxidised Fe0 expresses the amount of the total Fe0 that was oxidised, i.e. transformed into new Fe (oxyhydr)oxides (Table S3.2).*

The original nZVI and nZVI-BC were still present in the sorbent layer samples in amounts up to 53% and 64%, respectively (Fig. S3.16). Surprisingly, the highest amount of nZVI and nZVI-BC corresponded to the longer incubation time, implying that the oxidation of Fe^0 was not directly proportional to time. The formation of agglomerates(Ken & Sinha, 2020) which was observed by SEM in the sorbent layers (Figs. 3.3, 3.4) has reduced the reactive surface area

of nZVI. This could explain the variability in the nZVI oxidation rate because the core of the agglomerates was not in contact with O_2, not able to oxidise to other Fe phases and remained as Fe^0. Therefore, the size of the agglomerates directly affected the amount of oxidised Fe^0 in samples and subsequently the amounts of inorganic contaminants released over time, which was observed in the results from porewater and soil water extraction.

As secondary products of nZVI and nZVI-BC, ferrihydrite, lepidocrocite and magnetite were present in the sorbent layers. Overall, ferrihydrite was the most abundant newly formed Fe species, representing 19-50% of the total Fe (Fig. S3.16). The amount of lepidocrocite ranged between 11 and 29%. Magnetite represented 6-26% of the Fe species, with generally higher amounts in the nZVI-BC sorbent layer than in nZVI (Fig. S3.16). According to Fig. 3.6C, although the amount of oxidised Fe^0 increases, the newly-formed Fe phases are present in the same ratios (i.e. ratios of ferrihydrite / lepidocrocite, lepidocrocite / magnetite and magnetite / ferrihydrite) (Fig. 3.6C). This implies that the oxidation of the used nZVI materials under the given conditions results in the formation of specified by-products in certain proportions independently of time. Goethite was present only in the sorbent layer of nZVI-BC after 3 months of incubation (Fig. S3.16). In the same sample, nZVI-BC was completely transformed. This finding was in complete agreement with the preliminary XRD data (Figs. S3.15A, B). We suggest that the total transformation of Fe^0 (from the nZVI-BC layer) to Fe oxides and the presence of goethite after 3 months was governed by potentially more oxidising conditions in this individual sample, which favoured the occurrence of goethite over lepidocrocite (Bakshi, 2018).

Using the same nZVI product, Wu et al. (2019) reported magnetite (Eq. 1-3) and goethite (Eq. 4-6) as the main products of oxidation described by the following reactions:

(1) $Fe^0 + 2H_2O \rightarrow Fe^{2+} + H_2 + 2OH^-$
(2) $2Fe^0 + O_2 + 2H_2O \rightarrow 2Fe^{2+} + 4OH^-$
(3) $6Fe^0 + O_2 + 6H_2O \rightarrow 2Fe_3O_4(s) + 12H^+$
(4) $4Fe^0 + 3O_2 + 2H_2O \rightarrow 4\gamma\text{-FeOOH}$
(5) $4Fe^0 + O_2 + 6H_2O \rightarrow 4\gamma\text{-FeOOH} + 8H^+$
(6) $4Fe_3O_4 + O_2 + 6H_2O \rightarrow 12\gamma\text{-FeOOH}$

Rapid (within hours) oxidation of nZVI followed by the formation of magnetite was also reported by Liu et al. (2022) Generally, nZVI oxidation pathway is: $Fe^0 \rightarrow Fe(OH)_2$, ferrihydrite $\rightarrow Fe_3O_4 \rightarrow \gamma Fe_2O_3$ (Y. Wang et al., 2021). In our study, magnetite was present in all the samples regardless of the incubation step, implying that rapid nZVI oxidation likely occurred within 1 month (complying with the previous studies), but Fe transformations never ceased until the end of incubation. Since nZVI oxidation was not directly proportional to time in the layered samples, the coexistence of poorly crystalline (i.e. ferrihydrite) and more crystalline (i.e. goethite, lepidocrocite, magnetite) Fe oxides is possible. The presence of lepidocrocite was expected based on the reported results for water (Dong et al., 2020; A. Liu et al., 2014) and for this soil (S. Wu et al., 2019) and the given conditions (i.e. pH around 5 and oxic conditions) (A. Liu et al., 2017). Finally, higher adsorption of metal(loid)s could be expected when ferrihydrite is present due to its higher surface area compared to more crystalline Fe oxides (Danila et al., 2020; Kumpiene et al., 2012).

3.3.3 Elemental availability in the liquid phase

The results from the soil water extraction and pore water extractions are discussed together in the following section. Note that the actual available concentrations in the pore water were 10 times lower than those in the soil water extracts. Hence, the latter represent a "magnified picture" of the metal(loid) extractability and amendment efficiency.

The general time-dependent leaching trend in the soil water extracts was as follows: after the initial (1 month) decrease in all metal(loid)s' concentrations (except for Pb in BC-treated soil), a universal increase in the concentrations of Zn, Cd and As (and occasionally in Pb) was noticed, and then again a decrease in all contaminant concentrations was observed in all treatments, including control (Fig. 3.7). At the same time, the soil solution pH was higher in all the treated soils than in control (Fig. 3.7E) which affected the concentrations of Zn at least partially (see later in this section). However, after 3 months a sharp pH decrease was observed, which was linked to the sharp increase in all studied contaminant concentrations, in some cases even in control soil (Figs. 3.7A−D). Eventually, the pH of the treated samples reached the pH value corresponding to the control soil after 15 months (pH 5.6; Fig. 3.7E). This finding highlights the importance of long-term studies about risk element immobilisation in soils.

More importantly, it points to the role of natural immobilisation of contaminants with time, especially when the soil is modified with amendments that potentially enhance and accelerate the remediation process (Mulligan & Yong, 2004).

Considering the concentrations of NO_3^- and SO_4^- (Fig. S3.18) in the soil water extracts, we suggest that the significant fluctuations in soil pH over time are partially due to increased (up to 7x more) concentrations of these anions. The available sulphates followed by a pH decrease correspond to the potential oxidation of sulphides that are present in the soil as relicts from the metallurgical slags/matte of the nearby former smelter(Ettler et al., 2001). We assume that the activity of N (Alef & Nannipieri, 1995) and S (Wainwright, 1978) oxidising bacteria was taking place throughout the incubation period when the conditions (i.e. moisture, pH, aeration) were favourable for them. Therefore, the occasionally increasing concentrations of NO_3^- and SO_4^- can lead to the formation of acids and lower pH values following the principle of acid mine drainage(Skousen et al., 2019). Additionally, the alkalinity of BC, which is one of the major factors for its immobilisation efficiency, can be depleted over time due to the dissolution of alkaline minerals, resulting in an increase of risk element concentrations in soil (J. Wang et al., 2021b).
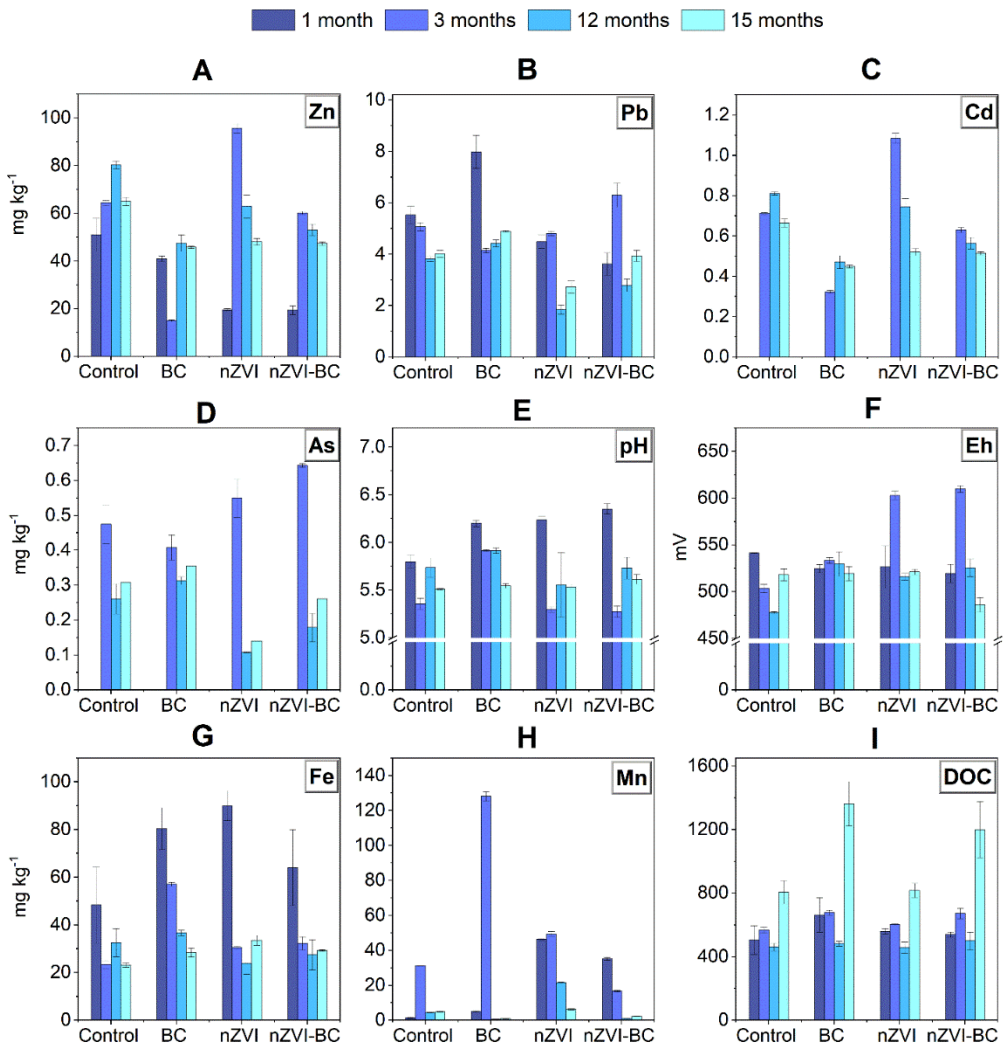
Figure 3.7: *Concentrations of Zn (A), Pb (B), Cd (C), As (D), Fe (G), Mn (H), and DOC (I), and pH–Eh values (E and F) in soil water extracts of mixed soil samples after 1, 3, 12 & 15 months of incubation.*

The concentrations of Zn and Pb were significantly lower in the treated soil samples compared to control already after 1 month of incubation (Fig. 3.7 A, B), while Cd and As were below the detection limit (0.005 ppb) in all the soil water extracts during the first month of incubation. Zinc was in most cases immobilised in BC-treated soil, although occasionally it was also effectively immobilised by nZVI and nZVI-BC. Although Zn concentrations were significantly higher after 3 months of incubation in all the treatments except for BC, in the treated soil samples, the concentrations gradually decreased over

time and remained lower than those in the control soil (Fig. 3.7A). Up to 52% of Pb was immobilised by the nZVI-containing treatments and particularly by nZVI. Lead concentrations were significantly lower after longer (mainly 12 and 15 months) incubation time-steps (Figs. 3.7B, 3.8B), which corresponded to a decrease in Mn concentrations (Figs. 3.7H, 3.8G). The increased occurrence of secondary Fe-Mn phases in the nZVI-containing samples, which were capable of scavenging up to 30 wt.% of Pb as observed by SEM/EDS (Fig. 3.3C), was previously reported in this soil (Mitzia et al., 2020; Vítková et al., 2017).Moreover, the low point of zero charge that is typical for many Mn oxides makes cation sorption possible even at low pH values unlike Fe oxides (Negra et al., 2005). This could explain why Pb (which showed the highest affinity to Mn oxides compared to the rest risk elements) was the only metal to show lower concentrations after longer incubation time despite the decrease in pH values. Cadmium varied between 0.32 and 1.08 mg kg^{-1} (Figs. 3.7C, D) in the water extracts and was most efficiently immobilised by BC (32-55%), which exhibited overall the lowest concentrations, followed by nZVI (up to 30%). The availability trend of Cd followed the behaviour of Zn with lower concentrations at longer incubation time (Fig. 3.7C). The increased immobilisation of Zn and Cd by BC compared to nZVI treatments (Fig. 3.7A, C) was also observed in our previous study with this soil although a different BC was used (Mitzia et al., 2020). The immobilisation of cationic metals (like Zn and Cd) by BC is mainly attributed to the liming effect and sorption on the BC surface and/or pores (Kumpiene et al., 2019b).The increase in soil pH that is induced by BC application is often reported as the critical factor in cationic metals immobilisation (El-Naggar et al., 2022; Fu et al., 2023; C. Yuan et al., 2021) and can be explained by its basic character (pH = 10, Table 3.1), as stated in other studies (Anawar et al., 2015; Palansooriya et al., 2020; Y. Zhang et al., 2021). In addition, Zn and Cd are dominantly immobilised by BC through the precipitation of metal carbonates, followed by surface cation exchange and complexation(Trakal et al., 2016b; C. Yuan et al., 2021). Moreover, cation exchange can be even strengthened after BC impregnation with Fe oxides, which minimises potential desorption of metals, as reported for Cd(Trakal et al., 2016b). Therefore, it can be assumed that the observed immobilisation of Zn and Cd by BC or nZVI-BC was attributed to a combination of factors. Furthermore, the retention of Cd and Zn by BC might not be immediately reversible once the pH decreases (Trakal et al., 2016b) which supports the idea of long-term metal immobilisation by BC compared to nZVI treatments.
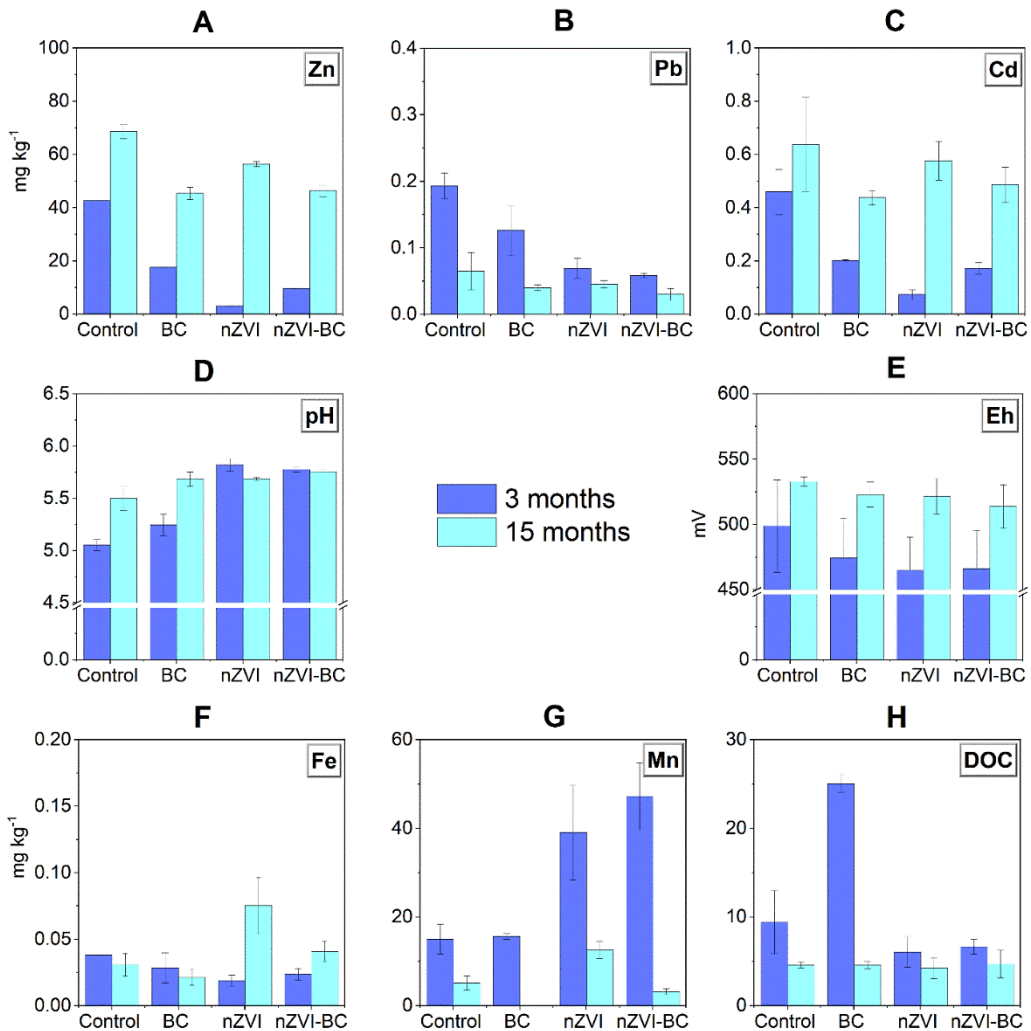
Figure 3.8: *Concentrations of Zn (A), Pb (B), Cd (C), Fe (F), Mn (G), and DOC (H), and pH–Eh values (D and E) in the pore water extracts of mixed soil samples after 3 and 15 months of soil incubation*

In the pore water, the concentrations of Zn, Pb and Cd in all treated samples were consistently lower than those in the control (Fig. 3.8A-C). The lowest values for Zn and Cd were recorded in nZVI-treated soil. Although nZVI was initially the most effective stabilising amendment for Zn and Cd in this case, eventually (after 15 months) BC-treated samples yielded lower values than nZVI-containing soil (Figs. 3.8A, C). Lead in the pore water was detected only in amounts up to 0.19 mg kg^{-1} and was immobilised by all treatments, with nZVI-BC being the most effective (Fig. 3.8B). According to Vítková et al., (2017)

a decrease in Zn and Cd leaching in this soil could be expected when pH>6 and for Pb when pH>5. Additionally, recent studies confirmed the nZVI immobilisation efficiency for selected metals even under acidic conditions, i.e. 4<pH<6 [44,27]. In this study, the ANC of the control soil was 0.04 mol kg^{-1} while those of BC, nZVI, and nZVI-BC were 0.17, 12.5 and 13.2 mol kg^{-1}, respectively (Fig. S3.17). Therefore, the resistance of the nZVI-based amendments to pH changes was more than 1.5 orders of magnitude higher than that of BC or the control soil. This can explain why nZVI-containing treatments were efficient for immobilisation in the short term (Figs. 3.7, 3.8). Similar to soil water extracts, the availability of Zn, Pb and Cd in the pore water was closely related to the changes in pH values, as supported by the determined Pearson correlations (pH–Zn up to r=−0.91, pH–Pb up to r=−0.98, pH–Cd up to r=−0.86; Table S3.3b). After an initial (after 3 months) increase in the pH values of all treatments (significant for nZVI and nZVI-BC), similar values (pH 5.7) were determined for all treatments after 15 months. The pH was significantly different ($p<0.05$) from the control in the case of nZVI and nZVI-BC samples, although the absolute pH values were higher in the BC-treated sample as well (Fig. 3.8D). The BC-treated soil presented similar time-related trend as control soil, while samples containing nZVI treatments had statistically the same pH in both time steps (Fig. 3.8D).

Arsenic was detectable from the 3- until the 15-months time steps with concentrations between 0.11–0.64 mg kg^{-1} (Fig. 3.7D). A decrease was observed after 12 months, and even lower values were determined after 15 months in the nZVI-based treatments (Fig. 3.7D), underlying the long-term immobilisation efficiency of nZVI in As-contaminated soil (Danila et al., 2020; Gil-Díaz et al., 2019). Particularly, As concentrations decreased by nZVI up to 59% and by nZVI-BC up to 31% (Fig. 3.7D). Although also BC rarely showed lower concentrations of As than control (1 month), it is suggested using BC with caution since higher pH values (>5) can promote As mobility (Beesley et al., 2010). Indeed, a strong positive Pearson correlation of pH–As (up to r=0.93; see Table S3.3a) was determined in our study. In addition, it has been demonstrated that BC has the ability to accept and/or donate electrons acting as a "geobattery" (Klüpfel et al., 2014; J. Yuan et al., 2022), which can be employed to immobilise redox-sensitive elements like As (Zhong et al., 2019). However, the electron storage capacity of BC is suggested to be reversible (Xin et al., 2019), implying that previously oxidised As(V) can be reduced again to

As(III) which is more toxic and more mobile in the environment (Moreno-Jiménez et al., 2012).This behaviour could explain the persistent availability of As in the soil extracts of BC-treated soil in concentrations similar or higher than control (Fig. 3.7D). In the pore water, As was below the detection limit of ICP OES in all the samples.

The increased metal(loid) immobilisation in the samples incubated for 1 and 12 months compared to the rest of the samples is in accordance with the results from the layers studied by XAS, where higher amounts of ferrihydrite were observed at the same time steps. However, when comparing the concentrations of the studied contaminants from the first and the last time step, they increased except for Pb (Figs. 3.7, 3.8), in all treatments including control. These results imply that kinetically driven long-term changes may appear in the incubated soil under given conditions. Seasonal changes in metal(loid) concentrations in the biomass of indigenous plant species from the studied contaminated area, which may be linked to this behaviour, have been reported (Teodoro et al., 2020). Based on these findings, we suggest that longer incubation periods demonstrate not only the immobilisation ability of amendments over time but also the natural processes occurring in the soil.

Regarding redox potential, despite some time-dependent oscillations in Eh values in the pore water, oxic conditions prevailed in all cases and no significant differences were observed among the treatments (Figs. 3.7F, 3.8E). In total, the Eh values both in the soil water extracts and the pore water ranged from 465 to 610 mV (mean value: 519; median value 521 mV). Based on the actual values, the redox conditions can be considered similar throughout the incubation experiment and due to the limited fluctuation, no significant effect of redox changes on metal(loid) availability was observed. The few observed fluctuations were more profound in the nZVI-containing samples (Figs. 3.7F, 3.8E) because of the nZVI oxidation process (Pasinszki & Krebsz, 2020). Generally, redox processes are one of the driving forces that affects metal(loid) mobility in soils (Frohne et al., 2011, 2014), either directly by changing the speciation of the metal(loid)s, or indirectly, by altering the pH of the soil, by inducing dissolution/precipitation, co-precipitation with Fe and Mn oxides or complexation with organic matter (Du Laing et al., 2009). However, in our study, the redox oscillations were minimal.

Potential excessive Fe release from the nZVI-containing soil was carefully considered when choosing the application rate of 2 wt.%. In fact, Fe availability remained stable from the 3-months step until the end of the incubation in the samples containing nZVI, contrary to the BC-treated samples, in which a fluctuation was observed (Figs. 3.7G). In the pore water, the leaching of Fe was lower than 0.10 mg kg^{-1}, and only a slight increase in the nZVI-containing treatments was observed (Fig. 3.8F). Manganese release was higher in the nZVI-treated samples both in the water extracts (Fig. 3.7H) and in the pore water (Fig. 3.8G). Similar release of Mn after a short-term interaction with nZVI treatments was previously reported in the same soil (Mitzia et al., 2020; Vítková et al., 2018) and is attributed to the strongly reducing character of nZVI, which may dissolve Mn (hydro)oxides (Wang, et al., 2022; Michálková et al., 2017). Despite the dissolution of the soil Mn (hydro)oxides by nZVI, immobilisation of inorganic contaminants on Fe-Mn oxides was promoted in the nZVI-containing samples because the newly formed Fe oxides and Mn phases compensated for the release of contaminants from the primary phases (M. Liu et al., 2021; Wang, et al., 2022). Elevated Mn release was occasionally observed also for BC-amended samples (Fig. 3.7H). In general, the release of Fe and Mn decreased over time in all the treatments. Although DOC concentrations were in most cases statistically similar ($p > 0.05$) among the treatments, BC-treated soil occasionally yielded significantly higher amounts of DOC than the rest of the treatments (Figs. 3.7I, 3.8H). In the soil extracts the release of DOC increased over time, with the highest concentrations being observed after 15 months of incubation, especially in the samples containing BC (Fig. 3.7G). Similarly, in the pore water, the release of DOC did not vary significantly ($p > 0.05$) over time except for the case of BC. In fact, the DOC values were practically the same in all treatments after 15 months of incubation, and no strong correlations between DOC contents and metals were established (Fig. 3.8H). The real-scale use of BC for metal(loid) immobilisation in soils might lead to increased leaching of DOC and/or Mn and consequently to the release of contaminants due to co-mobilisation of DOC and metal(loid)s(Beesley et al., 2015; J. Wang et al., 2021b), as observed here for Pb (Pb-DOC correlation up to r=0.75; Table S3.3a).

3.3.4 Geochemical modelling predictions in the liquid phase

The use of geochemical modelling (PHREEQC-3 code) in this study enabled 1) the understanding of the speciation of Zn, Pb, Cd and As in the aqueous phase and 2) the projection of the chance that important solubility-controlling phases would be dissolved or precipitate. The most important findings in connection with the analytical results are summarised and discussed here and the individual metal species in soil/pore water extracts and saturation indices of potential mineral phases are listed in Tables S3.4-7.

Both in the soil water extracts and the pore water, Zn and Cd were mostly projected to be in their free cationic form (i.e. Zn^{2+}, Cd^{2+}) regardless of the treatment and the incubation step (Tables S3.4, 7). In contrast, Pb was more likely to be in its cationic form in percentages up to 82 % in the pore water extracts of all treatments and partly as $PbNO_3^+$ and $PbHCO_3^+$ (Table S3.4). In contrast, predominant Pb carbonate complexes in the pore water of nZVI-treated soil were reported by Vítková et al. (Vítková et al., 2018). In the soil extracts, Pb^{2+} was the prevailing form of Pb in the long-term, while up to 62 % of Pb carbonates were predicted after 1-month incubation with BC, nZVI, and nZVI-BC (Table S3.6). Important solubility-controlling phases, such as jarosite ($KFe^{3+}_3(SO_4)_2(OH)_6$) and rhodochrosite ($MnCO_3$), were suggested to be mostly dissolved in the pore water, similar to metal sulphates and carbonates, including $PbSO_4$, $PbCO_3$ and $ZnCO_3$ (Table S3.5). Jarosite typically forms under oxic acidic conditions and can be classified as a layered mineral; its properties allow to incorporate various metals and metalloids (Pb, Zn, Cu, Cd, As, and Cr) in the crystal structure(Shi et al., 2021). However, when soil pH increases to 7–8, metal carbonates play crucial role in the scavenging mechanisms(Vítková et al., 2017). The absence of precipitated sulphate and carbonate phases partially explains the increased amounts of available Zn and Pb in the pore water after 15 months of incubation. The suggested dissolution of $Fe(OH)_3$ both in the pore water and the soil extracts (Tables S3.5, S3.7) is considered an important factor affecting the concentrations of the studied contaminants, especially because Fe (oxy)hydroxides are key scavenging phases and the calculated saturation indices values were very close to equilibrium.

3.3.5 Environmental implications of long-term effects of soil amendments

The study of possible negative effects (e.g. toxicity, metal(loid) release) of amendment application in soils is crucial before field application of BC-based(Sun et al., 2021; Urra et al., 2019; Y. Zhang et al., 2021) and Fe-based amendments (Anza et al., 2019; Ken & Sinha, 2020; J. Wang et al., 2016). It is important though, to predict the long-term behaviour of soil amendments even if their effects are positive so that we can make a sustainable choice of amendment and application rate both in terms of environmental and financial efficiency (Taraqqi-A-Kamal et al., 2021).

The layered design that was used in this study could be a simulation of field application of soil amendments in the form of reactive barriers that are not mixed with the soil and could potentially be later removed from it. In addition, our results can assist in a future enhanced experimental design in which the sorbent layer will be more reactive. Potential solutions could be the use of increased doses of nZVI for the formation of a reactive barrier but limiting the thickness of the layers and/or application of multiple layers for extended surface area. Additionally, modified nZVI products were reported to show increased immobilisation efficiency compared to plain nZVI (Alazaiza et al., 2022; Petala et al., 2022; Santos et al., 2022). The use of BC support in particular makes nZVI particles less prone to agglomeration and increases their dispersion ability in the soil matrix (S. Wang et al., 2019a).

The lowest leaching of all studied metals in the sand layer was observed in the BC-treated samples (Fig. S3.19). This could be linked to the property of BC to significantly increase the WHC (Jačka et al., 2018) and the available water content of the soil (Seyedsadr et al., 2022) and therefore limit the transport of risk elements through the soil profile (Pračke et al., 2022). Based on that, BC could be suggested as the least permeable sorbent layer even though fluctuations in time occurred in this case as well (Fig. S3.19). On the other hand, the most significant positive effect of BC application in this soil was the long-lasting pH increase that it provoked (Fig. 3.7E). Based on the ANC results, however, the ANC of BC was similar to that of the control soil, unlike the nZVI-containing sorbents (Fig. S3.17). In the long term, the pH of all samples was around 5.5 in both the pore water and the soil extracts (Figs. 3.7, 3.8). Therefore, a higher dosage of a nZVI amendment (which has significantly

higher ANC than BC) could promote both risk element immobilisation and pH retention.

In such cases that nZVI would be applied at higher dosages, the potential toxic effects of nZVI in the soil biota need to be extensively studied. The use of nZVI carries the risks of migration out of the medium (e.g. to plant tissues) and the sedimentation of nZVI particles due to their agglomeration (X. Li & Liu, 2021). If possible, the effect of nZVI on microorganism populations and potential migration to plant tissues needs to be projected before application. A dosage of 2 wt.% (Gómez-Sagasti et al., 2019) or up to 10 wt.% nZVI (Fajardo et al., 2019) was reported to possibly affect the soil microbial community, but the effect mainly depended on the soil type. An amount of 20 wt.% nZVI slurry was not found to be harmful to the biological and physico-chemical properties of the soil but actually increased the soil respiration (Gil-Díaz et al., 2014). Wu et al. (2019) applied 20 wt.% nZVI in the same soil as in our study and concluded that the interactions between nZVI and soil biota are bilateral. It was also reported that nZVI ageing limits its possible toxic effects (Mukhopadhyay et al., 2021; S. Wu et al., 2019)᾽ concluding that more studies are necessary to assess the ageing effect of nZVI in various types of soils to understand its behaviour.

Another point that needs to be addressed is the potential release of the previously immobilised contaminants in the long term. Based on the results of this study, the risk element concentrations increased both in the pore water and soil extracts at a specific point and decreased again after a longer time, which implies that the mechanisms of retention need to be extensively studied to predict the behaviour of the amendments. The metal(loid) retention mechanisms in the soil are still lacking detailed research and understanding compared to water solutions and future studies need to address this (Mazarji et al., 2023). Long-term studies on the efficiency of BC and the changes it provokes in the soil are still scarce, and the mechanisms involved are not yet fully explained (Taraqqi-A-Kamal et al., 2021). Although a wide range of pyrolysis temperature (400–700 °C) has been reported to produce biochar efficient for the immobilisation of Zn and Pb (Palansooriya et al., 2020), high temperatures (i.e. 700 °C) generally result in limited functional groups on the surface of BC and could lead to a decrease in the metal removal efficiency of BC (H. Li et al., 2017). In addition, there is evidence that the release of contaminants in untreated soil is more likely when nonspecific adsorption takes

place, especially in the case of multiple element contamination (Campillo-Cora et al., 2020). In the case of nZVI, some explanations for the release of contaminants have been given by Danila et al. (2020), who reported that the formation of crystalline Fe phases during nZVI ageing resulted in contaminant release. The immobilisation efficiency of Fe (oxyhydr)oxides is significantly affected by their size, structure, specific surface area, prevailing physicochemical conditions, metal(loid) concentrations and more (Shi et al., 2021), implying that the same material (in this case nZVI) might not always behave in the same way in different contaminated environments/areas. However, attention should be given to coprecipitation; it has been reported that under specific conditions, risk metal(loid)s coprecipitated with Fe (oxyhydr)oxides might be either released in the remediated matrix or redistributed in the emerging crystalline structure (Shi et al., 2021). Redox changes are a major factor affecting metal(loid)s co-precipitation with Fe and Mn oxides since the dissolution of the latter ones under reducing conditions can result in the release of risk elements in the environment (Du Laing et al., 2009). It is therefore suggested that attention to the redox oscillations is given in the future studies.

Our results stress that natural attenuation in this soil plays a crucial role in risk element behaviour. Natural attenuation is based on naturally occurring processes in the soil aiming to limit the existing contamination without human interaction. The potential mechanisms employed are, among others: 1) biodegradation or abiotic processes including hydrolysis and redox transformations, 2) a decrease in available contaminant concentrations by dilution or diffusion, dispersion, and volatilisation, and 3) contaminant adsorption, resulting in limited bioavailability and toxicity (Fernández Rodríguez et al., 2014). The observed pH and metal(loid) release changes over time indicate that natural scavenging mechanisms work and can be supported with wisely selected amendments. In the end (after 15 months), the metal(loid) extracted fraction (expressed in % of the total amount) was up to 0.6% lower in the treated samples compared to control (Fig. S3.20). This finding proves that natural attenuation was enhanced by the used amendments in this soil. The natural attenuation of a highly contaminated mining site has been suggested by Jurkovič et al. (2019) as a potential remediation method. However, relying on the possible effect of natural attenuation can be toxic for the biota at the contaminated site, and a sustainable solution needs to be

applied at the moment even for short-term remediation. Dovletyarova et al. (2022) recently showed that natural Fe oxides and BC-supported nZVI and ZVI microparticles had similar efficiency in the short time at immobilising metals in Cu- and Ni-contaminated soil. Therefore, possible modifications of the amendments could result in significantly more efficient BC-based materials for soil remediation (Taraqqi-A-Kamal et al., 2021) and limit the aggregation and potential toxicity of nZVI (Xue et al., 2018).

In our study, the dose of amendments that was used was only 2 wt.%, which could be a limiting factor in terms of immobilisation. An increased dosage of nZVI is usually connected with increased contaminant immobilisation (Ganie et al., 2021; Gil-Díaz et al., 2016), while Wu et al. (2019) used up to 20 wt.% nZVI in this soil and did not report alarming changes to the soil biota due to nZVI. Based on the contaminant concentration fluctuations over time, we suggest that 2 wt.% nZVI in this study was not enough to immobilise the studied contaminants efficiently in the long term. However, the use of a higher dosage would increase the cost of field application. The most promising, feasible and sustainable approach is the application of amendments with the aim of enhancing the natural attenuation processes (Hiller et al., 2021) rather than targeting complete risk element immobilisation by the amendments only.

3.4 Conclusions

Our findings will be useful in decision-making about suitable and sustainable solutions for soil remediation where the use of nZVI products and BC is intended. Here, we summarised the key conclusions:

- Biochar-based treatments (i.e. BC and nZVI-BC) were mostly efficient for Zn and Cd immobilisation while nZVI for Pb and As.
- The studied nZVI-based sorbents were mainly effective for short-term remediation, while BC for the long-term (considering the contaminant release and pH values over time).
- The metal(loid) immobilisation efficiency of the studied nZVI, nZVI-BC, and BC did not increase with longer time.
- Accumulation of risk metal(loid)s on Fe and/or Mn oxides was repeatedly suggested to be the most important immobilisation mechanism. Although these oxides were commonly found in the contaminated soil (natural attenuation), the combined occurrence of Fe

and/or Mn oxides and Zn, Pb and As increased 2× after the amendment application.

- The oxidation of Fe^0 was more intense in the short term (1 and 3 months) and not directly proportional to time, unlike what was hypothesised. Ferrihydrite, lepidocrocite, and magnetite were formed as secondary products regardless of the amount of oxidised Fe^0.

3.5 Supplementary Information

Materials and methods

Activation procedure for the studied amendments

Before application to soil, the activation of NANOFER STAR was performed as recommended by the manufacturer. NANOFER STAR is an air-stable nZVI product in which the Fe^0 core is covered by Fe oxides. The aim of activation is to remove the protective Fe oxide layer coating the nanoparticles, which has been reported to make nZVI more efficient for contaminant immobilisation (Ribas et al., 2017). A suspension of nZVI in demineralised water (ratio 1:4 wt.%) was prepared and thoroughly mixed using a vortex device. The suspension was preserved in a closed reactor at ambient temperature for 48 h and then mixed again and immediately applied to the soil, followed by manual homogenisation of the soil with the activated suspension. The same activation procedure was performed for the pure BC and nZVI-BC composite to maintain consistent conditions.

Recalculation of concentrations of elements in pore water

The concentrations in the pore water (mg L^{-1}) were recalculated to mg kg^{-1} using Eq. 1:

$$C = C_{pw} * V / m \quad (1)$$

where C is the concentration in mg kg^{-1} of soil, C_{pw} is the concentration in mg L^{-1} of pore water, V is the total volume of water in the pot in L, and m is the total dry mass of the solid in the pot (soil + sorbent) in kg.

Experimental conditions of the full-frame SEM/EDS session

Extensive scanning of the samples after 15 months of incubation and selective mapping were conducted and further treated using AZtec software. Feature analysis was used for large sample mapping. Particle classification was fitted to the BSE figure, and then feature analysis was performed with a constant 50000 counts by EDS at a 25 keV accelerating voltage. The average analysis time was 48 hours per sample. Selected particles of interest were analysed in detail.

Input details for the geochemical modelling

Analytical data from 1) the soil water extractions and 2) the pore water were treated appropriately to prepare an input for the PHREEQC geochemical code (version 3 for Windows)(Parkhurst & Apello, 2013). The necessary parameters that were included in the modelling were pH, Eh (recalculated to pe according to the Nernst equation), concentrations of major and trace elements including both cations and anions to ensure that the ion balance was determined. The content of inorganic carbon was recalculated to the concentration of HCO_3^- ions and used in the model input. In addition, dissolved organic carbon (DOC) was included in the calculations in the form of humates and fulvates (Michálková, Komárek, Veselská, et al., 2016) using thermodynamic data from the T&H.dat database. In particular, the DOC was calculated as humate (30%) and fulvate (70%) according to Borůvka and Vácha (2006)(Boruvka & Vacha, 2006), who studied the fractionation of DOC in the soil used in our study.

Results and Discussion
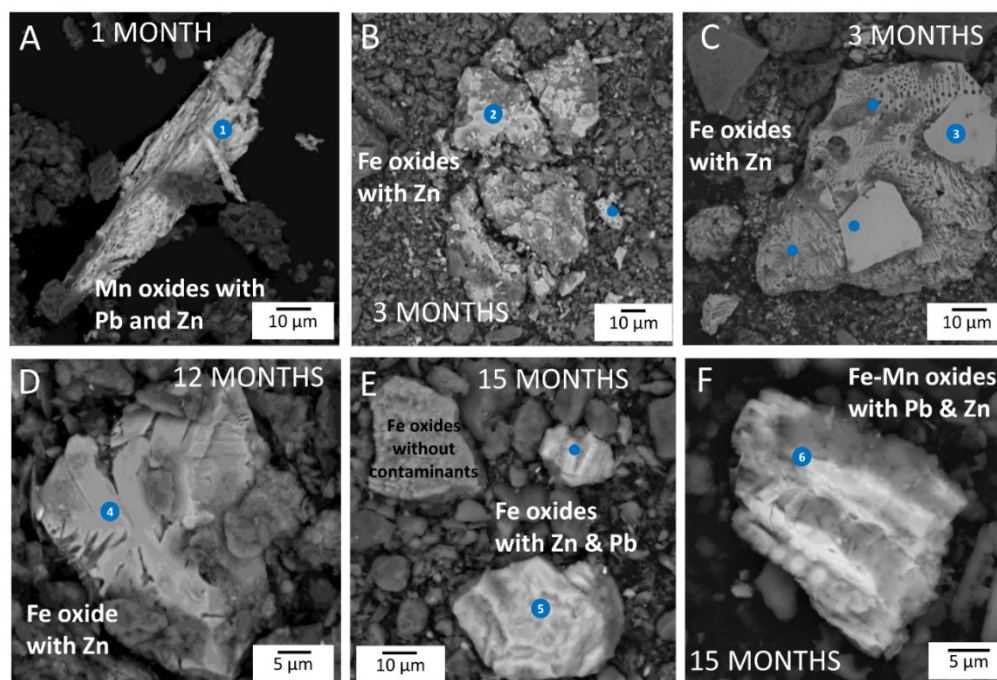
Figure S3.1: *Backscattered electron images (BSE) of control soil. The respective EDS spectra (numbered points) can be found in Fig. S3.6. A) Mn oxides with 4 wt. % Zn and 35 wt. % Pb on the surface of soil particles. B) Fe oxides with up to 10 wt. %, C) up to 5.7 wt. % and D) 7.8 wt. % Zn. E) Soil Fe oxides with no contaminants and Fe oxides with up to 1.6 wt. % Zn and 3.2 wt. % Pb. F) Soil particle covered by Fe-Mn oxides with 4.1 wt. % Zn and 13.2 wt. % Pb.*
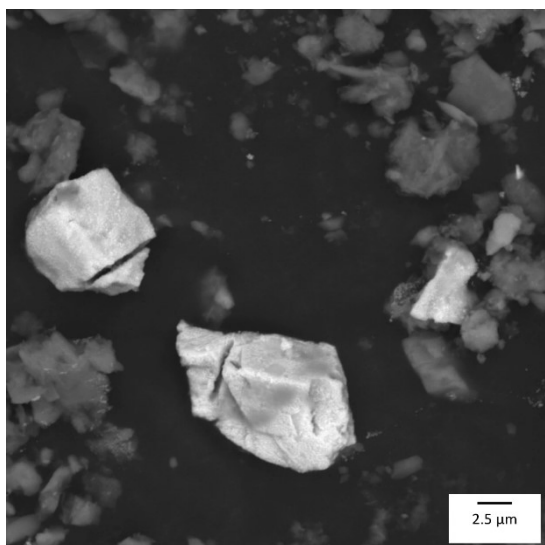
Figure S3.2: *Sphalerite (ZnS) captured in control soil sample by SEM.*
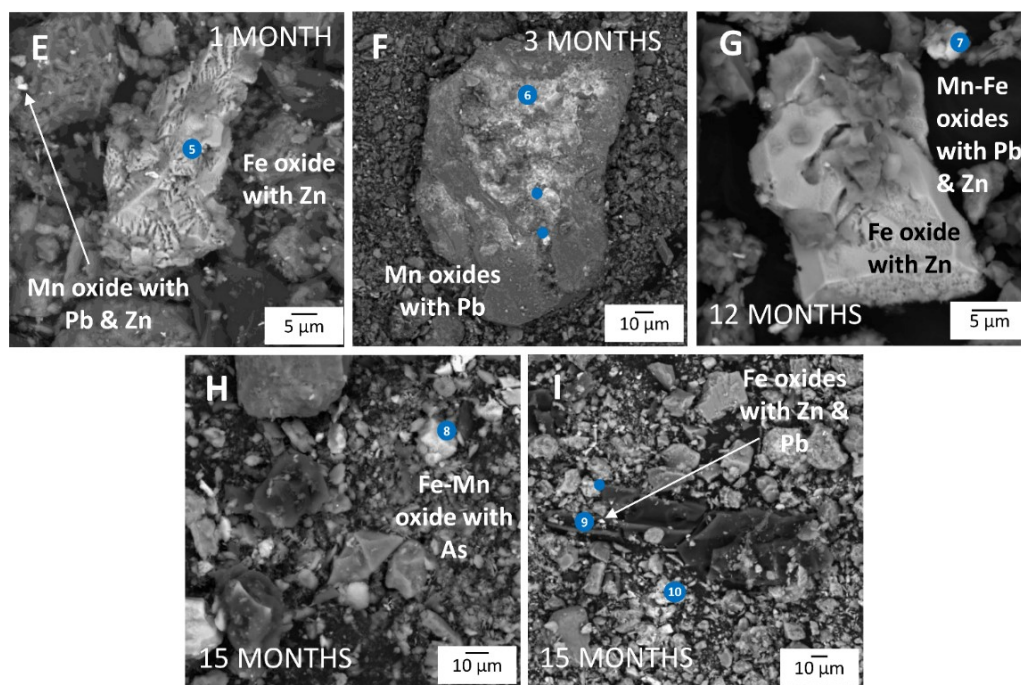
Figure S3.3: *Images of BC-treated soil in BSE mode. The corresponding EDS spectra are indicated by number(s) (Fig. S3.7). Images G and H are taken from the mixed soil, images E, F and I are from the soil-BC interface. E) Mn oxide (7 wt.% Zn and 16 wt.% Pb) and Fe oxide (7 wt.% Zn). F) Mn oxides with up to 17. 8 wt. % Pb. G) Fe oxides (6.3 wt.% Zn) and Mn-Fe oxides (6.2 wt.% Zn and 15 wt.% Pb). H) Fe-Mn oxides with up to 1.2 wt. % of As. I) Soil particles containing Fe oxides on top of or adjacent to BC particle (up to 3 wt.% Zn and 7.7 wt.% Pb).*
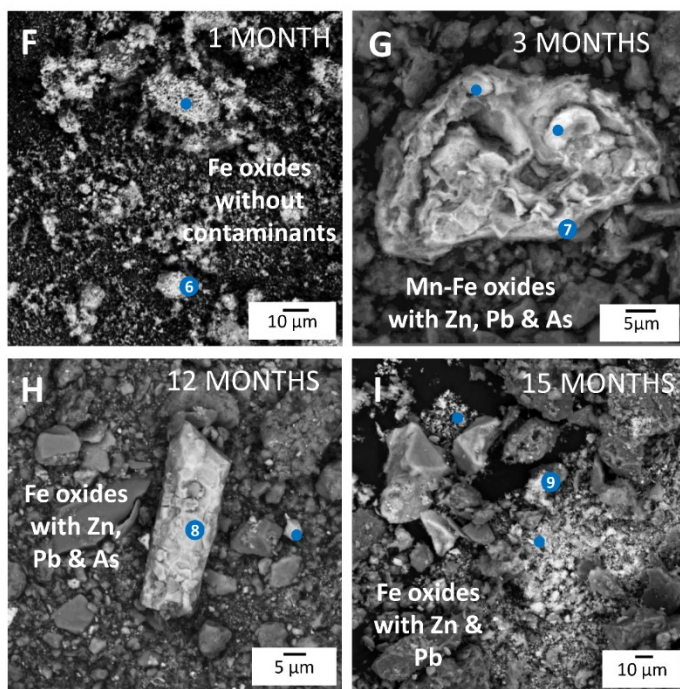
Figure S3.4: SEM images of the nZVI treatment with numbered EDS spectra (Fig. S3.8). Image F is taken from the sorbent layer, image B from the mixed soil and images H and I are taken from the soil-nZVI interface. F) nZVI particles without contaminants. G) Fe-Mn oxides (2.8 wt.% Zn, 30.5 wt.% Pb and 2.8 wt.% As. H) Fe oxides (1.8 wt.% Zn, 2.9 wt.% Pb and 0.6 wt.% As). I) traces of Zn and Pb (< 1 wt.%) bound to Fe oxides.
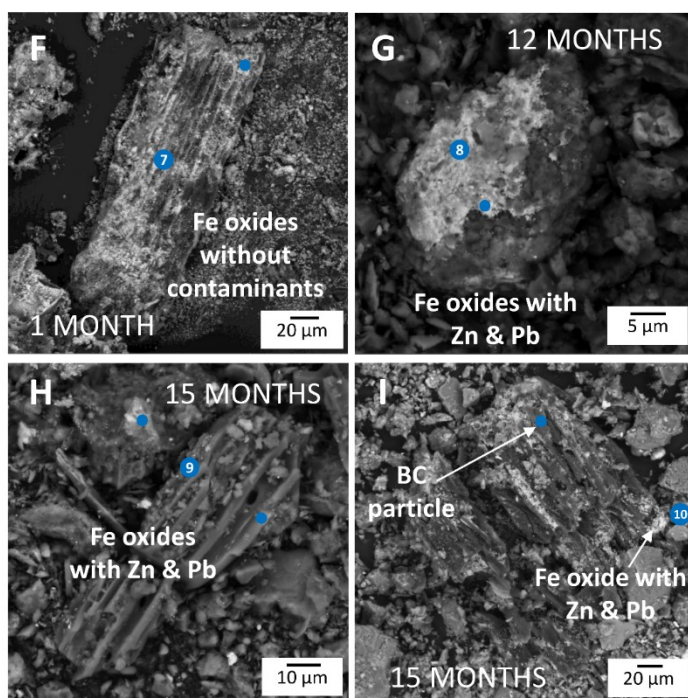
Figure S3.5: *SEM images from the nZVI-BC treatment with numbered EDS spectra (Fig. S3.9). Image F is from the sorbent layer and images H and I are from the soil-nZVI-BC interface. F) nZVI on a BC particle (no contaminants). G) Fe oxides with 19.7 wt.% Zn, 1.8 wt.% Pb and 0.6 wt.% As. H) Fe oxides on the surface of a BC particle (up to 2.6 and 7.3 wt.% Zn and Pb, respectively). I) Traces (<1 wt.%) of Zn and Pb bound on Fe oxide on the surface of BC.*
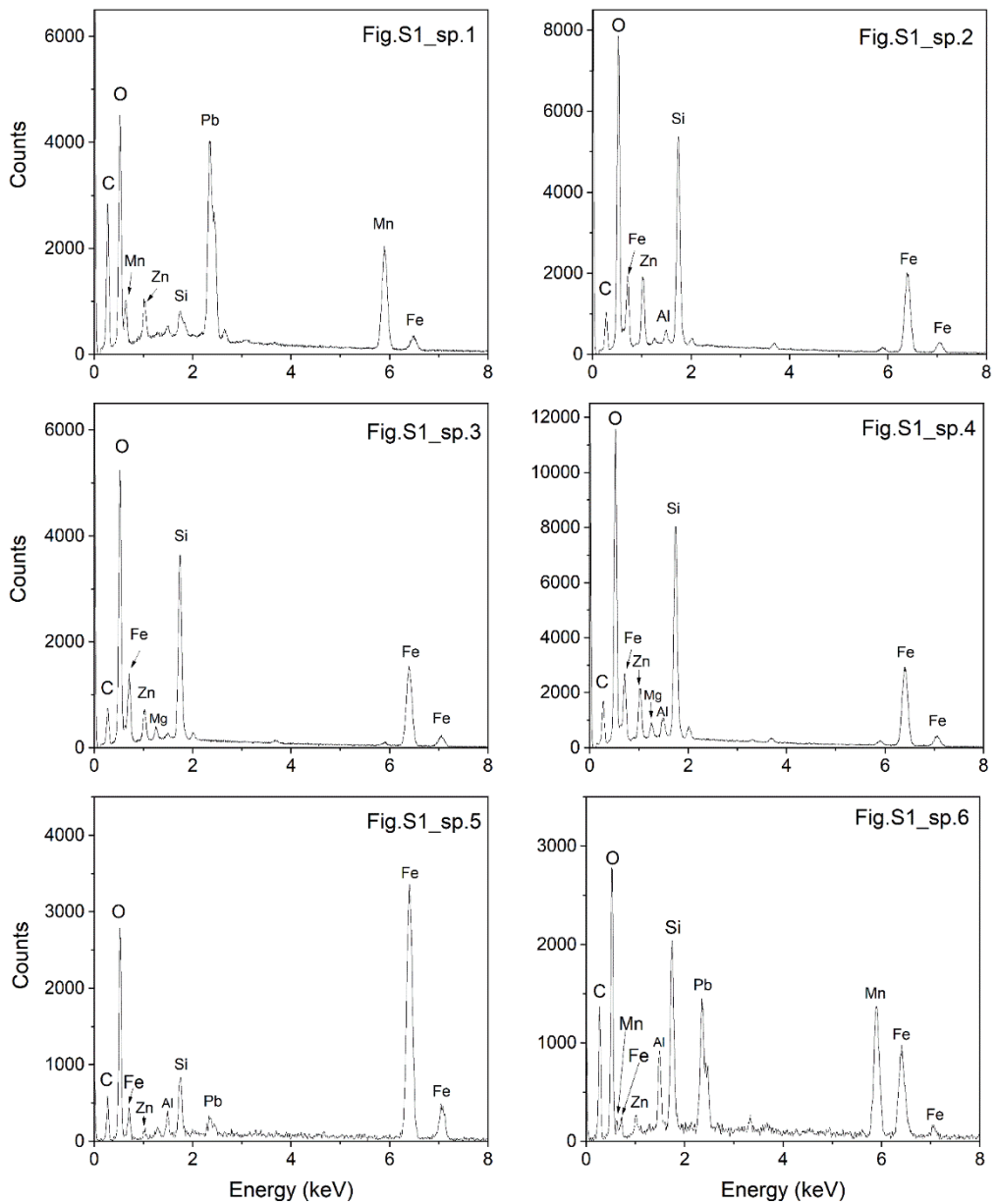
Figure S3.6: *Spectra from the EDS analysis of selected points in control soil samples (Fig. S3.1).*
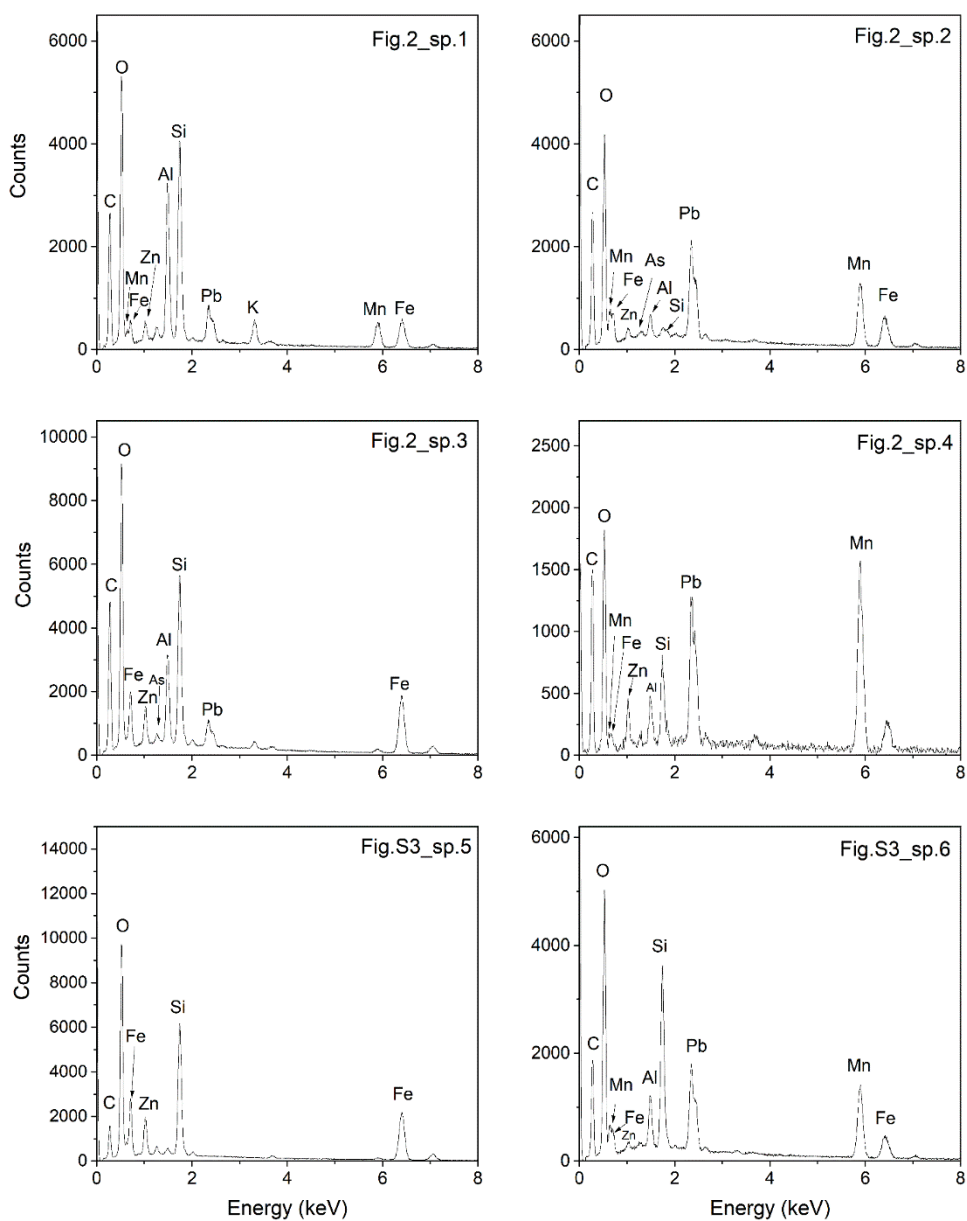
Figure S3.7: *Spectra from the EDS analysis of selected points in BC-treated soil samples (Fig. S3.3).*
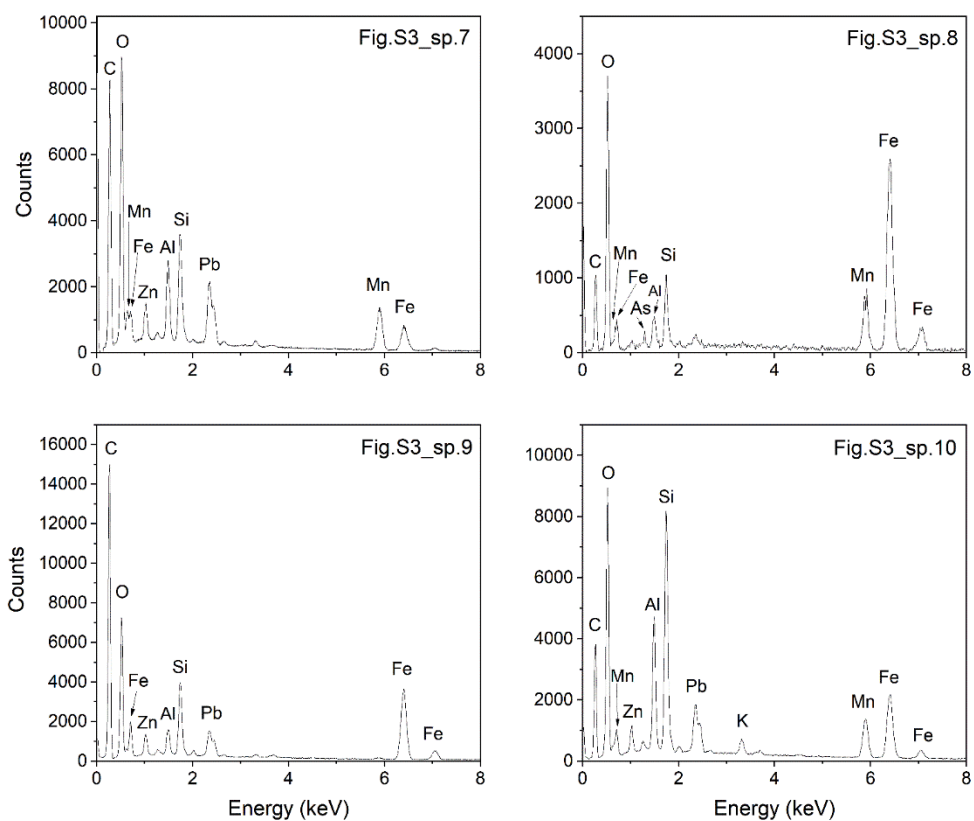
Figure S3.7: Spectra from the EDS analysis of selected points in BC-treated soil samples (Fig. S3.4) (continuation).
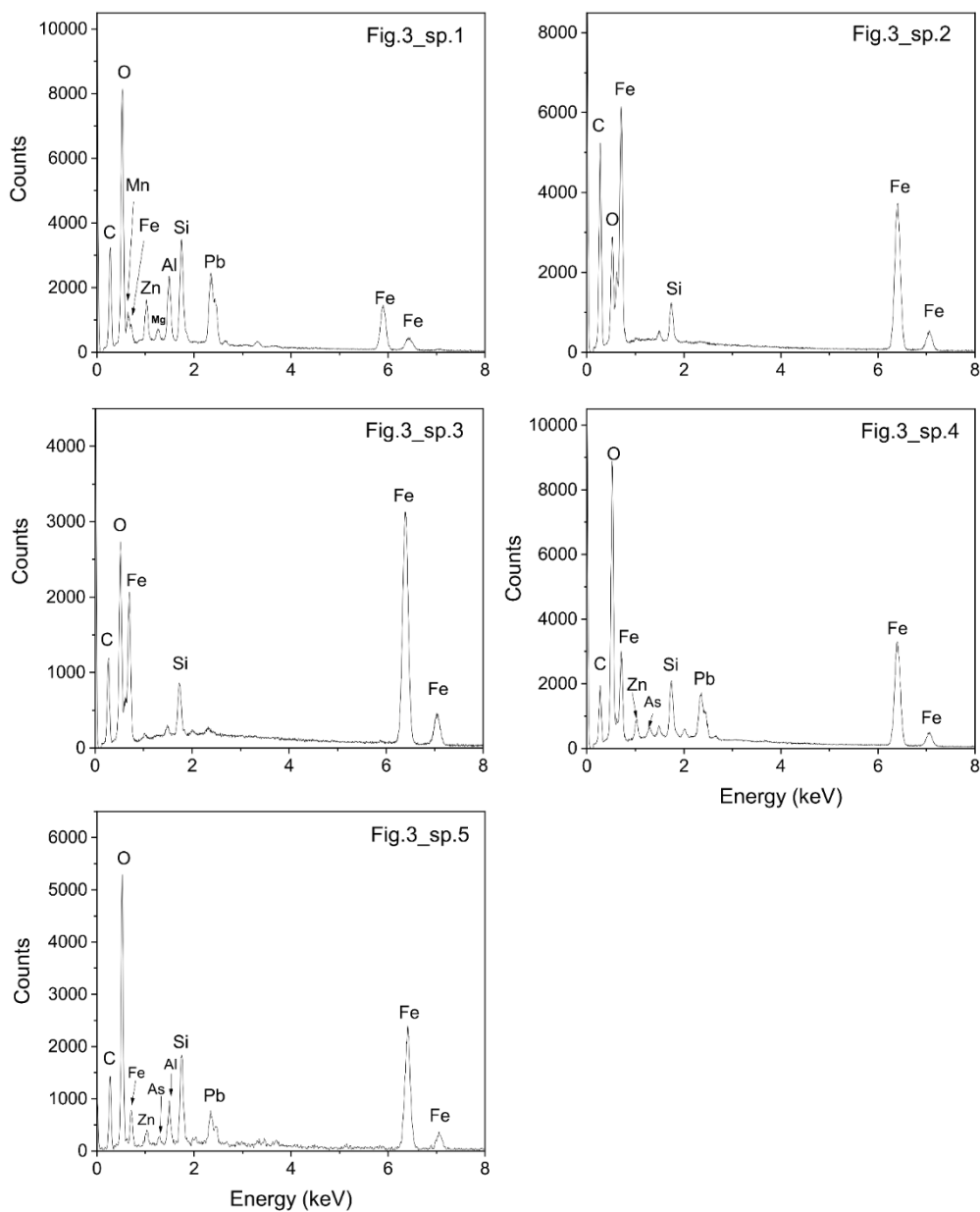
Figure S3.8: Spectra from the EDS analysis of selected points in nZVI-treated soil samples 9Fig. S3.5).
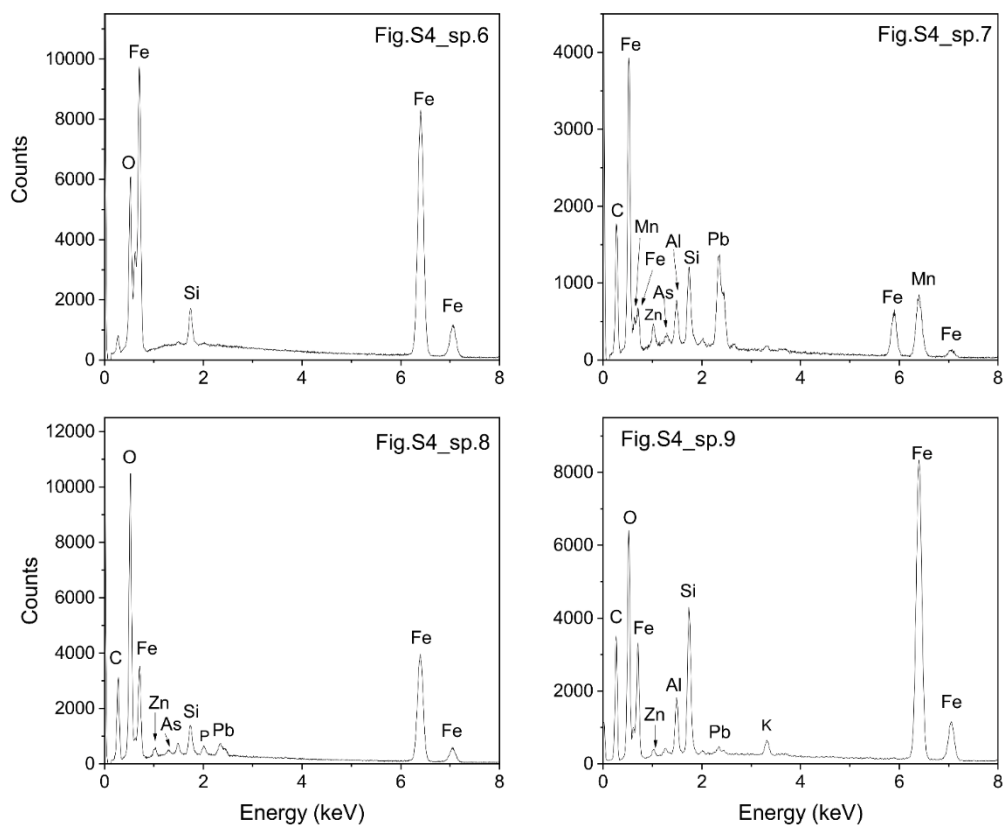
Figure S3.8: *Spectra from the EDS analysis of selected points in nZVI-treated soil samples (Fig. S3.5) (continuation).*
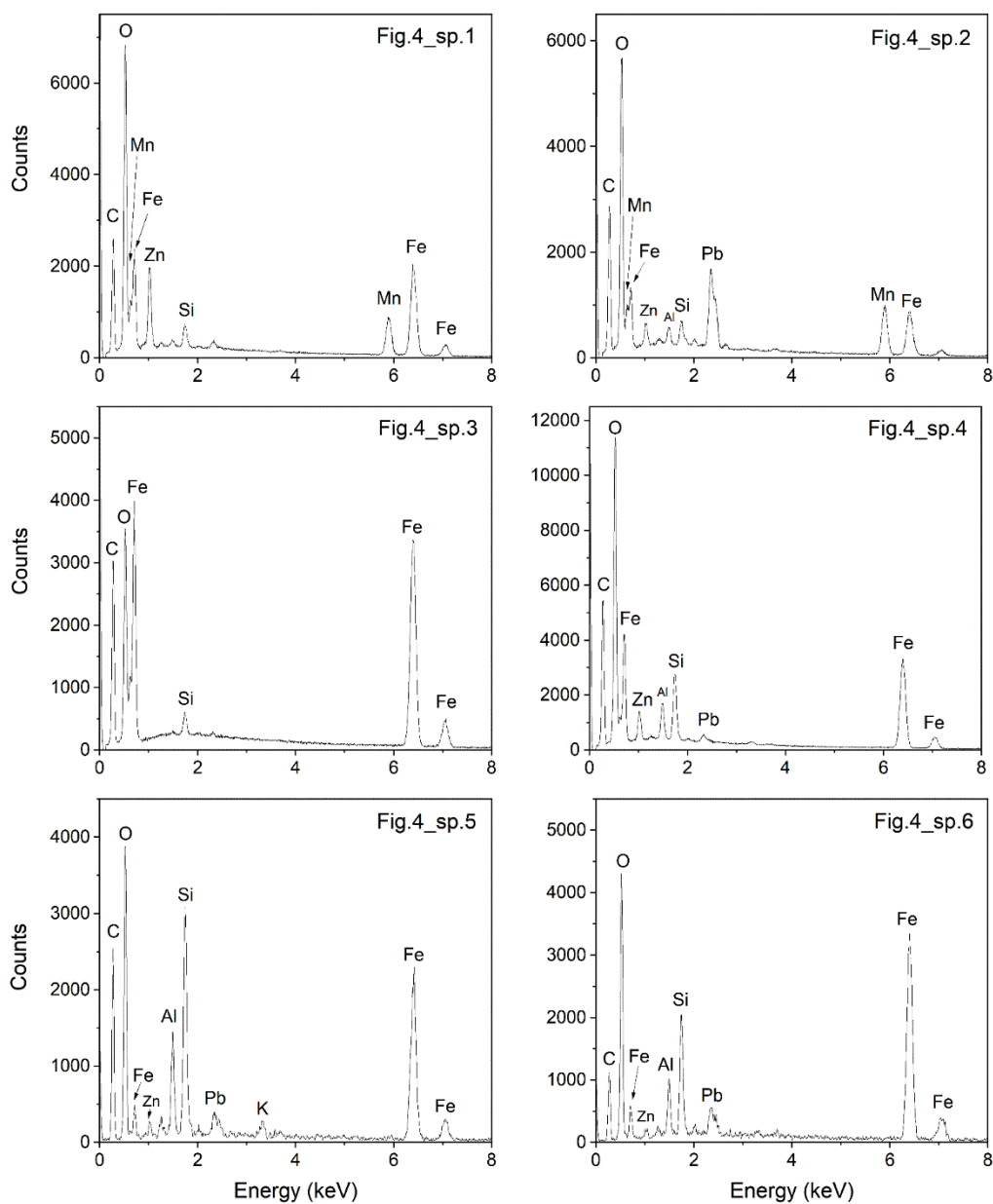
Figure S3.9: *Spectra from the EDS analysis of selected points in nZVI-BC-treated soil samples (Fig. S3.6).*
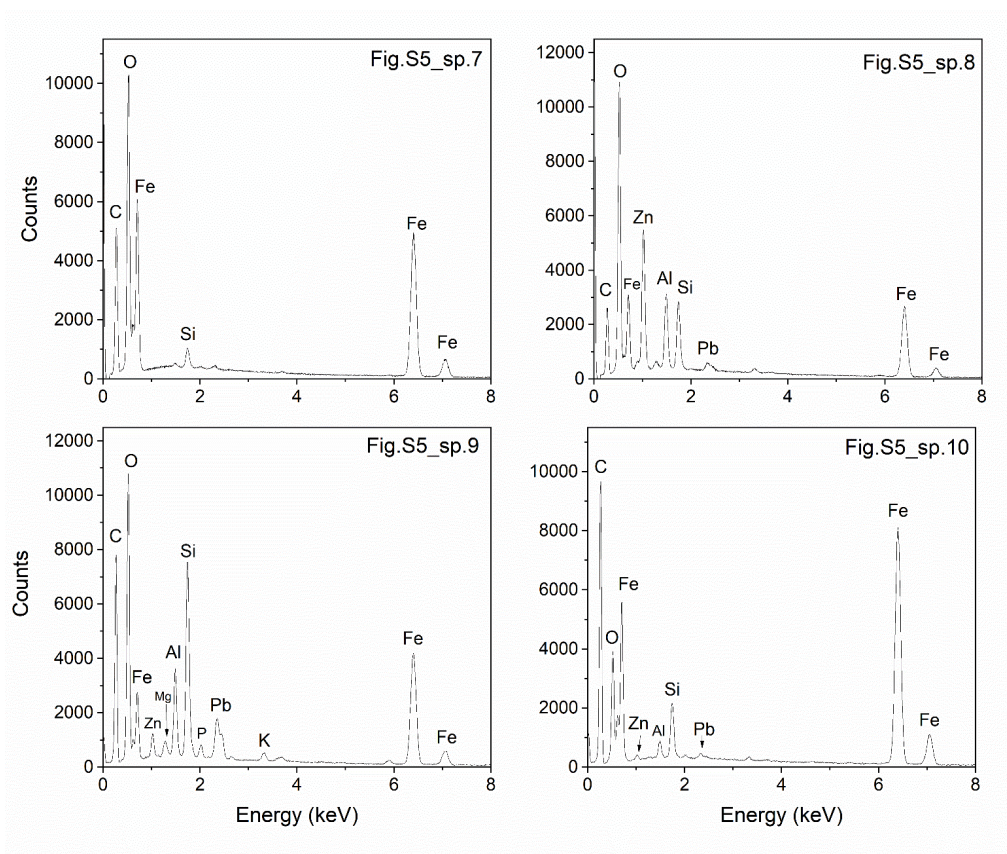
Figure S3.9: *Spectra from the EDS analysis of selected points in nZVI-BC-treated soil samples (Fig. S3.6) (continuation).*
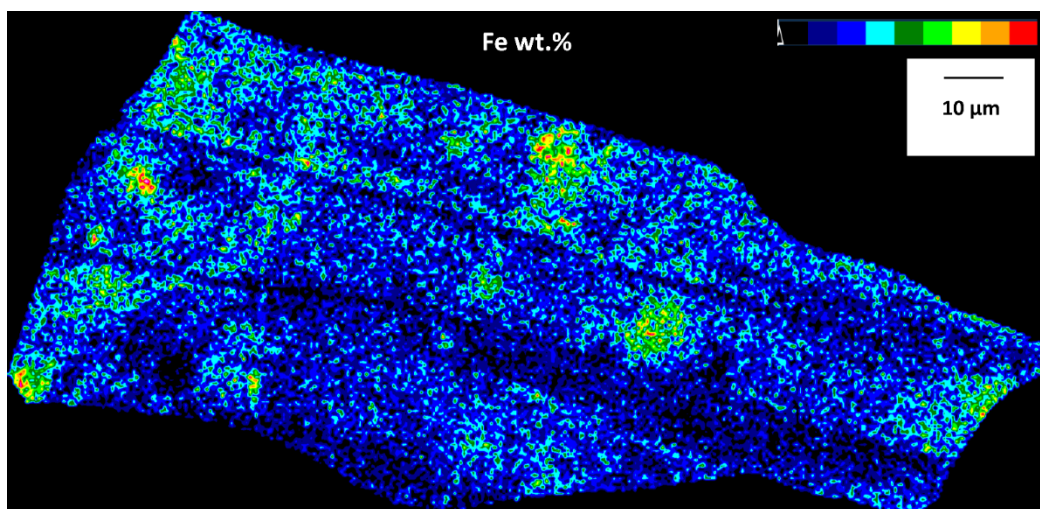
Figure S3.10: *Fe distribution on the BC particle of Fig. 3.4D.*

During the analysis of the 15-month incubated samples, the EDS chemical composition of the particles was used to determine the different classes presented in Table S3.1. According to these classes, ternary diagrams were prepared to examine the relationships between the studied contaminants and metal(loid) scavengers (i.e. Fe/Mn/Al oxides).

Table S3.1: Description of the established classes used during SEM/EDS analysis to check the combined affinity of risk elements to Fe and Mn mineral phases.

Element	Minimum value (wt.%)	Maximum value (wt.%)	Class
Pb	10	100	
Mn	0	10	
Si	0	6	▬ 1
Zn	0	100	
Fe	20	100	
Si	0	6	▬ 2
As	0	100	
Fe	0	100	▬ 3
Fe	20	100	
Pb	0	100	▬ 4
Cd	0	100	▬ 5
Sb	0	100	▬ 6
Pb	0	100	
Zn	0	100	
Fe	15	100	▬ 7
No classification			▬
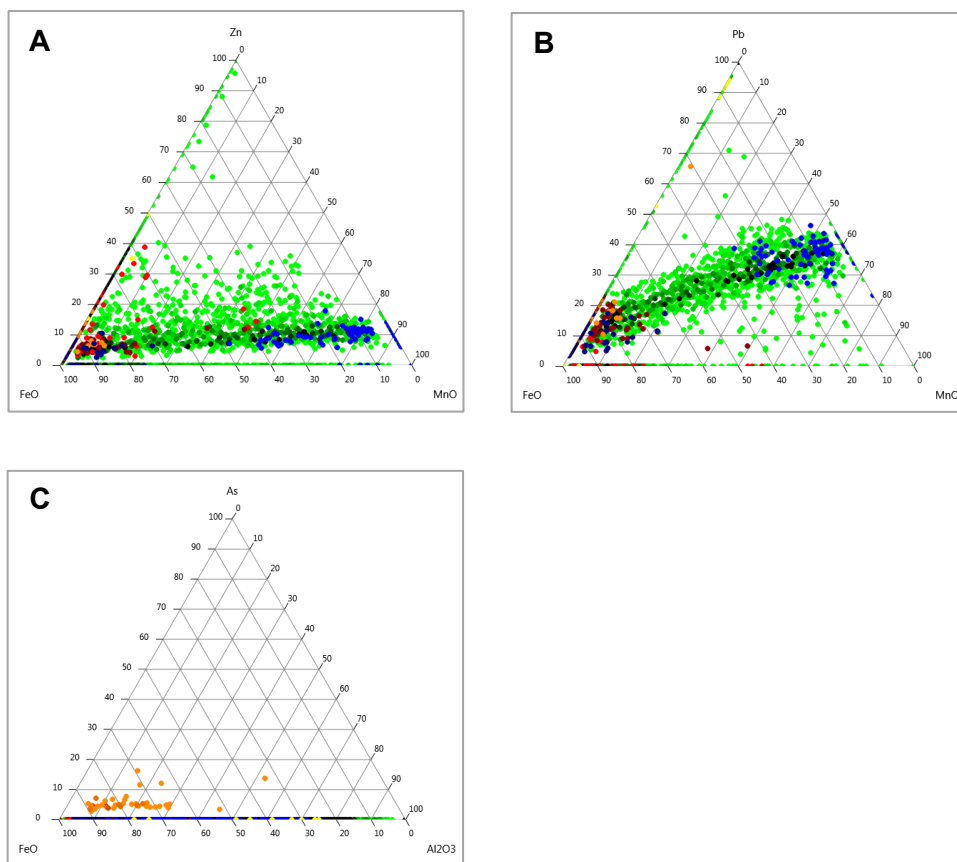
Figure S3.11: *Ternary plots presenting combinations of A) Zn and Fe/ Mn oxides B) Pb and Fe/ Mn oxides and C) As and Fe/Al oxides in the control soil samples.*
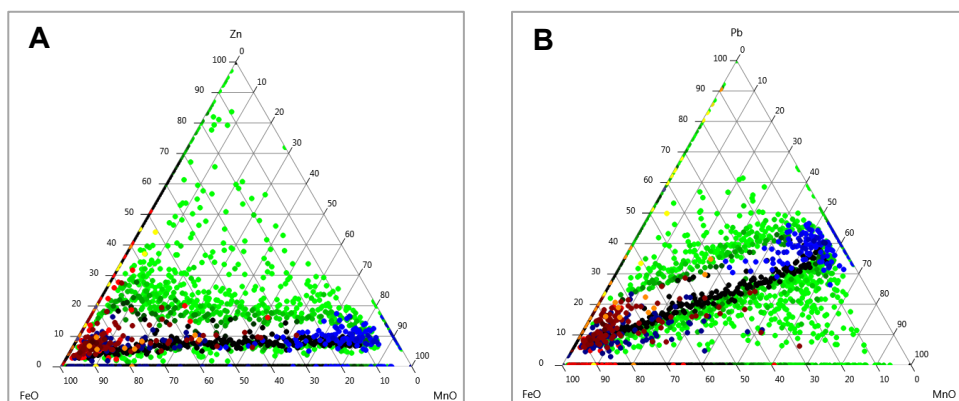
Figure S3.12: *Ternary plots presenting combinations of A) Zn and Fe/ Mn oxides and B) Pb and Fe/ Mn oxides in the BC-treated soil samples.*
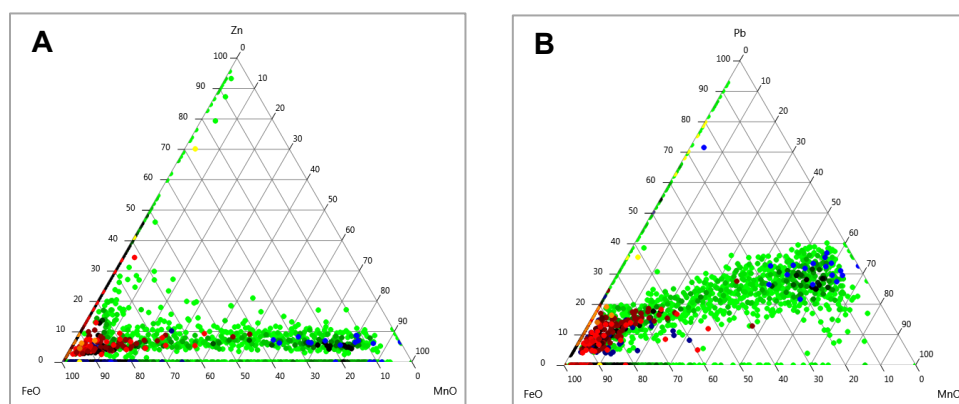
Figure S3.13: *Ternary plots presenting combinations of A) Zn and Fe/ Mn oxides and B) Pb and Fe/ Mn oxides in the nZVI-treated soil samples.*
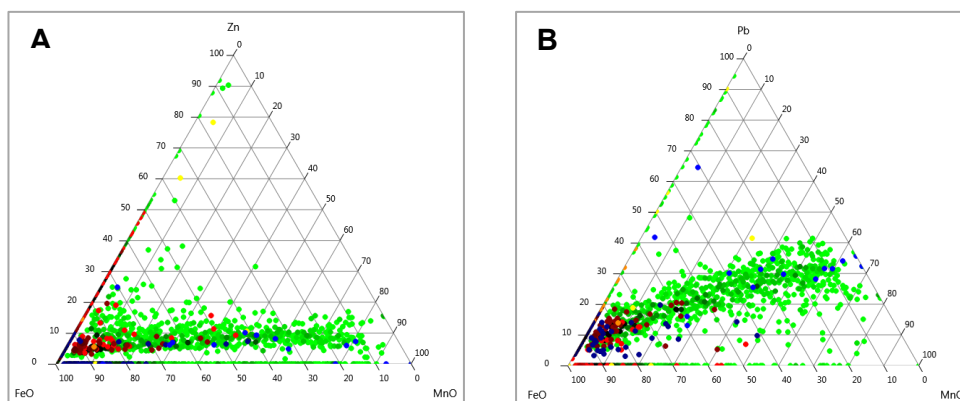
Figure S3.14: *Ternary plots presenting combinations of A) Zn and Fe/ Mn oxides and B) Pb and Fe/ Mn oxides in the nZVI-BC-treated soil samples.*
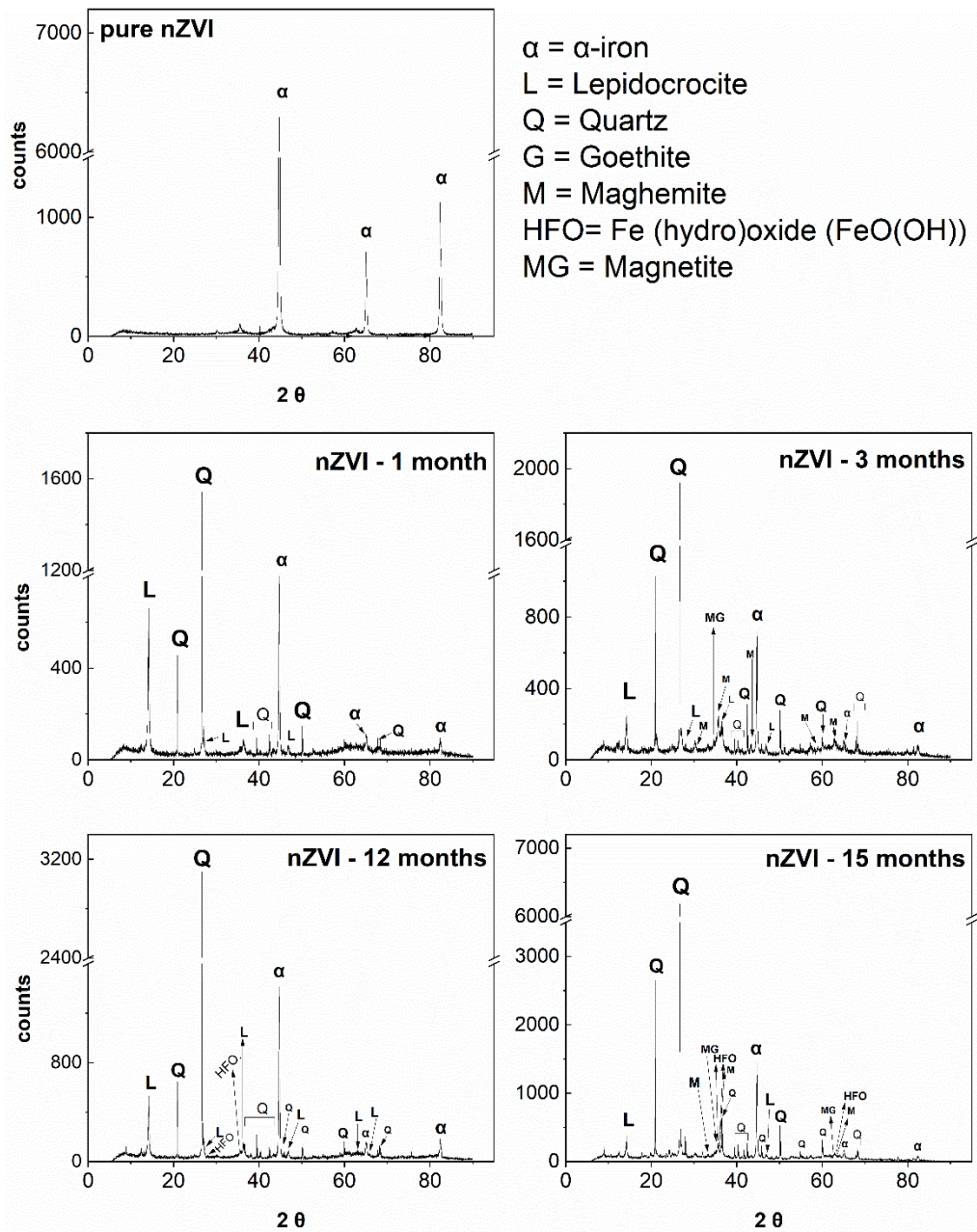
Figure S3.15A: Diffractograms derived from the XRD analysis of the sorbent layer of nZVI after different incubation time
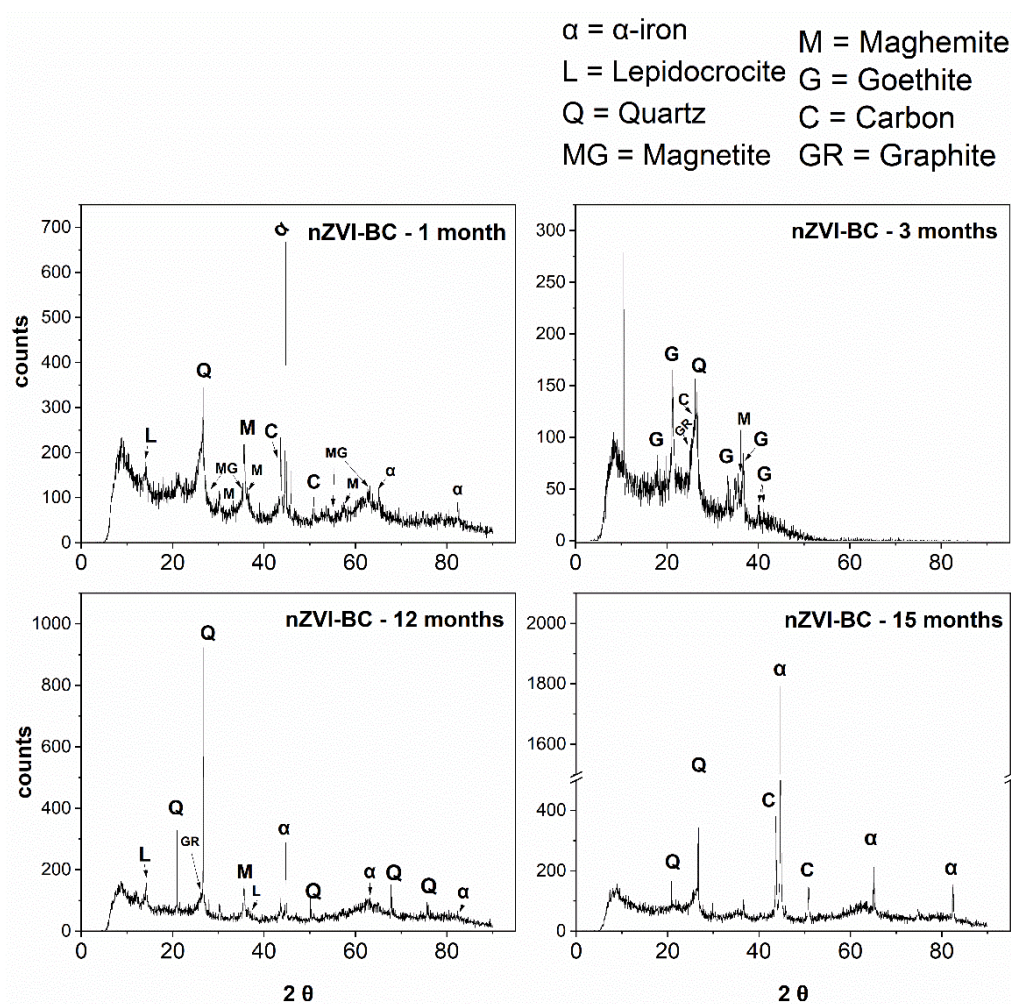
Figure S3.15B: *Diffractograms derived from the XRD analysis of the sorbent layer of nZVI-BC after different incubation time.*
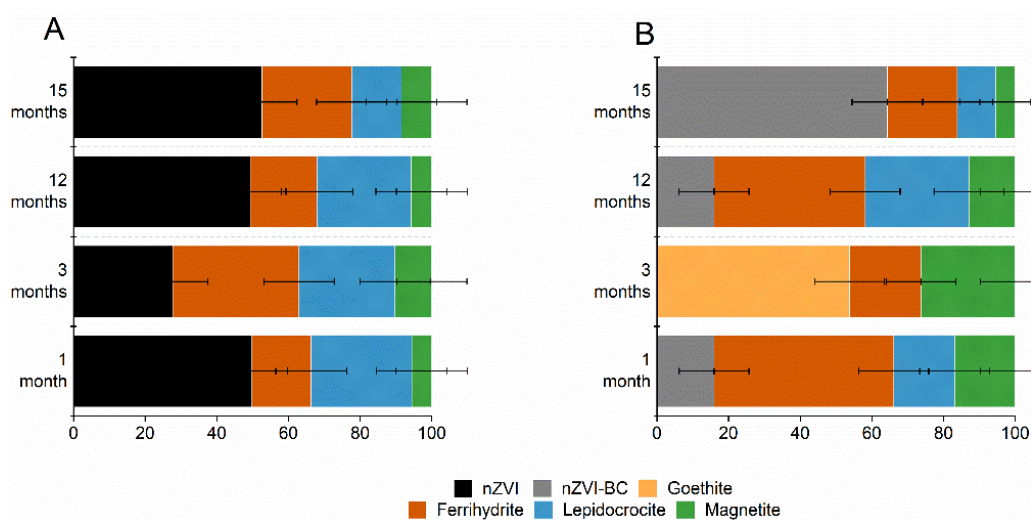
Figure S3.16: *Proportional Fe solid speciation based on Fe K-edge XANES spectra for the sorbent layers of A) nZVI and B) nZVI-BC from the different incubation time steps.*

Table S3.2: *Values used for the calculation of proportions of the most abundant phases according to XANES. The Fe0 oxidation rate of Fig. 3.7C is calculated from the sum of the Fe (oxyhydr)oxides of each sample*.

sample	R factor	nZVI weight	Lepidocrocite weight	Ferrihydrite weight	Magnetite weight
nZVI 1 month	0.00034	0.50	0.28	0.17	0.06
nZVI 3 months	0.00010	0.28	0.27	0.36	0.10
nZVI 12 months	0.00030	0.50	0.27	0.19	0.06
nZVI 15 months	0.00006	0.54	0.14	0.26	0.09

	R factor	nZVI-BC weight	Lepidocrocite weight	Ferrihydrite weight	Goethite weight	Magnetite weight
nZVI-BC 1 month	0.00006	0.16	0.17	0.51		0.17
nZVI-BC 3 months	0.00010			0.20	0.55	0.27
nZVI-BC 12 months	0.00013	0.16	0.30	0.43		0.13
nZVI-BC 15 months	0.00009	0.65	0.11	0.20		0.06

	R factor	Montmorillonite weight	Muscovite weight	Haematite weight	Goethite weight	Magnetite weight
Control soil average	0.00011	0.20	0.14	0.22	0.25	0.18

	R factor	Control weight	nZVI weight
nZVI mix 1 month	0.00022	0.91	0.09
nZVI mix 3 months	0.00111	0.90	0.10
nZVI mix 12 months	0.00025	0.98	0.02
nZVI mix 15 months	0.00064	0.96	0.04

	R factor	Control weight	nZVI-BC weight
nZVI-BC mix 1 month	0.00028	0.98	0.02
nZVI-BC mix 3 months	0.00101	0.92	0.08
nZVI-BC mix 12 months	0.00010	0.95	0.05
nZVI-BC mix 15 months	0.00005	0.97	0.03

Table S3.3a: Correlation matrices of soil extraction data based on the Pearson coefficient.

1 month	Zn	Pb	pH	Eh	Fe	Mn	DOC		
Zn		0.60	-0.86	0.79	-0.57	-0.96	0.03		
Pb	0.60		-0.12	0.03	0.11	-0.73	0.81		
pH	-0.86	-0.12		-0.99	0.65	0.69	0.42		
Eh	0.79	0.03	-0.99		-0.59	-0.59	-0.47		
Fe	-0.57	0.11	0.65	-0.59		0.55	0.63		
Mn	-0.96	-0.73	0.69	-0.59	0.55		-0.20		
DOC	0.03	0.81	0.42	-0.47	0.63	-0.20			
3 months	**Zn**	**Pb**	**As**	**Cd**	**pH**	**Eh**	**Fe**	**Mn**	**DOC**
Zn		0.36	0.59	0.98	-0.88	0.48	-0.82	-0.73	-0.63
Pb	0.36		0.91	0.19	-0.73	0.53	-0.57	-0.84	0.10
As	0.59	0.91		0.47	-0.80	0.82	-0.54	-0.80	0.11
Cd	0.98	0.19	0.47		-0.78	0.46	-0.72	-0.58	-0.64
pH	-0.88	-0.73	-0.80	-0.78		-0.47	0.93	0.96	0.50
Eh	0.48	0.53	0.82	0.46	-0.47		-0.12	-0.35	0.38
Fe	-0.82	-0.57	-0.54	-0.72	0.93	-0.12		0.92	0.75
Mn	-0.73	-0.84	-0.80	-0.58	0.96	-0.35	0.92		0.44
DOC	-0.63	0.10	0.11	-0.64	0.50	0.38	0.75	0.44	
12 months	**Zn**	**Pb**	**As**	**Cd**	**pH**	**Eh**	**Fe**	**Mn**	**DOC**
Zn		-0.08	-0.09	0.94	-0.43	-0.98	-0.13	0.26	-0.69
Pb	-0.08		1.00	-0.39	0.93	-0.13	0.99	-0.79	0.20
As	-0.09	1.00		-0.40	0.93	-0.12	1.00	-0.78	0.19
Cd	0.94	-0.39	-0.40		-0.70	-0.85	-0.43	0.56	-0.78
pH	-0.43	0.93	0.93	-0.70		0.23	0.93	-0.86	0.49
Eh	-0.98	-0.13	-0.12	-0.85	0.23		-0.07	-0.06	0.61
Fe	-0.13	0.99	1.00	-0.43	0.93	-0.07		-0.74	0.16
Mn	0.26	-0.79	-0.78	0.56	-0.86	-0.06	-0.74		-0.70
DOC	-0.69	0.20	0.19	-0.78	0.49	0.61	0.16	-0.70	
15 months	**Zn**	**Pb**	**As**	**Cd**	**pH**	**Eh**	**Fe**	**Mn**	**DOC**
Zn		-0.02	0.20	0.97	-0.59	0.26	-0.80	0.44	-0.65
Pb	-0.02		0.98	-0.22	0.11	-0.08	-0.57	-0.88	0.75
As	0.20	0.98		-0.01	-0.01	-0.02	-0.73	-0.76	0.60
Cd	0.97	-0.22	-0.01		-0.47	0.13	-0.67	0.58	-0.76
pH	-0.59	0.11	-0.01	-0.47		-0.93	0.30	-0.52	0.58
Eh	0.26	-0.08	-0.02	0.13	-0.93		-0.04	0.39	-0.37
Fe	-0.80	-0.57	-0.73	-0.67	0.30	-0.04		0.18	0.07
Mn	0.44	-0.88	-0.76	0.58	-0.52	0.39	0.18		-0.97
DOC	-0.65	0.75	0.60	-0.76	0.58	-0.37	0.07	-0.97	

Significant ($p < 0.05$) correlations are represented by red coloured numbers

Table S3.3b: *Correlation matrices of pore water data based on the Pearson coefficient*

3 months	Zn	Pb	Cd	pH	Eh	Fe	Mn	DOC
Zn		0.45	0.46	-0.91	0.35	0.11	-0.51	0.14
Pb	0.45		0.94	-0.98	0.23	0.43	-0.63	0.39
Cd	0.46	0.94		-0.86	0.07	0.55	-0.53	0.39
pH	-0.91	-0.98	-0.86		-0.50	-0.23	0.50	-0.41
Eh	0.35	0.23	0.07	-0.50		-0.37	-0.03	0.30
Fe	0.11	0.43	0.55	-0.23	-0.37		-0.09	-0.47
Mn	-0.51	-0.63	-0.53	0.50	-0.03	-0.09		-0.12
DOC	0.14	0.39	0.39	-0.41	0.30	-0.47	-0.12	
15 months	Zn	Pb	Cd	pH	Eh	Fe	Mn	DOC
Zn		0.88	0.98	-0.37	0.07	0.47	0.43	-0.11
Pb	0.88		0.83	-0.59	0.21	0.75	0.24	-0.02
Cd	0.98	0.83		-0.27	-0.01	0.46	0.54	-0.15
pH	-0.37	-0.59	-0.27		-0.58	-0.61	0.25	-0.29
Eh	0.07	0.21	-0.01	-0.58		0.41	-0.22	0.14
Fe	0.47	0.75	0.46	-0.61	0.41		0.02	0.11
Mn	0.43	0.24	0.54	0.25	-0.22	0.02		-0.52
DOC	-0.11	-0.02	-0.15	-0.29	0.14	0.11	-0.52	

Significant (p<0.05) correlations are represented by red coloured numbers
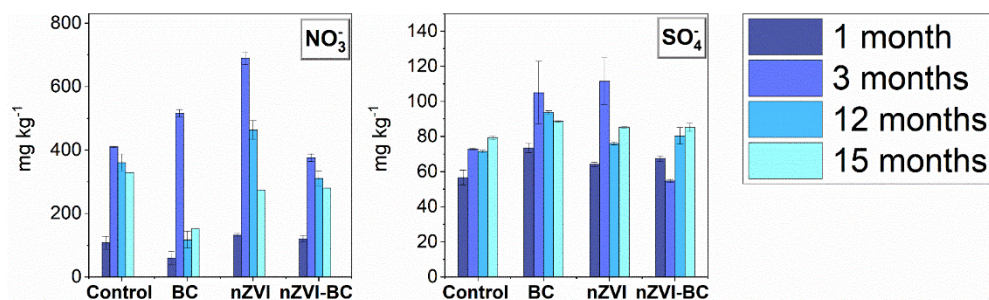
Figure S3.17: *Concentrations of NO-3 and SO-4 in the soil H2O extracts after 1, 3, 12 & 15 months of incubation.*
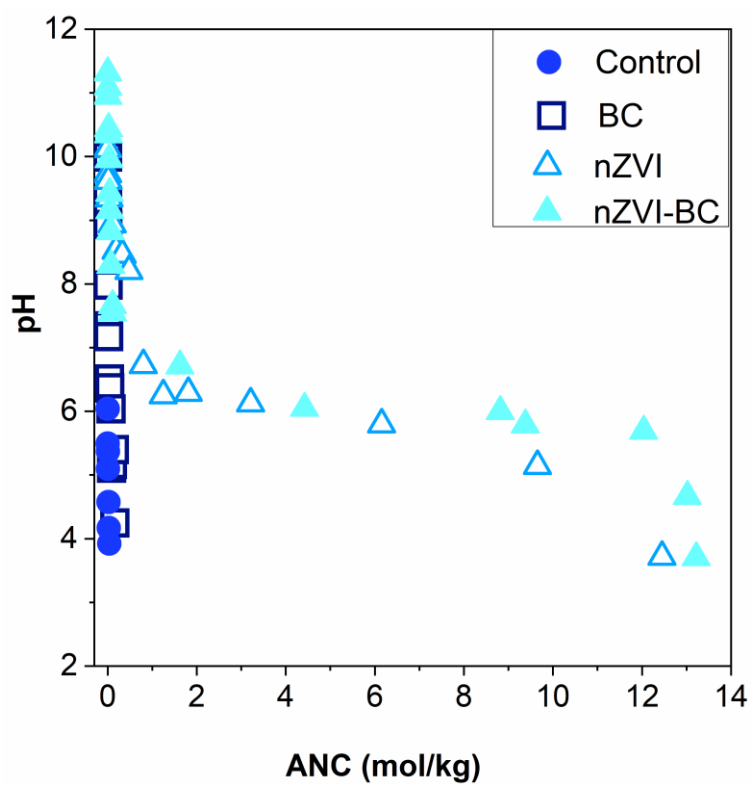
Figure S3.18: The acid neutralisation capacity (ANC) of the studied treatments and control soil (n=2).

Table S3.4 Speciation of Cd, Pb and Zn in the pore water samples as calculated by the PHREEQC-3 geochemical code

	15 months				3 months			
	nZVI-BC	nZVI	BC	Control	nZVI-BC	nZVI	BC	Control
pH	5.76	5.69	5.69	5.50	5.78	5.82	5.25	5.05
Cd^{2+}	95%	94%	96%	94%	96%	97%	97%	95%
$CdNO_3^+$	5%	6%	4%	6%	4%	3%	3%	5%
Pb^{2+}	69%	69%	77%	70%	75%	78%	82%	77%
$PbNO_3^+$	23%	26%	19%	27%	19%	14%	14%	21%
$PbHCO_3^+$	8%	4%	4%	3%	7%	7%	3%	1%
Zn^{2+}	97%	98%	96%	98%	97%	98%	96%	99%
$ZnSO_4$	1%	1%	3%	2%	1%	1%	3%	1%
$ZnHCO_3^+$	2%	1%	1%	1%	1%	2%	1%	0%

Table S3.5 Saturation indices of selected phases found in the pore water as calculated by the PHREEQC-3 geochemical code.

	15 months				3 months					Formula
	nZVI-BC	nZVI	BC	Control	nZVI-BC	nZVI	BC	Control		
Gibbsite	**1.73**	**1.78**	**1.86**	**1.23**	–	–	–	**1.17**	Gibbsite	$Al(OH)_3$
Jurbanite	-2.47	-2.35	-1.80	-2.27	–	–	–	-1.63	Jurbanite	$Al(SO_4)(OH) \cdot 5H_2O$
Otavite	-1.39	-1.67	-1.80	-1.86	-1.93	-2.21	-2.74	-2.82	Otavite	$CdCO_3$
Fe(OH)3	-0.33	-0.40	-0.39	**0.24**	**0.39**	**0.37**	-0.40	-0.10	$Fe(OH)_3$	$Fe(OH)_3$
Fe3(OH)8	-7.97	-8.25	-8.23	-6.31	-5.03	-5.08	-6.98	-6.31	$Fe_3(OH)_8$	$Fe_3(OH)_8$
Jarosite	-2.40	-1.57	-2.54	-1.82	-3.70	-4.56	-3.68	-4.54	Jarosite	$KFe^{3+}_3(SO_4)_2(OH)_6$
Rhodochrosite	-1.29	-0.98	-3.54	-1.54	-0.11	-0.12	-1.47	-1.91	Rhodochrosite	$MnCO_3$
Anglesite	-3.20	-3.08	-2.57	-2.61	-2.84	-2.89	-2.01	-2.24	Anglesite	$PbSO_4$
Cerussite	-2.00	-2.15	-2.18	-2.23	-1.77	-1.59	-2.26	-2.52	Cerussite	$PbCO_3$
Pb(OH)2	-3.60	-3.55	-3.51	-3.70	-3.20	-2.97	-3.84	-4.04	$Pb(OH)_2$	$Pb(OH)_2$
Smithsonite	-1.23	-1.53	-1.60	-1.63	-2.01	-2.43	-2.63	-2.65	Smithsonite	$ZnCO_3$

Saturation indices in the interval <-1.5 - 1.5> are highlighted with grey background, values >0 are given in bold.

Table S3.6 Speciation of Cd, Pb and Zn in the soil extracts as calculated by the PHREEQC-3 geochemical code.

	15 months				12 months				3 months				1 month			
	nZVI-BC	nZVI	BC	Control	nZVI-BC	nZVI	BC	Control	nZVI-BC	nZVI	BC	Control	nZVI-BC	nZVI	BC	Control
pH	5.62	5.53	5.55	5.51	5.73	5.56	5.92	5.74	5.28	5.30	5.92	5.36	6.35	6.24	6.20	5.80
Cd^{2+}	–	–	–	100%	100%	100%	100%	100%	100%	100%	100%	100%	–	–	–	–
Pb^{2+}	91%	92%	90%	95%	72%	81%	59%	70%	97%	97%	90%	95%	37%	43%	38%	69%
$PbCO_3^0$	3%	2%	3%	1%	10%	5%	19%	10%	0%	0%	5%	1%	43%	36%	38%	12%
$PbHCO_3^+$	6%	6%	8%	4%	18%	14%	23%	19%	2%	2%	6%	4%	19%	21%	24%	19%
Zn^{2+}	98%	98%	98%	98%	95%	97%	93%	95%	99%	98%	98%	98%	92%	92%	90%	95%
$ZnHCO_3^+$	1%	1%	1%	1%	4%	3%	6%	4%	0%	0%	1%	1%	8%	7%	9%	4%
$ZnSO_4^0$	1%	1%	1%	1%	1%	1%	1%	1%	1%	1%	1%	1%	1%	1%	1%	1%

Table S3.7 Saturation indices of selected phases found in the soil extracts as calculated by the PHREEQC-3 geochemical code

	15 months				12 months				3 months				1 month					Formula
	nZVI-BC	nZVI	BC	Control	nZVI-BC	nZVI	BC	Control	nZVI-BC	nZVI	BC	Control	nZVI-BC	nZVI	BC	Control		
	0.19	**0.01**	**0.24**	**0.21**	**0.62**	**0.05**	**1.05**	**0.88**	-0.13	-0.13	**0.70**	-0.06	**1.51**	**1.30**	**1.58**	**1.11**	Gibbsite	$Al(OH)_3$
	-1.28	-1.28	-1.06	-1.03	-1.10	-1.36	-0.97	-0.87	-1.13	-0.90	-1.31	-1.05	-1.52	-1.52	-1.11	-0.84	Jurbanite	$Al(SO_4)(OH) \cdot 5H_2O$
	–	–	–	-3.07	-2.48	-2.83	-2.11	-2.19	-3.85	-3.66	-3.19	-3.45	–	–	–	–	Otavite	$CdCO_3$
	1.88	**1.91**	**1.86**	**1.76**	**2.02**	**1.65**	**2.34**	**2.11**	**1.66**	**1.65**	**2.52**	**1.54**	**2.95**	**3.00**	**2.92**	**2.40**	$Fe(OH)_3$	$Fe(OH)_3$
	-0.74	-1.15	-1.29	-1.51	-1.08	-1.86	-0.40	-0.01	-3.13	-3.07	**0.09**	-1.78	**1.17**	**1.33**	**1.16**	-0.28	$Fe_3(OH)_8$	$Fe_3(OH)_8$
	0.52	**0.85**	**0.64**	**0.60**	**0.59**	-0.19	**1.03**	**0.85**	**0.18**	**0.71**	**1.25**	-0.03	**1.04**	**1.51**	**1.60**	**1.34**	Jarosite	$KFe^{3+}_3(SO_4)_2(OH)_6$
	-3.11	-2.82	-3.39	-3.13	-2.74	-1.98	-2.60	-2.10	-3.10	-2.64	-1.16	-2.44	-0.39	-0.41	-1.30	-2.44	Rhodochrosite	$MnCO_3$
	-2.45	-2.62	-2.29	-2.30	-2.74	-3.01	-2.52	-2.56	-2.43	-2.31	-2.40	-2.32	-2.85	-2.82	-2.56	-2.47	Anglesite	$PbSO_4$
	-1.56	-1.84	-1.42	-1.75	-1.14	-1.72	-0.64	-0.90	-2.13	-2.26	-1.29	-1.86	-0.26	-0.35	-0.08	-0.67	Cerussite	$PbCO_3$
	-2.89	-3.24	-2.89	-2.98	-2.92	-3.50	-2.41	-2.72	-3.34	-3.45	-2.29	-3.24	-1.73	-1.91	-1.78	-2.43	$Pb(OH)_2$	$Pb(OH)_2$
	-3.06	-3.15	-3.05	-3.18	-2.34	-2.72	-2.02	-2.06	-3.75	-3.56	-3.30	-3.34	-1.87	-2.01	-1.62	-2.18	Smithsonite	$ZnCO_3$

Saturation indices in the interval $<-1.5 - 1.5>$ are highlighted with grey background, values >0 are given in bold.

143
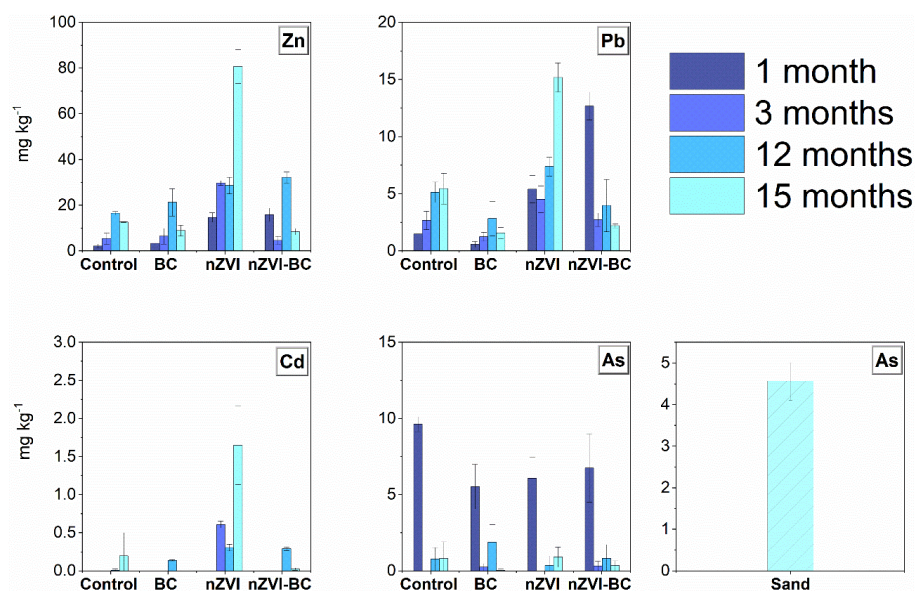
Figure S3.19: *Total concentrations of the studied risk elements in the sand layer after 1, 3, 12 & 15 months of incubation and total concentration of As in the pure sand sample.*
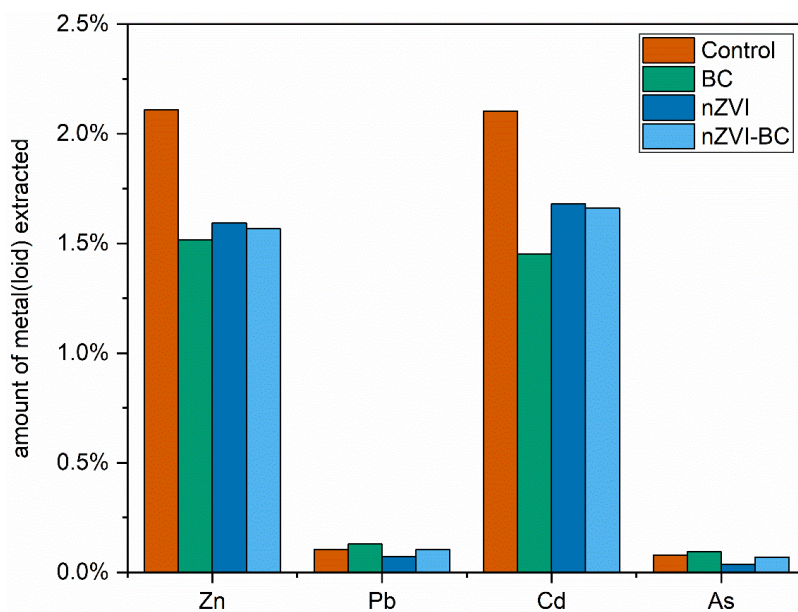
Figure S3.20: *The amount of metal(loid)s extracted by H2O extraction from the mixed soil samples after 15 months of incubation (expressed as % proportion of the total concentrations).*

Chapter IV

Pyrolysed sewage sludge for metal(loid) removal and immobilisation in contrasting soils: exploring variety of risk elements across contamination levels

Aikaterini Mitzia, Barbora Böserle Hudcová, Martina Vítková, Barbora Kunteová, Daniela Casadiego Hernandez, Jaroslav Moško, Michael Pohořelý, Alena Grasserová, Tomáš Cajthaml, Michael Komárek

Content

Abstract

Efficient treatment of sewage sludge may transform waste into stable materials with minimised hazardous properties ready for secondary use. Pyrolysed sewage sludge, sludgechar, has multiple environmental benefits including contaminant sorption capacity and nutrient recycling. The properties of five sludgechars were tested firstly for adsorption efficiency in laboratory solutions before prospective application to soils. A wide variety of metal(loid)s (As, Cd, Co, Cr, Cu, Ni, Pb, Sb, and Zn) was involved. Secondly, the sludgechars (3% v/v) were incubated in five soils differing in (multi)-metal(loid) presence and the level of contamination. The main aim was to evaluate the metal(loid) immobilisation potential of the sludgechars for soil remediation. Moreover, nutrient supply was investigated to comprehensively assess the material's benefits for soils. All sludgechars were efficient (up to 100%) for the removal of metal cations while their efficiency for metal(loid) anions was limited in aqueous solutions. Phosphates and sulphates were identified crucial for metal(loid) capture, based on SEM/EDS, XRD and MINTEQ findings. In soils, important fluctuations were observed for Zn, being partially immobilised by the sludgechars in high-Zn_{tot} soils, while partially solubilised in moderate to low-Zn_{tot} soils. Moreover, pH showed to be crucial for material stability, metal(loid) adsorption ability and their immobilisation in soils. Although metal(loid) retention was generally low in soils, nutrient enrichment was significant after sludgechar application. Long-term evaluation of the material sorption efficiency, nutrient supply, and ageing in soil environments will be necessary in future studies.

4.1 Introduction

In recent years, significant interest has been focused on the production of carbon-based materials from various waste residues, including sewage sludge, and their possible use for soil and water remediation (Wang et al., 2020). A widely used and effective technique for the preparation of such materials is pyrolysis, a thermochemical conversion of carbonaceous materials in the absence of oxygen (Rangabhashiyam et al., 2022). Numerous publications have been devoted to the production of carbon-based solid materials from pristine (plant-based) pyrolysed biomass (so-called biochar; BC), and its use as a sorbent or soil improver. Pyrolysed sewage sludge (denoted here as sludgechar; SC) can be considered a beneficial material with regard to nutrient content and direct reuse of otherwise potentially hazardous waste material (Rangabhashiyam et al., 2022; Wang et al., 2020; Zhao et al., 2023).

Sludgechars, similarly to BCs, have been intensively tested for their metal(loid) adsorption characteristics (Chen et al., 2014; Gao et al., 2019) as promising metal(loid) sorbents in water (Gopinath et al., 2021). However, its full-scale application to soil is still a matter of debate, regarding the increased risk of metal(loid)s release and plant uptake (Zhang et al., 2021). On the other hand, pyrolysis promotes conversion of mobile fractions of hazardous metal(loid)s into stable forms, which limits their possible leaching into the environment (Agrafioti et al., 2013; Cui et al., 2022). In addition, the mineral components in SCs can significantly contribute to metal(loid) retention, playing an important role in the ion exchange processes and taking part in surface complexation by providing a specific interface for further metal(loid)-solid phase interactions (Shen et al., 2018). In particular, the abundance of Fe or Al minerals may greatly increase the SC sorption ability, since sludge-derived BCs have much higher mineral content compared to plant-derived BCs (Shen et al., 2018; Xu et al., 2017). It can be advantageous especially for the capture of metal(loid) anions, since carbonaceous sorbents themselves have negatively charged surface over a wide pH range, thus limiting anion sorption (Fu et al., 2023). Generally, the ash content may significantly affect the SC sorption properties as well as increase soil fertility (Fan et al., 2020). Although metal(loid) immobilisation by SC in soil has been already documented (He et al., 2019; Rashid et al., 2022), the number of studies dealing with SC behaviour in contrasting soil types and various contaminants is still limited (Álvarez-Rogel et al., 2018; Khan et al., 2023). Yet, it is crucial, because robust datasets may

provide key answers in decision-making about the use of sludge for soil remediation or reclamation of contaminated or degraded soils. As such, it represents sustainable solution to the waste disposal issues and the need for soil quality improvement (Khan et al., 2023).

In this context, we aimed to assess the potential of five different SCs for metal(loid) immobilisation in five contrasting soils differing in risk metal(loid) type and concentration levels, pH, and current land-use. We hypothesise that SC is a stable material with low risk of metal(loid) leachability but with high potential for remediation of various soil types and contaminants. Different sludge sources were selected to verify our hypothesis on a representative sample. Furthermore, one of the SC has been certified as soil improver and after proper testing in a small-scale, it will be ready to be produced in an industrial scale for field use. Therefore, the SCs efficiency for metal(loid) retention was investigated under different experimental (pH, adsorption time) and environmental conditions (soil pH, metal(loid) presence or co-existence and concentration level). Considering the importance of solid-phase stability when waste-derived amendments are applied to the environment, our study combines detailed characterisation of SCs from chemical and mineralogical points of view and material stability testing (leachability of potentially hazardous components). To achieve the main objective, 1) time-dependent adsorption efficiency was tested towards a wide range of metal(loid)s at different pH values, followed by 2) the investigation of metal(loid) behaviour after the application of SCs in contrasting metal(loid)-contaminated soils. Only such a comprehensive study of the material's behaviour in different soil conditions can help evaluate the application potential of SCs and their subsequent safe use in remediation technologies.

4.2 Materials and methods

4.2.1 Preparation of sludgechars

Five sludges were selected originating from different wastewater treatment plants (WWTPs) in the Czech Republic, differing in size, technology, location, and the presence of industry (Table S4.1). The technologies include mechanical-biological wastewater treatment with/without tertiary treatment and with/without sludge stabilisation. Due to existing non-disclosure

agreements with the WWTPs that provided us with the studied sludges, information regarding the exact locations and specific treatment technologies of each WWTP remains confidential. The five sludges reflect the industrial and population dynamics covering large, medium, and small population areas. Individual sludges were air-dried and subsequently pyrolysed at a final temperature of 600–650 °C per each sludge in an inert nitrogen atmosphere using forced evacuation (fan) of primary pyrolysis products (condensate and gas). The range indicates the inevitable fluctuations in temperature during the process. Temperature increase was 10 °C/min and the residence time of the material at the final temperature was until the end of the development of primary pyrolysis products (90–120 min). These conditions were used based to our previous findings (Moško et al., 2021b) to achieve the required sludge properties. One of the studied SCs is produced in industrial scale and has been certified as soil improver according to the *Central Institute for Supervising and Testing in Agriculture* of the Czech Republic (ÚKZÚZ). The sewage sludge treatment methodology that was used (Pohořelý et al., 2023) is currently a verified technology to process sewage sludge and produce biochar without organic pollutants. However, for the certified and the rest of the SCs additional characterisation was necessary to assess their environmental safety before further field applications. The five studied sludgechars were denoted as SC1, SC2, SC3, SC4, and SC5 in this study.

4.2.2 Characterisation of sludgechars

The basic physical and chemical properties of the SCs were determined using ČSN EN ISO 21656 (ash content; A), ČSN EN ISO 22167 (volatile content; V), a Flash EA 1112 Series CHNS/O Analyser (Thermo Finnigan; elemental analysis), and IKA C 2000 calorimeter (IKA-Werke GmbH & Co; Higher heating value and Lower heating value, HHV/LHV). The specific surface area (S_{BET}) was determined by the standard Brunauer–Emmett–Teller (BET) procedure, i.e. nitrogen physisorption measurements at 77 K (ASAP 2050; Micromeritics). Sludgechar pH was measured in deionised water (pH_{H2O}), 1 M KCl (pH_{KCl}), and 0.01 M $CaCl_2$ (pH_{CaCl2}) in individual suspensions at a ratio of 1:5 w/v (ISO 10390:2005). Cation exchange capacity (CEC) was determined using 0.1 M $BaCl_2$ at a solid/liquid ratio (S/L) of 1/60 (Carter and Gregorich, 2007). Total elemental composition of individual SCs (and input raw sewage sludges) was determined by inductively coupled plasma atomic emission spectroscopy (ICP

OES; Thermo Scientific iCAP 7000) and/or inductively coupled plasma mass spectrometry (ICP MS; Thermo Scientific iCAP Q) methods after microwave decomposition according to EPA 3051A (2007). Micropollutant analyses were done according to previously published methods (Innemanová et al., 2022; Semerád et al., 2020).

Briefly, both sludgechar and sewage sludge materials were extracted for pharmaceuticals and personal care products (PPCPs), endocrine disruptors (EDs), and per/poly-fluorinated compounds (PFCs) by Accelerated Solvent Extractor ASE 200 (Dionex; Plaiseaut, France) with heated methanol as an extraction solvent (temperature 80 °C, pressure 10.3 MPa). Final solutes were analysed for PPCPs and EDs using liquid chromatography coupled with mass spectrometry (Agilent 6470 Triple Quadrupole LC/MS System) (Innemanová et al., 2022; Dume et al., 2023). The solutes were further cleaned using Superclean ENVI-Carb SPE tubes, eluted with methanol + 1% formic acid, and analysed for PFCs by LC-MS (Shimadzu Nexera X2 LC/Sciex 4500) (Semerád et al., 2020). The structure identification of SCs was determined by X-ray diffractometry (XRD; D2 PHASER XE-T, Bruker); step size was 0.04º 2θ and counting time was 2.00 s per step (5–70°). Individual phases were identified using PANalytical X'Pert HighScore Plus software (version 3) and ICDD PDF-2 database (2003). Sludgechar samples were prepared both as individual particles attached to carbon tape (to study the morphology and chemical composition of individual specimens) and as polished thin sections (to evaluate the mineral phase composition). All the samples were carbon-coated and investigated by scanning electron microscopy (SEM; TESCAN VEGA 3 XMU) coupled with energy dispersive X-ray spectroscopy (EDS; Oxford Instruments Aztec X-MaxN 50); voltage was set at 20 kV and occasionally at 15 kV (i.e. when accessing the image-capture mode).

4.2.3 Metal(loid) removal from aqueous solutions

Sorption kinetic experiments were performed to obtain basic information on the SC sorption efficiency against individual metal(loid)s and the time required to establish equilibrium. To further evaluate the metal removal process in the pH range relevant for the studied soil environments, the following conditions were tested: 1) without pH adjustment, i.e. simulating the natural pH after the SC–metal(loid) interaction; 2) at controlled pH 5, i.e. weakly acidic conditions; and 3) at controlled pH 7, i.e. neutral pH. A number of metal(loid)s were tested

to thoroughly evaluate the effectiveness of the materials, namely As(V), Cr(VI), Sb(V), Cd(II), Co(II), Cu(II), Ni(II), Pb(II), and Zn(II). Individual solutions were prepared by dissolution of $HAsNa_2O_4 \cdot 7H_2O$, $Cr_2Na_2O_7 \cdot 2H_2O$, $K[Sb(OH)_6]$, $Cd(NO_3)_2 \cdot 4H_2O$, $Co(NO_3)_2 \cdot 6H_2O$, $Cu(NO_3)_2 \cdot 3H_2O$, $Ni(NO_3)_2 \cdot 6H_2O$, $Pb(NO_3)_2$, and $Zn(NO_3)_2 \cdot 6H_2O$ in deionised water to obtain a metal(loid) concentration of 0.1 mM. The concentration was selected based on our previous experimental conditions for adsorption kinetics using BC-composites (Hudcová et al., 2022) and it corresponds to values observed for moderately-to-highly contaminated soils (Table 4.1). Each sludgechar (sieved through a 250 μm sieve; 1 g/L) was added to a single-metal(loid) solution, vigorously stirred on a magnetic stirrer (550 rpm), and 10 mL of suspension was sampled at specific time intervals up to 120 min. The samples were filtered using a 0.45 μm cellulose acetate membrane and subsequently analysed by ICP OES. For comparison, the same kinetic experiment was performed in deionised water without metal(loid)s. Here, possible leaching of elements was monitored using ICP OES and ion chromatography (IC; Dionex ICS-242 5000+, Thermo Fisher Scientific, USA). Dissolved inorganic carbon was measured with a carbon analyser (TOC-L CPH, Shimadzu, Japan). The experiments were performed in duplicates. The possible influence of metal(loid) precipitation under the given experimental conditions on the overall removal process was evaluated using the Visual MINTEQ 3.1 program.

4.2.4 Pot experiment and pore water sampling

To investigate the efficiency of the SCs for soil remediation, a pot experiment with five different soils was conducted. The soils were collected from contrasting areas of the Czech Republic, yielding distinct levels of metal(loid) contaminants. For confidentiality reasons the exact locations are not disclosed. The soils were sampled from 0-25 cm depth, air-dried, and sieved (< 2 mm). The field bulk density of each soil was determined using 100 cm^3 rings placed on the soil surface. A total of 6 soil rings (Ejikelkamp, Netherlands) per location were used. The soil was weighed in wet state, dried at 105 °C, and weighed again. Hence, the bulk density of each sample was calculated by dividing dry soil mass with the known volume of the sample (100 cm^3). Soil texture was tested in duplicates using the standard hydrometer method (CEN ISO/TS 17892-4, 2004) and, consequently, the particle size classification was determined according to Gee and Or (2002). Soil pH was determined in

duplicates for each soil type using ISO 10390 (2005). Soil samples in triplicates were subjected to microwave-assisted total digestion according to the EPA 3051a method (2007) to assess their total content of elements. Total C and total N content of the studied soils were measured in dry state using TN/TC analyser PrimacsSCN (Skalar, the Netherlands). Basic identification of each soil, including a classification based on the contamination level, is given in Table 4.1. Detailed characteristics (i.e. total element concentrations, texture, etc.) are given in Table S4.2. For the incubation experiments, the five SCs were individually applied by mixing each one of the five studied soils at a 3% v/v ratio in a separate pot. A control sample of each soil without SC was present in every set. Each pot had approximately 150 mL of soil and 4.5 mL of SC. The exact volumes were calculated based on the bulk density of each soil and the volume of the individual SC. For each combination of sludgechar and soil, separate pots were prepared for pore water sampling (with a rhizon sampler inserted; Rhizon, The Netherlands) and for soil extractions (without a rhizon). The incubation period was 30 days, during which the pots were maintained at 70% of each soil's water holding capacity. At the end of the incubation period, pore water samples were collected using rhizons. The experiment was performed in duplicates. Each sample was immediately subjected to pH, Eh, and conductivity measurements and subsequently analysed for major and trace elements by ICP OES and/or ICP MS after acidification with 2% HNO_3. An unacidified aliquot was used to determine anions, total carbon and dissolved organic carbon (DOC) in the pore water using the same equipment as described previously

Table 4.1 *Soil identification and origin, classification based on the total content of each contaminant, source of contamination and land use (main contaminants for each soil are given in red).*

Soil ID	Soil classification (contaminant total content[a])	Source of contamination	Land use
Zn-rich	Zn; high (3000−3600 mg/kg) Pb; high (3900−8600 mg/kg) Cd; high (30−50 mg/kg) Cu; moderate (~80 mg/kg)[b] As; moderate (310−390 mg/kg)[b] Sb; moderate (~60 mg/kg)[b]	Mining & smelting affected area	Occasional grazing/ Agriculture
Smelter	Pb; high (3900−8600 mg/kg) Zn; high (3000−3600 mg/kg) Sb; high (~230 mg/kg) Cd; high (30−50 mg/kg) Cu; high (~310 mg/kg) As; moderate (310−390 mg/kg)	Former smelter area	Brownfield
As-rich	As; high (~18000 mg/kg) Zn; moderate (~200 mg/kg)[b] Cd; moderate (1−3 mg/kg)[b] Pb; low (70−80 mg/kg)[b] Cu; low (13−60 mg/kg)	Natural enrichment, historical Au mining	Forest
Brownfield	Pb; moderate (110−150 mg/kg) Zn; low (90−130 mg/kg)[b] Cu; low (13−60 mg/kg) As; low (7−15 mg/kg) Sb; low (2−20 mg/kg)[b]	Landfill, coal mining in the vicinity	Brownfield
Garden	Cd; moderate (1−3 mg/kg)[b] Cu; low (13−60 mg/kg) Pb; low (70−80 mg/kg)[b] Zn; low (90−130 mg/kg)[b] As; low (7−15 mg/kg)[b] Sb; low (2−20 mg/kg)	Former landfill	Gardening/ Landfill ballast (backfilling)

[a] The classification is based on the total concentrations of each element (Table S4.2) by relative comparison between the soils.

[b] Value higher or at the limit based on the Decree No. 153/2016 Coll (Czech regulatory limits for individual risk elements in common soils). No limits for Sb given in the current legislation, so the value given for As was used as a reference value here.

4.2.5 Soil extractions

After the incubation period, soil from pot variants without rhizons was dried (40 °C) and subjected to the first step of the sequential extraction procedures. In particular, exchangeable metals were determined in 0.11 M acetic acid (CH_3COOH) extracts (Quevauviller, 1998), while ammonium sulphate [$(NH_4)_2SO_4$] was used to determine exchangeable As and Sb (Wenzel et al., 2001). The extractions were performed in duplicates with procedural blanks. The extractants from both procedures were centrifuged, filtered with 0.45 μm nitrocellulose filters, acidified with 2% HNO_3, and subsequently subjected to trace and major elements measurements by ICP OES and/or ICP MS.

4.3 Results and Discussion

4.3.1 Physical and chemical properties of sludgechars

The basic physical and chemical characteristics of the SCs are given in Table 4.2. Generally, sludgechar SC2 showed very distinct properties compared to the other materials, which can be related to the fact that the raw sludge was not stabilised (only mechanically treated). In particular, it had significantly lower ash content (i.e. the level of mineral fraction incorporation into pyrolysed materials; Jin et al., 2016) compared to the other SCs in this study as well as those described in our previous paper by Moško et al. (2021a). Further, the C and N contents were almost double in the case of SC2 compared to the other sludgechars (Table 4.2). Finally, the specific surface area was only 5.6 m^2/g for SC2 compared to 44–77 m^2/g for the other SCs, despite their higher ash content that often decreases the specific surface. However, higher S_{BET} was usually reported for anaerobically stabilised input sludges (SC1, SC3, SC4, SC5) in contrast to non-stabilised ones (SC2) (Moško et al., 2021a; Giwa et al., 2023). In general, the specific surface area of SCs (Rangabhashiyam et al., 2022) is lower compared to BC produced from woody/plant biomass (Trakal et al., 2014), which was explained by clogging of pores due to adhesion of tar produced during sludge pyrolysis (Jin et al., 2016). In addition, SCs prepared under the given laboratory conditions show typical porosity values of 45–55 % and a total liquid pore volume of about 100 mm^3/g mainly in the meso-macropore range (Moško et al., 2021b), whereas lower values of these

parameters can be expected for commercial production. However, previous studies dealing with pyrolysed materials have shown that higher specific surface area does not necessarily mean better adsorption properties (Hudcová et al., 2022; Trakal et al., 2014). On the contrary, an important parameter influencing the material usability as an effective sorbent is its natural pH. Here, very high values were reached for all the studied materials (pH range of 10–12; Table 4.2), with the lowest values observed for SC4. High sludgechar pH values are attributed to the content of mineral phases, especially those of an amorphous nature (e.g. calcium/magnesium oxides (Bandosz & Block, 2006), and/or formation of carbonates during pyrolysis (Méndez et al., 2005). Cation exchange capacity, described as one of the factors influencing metal removal (Rangabhashiyam et al., 2022), reached the highest values of 48.2 and 46.1 cmol/kg for SC2 and SC3, respectively (Table 4.2). This can be related to the high content of exchangeable Ca.

Total elemental composition (including toxic metals and metalloids) is given in Table S4.3 and organic micropollutant content (PPCPs, EDs, and PFCs) in Fig. S4.1. Emerging micropollutants in sewage sludges are currently at the forefront of concern in terms of their persistence and ubiquity (W. Zhang et al., 2022). Therefore, it is crucial to mention that pyrolysis conditions in this study resulted in the complete removal of EDs and PFCs, as well as minimisation of PPCPs content (Fig. S4.1). Moreover, it is noteworthy that traditional organic pollutant content in the raw sludge (i.e. polycyclic aromatic hydrocarbons, PAH, and polychlorinated biphenyls, PCB) was below the safety limits required for waste intended to be disposed of on land (6 mg/kg for PAH and 0.2 mg/kg for PCBs according to Decree No. 294/2005 Coll., Annex 10), and even two orders of magnitude lower in the pyrolysed ones (data not shown).

Table 4.2 *Basic characteristics of the studied sludgechars.*

Sample		SC1	SC2	SC3	SC4	SC5
Proximate analysis[d]						
Ash (A)	*wt. %*	74.6	47.4	68.4	76.6	75.3
Volatiles (V)	*wt. %*	2.71	3.32	3.86	3.65	4.65
Fixed carbon (FC)	*wt. %*	22.7	49.3	27.7	19.8	20.1
Ultimate analysis[d]						
Carbon	*wt. %*	21.5	46.8	27	20.1	21.4
Hydrogen	*wt. %*	0.40	0.68	0.57	0.36	0.50
Nitrogen	*wt. %*	1.14	3.24	1.56	0.92	1.46
Sulphur	*wt. %*	1.35	1.04	1.75	1.39	0.70
Oxygen	*wt. %*	1.01	0.84	0.72	0.63	0.64
H/C atomic ratio	–	0.22	0.17	0.25	0.21	0.28
O/C atomic ratio	–	0.04	0.01	0.02	0.02	0.02
(O+N)/C atomic ratio	–	0.08	0.07	0.07	0.06	0.08
Energy value of dry matter[d]						
Higher heating value (HHV)	*MJ/kg*	8.66	16.3	10.2	7.50	7.67
Lower heating value (LHV)	*MJ/kg*	8.57	16.2	10.1	7.42	7.56
Other analyses						
S_{BET}	*m²/g*	77	5.6	63	62	44
pH_{H2O}	–	11.3±0.03	12.3±0.02	12.1±0.01	10.7±0.08	12.1±0.01
pH_{KCl}	–	10.6±0.08	12.3±0.05	11.9±0.03	10.0±0.00	11.8±0.01
pH_{CaCl2}	–	11.2±0.01	12.3±0.00	12.0±0.00	10.5±0.03	12.0±0.01
CEC	*cmol/kg*	30.3	48.2	46.1	25.8	28.9

[d] in dry matter

Concentrations of major elements (i.e. Ca and Fe) significantly differed between individual SCs, resulting in two groups: 1) with higher Ca content (SC1, SC2 and SC3), and 2) with higher Fe content (SC4 and SC5). The highest concentration of P was observed in SC2 (Table S4.3). In general, the resulting characteristics of SCs including the chemical composition are strongly dependent on the composition of the input raw material (Rangabhashiyam et al., 2022). Concerning potentially toxic metals, the pyrolytic process resulted in

increased concentrations compared to raw sludge, while volatile components were efficiently removed. In particular, high concentrations of Cu (especially SC3), Ni (especially SC3 and SC4), and Zn (especially SC2) were determined in the sludgechars. In the case of SC3, concentration limits given in Decree No. 273/2021 Coll., Annex 38, were exceeded for Cu (3.5×) and Ni (7×). However, it is important to note that although metals are usually "concentrated" due to the pyrolysis process, their availability is significantly reduced compared to raw sludge (Cui et al., 2022; Yuan et al., 2015).

4.3.2 Structural properties and mineralogical implications of sludgechars

The overall morphology (Fig. S4.2) of all SCs appears visually similar, but the chemical composition (measured by EDS) of individual particles (Figs. S4.2, S4.3) shows important differences. Mainly Ca, Fe, O, Mg, Al, Si, and P were detected. The predominant occurrence of Ca and Fe corresponded to the bulk chemistry of the SCs (Table S4.3). Regarding the pyrolysed organic matter, it was observed in rather smaller amounts for all sludgechars, although total C content reached 22–51 wt.% (Table 4.2). Nevertheless, the SEM images indicate that the organic matter was coated with mineral surfaces (Fig. 4.1f, Fig. S4.2), and the presence of carbon particles with porous BC structure was occasionally confirmed by SEM/EDS (Fig. S4.2_2, SC2-3a, 3c, and corresponding EDS spectra in Fig. S4.3). Due to the richness of major elements (Ca, Mg, P, S) in the raw material, we suggest that BC pores were clogged with new phases formed during pyrolysis (also in Raj et al., 2021). The occurrence of mineral phases can further facilitate ion exchange and surface complexation (Shen et al., 2018). Generally, the presence of different sorption sites on the SC surface may subsequently influence the removal of hazardous metal(loid)s (Rangabhashiyam et al., 2022). Mineral phases components were further investigated and the key features are shown in Fig. 4.1 (with corresponding spectra depicted in Fig. 4.2). The microscopic appearance and elemental ratios derived from EDS indicate that 1) Fe and Ca phosphates (including the formations of apatite; Fig. 4.1b) and 2) Fe and Ca sulphates were the most frequently observed mineral phases (also determined by Mahieux et al., 2010). Ubiquitous silicates were monitored during SEM/EDS analysis (Fig. 4.1d) and confirmed by XRD (see the text below). Risk elements known to be present in the raw sludges and even concentrated in the sludgechars (Table S4.3) were

rarely detected by EDS, most likely due to the detection limits of the method and the spatial distribution of trace elements in the specimens. Nevertheless, spots with detectable concentrations of mainly Cu and Zn were found in combination with phosphates (Fig. 4.1c) and sulphates (Fig. 4.1d). Therefore, potential formation of stable compounds of Cu and Zn with phosphate radicals coming from the decomposition of Ca phosphate phases (Gu et al., 2022) may be responsible for generally limited risk element leachability in the sludgechars (see later in text). Phosphates are one of the most common ligands that cationic metals precipitate with, leading to their effective immobilisation by sewage sludge-derived BCs (Xing et al., 2021). In addition, based on the frequent occurrence of P-rich phases detected by SEM/EDS, we suggest that P was present in the form of stable Ca-, Mg- and Fe- mineral phases in the SCs (Fig. 4.1e). On the other hand, the mineral elements in SC or BC can improve the soil nutrient content and effectively regulate the nutrients balance in the soil (Zhao et al., 2023), as demonstrated further on pore water results (see later in text; Fig. S4.9).
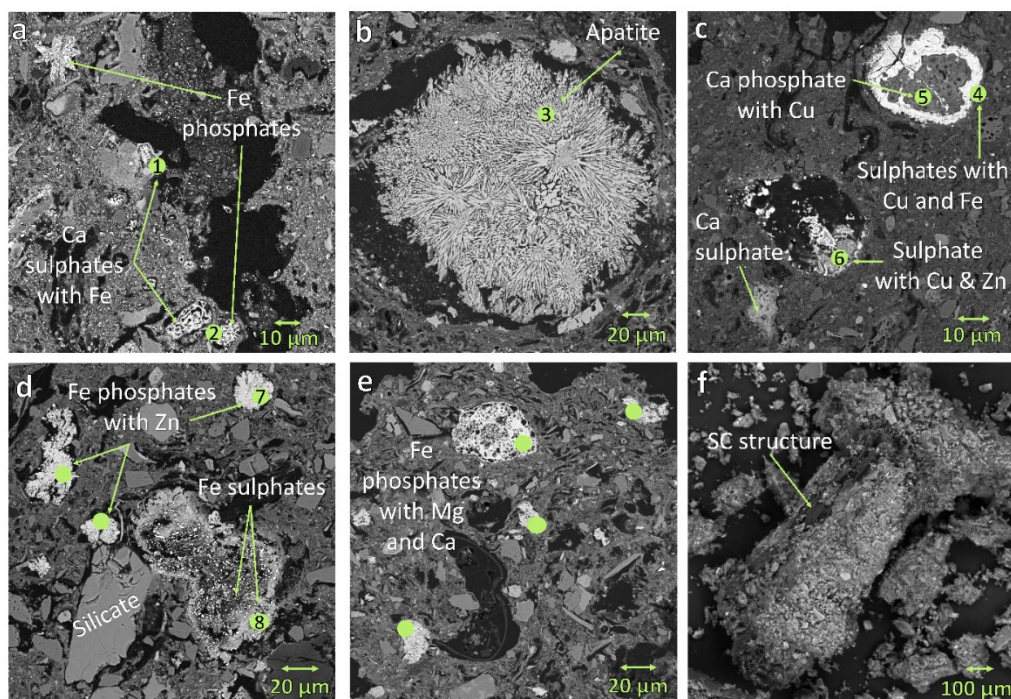
Figure 4.1 *Selected back-scattered electron images from SEM/EDS analysis of the sludgechars prepared as polished thin sections (a-e) and pins (f). a) SC1: Fe phosphates with Ca (up to 30 wt.%) and Mg (≈ 1 wt.%), Ca sulphates with Fe (≈ 1 wt.%); b) SC2: formation of apatite (Ca5(PO4)3); c) SC3: Ca phosphates with up to 15 wt.% Cu, sulphates with up to 41 wt. % Cu and up to 7 wt.% Fe, Ca sulphate with trace amount of Mg (< 1 wt.%), sulphates with up to 3 wt.% Cu and 32 wt.% Zn ; d) SC4: Fe phosphates with up to 2 wt.% Zn and Fe sulphates with trace amounts of Ca (< 1 wt.%); e) SC5: Fe phosphates with Ca (≈ 1 wt.%) and Mg (1-5 wt.%). The respective EDS spectra of the numbered points are presented in (Fig. 4.2) below, points in image e) have similar composition to sp. 2 and sp.7, more details of image f) can be found in the SI (Fig.S4.2_5 and Fig.S4.3).*
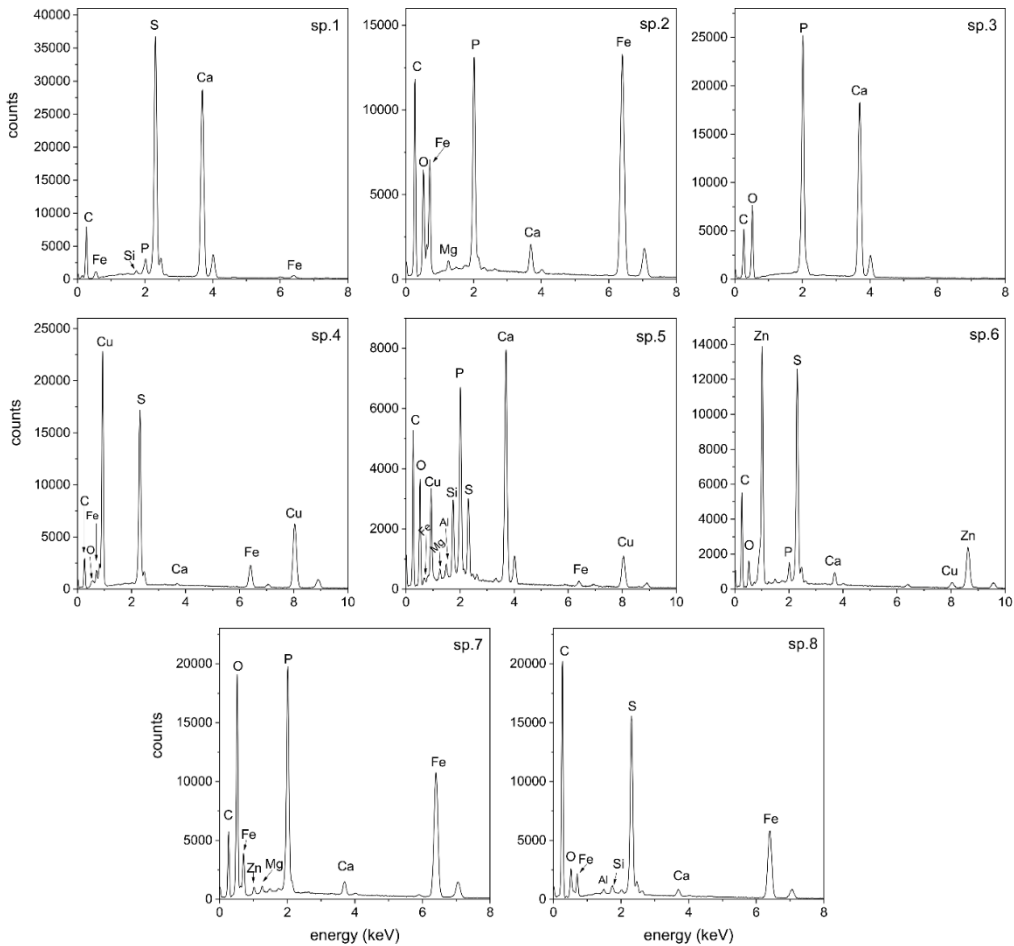
Figure 4.2 *Corresponding EDS spectra of numbered points 1-8 from SEM images of Fig. 4.1*

Mineral particles of similar morphology (i.e. prevailing amorphous and granular morphology) were observed by Lu et al. (2013). In addition, well-developed crystals may occasionally occur (e.g. quartz, calcite, apatite, or ilmenite). In order to further identify material structure and bulk mineralogical composition, XRD measurements were performed on individual SCs (Fig. S4.4). Apart from the amorphous part, the occurrence of crystalline mineral phases was evident, which is closely related to structural changes promoted by the high-temperature pyrolysis process (Ábrego et al., 2009). Generally, the diffractograms of all the studied SCs were very similar, indicating that, despite differences in the concentration level of elements, the dominant mineral phases were the same. However, the large number of lines in all diffractograms

indicated overall heterogeneity in the composition of SCs and the complex multi-phase character of the sludges. Therefore, only well-defined structures are presented in this section. The major crystalline phases were quartz (PDF-2 card 01-078-1254) and (Ca-)whitlockite (PDF-2 cards 01-073-1140 and 00-003-0713) observed in all SCs. Moreover, these were the only crystalline phases detected in SC2, which can be related to the lowest ash content (more ash = more crystalline phases, and vice versa; Ábrego et al., 2009). Calcite (PDF-2 card 00-002-0629), which is commonly detected in diffractograms of sludge pyrolysed below 700 °C, i.e. before its decomposition to CaO (Ábrego et al., 2009), was determined in SC1, SC3, and SC5. Other phases detected by XRD included various aluminosilicates, especially clays (e.g. muscovite and/or illite; PDF-2 cards 00-002-0058 and/or 00-026-0911). Additionally, other important phases might also be present in minor amounts, not detectable by XRD (e.g. iron phosphates/sulphates, calcium sulphates, Fe/Ca sulphides, or other silicates; Bandosz & Block, 2006; Figueiredo et al., 2021; Mahieux et al., 2010), many of which were identified using microscopic analyses (Figs. 4.1, 4.2). Furthermore, the partially amorphous character of the diffractograms can be attributed to 1) amorphous carbon, which is characteristic for the BC structure (Gale et al., 2021), and 2) amorphous oxides, carbonates, or phosphates (Bandosz & Block, 2006; Clemente et al., 2018; Méndez et al., 2005).

4.3.3 Time-dependent metal(loid) removal from aqueous solutions

Prior to the application of SCs in real contaminated soil environments, testing in simplified laboratory experiments is necessary to determine: 1) the overall ability of the SCs to remove the target risk metal(loid)s at different pH values; 2) potential leaching of risk elements and nutrients from the SC matrix; and 3) possible capture mechanisms (including precipitation of new solid phases). The pH values during metal(loid) removal significantly increased after the addition of SCs (see the lines in Fig. 4.3), indicating a strong buffering effect of all materials. The lowest increase was observed for SC4, which is in accordance with the natural pH values measured for the individual materials (Table 4.2). Such an increase in pH may have an indirect positive effect on metal removal due to (co)precipitation of new metal-based solid phases and further immobilisation of metals in soils. However, the opposite effect of the pH increase can be expected for anionic species (As, Cr and Sb), which is usually caused by: 1) predominantly negatively charged surface sites throughout the

pH range or the presence of cation exchangers (e.g. BC or clays; Gao et al., 2020 or Osuna et al., 2019); 2) the negative charge of some sorption sites on the SC surface at higher pH values (e.g. Fe/Mn/Al oxides and hydroxides; Sverjensky, 2005); and/or 3) unsuitable conditions for precipitation of metalloid solid phases under given conditions (e.g. low stability of Ca arsenates due to preferable formation of Ca carbonates; Zhu et al., 2006). In fact, the removal efficiency without pH control followed exactly the above-mentioned effect of the increasing pH values (see points in Fig. 4.3, Fig. S4.5). High efficiency towards metal cations was determined, yet significant differences in the overall removal course were observed between individual SCs. In particular, the removal efficiency and rate were significantly lower for SC4 (70% Cd removal efficiency) followed by SC1. This behaviour was attributed to low pH of these two materials. Similar results (but during multi-metal sorption experiments) were reported in the study of Zhao et al. (2019), where the efficiency without pH adjustment was Pb ≈ Cu (100%) > Cd (60%). In general, SC3 appeared to be the most effective towards metal cations under these conditions. As expected, the materials were not effective against metal(loid) anions, i.e. As (max. 4%), Cr (max. 9%) and Sb (max. 2%). In particular, SC5 appeared to be the most effective, while SC2 was the least effective, which can be attributed to the lowest mineral ash content (Table 4.2) and the lowest amount of Fe (Table S4.3) and thus potential mineral phases for metalloid sorption in SC2. Although Agrafioti et al. (2014) demonstrated some effectiveness of sludgechars against As and Cr without pH control, electrostatic interactions with Fe phases on the surface were considered to be the main removal mechanism. Considering the variability in SCs properties, Rangabhashiyam et al. (2022) highlighted the necessity to evaluate the connection between the material's characteristics and its ability to remove hazardous components when used as an adsorbent.
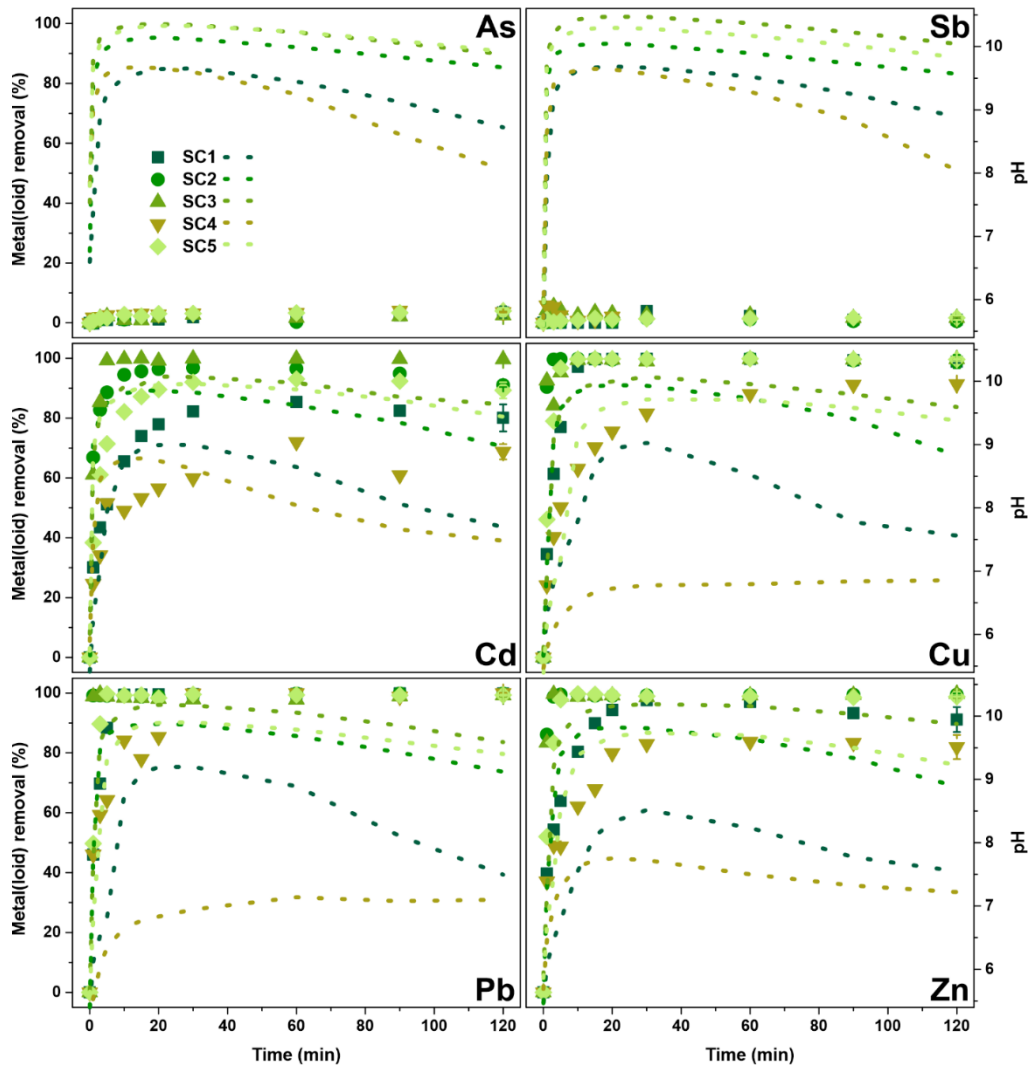
Figure 4.3 *Sorption efficiency (points) of the five sludgechars in single solutions of metalloid anions (As, and Sb) and metal cations (Cd, Cu, Pb, and Zn) at natural pH (i.e. without control shown by dotted lines).*

At controlled pH 7 (Fig. S4.6), a slight improvement towards As (max. 16%; SC3), Cr (max. 6%; SC3) and Sb (max. 6%; SC2) was observed. In line with expectations, the removal efficiency of all metals decreased compared to the experiments without pH control in the order Pb > Cu > Zn > Cd > Co ≈ Ni. At controlled pH 5 (Fig. S4.7) the effectiveness towards As (max. 13%; SC3) and Sb (max. 3%; SC3) was almost identical, while a significant improvement was observed for Cr (i.e. up to 72%, max. SC3, min. SC5). The higher removal

efficiency at lower pH values may be the result of electrostatic interactions between positively charged sites on the SC surface, including (amorphous) metal oxide surfaces, and the anionic species (Agrafioti et al., 2014). Similarly, Kaljunen et al. (2022) observed increased removal of anionic species at lower pH values by SCs. This phenomenon was explained as follows: although the SC surface is negatively charged in a wide pH range, a decrease in pH causes a decrease in the total negative charge, which leads to a decrease in the repulsion between the SC surface and the anionic species in the solution. Compared to higher pH values, a significant decrease in removal efficiency was observed for all metal cations, which indicate potentially lower efficiency for acidic soils. Nevertheless, the order of metal cation removal efficiency was similar to that of pH 7, with the only difference in the order of Cd > Zn. In addition, gradual release of trapped metals was observed for most metal cations at pH 5, which can be attributed to the influence of: 1) metal leaching from sludgechar matrix (later excluded; see text for details), and/or 2) competition with H^+ for binding sites (Yang et al., 2019).

4.3.4 Potential time-dependent leaching from sludgechars

Potential metal(loid) leaching

Possible hazards related to the release of risk elements from SCs need to be evaluated before application of SCs as soil amendments. Noteworthy, no leaching was observed for any of the studied risk metal(loid)s from the SCs at the natural pH, pH 7, or even at pH 5 in our leaching experiment (values below detection limits, not shown). Therefore, the aforementioned possibility of metal(loid) release due to dissolution of mineral phases of the SCs during the kinetic experiment at pH 5 was rebutted. Similar results with regard to risk metal(loid) leachability were observed by Chen et al. (2014), under significantly more acidic conditions compared to this study. This finding thus confirmed the theory that despite increased total metal(loid) concentration in the pyrolysed sludge (Table S4.3), the risk elements are strongly bound in the SC and their availability is limited compared to the raw sludge (Yuan et al., 2015), especially when pyrolysed at 600–800 °C (Cui et al., 2022; Jin et al., 2016). This result further supports the suitability of SCs for soil application.

4.3.5 Availability of nutrients

The reduced leachability of metals even under acidic conditions confirmed their competing effects with major cations and H^+. The release of major elements at different pH is depicted in Fig. 4.4. The release of Ca, which was determined as the main exchangeable cation, was controlled by its availability. That means it was higher from SCs with a higher concentration of total Ca. Interestingly, the Ca concentration was the same if performed only in deionised water (Fig. 4.4) or in the presence of metal(loid)s during adsorption kinetic experiments (data not shown). Contrasting results were presented by Chen et al. (2014), who showed an increase in Ca leaching by increasing Cd concentrations in laboratory solution, while Gao et al. (2019) presented that cation exchange does not necessarily play a major role. Nevertheless, there is still the possibility that the binding sites formed after the release of Ca (i.e. negatively charged sites) may subsequently be occupied by metal cations from the solutions due to electrostatic forces (Hudcová et al., 2021). However, the already mentioned competition with H^+ ions needs to be considered, especially at pH 5. Other major cations (namely Mg and K) were released in smaller quantities (Fig. 4.4). For P, the released P concentration was only 0.2–0.6 mg/L. Noteworthy, a significant decrease in P concentration was observed in solutions containing metals during the kinetic experiment (data not shown), indicating possible precipitation of metals with P. On the other hand, S release was similar regardless of the presence of metals and metalloids in the solution, so the influence of sulphate precipitation was assumed to be minor. According to Mercl et al. (2020), pyrolysis temperatures above 420 °C promote lower availability of nutrients in sludgechar compared to the raw sludge. Considering the content of organic matter in the sludgechars, surprisingly, no leaching of DOC was observed under the given experimental conditions.
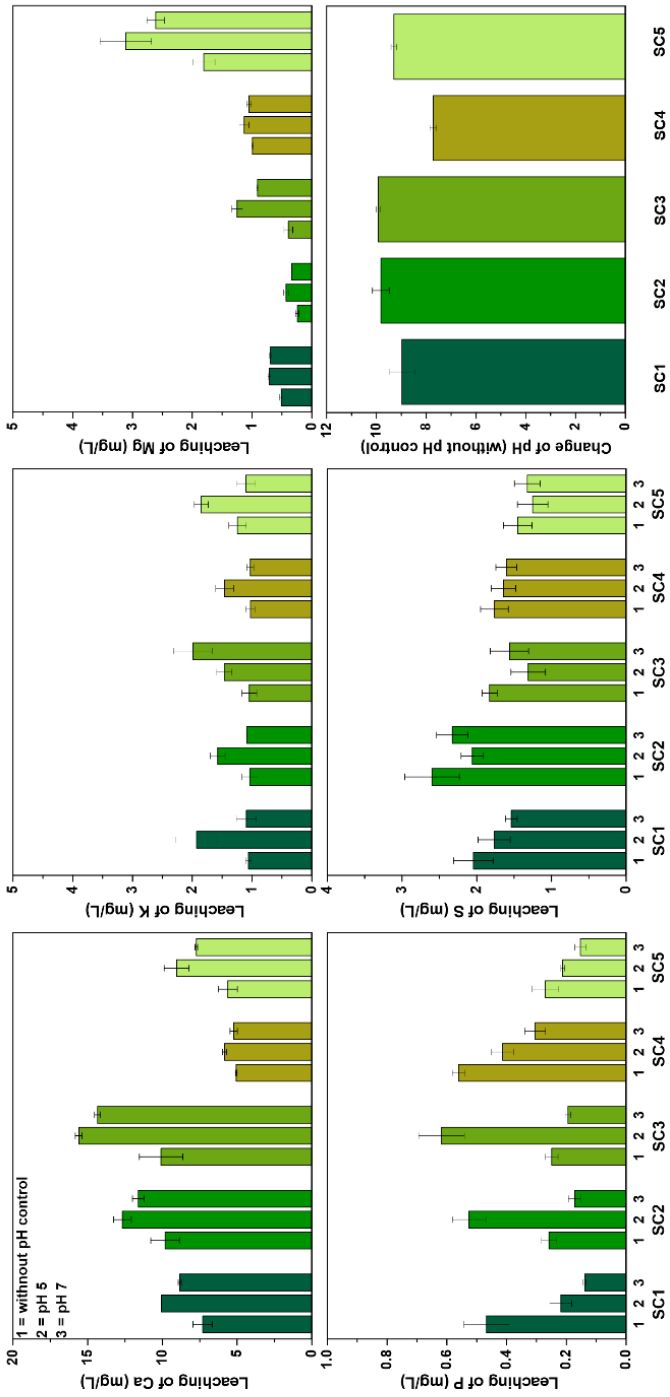
Figure 4.4 *Release of nutrients from the studied sludgechars during leaching in demineralised water (2 hours) at pH 5, pH 7, and natural pH (the pH evolution without control is depicted separately).*

4.3.6 Model of potential phase precipitation in aqueous solutions

With regard to the above-mentioned changes and the possible effect of pH on metal and metalloid removal, a simple simulation was performed under the given experimental conditions (i.e. pH value, initial metal concentration, major elements release, and atmospheric CO_2) to evaluate the possible precipitation of new phases (Table S4.4). It is evident that without pH control, the formation of metal phosphates and/or sulphates can be observed, in addition to the expected predominant precipitation of metal carbonates and hydroxides. This finding further complies with the SEM/EDS observations of metal-rich phosphates and sulphates (Figs. 4.1, 4.2). Moreover, such formations may have significant implications both for nutrient and metal behaviour when further applied to soils for metal(loid) immobilisation. The possible precipitation of P with Cd (released from sludgechar) as one possible metal removal mechanism was previously discussed by Gao et al. (2019). With decreasing pH values, the possibility of metal precipitation decreases, depending on metal type. At pH 5, the formation of new phases was predicted only for Pb. However, it is necessary to mention that so-called surface-induced precipitation of metals (which occurs at lower pH values than in pure aqueous solutions), caused by the high pH on the material surface, may significantly influence the overall removal process (Hudcová et al., 2019). Although the main credit for metal removal is often given to cation exchange (Rangabhashiyam et al., 2022), it can be seen that at higher pH values (generally at pH $\geq$ 7), precipitation of new phases can be considered the main metal removal mechanism using SC (Chen et al., 2014; Gao et al., 2019). Conversely, Fan et al. (2020) and Shen et al. (2018) identified the surface complexation of Cu and/or interaction with mineral phases on the SC surface as the main mechanism. Additionally, it has been reported that metal precipitation on carbon sorbents tends to have faster kinetics than other processes (Yang et al., 2019). The effect of adsorption (i.e. surface complexation, including cation exchange) can only be expected at lower pH values (or as an additional mechanism). Regarding metal(loid) anions (i.e. As, Cr, Sb), there was no evidence of metal(loid) anion precipitation in our experiments. Therefore, surface complexation, especially electrostatic interaction at lower pH values, was assumed to be the most probable removal mechanism of these elements, based on the previous studies dealing with removal of anionic species using SCs (Agrafioti et al., 2014; Kaljunen et al., 2022). However, to distinguish the removal mechanisms in detail, especially

the role of chemical and physical adsorption, further measurements should be provided in future studies.

4.3.7 Availability of risk elements and nutrients in the soil

After testing the materials removal efficiency under different conditions in laboratory aqueous solutions, their efficiency for metal(loid) immobilisation was investigated in soils. The five studied soils (Tables 4.1 and S4.2) represent contaminated and/or degraded substrates that could potentially benefit from application of sludgechars. For the purposes of this study, soils with contrasting characteristics mainly regarding soil pH and various metal(loid) combinations and their concentration levels were selected. It is well-known that removal efficiencies in single-metal systems are increased compared to multiple-metal systems due to the competition between individual species for sorption sites (Zhao et al., 2019). Also, maximum sorption capacities differ among the sorbent materials and metal(loid) types, as reviewed by Yang et al. (2019) and demonstrated for various BCs regarding Cd, Cr, Cu, and Pb (Zhao et al., 2019) as well as As (Agrafioti et al., 2014). Concentration level and contaminant type further influence the relative immobilisation efficiency in soils, as documented for example by Vítková et al. (2018) on two contrasting soils with extremely distinct As and Zn contents. For this reason, our soils were classified as high-, moderate- and low-contaminated soils (Table 4.1), based on their total amount of each risk element (Table S4.2). The classification assisted in showing the major differences between the soils and highlighting contaminants of the biggest concern, and subsequently in assessing the efficiency of the SC treatments as a function of the metal(loid) concentration level in each soil. Moreover, changes in the nutrient availability after applying the SC amendments was monitored to 1) assess the overall material stability under various soil conditions, 2) be able to better describe the reactivity on the SC–soil interface, and 3) evaluate the complex potential of the material for soil reclamation and revegetation.

4.3.8 Availability of risk elements in the soil extracts

The exchangeable amount of risk metals in the acetic acid or metalloids in ammonium sulphate soil extracts followed the sequence: Zn>>Pb>Cd>Cu>As>Sb; the distribution in the different soils is presented in

Fig. 4.5. Smelting-affected soils (Zn-rich and Smelter) commonly yielded at least one or two orders of magnitude higher extractable metal concentrations (Zn, Pb, Cd, and Cu) compared to the other soils. In particular, Zn was the main contaminant in Zn-rich soil extracts, with concentrations up to 2095 mg/kg, and in Smelter soil extracts with up to 829 mg/kg (Fig. 4.5), representing 68% and 23% of the total Zn, respectively (Table S4.2). Although the total Zn concentrations of Zn-rich and Smelter soil were similar (Table S4.2), the extractable amounts differ by one order of magnitude. Similar behaviour was observed in the pore water with maximum Zn available concentrations reaching 42 and 2.8 mg/L in Zn-rich and Smelter soil, respectively (Fig. S4.8). This observation highlights the importance of physico-chemical, structural, and biotic factors of each soil, which altogether affect the actual risk element availability (Rieuwerts et al., 1998). The effect of amendments on Zn immobilisation for the high-Zn_{tot} soils was not significant except for soil treated with SC1, yielding the highest S_{BET} among the SCs (Table 4.2). For the other soil types, exchangeable Zn concentrations ranged between 2.3 and 23 mg/kg. In contrast to high-Zn_{tot} soils, significant differences were observed between treatments in the moderate- and low-Zn_{tot} soils, yet the addition of sludgechars usually lead to mobilisation of Zn. Although possible metal leaching from the sludgechars was excluded during the kinetic experiment (Fig. 4.4), the potential Zn leachability under much more complex soil environment cannot be completely avoided, especially in acidic soils. For instance, Y. Zhao et al. (2018) found that Zn release from SC was higher in acidic rather than alkaline soil, despite the low Zn leachability when the SC was tested alone. In contrast, the application of sewage sludge-derived BC provoked a decrease in Zn pore water concentrations in acidic but not alkaline mining soils (Álvarez-Rogel et al., 2018). Besides the effect of pH, changes in the availability of metals contained in SCs can occur over time as a result of the interactions between soil and SC particles (E. He et al., 2019). Interestingly, in our study, the pattern of Zn exchangeable concentrations as a function of the SC amendment was similar in As-rich, Brownfield, and Garden soils (Fig. 4.5). Namely, SC3 showed increased Zn release compared to the other sludgechars and control, yet the concentration level was marginal and not considered hazardous. This implies that the amendments used in this study were resistant enough to external conditions and material–soil interactions and, despite high total Zn concentrations in the sludgechars (Table S4.3), leaching of Zn was very limited (<1 %). Such high material stability is related to the

high pyrolysis temperature (600–650 °C) used for the amendment production (Figueiredo et al., 2021; X. Zhang et al., 2022).
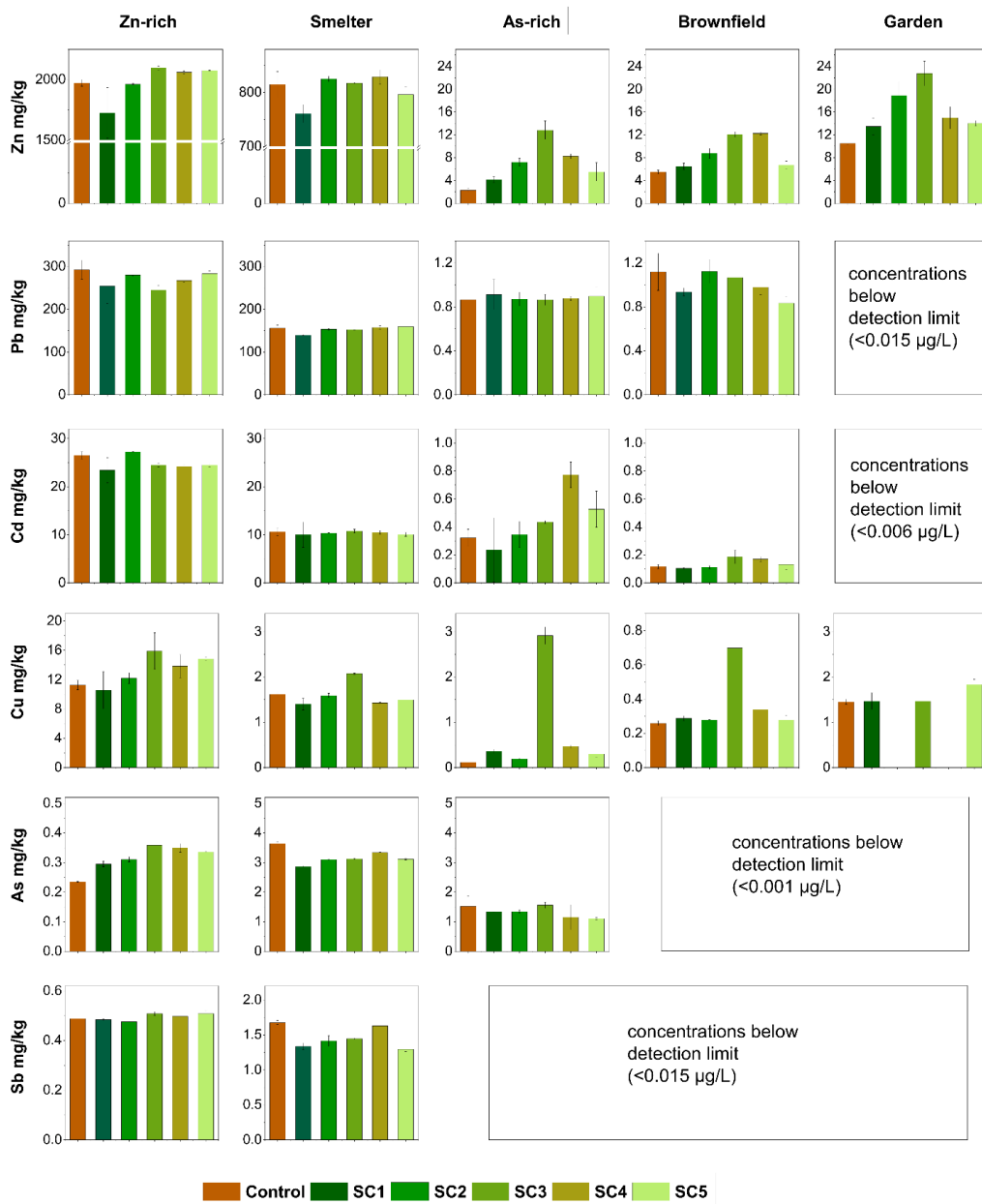
Figure 4.5 *Easily available concentrations of metals (in CH₃COOH extracts) and metalloids (in (NH₄)₂SO₄ extracts).*

The highest amounts of exchangeable Pb (140–293 mg/kg) were observed in high-Pb$_{tot}$ soils (i.e. Zn-rich and Smelter). Although not considered significant, SC3 and SC1 treatments resulted in the biggest decrease in Pb concentrations in Zn-rich and Smelter soils, respectively (Fig. 4.5). Wang et al. (2021) showed that SCs were always somewhat efficient for Pb immobilisation. This effect can be explained by ionic exchange and precipitation of pyromorphite-type minerals [Pb$_5$(PO$_4$)$_3$X; X = F, Cl, B or OH], which might be formed when P-rich amendments are added in Pb-contaminated soils (Kumpiene et al., 2008). In the moderate Pb$_{tot}$ Brownfield soil, the lowest Pb concentration was detected in SC5-treated soil. In general, Pb was not very mobile in the soils, as documented, e.g. by Cerqueira et al. (2011) who studied Pb migration in different soil horizons.

Maximum available Cd was observed for SC2-treated Zn-rich soil (27.3 mg/kg), followed by control soil, while slightly decreased Cd values were determined for the other sludgechar-treated samples (Fig. 4.5). Low efficiency of SC2 can be related to generally not favourable properties of this material for adsorption (Table 4.2 and previous discussion). In high-Cd$_{tot}$ Smelter soil, Cd behaviour was independent of the treatment. In contrast, despite low extractable Cd in As-rich (moderate-Cd$_{tot}$) and Brownfield (low-Cd$_{tot}$) soils, the highest concentrations were determined for the SC-treated samples (Fig. 4.5), indicating Cd release from the SC matrix. Moreover, the release trend corresponds to the highest Cd contents in SC-3 and SC-4 (Table S4.3). Although BCs are typically efficient for immobilisation of divalent metals, a long-term study using sewage sludge-derived BC revealed no changes in the availability of Cd and Pb over time (Chagas et al., 2021), while Khan et al. (2013) reported an increase in bioavailable Zn, Cd, and Cu in soil after the application of sewage sludge-derived BC.

The highest available Cu was observed in SC3-treated samples and was even more pronounced in the low-Cu$_{tot}$ soils, As-rich and Brownfield (Fig. 4.5). This observation is clearly associated with the SC3 treatment, which had at least 4× higher Cu content than the other SCs (Table S4.3), and with low pH of these soils (pH 6.1 and 5.2, respectively; Table S4.2). In contrast, no elevated Cu leachability was observed for Garden soil (pH 7.4; Table S4.2) after any SC treatment. Since Cu is an essential trace element for plants, determined in concentration range of 2–20 mg/kg in plant dry mass (Cruz et al., 2022), attention should be given when applying BC to soils, so as not to completely immobilise Cu in soils or make it unavailable to plants (Hartley et al., 2016).

Available As was detected only in the smelter-affected soils or in the naturally As-enriched one in the following sequence: up to 3.64, 1.56, and 0.36 mg/kg in the Smelter (moderate As_{tot}), As-rich (high As_{tot}), and Zn-rich (moderate As_{tot}) soils, respectively (Fig. 4.5). Interestingly, the available concentrations did not follow the order of the total concentrations of As in these soils (i.e. As-rich>>Zn-rich> Smelter) but rather the sequence of the most acidic to most alkaline soil pH (Table S4.2). The same sequence in As concentrations was observed in the pore water extracts (max 700 µg/L; Fig. S4.8). These findings underline the fact that As availability is strongly dependent on the soil type and physicochemical properties (Bissen & Frimmel, 2003; Singh & Srivastava, 2020) but also on the source of contamination (geogenic vs anthropogenic). The availability of As in anthropogenically contaminated soils is reported to be increased compared to naturally enriched ones (Shaheen et al., 2017; Skála et al., 2011). Regarding sludgechar efficiency, distinct As behaviour was observed as a response to different treatments in the soil extracts (Fig. 4.5). For Smelter soil, SC1 was the most efficient As-immobilising agent, which can be related to its high ash content and the highest S_{BET} (Table 4.2). For As-rich soil, the highest immobilisation potential was observed for SC5, which was the most effective SC for metalloids in aqueous solutions and in pore water extracts (see Fig. S4.8). On the contrary, for Zn-rich soil, the control sample yielded the lowest amount of exchangeable As, followed by SC1 (Fig. 4.5). Mitzia et al. (2023) also observed lower amounts of As in control samples compared to woody BC-treated samples. This result was expected since BCs are typically not efficient for immobilisation of As and other anionic metal(loid)s (Sb, Mo), as already discussed previously. Furthermore, the variations in SC efficiency in different soils can be related both to sludgechar pH (pH>10; Table 4.2) and especially to soil pH (pH 5.2–7.5; Table S4.2) as the main drivers of As availability. Additionally, the efficiency of SC1 and SC5 could be attributed to their high total Fe content (>2 wt.%; Table S4.3), which indicates potential sorption of As onto Fe oxyhydroxides (Agrafioti et al., 2014; Simón et al., 2018). In general, all the treatments showed some efficiency in As immobilisation in Smelter soil as well as in As-rich soil (except SC3), yet very similar concentrations were detected for the latter (Fig. 4.5). Noteworthy, although SC4 had the highest total content of As among the treatments (Table S4.3), it did not yield the highest extractable concentrations, most likely because As was well-stabilised in the BC structure.

Exchangeable Sb was detected exclusively in the smelter-affected soils (i.e. Smelter up to 1.68 mg/kg, and Zn-rich up to 0.51 mg/kg) (Fig. 4.5). In the high-Sb_{tot} Smelter soil, SC5 and SC1 yielded the lowest amounts of available Sb, while for the moderate-Sb_{tot} Zn-rich soil, negligible differences were observed between the treatments and control. As observed also during the kinetic experiment and despite the highest total content of Sb in SC5 (Table S4.3), SC5 showed the highest efficiency towards Sb. Similarly to As, Sb has high affinity to Fe oxides (Chang et al., 2022; Vidya et al., 2022), which could explain the increased efficiency of SC1 and SC5, yielding higher Fe content than the other SCs (Table S4.3). A different picture was observed in the soil pore water where Sb was present in all samples except for Garden (Fig. S4.8). Different SCs were efficient in different soil types, mainly as a result of different soil pore water pH (Fig. 4.6). For instance, high-As_{tot}/Sb_{tot} Smelter soil pore water pH was 7.5 and the application of SCs resulted in a slight decrease both in As and Sb available concentrations. Nevertheless, the efficiency of the studied materials towards both metalloids was in general low in the soil, as also observed in the aqueous solutions (see previous text).

Despite the occasionally observed increase in metal release related to high total metal contents in SCs, the extractable amounts were very low, which implies generally efficient metal stabilisation in the SC matrix. As already mentioned, the higher the pyrolysis temperature, the more stabilised risk elements in the sewage sludge-derived BC (X. Zhang et al., 2022). The possible mechanisms by which this stabilisation is achieved are 1) the formation of new crystal phases (silicate and phosphate minerals) by incorporation of risk elements and vitrification, and 2) encapsulation, leaving low concentrations of risk elements on the BC surface (Li et al., 2018).

pH, DOC, and (macro)nutrients in the soil pore water

Soil pH (Table S4.2) and soil pore water pH (Fig. 4.6) was considered one of the key parameters influencing the available metal(loid) fraction. The soil pore water pH values of the different soils and treatments ranged between 4.6 and 7.6 (corresponding to the tested pH range of the kinetic experiment). For acidic soils (i.e. Zn-rich, Brownfield, and As-rich), all the SCs increased the pH values compared to control (Fig. 4.6). The greatest difference compared to control was observed for Zn-rich soil treated with SC2 and As-rich soil treated with SC5. At the same time, SC2 and SC5 yielded the lowest available concentrations of Zn and Pb in Zn-rich and Smelter soils, yielding Pearson correlations of pH–

Pb up to r=−0.90. For circumneutral soils (i.e. Smelter and Garden), the addition of SCs did not change or even decreased the pore water pH (Fig. 4.6), particularly SC4. These results are aligned with studies revealing that BCs are more likely to increase pH and promote risk metal immobilisation in acidic soils rather than in neutral or alkaline soils (Meng et al., 2022; Yang et al., 2021). Adverse impacts were determined for metalloids, showing significant correlations for pH–As (up to r=0.90) and pH–Sb (up to r=0.80) in Smelter and Zn-rich soils, underlying that higher pH values promote anionic metal(loid) availability.
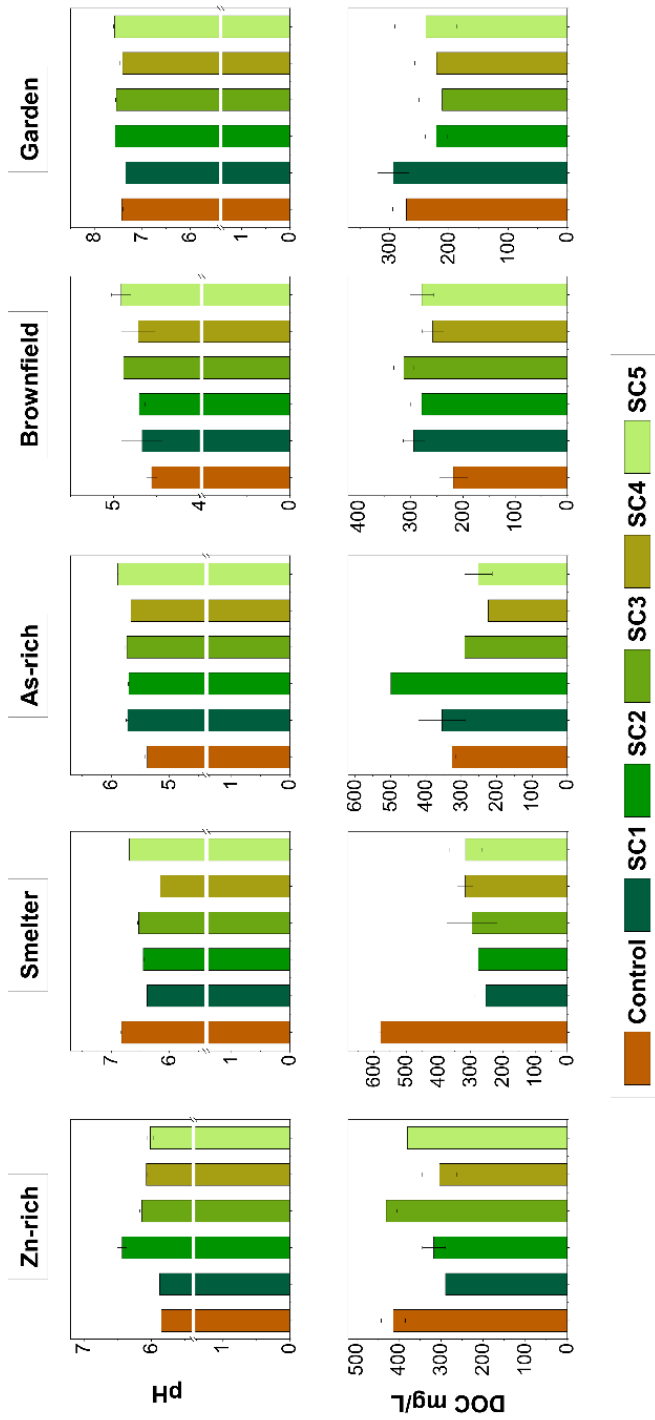
Figure 4.6 *pH values and DOC contents in the pore water of the five studied soils.*

In terms of DOC, the concentrations in the pore water varied from 211 to 579 mg/L among the different soils but the presence of SCs did not lead to an excessive release of DOC (Fig. 4.6). In this context, these results support the idea of using SCs as soil amendments with the potential for carbon sequestration (Gievers et al., 2021).

Regarding major elements, Ca was the most abundant ion in the pore water (up to 691 mg/L; Fig. S4.9) as expected from the high total concentrations of Ca in the SCs (up to 67 g/kg; Table S4.3), its solubility, and the fact that Ca was the main exchangeable cation (see earlier in text). Generally, nutrients (Ca, K, and Mg) content significantly increased in the soil pore water after SC application (Fig. S4.8), although it is assumed that pyrolysis temperatures above 420 °C promote lower availability of nutrients in SCs (Mercl et al., 2020). On the other hand, available nutrients can have a positive effect on soil health (e.g. increase soil fertility) and enhance revegetation of degraded areas, even though it might not lead to metal(loid) immobilisation. Furthermore, the presence of divalent nutrients on the SC surface may support ion exchange and indirectly promote metal(loid) retention. The release of P was generally very low among treatments, yet in most cases it was increased by the addition of SCs compared to control (Fig. S4.9). Nevertheless, stability of P can be expected in SCs due to formation of less soluble Mg- and Ca- minerals during pyrolysis (Figueiredo et al., 2021; Frišták et al., 2018), which was confirmed during SEM/EDS analyses (Figs. 4.1, 4.2).

4.3.9 Suitability of sludgechars for soil remediation

Based on both the results from the soil extractions and pore water, SC1, SC2, and SC3 treatments are suggested as efficient for immobilisation of metal cations, while SC5 and SC2 were efficient for metalloid anions (As and Sb). In particular, Zn was most efficiently immobilised by SC1 and SC2, Pb by SC1 and SC3, Cd by SC3, SC4, and SC5, Cu by SC1, As by SC5 and SC1, and Sb by SC2 and SC5 (Table S4.5). Treatment SC4 was universally not efficient for risk element immobilisation in soils. These findings are comparable to the adsorption experiment results, although not identical due to different interactions between SC–metal(loid) only and SC–soil–metal(loid) and the indirect effects that may occur (L. He et al., 2019; Rangabhashiyam et al., 2022; Sun et al., 2022). According to our findings, the efficiency of the studied sludgechars for anionic metal(loid) immobilisation was very limited, as also

reported in other studies (Ahmad et al., 2017; Amin et al., 2020; Lomaglio et al., 2017). However, the Fe content of SCs is of particular importance when dealing with metalloids due to their high affinity for Fe phases, which can promote metalloid immobilisation (Agrafioti et al., 2014; Yu et al., 2021). Therefore, Fe-rich sludges can represent perspective immobilising amendments in multi- or metalloid- contaminated soils (Fu et al., 2023). At the same time, soil texture could play a key role in affecting As and Sb mobility, with sandy soils presenting the greatest risk (Chang et al., 2022; Gerdelidani et al., 2021). In addition, we observed different behaviour of the same amendment in the different soils, affected by the total concentrations of contaminants, available contaminant fraction, physicochemical properties, soil type, and organic matter content of each soil (Table S4.2). Likewise, other studies with BCs derived from sewage sludge (Penido et al., 2019), wood (Ali et al., 2019), and swine manure (Yang et al., 2021) have reported variable BC efficiency. Mutual impacts always occur between the amendment and the soil (Lian & Xing, 2017).

With regard to the discussion in the previous sections and taking into account that all SCs were strongly alkaline, we suggest that the main parameters affecting the extent of metal(loid) immobilisation by SCs are: 1) pH of the SC as well as initial pH of the soil (Table 4.2, Table S4.2); 2) CEC (i.e. the presence of exchangeable cations like Ca) of SCs, especially for cationic metals (Pearson correlations between metal removal/immobilisation and CEC were determined as follows: CEC-Zn up to r=0.85; CEC-Pb up to r=0.65 ,CEC- Cd up to r=0.78), 3) P content which promotes phosphate mineral formation with metals (Figs.4.1 and 4.2, Table S4.4), and 4) Fe content and potential Fe (oxyhydr)oxide formation as metal(loid) scavengers (As-Fe up to r=0.73). The observed immobilisation of metal(loid)s is a promising step towards the use of SCs for soil remediation. However, an increase in risk elements in the soil solutions was observed and, therefore, their potential leaching under acidic soil environment need to be further monitored. Overall, SC immobilisation efficiency is expected to be affected by individual soil properties, especially by soil constitution, pH, organic matter, and co-existing ions (Li et al., 2015).

Regarding the long-term perspective of SC use for soil remediation, ageing plays a key role. Particularly, ageing can change some BC properties, such as pH and alkalinity, CEC, Fe species on their surface, and the number of functional groups; consequently, such changes affect their immobilisation efficiency (E. He et al., 2019; Wang et al., 2017). In a 2.5-year field study, Farkas et al., (2020) reported positive direct and indirect effects of SC

application such as alkaline pH retention and P and K availability in the long-term. Therefore, despite the general low retention of metal(loid)s by the studied SCs, it can be assumed that longer experiments will have more promising results due to the positive effect of ageing. Enhanced immobilisation could be the result of more reducing conditions prevailing after a longer time (Álvarez-Rogel et al., 2018). On the other hand, sewage sludge-derived BCs have shown increased resistance to ageing and/or increased immobilisation efficiency compared to BCs from another feedstock (Álvarez-Rogel et al., 2018; E. He et al., 2019; Yang et al., 2022). At last, the common presence of phosphates (as observed by SEM/EDS) is valuable for applications of SCs in degraded soils. The retention of P in soils is currently a hot topic due to the depletion of global P reservoirs (Alewell et al., 2020; Ringeval et al., 2017) and, therefore, the use of SC as a treatment with the potential to recover P in soils is a promising and sustainable solution (Hušek et al., 2022). Overall, the studied materials could be considered environmentally safe and promising for applications in soil remediation. Future research focusing on the possible interactions of SCs and individual soil components, plants and biota, preferably in a field-scale, will be beneficial for the complete assessment of SCs. Combinations of SC and other metal(loid) immobilising agents such as Fe-based amendments will also be valuable in the case of multi-element contamination.

4.4 Conclusion

Five pyrolysed sludges were tested for metal(loid) removal and immobilisation for further use as soil amendments. Despite the great variability in their composition and properties, inevitably affecting their efficiency in metal(loid) capture, all sludgechars were highly efficient (up to 100 %) for Cd, Co, Cu, Ni, Pb, and Zn removal from aqueous solutions. Unlike metal cations, the removal of As, Cr, and Sb was limited. The SEM/EDS investigations revealed the formations of phosphates and sulphates that were often associated with Cu and Zn. Therefore, these mineral phases were found crucial for the sludgechar stability and for minimising the risk of metal(loid) leachability from the pyrolysed matrix. When applied to contaminated soil environments, the sludgechar immobilisation efficiency towards metal(loid)s was significantly lower compared to laboratory testing. Yet, specific sludgechars were suggested as potential immobilising agents for metals (Zn, Pb, Cd, and Cu) and other(s)

for metalloids (As and Sb) in soils. Studying contradictory soils, which represent real remediation targets, indicated that metal(loid) immobilisation efficiency was soil-specific and closely related to 1) the level of contamination and 2) soil pH. Zinc was a great example of distinct response to the sludgechars applied in soils with high, moderate, and low Zn_{tot} contents and availability. Moreover, our study showed availability of nutrients, while limited leachability of risk elements from the sludgechars, both indicating the benefits for material reuse and nutrient recycling. All these aspects are favourable for their application in multi-element contaminated sites and to assist decision-making for immobilisation in various soil types with different use (i.e. smelter-affected, brownfield, landfill).

4.5 Supplementary Information

Table S4.1 *Classification of wastewater treatment plants (sources of the input raw sludges) according to city population.*

WWTP[a]		1	2	3	4	5
Category	–	Large	Extra small	Small	Medium	Medium
City population	*Number of residents*	>100,000	<1000	<20,000	20,000–100,000	20,000–100,000
Industry or important pollution sources	*Impact*	High	Low–Medium	High	High	Medium

[a] *With respect to the existing non-disclosure agreement with the individual wastewater treatment plants (WWTPs), all the names, locations, as well as specific technologies are kept confidential.*

Table S4.2 *Basic characteristics and bulk chemical composition of the tested soil samples.*

Soil ID	Particle size distribution (%)			mg/kg												pH_{H_2O}[a]	TC (%)	TN (%)
	Sand	Silt	Clay	As	Cd	Cu	Pb	Sb	Zn	Ca	Fe	K	Mg	Mn	Na			
Zn-rich	75	20	5	385 ±11	31.6 ±1	82 ±1	3854 ±121	63.7 ±4.7	3082 ±83	1436 ±26	32974 ±629	1529 ±43	2453 ±40	4695 ±99	402 ±7	5.95	1.9 ±0.01	<0.07
Smelter	81	11	8	307 ±45	48 ±5	309 ±13	8604 ±675	231 ±86	3559 ±207	11120 ±605	45143 ±1656	7704 ±452	1612 ±121	2299 ±136	4356 ±132	7.49	4.3 ±0.01	<0.07
As-rich	89	6	5	17563 ±280	3 ±0.001	51 ±5	73 ±12	<15 $\times10^{-6}$	193 ±12	8574 ±648	68910 ±4274	2900 ±522	13179 ±857	1096 ±124	214 ±15	6.09	3.8 ±0.4	0.4 ±0.001
Brown-field	43	37	20	7 ±0.001	<6 $\times10^{-6}$	13 ±0.001	130 ±16	20 ±0.001	86 ±7	669 ±69	29606 ±1032	5818 ±4414	147 ±39	465 ±110	3026 ±2320	5.19	9.7 ±0.3	0.3 ±0.001
Garden	39	45	16	15 ±1	1 ±0.001	38 ±2	79 ±10	2 ±0.001	128 ±10	4497 ±342	22421 ±1023	10431 ±735	76 ±15	536 ±35	4044 ±266	7.38	16 ±0.01	0.2 ±0.001

[a] According to ISO 10390 (2005).
Red values represent the detection limit

Table S4.3 *Bulk concentration of elements after total digestion of input raw sludges (S) and studied sludgechars (SC) (part 1/2).*

	Materials									
	S1	SC1	S2	SC2	S3	SC3	S4	SC4	S5	SC5
Risk metals and metalloids in mg/kg										
As*	3.37 ±0.39	6.51 ±0.12	2.46 ±0.01	7.58 ±3.36	6.12 ±0.19	8.65 ±5.21	5.36 ±0.60	12.5 ±4.13	12.1 ±0.10	10.7 ±2.32
Cd*	1.05 ±0.03	1.66 ±0.28	0.75 ±0.01	1.58 ±0.14	1.04 ±0.09	3.19 ±0.19	0.92 ±0.01	3.06 ±1.36	1.37 ±0.01	2.03 ±0.18
Co	6.40 ±0.04	12.9 ±0.10	3.34 ±0.04	7.42 ±0.23	9.38 ±0.44	18.1 ±0.95	8.66 ±0.15	19.8 ±0.04	5.70 ±0.12	10.4 ±0.20
Cr*	42.2 ±6.29	15.5 ±3.84	25.0 ±1.97	39.4 ±4.85	51.1 ±3.22	25.1 ±4.36	53.9 ±3.26	47.2 ±20.9	51.7 ±0.59	27.2 ±5.23
Cu*	218 ±8.81	332 ±28.2	134 ±2.60	190 ±36.7	1265 ±111	1776 ±229	253 ±12.4	410 ±45.5	204 ±3.33	268 ±29.2
Ni*	23.7 ±0.96	49.6 ±1.53	19.5 ±0.31	46.8 ±2.17	410 ±27.2	692 ±50.3	55.0 ±1.33	116 ±2.7	26.5 ±0.33	53.8 ±2.80
Pb*	28.0 ±5.61	27.9 ±3.46	14.0 ±0.99	22.3 ±3.10	35.9 ±4.44	20.1 ±0.57	28.9 ±7.81	28.8 ±12.1	22.4 ±1.65	36.2 ±8.87
Sb	2.92 ±0.47	2.24 ±0.65	3.50 ±0.06	4.02 ±0.66	3.53 ±0.35	3.09 ±0.20	15 ±4.49	4.91 ±2.08	57.1 ±0.81	8.70 ±2.15
Zn*	736 ±23.6	1428 ±9.78	804 ±11.5	2155 ±70.2	906 ±47.2	1717 ±115	930 ±72.3	1732 ±17.0	843 ±13.0	1593 ±48.9
Hg*	1.51 ±0.21	<0.01	0.68 ±0.04	<0.01	1.41 ±0.32	<0.01	1.87 ±0.16	<0.01	1.76 ±0.19	<0.01

Table S4.3 Bulk concentration of elements after total digestion of input raw sludges (S) and studied sludgechars (SC) (part 2/2).

Materials	S1	SC1	S2	SC2	S3	SC3	S4	SC4	S5	SC5
Other metals and nutrients in mg/kg										
Ca	18193 ±525	63968 ±1700	17449 ±813	59869 ±1349	19350 ±226	66673 ±5734	11454 ±1885	52844 ±307	11587 ±859	46984 ±1107
Fe	19286 ±4906	22142 ±4552	4821 ±695	10972 ±1388	11666 ±228	18704 ±79.5	17006 ±226	38387 ±15345	13401 ±122	24210 ±2710
K	2682 ±73.9	4786 ±77.4	2911 ±296	7821 ±332	3658 ±157	5478 ±804	3550 ±606	5049 ±32.7	4465 ±225	5255 ±85.6
Mg	1544 ±15.4	9611 ±308	1138 ±136	9345 ±251	1487 ±64.6	11969 ±850	898 ±89.3	8529 ±8.63	1333 ±167	14114 ±197
Mn	296 ±7.58	555 ±12.4	135 ±1.49	281 ±8.43	228 ±13.5	393 ±26.3	376 ±29.8	623 ±4.86	233 ±3.73	436 ±8.61
Na	1042 ±134	1313 ±40.3	1421 ±27.6	2883 ±110	1244 ±78.1	1633 ±120	2003 ±16.3	1837 ±8.56	1562 ±31.4	1114 ±40.0
P	11560 ±2938	10428 ±4558	14973 ±1000	30239 ±1861	14196 ±1973	18075 ±1840	12192 ±1589	24514 ±9542	11295 ±142	16066 ±1718
S	7128 ±609	4527 ±700	12756 ±263	9315 ±181	14666 ±855	11384 ±2112	9419 ±1708	11958 ±656	8984 ±289	5358 ±605

*The Decree No 273/2021 Coll., Annex 38 establishes limit concentrations for the given elements, i.e. 30 mg/kg for As, 5 mg/kg for Cd, 200 mg/kg for Cr, 500 mg/kg for Cu, 100 mg/kg for Ni, 200 mg/kg for Pb, 2500 mg/kg for Zn, and 4 mg/kg for Hg; (exceeded limits marked in red).
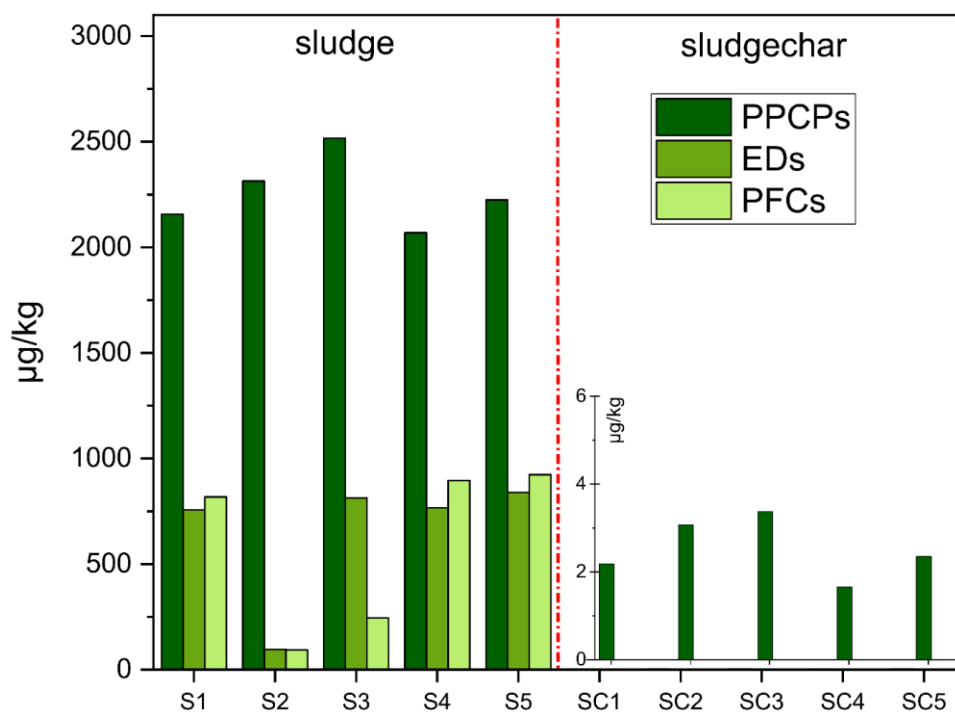
Figure S4.1 *Concentrations of pharmaceutical and personal care products (PPCPs), endocrine disruptors (EDs), and per/poly-fluorinated compounds (PFCs) determined in input raw sludges (S) and studied sludgechars (SC).*
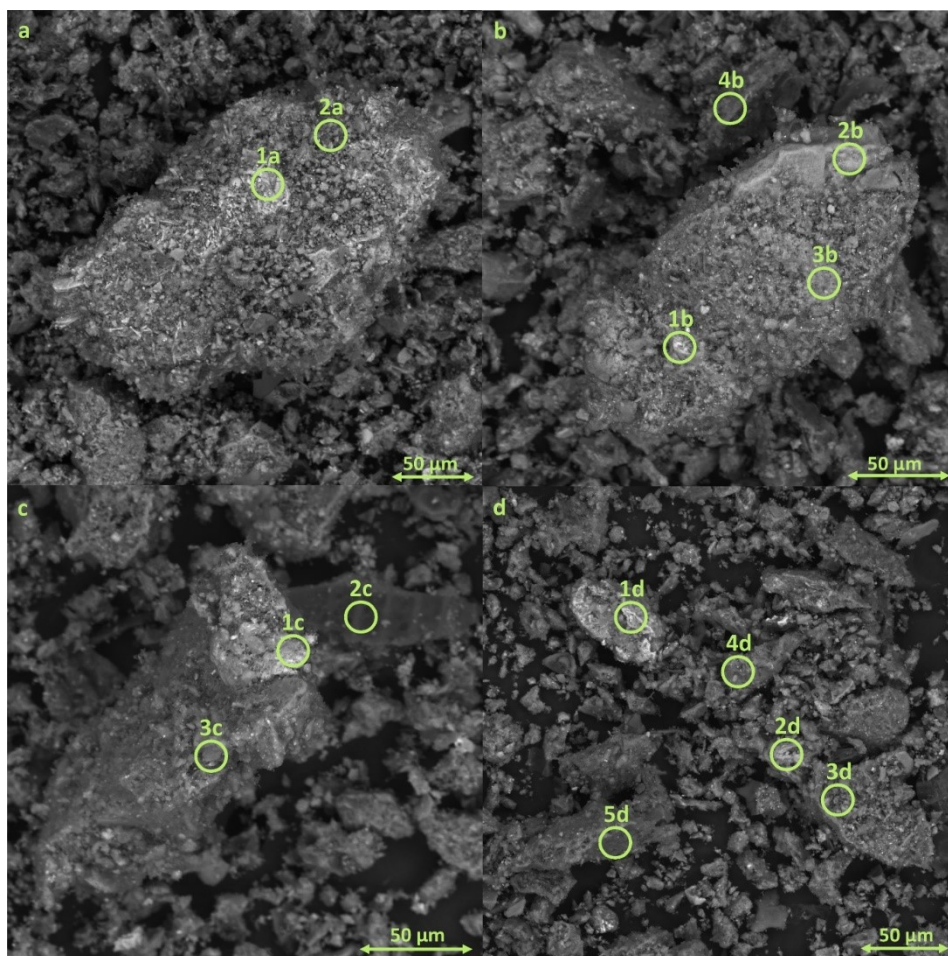
Figure S4.2_1 *Selected back-scattered electron images from the SEM/EDS analysis of SC1 on carbon-coated pins.1a) possibly phosphate particle rich in Fe (>30 wt.%), P (~16 wt.%), Mg (~5 wt.%) and trace amounts (<1 wt.%) of Ca and Zn; 2a) possibly silicate particles with Fe, Ca, and P with small amounts (1-5 wt.%) of Al, Mg and S; 1b) C-rich particle covered with Ca-S rich formation with traces of Fe (<2 wt.%); 2b) possibly Ca-Mg sulphate (Ca >30 wt.%, Mg >20 wt.%, S >20 wt.%); 3b) formation rich in Ca and P; 4b) silicate with Fe, Al, Ca, and P; 1c) possible phosphate rich in Fe (>30 wt.%) with Ca and Mg (<5 wt.%) and trace amounts (<1 wt.%) of Zn, see respective EDS spectrum in Fig. S4.3a; 2c) carbon particle with small to trace amounts of Fe, Ca, and P, see respective EDS spectrum in Fig. S4.3b; 3c) mixed analysis of several compounds containing Fe, Si, Ca, P, and Al (≤10 wt.%) and high amount of oxygen; 1d) particle rich in Fe (>45 wt.%) and S (>20 wt.%) with low amount of oxygen; 2d) possible phosphate with Fe (>30 wt.%), Ca and Mg (<5 wt.%), P (~15 wt.%); 3d) possible silicate with Fe, Ca, Al, and P (≤10 wt.%) and traces (~1 wt.%) of Mg and S; 4d) mixed analysis with mainly P, Fe, Ca, Si and low oxygen content; 5d) quartz particle.*
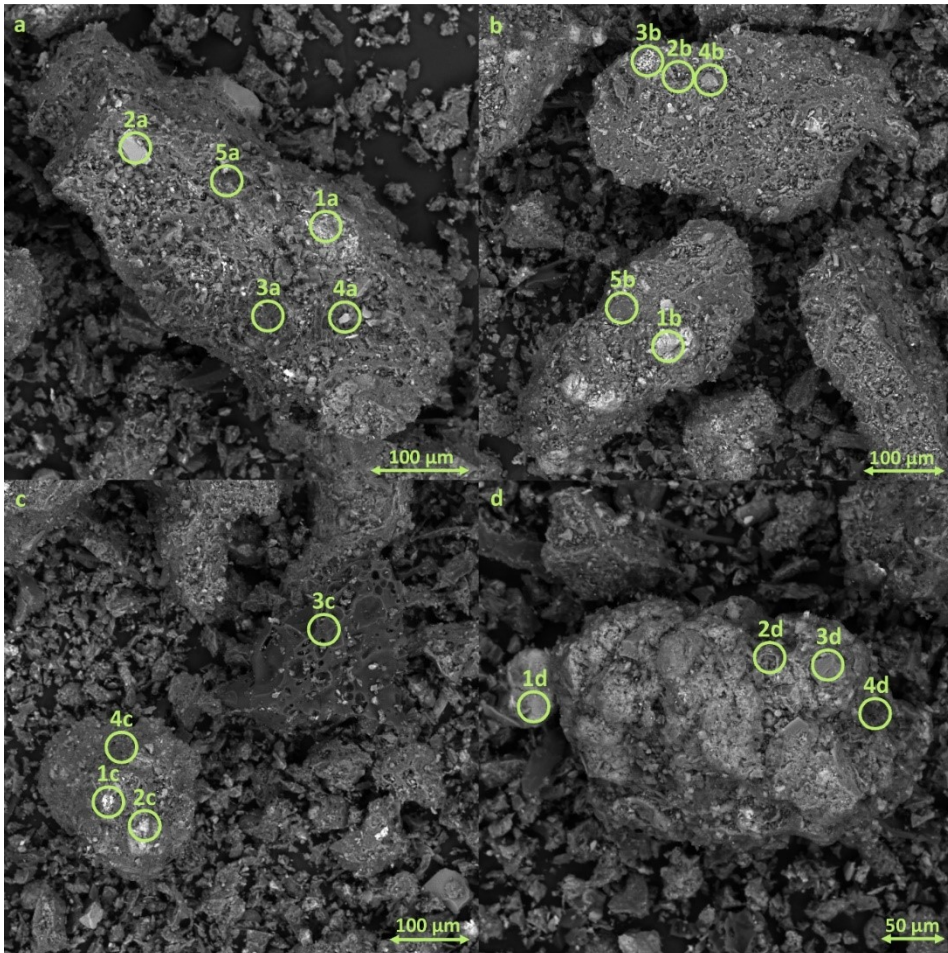
Figure S4.2_2 *Selected back-scattered electron images from the SEM/EDS analysis of SC2 on carbon-coated pins. 1a) formation containing mainly Ca, Fe, S, and oxygen adhering to carbon particle; 2a) particle with Fe, Ca, and Si with low oxygen content (<10 wt.%) on top of carbon particle; 3a) carbon particle; 4a) (alumino)silicates with Fe, K, Ca, and Mg; 5a) mixed analysis of several compounds with Ca >>P >Fe >Si, Al, S with moderate oxygen (~20 wt.%), and high carbon; 1b) particle containing mainly Ca and S with low oxygen amount; 2b) mixed analysis of several compounds including Cu-S rich particle with low oxygen amount; 3b) possible Ca phosphate with Fe; 4b) quartz particle; 5b) mixed analysis of several compounds containing P >>Ca >>Si >Mg >Na, K; 1c) particle point rich in Fe (≥80 wt.%) with low oxygen content; 2c) Ca sulphate particle; 3c) carbon particle with porous structure, see respective EDS spectrum in Fig. S4.3c; 4c) mixed analysis of carbon particle and adhering compounds containing Ca >P >Si >Al, Mg, Fe, S > K and moderate oxygen; 1d) possible Fe phosphate particle with Ca and Mg, see respective EDS spectrum in Fig. S4.3d; 2d) possible Ca-Fe phosphate; 3d) quartz; 4d) mixed analysis of carbon particle and adhering compounds containing Ca >P > Si > Fe > Al > Mg, Zn, S and high oxygen (> 30 wt.%).*
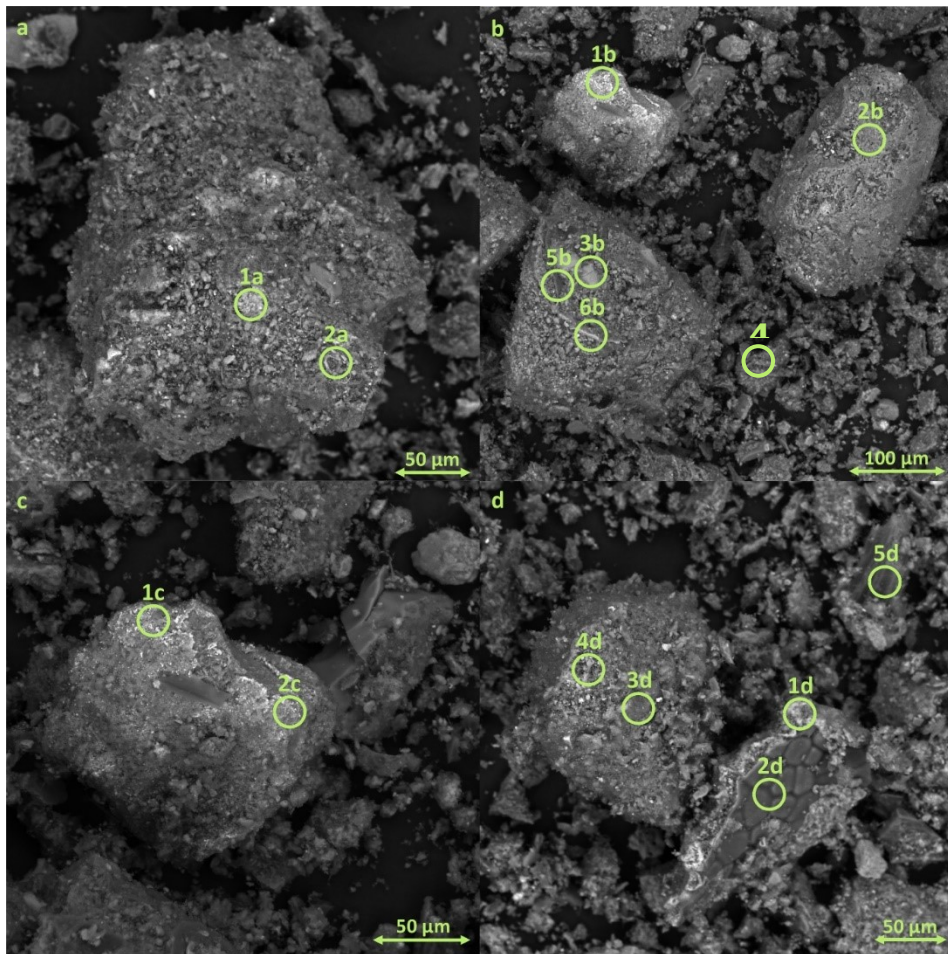
Figure S4.2_3 *Selected back-scattered electron images from the SEM/EDS analysis of SC3 on carbon-coated pins.1a) mixed analysis of several compounds including Ca sulphate and traces (~1 wt.%) of P and Fe. 2a) (alumino)silicates with Fe, Mg, Ca, and K; 1b) metallic formation rich in Fe (≥30 wt.%) and S with low oxygen amount (<10 wt.%) and trace Cu (<1 wt.%), see respective EDS spectrum in Fig. S4.3e; 2b) mixed analysis of carbon particle covered with aluminosilicates; 3b) and 4b) possible formations of Ca phosphates with up to ~6 wt.% of F and traces (<1 wt.%) of Fe and Mg; 5b) mixed analysis of carbon particle and adhering compounds containing Ca, Fe, S, Mg, and traces (<1 wt.%) of Cu; 6b) mixed analysis of carbon particle and adhering compounds including possible Ca-Fe phosphate; 1c) and 2c) formations rich in Fe and S with low amount of oxygen; 1d) possible Ca sulphate with <5 wt.% of Fe; 2d) mixed analysis of carbon particle with increased amount of Fe (<20 wt.%), S (<5 wt.%) and traces of Ca; 3d) mixed analysis of carbon particle and adhering compounds containing Ca >>Si >S >Fe, Al, P >Mg and moderate oxygen (<20 wt.%); 4d) mixed analysis of potential Ca sulphate and aluminosilicates; 5d) carbon particle with small amounts (<5 wt.%) of Ca and Fe, and trace amounts (~1 wt.%) of P and S.*
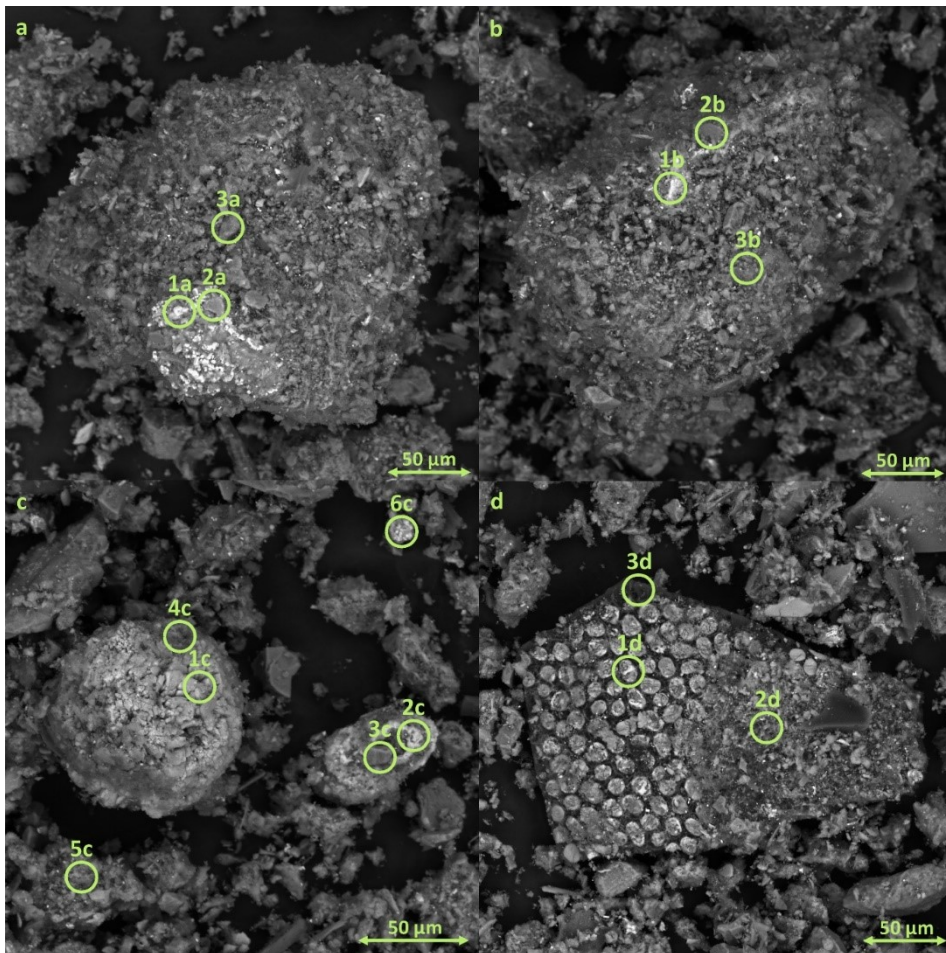
Figure S4.2_4 *Selected back-scattered electron images from the SEM/EDS analysis of SC4 on carbon-coated pins. 1a) possible Fe sulphate with traces (<1 wt.%) of Cu, see respective EDS spectrum in Fig. S4.3f; 2a) aluminosilicate containing Fe >>K, S >Na >Ca; 3a) mixed analysis of several compounds containing Ca >Fe, P >>Si, Al >Mg, S >K and oxygen; 1b) mixed analysis of several compounds with prevailing Fe and low oxygen contents (≤10 wt.%); 2b) aluminosilicate containing K >>Fe >Mg >Ca, Na; 3b) mixed analysis of several compounds containing Fe >Ca >P, Si >Al >Mg >Na, K and oxygen; 1c) mixed analysis of several compounds with potential Fe phosphate formation; 2c) mixed analysis of carbon particle and adhering compounds containing Ca and S; 3c) possible Si layer covering carbon particle; 4c) mixed analysis of several compounds with prevailing Fe phosphate; 5c) mixed analysis with prevailing Ca silicate and containing Fe, P >>Mg, S >K; 6c) mixed analysis of several compounds containing mainly Fe >>P >>Ca > Mg and low content of oxygen; 1d) Ca sulphate,; 2d) mixed analysis of C-rich particle and adhering compounds containing Ca >>S >>Fe, P, Al, Si; 3d) analysis of carbon particle containing traces (<1 wt.%) of Ca, S, and Si.*
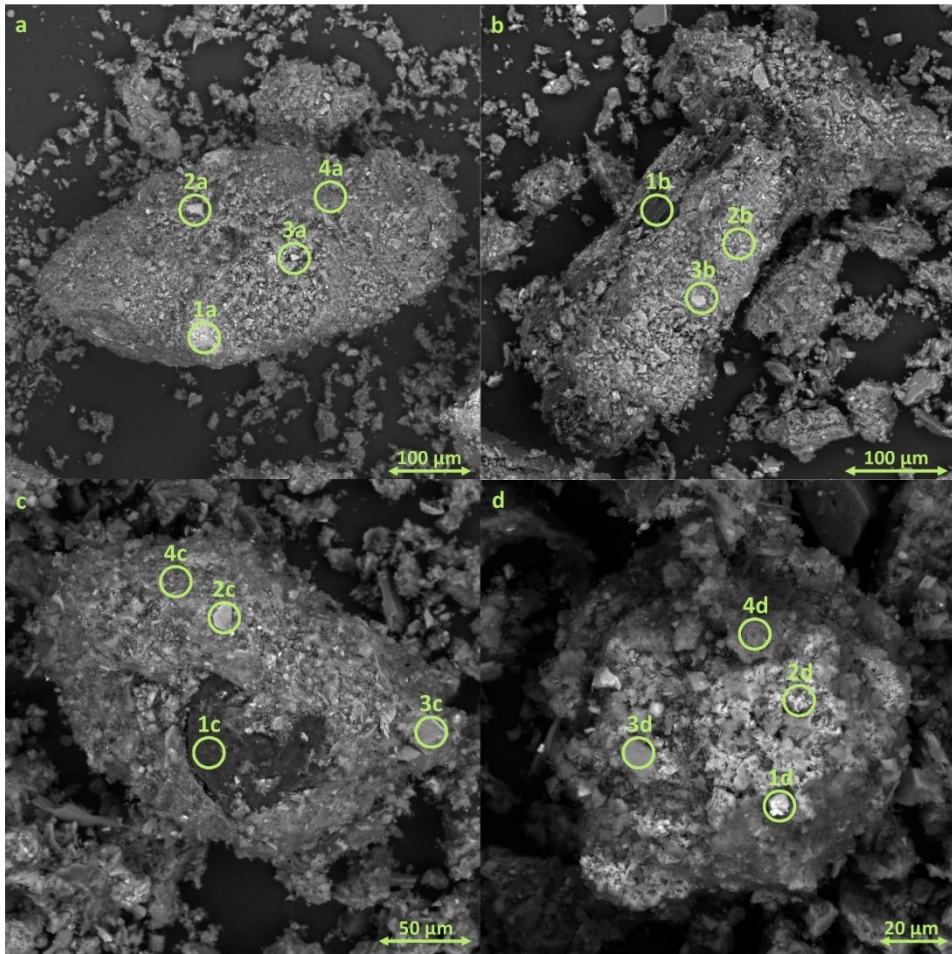
Figure S4.2_5 *Selected back-scattered electron images from the SEM/EDS analysis of SC5 on carbon-coated pins.1a) possible Fe phosphate with minor to trace amounts of Ca and Mg; 2a) aluminosilicate rich in Fe > Mg >K >> Ca; 3a) possible Fe phosphate particle; 4a) mixed analysis of several compounds containing Fe >>S, Si >P >Al, Ca >> Mg, K and oxygen;1b) carbon particle contaning traces of Ca and P with low amount of oxygen (< 10 wt%); 2b) mixed analysis of carbon particle and adhering compounds containing Fe, Ca >P, Si >Al >>Na, K and low amount of oxygen; 3b) aluminosilicate with Fe >>K >Mg contents; 1c) pure carbon particle; 2c) possible Ca-Mg sulphate; 3c) feldspar with K, Al, Si, and oxygen; 4c) mixed analysis of several compounds containing mainly Fe, Ca, P, and oxygen ; 1d) mixed analysis of several compounds rich in Fe with moderate oxygen content (<20 wt.%); 2d) possible Fe(-Ca) phosphate with trace amounts of Zn see respective EDS spectrum in Fig. S4.3g; 3d) silicate with Al >>Fe >>K, P>> Ca and traces (<1 wt.%) of Mg and Na, see respective EDS spectrum in Fig. S4.3h; 4d) mixed analysis of C-rich particle and adhering compounds containing Fe, Ca, P, Si >>Al >Mg >K >>Na and oxygen.*
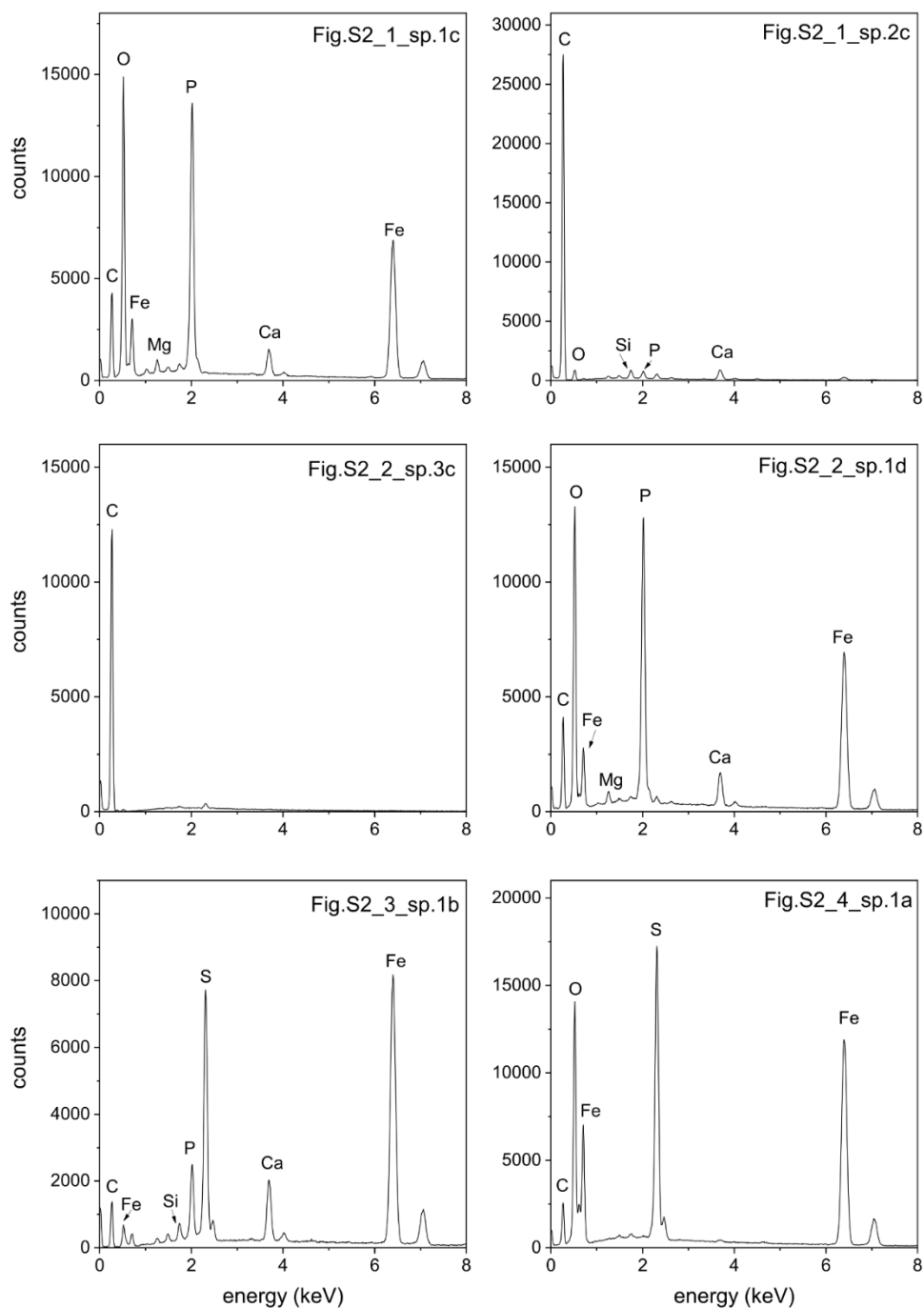
Figure S4.3_1 *Corresponding spectra from the EDS analysis of selected points as depicted in Fig. S4.2.*
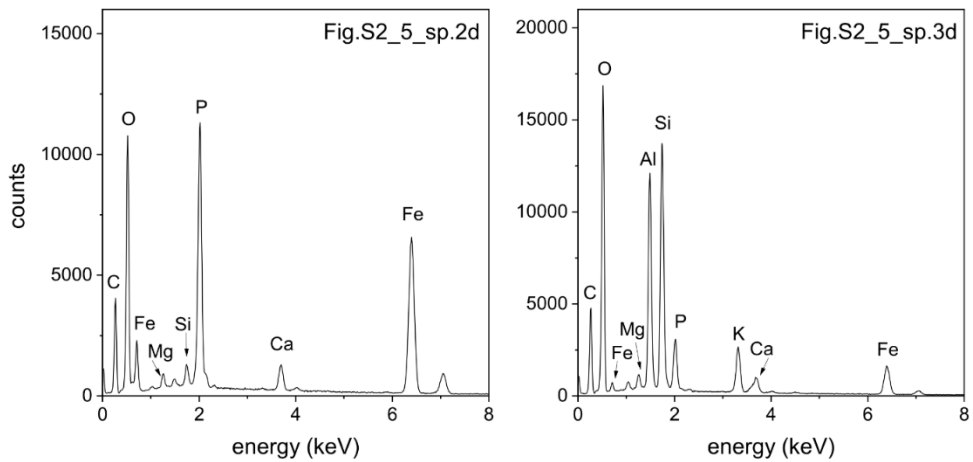
Figure S4.3_2 Corresponding spectra from the EDS analysis of selected points as depicted in Fig. S4.2 (continuation).
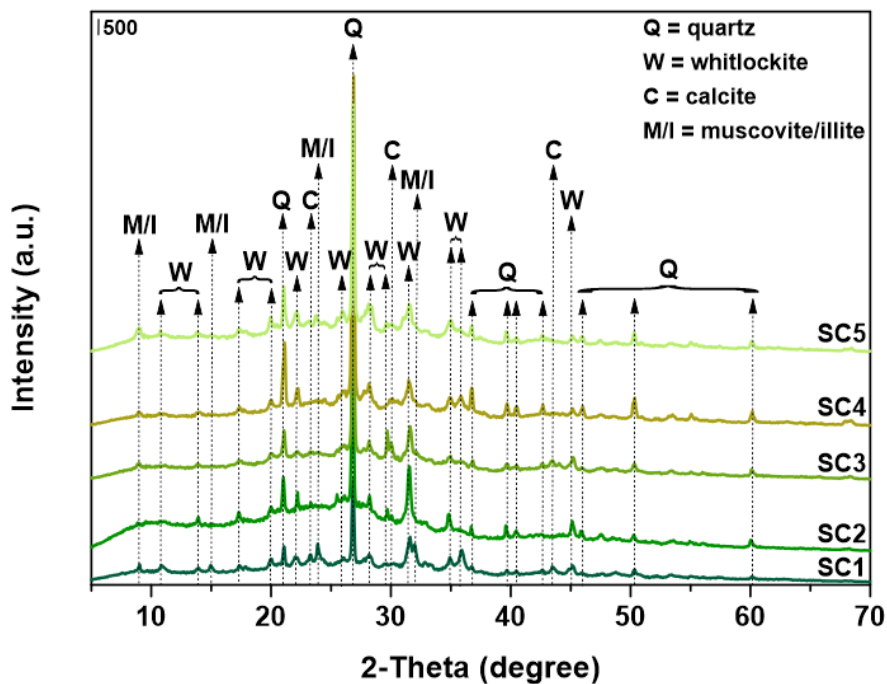
Figure S4.4 Diffractograms from the XRD analysis of the five studied sludgechars. In addition to crystalline phases, an amorphous character of SCs is also evident, i.e. broadening of some diffraction lines and the presence of an amorphous hump between 15–30 2θ.
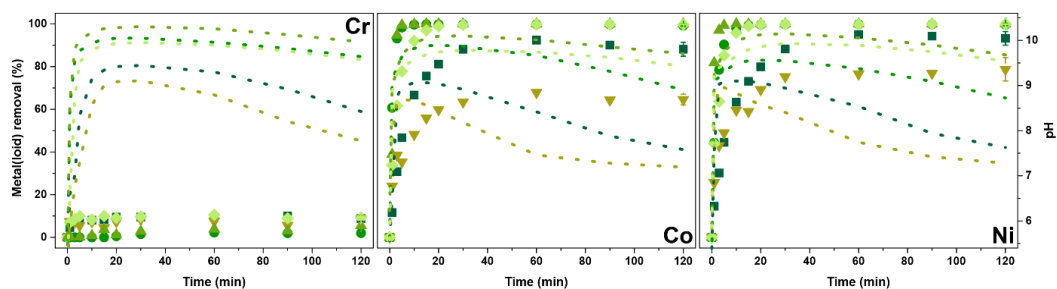
Figure S4.5 *Sorption efficiency (points) of the five sludgechars in single solutions of additional metal anions (Cr) and cations (Co and Ni) at natural pH (i.e. without control shown by dotted lines).*
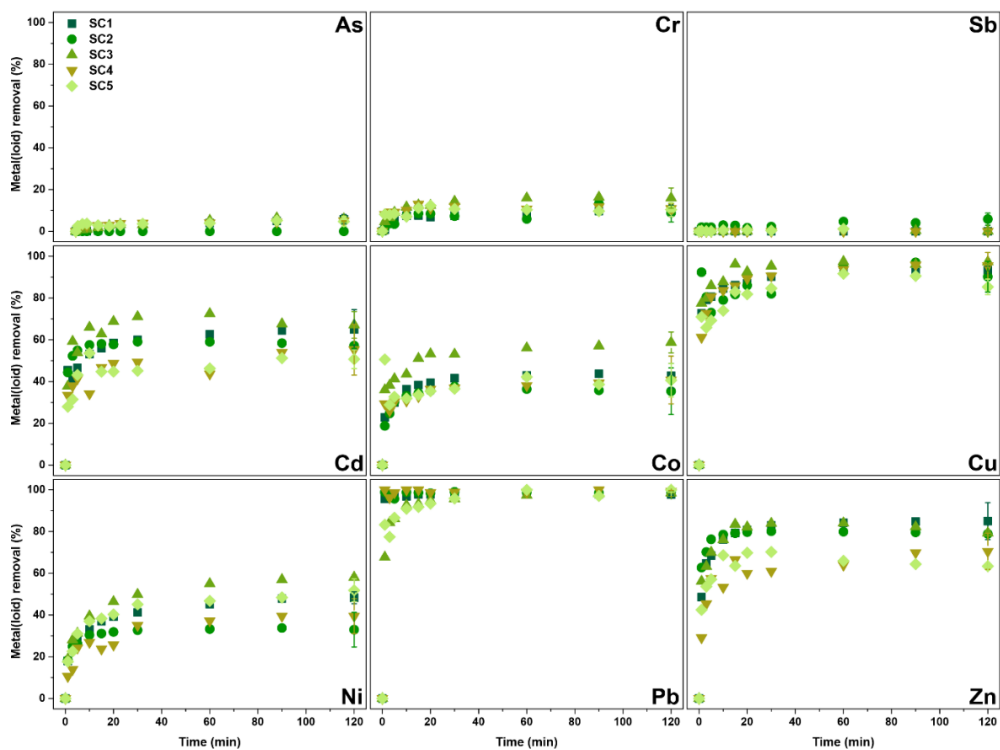
Figure S4.6 *Sorption efficiency of the five sludgechars in single solutions of metal(loid) anions (As, Cr, and Sb) and cations (Cd, Co, Cu, Ni, Pb, and Zn) at pH 7.*
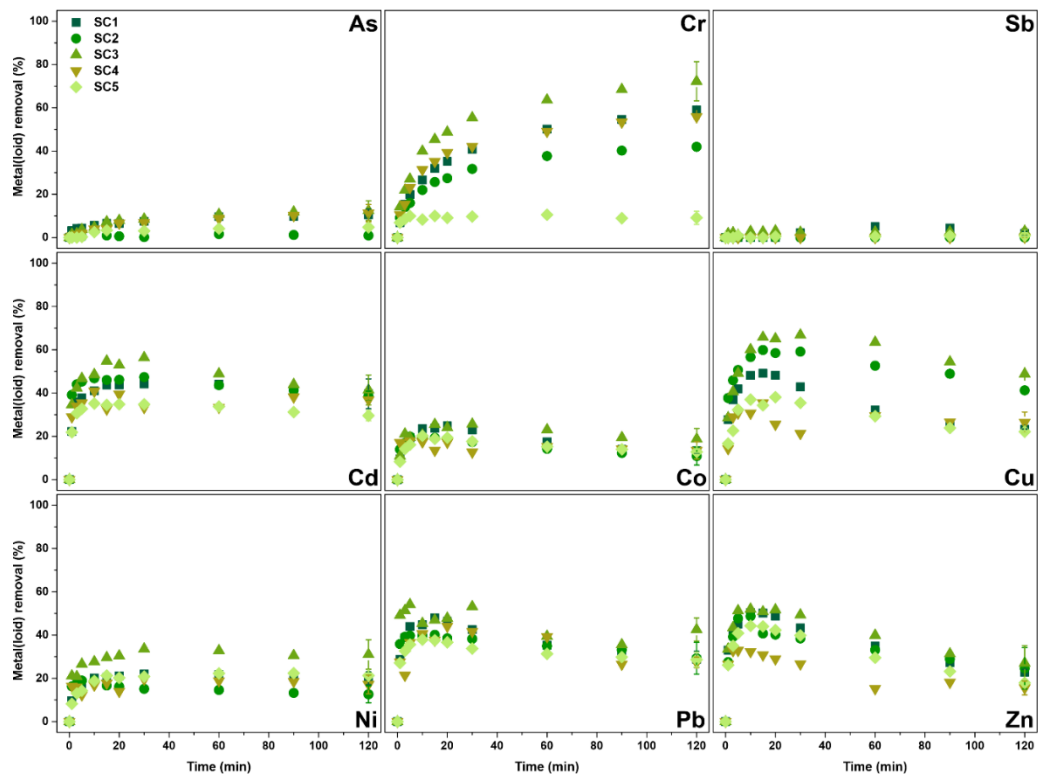
Figure S4.7 Sorption efficiency of the five sludgechars in single solutions of metal(loid) anions (As, Cr and, Sb) and cations (Cd, Co, Cu, Ni, Pb, and Zn) at pH 5.

Table S4.4 *Saturation indices (SI) of selected solubility-controlling phases during kinetic experiment calculated by MINTEQ 3.1 (bold = SI > 0, i.e. supersaturation of the leachates with respect to the solid phase; grey filling = -1 < SI > 1, i.e. saturation close to zero) (part 1/5).*

	Phase	SC1			SC2			SC3			SC4			SC5		
								pH								
		natural[a]	5	7	natural[a]	5	7	natural[a]	5	7	natural[a]	5	7	natural[a]	5	7
Cd	Cd(OH)₂(s)	-2.32	-7.69	-3.70	-0.63	-7.70	-3.70	-1.37	-7.70	-3.71	-2.75	-7.70	-3.70	-0.99	-7.68	-3.70
	Cd₃(PO4)₂(s)	**0.84**	-9.01	-2.01	**0.59**	-8.29	-1.85	-4.66	-8.16	-1.75	-0.17	-8.48	-1.33	-2.52	-9.00	-1.93
	Cd₄(OH)₆SO₄(s)	-2.76	-18.9	-6.99	**1.53**	-18.87	-6.83	-3.11	-19.1	-7.02	-3.91	-18.9	-6.97	-1.24	-20.0	-7.05
	Otavite	**1.76**	-3.60	**0.39**	**3.46**	-3.62	**0.38**	**2.72**	-3.62	**0.38**	**1.34**	-3.61	**0.39**	**3.09**	-3.59	**0.39**
Co	Co(OH)₂(am)	-2.00	-7.14	-3.15	-0.01	-7.15	-3.15	**0.17**	-7.15	-3.15	-2.76	-7.14	-3.14	**0.14**	-7.13	-3.15
	Co(OH)₂(c)	-1.19	-6.33	-2.34	**0.80**	-6.34	-2.35	**0.97**	-6.35	-2.35	-2.00	-6.34	-2.34	**0.95**	-6.32	-2.34
	Co₃(PO4)₂(s)	**2.84**	-6.92	**0.19**	**3.19**	-6.19	**0.35**	**0.02**	-6.06	**0.45**	**2.00**	-6.38	**0.88**	**1.38**	-6.91	**0.27**
	CoCO₃(s)	**0.73**	-4.41	-0.42	**2.72**	-4.42	-0.43	**2.89**	-4.43	-0.43	-0.04	-4.42	-0.42	**2.87**	-4.40	**-0.42**
	CoO(s)	-2.49	-7.63	-3.64	-0.50	-7.64	-3.64	**-0.33**	-7.64	-3.64	-3.25	-7.63	-3.64	-0.35	-7.62	-3.64

[a] natural pH = measured pH value after 120 min of kinetic experiments with individual metals (see Figs. 4.3, S4.5)

Table S4.4 Saturation indices (SI) of selected solubility-controlling phases during kinetic experiment calculated by MINTEQ 3.1 (bold = SI > 0, i.e. supersaturation of the leachates with respect to the solid phase; grey filling = -1 < SI > 1, i.e. saturation close to zero) (part 2/5).

	Phase	SC1			SC2			SC3			SC4			SC5		
								pH								
		natural[a]	5	7	natural[a]	5	7	natural[a]	5	7	natural[a]	5	7	natural[a]	5	7
	Antlerite	**2.60**	-5.23	**1.89**	**1.24**	-5.21	**2.05**	-4.17	-5.41	**1.87**	**1.63**	-5.28	**1.91**	-2.37	-6.34	**1.82**
	Atacamite	-10.5	-4.85	**0.66**	-11.0	-16.5	-11.1	-14.2	-16.5	**0.63**	**0.20**	-4.91	**0.38**	-1.51	-4.97	**0.35**
	Azurite	**5.01**	-7.87	**3.31**	**6.13**	-7.91	**3.29**	**2.60**	-7.92	**3.29**	**2.69**	-7.89	**3.30**	**3.99**	-7.84	**3.30**
	Brochantite	**6.42**	-5.71	**5.14**	**5.43**	-5.70	**5.29**	-1.16	-5.91	**5.12**	**4.67**	-5.76	**5.15**	**1.11**	-6.81	**5.07**
	Cu(OH)₂(s)	**0.96**	-3.34	**0.39**	**1.33**	-3.35	**0.39**	**0.16**	-3.35	**0.39**	**0.19**	-3.34	**0.39**	**0.62**	-3.32	**0.39**
	Cu₂(OH)₃NO₃(s)	-12.3	-6.47	-0.48	-1.41	-5.61	-0.25	-4.27	-5.46	-0.14	-2.33	-5.88	-0.71	-3.15	-6.61	-0.33
Cu	*Cu₃(PO₄)₂(s)*	**2.49**	-4.77	**1.40**	-1.71	-4.04	**1.56**	-8.70	-3.91	**1.67**	**2.39**	-4.23	**2.08**	-6.23	-4.76	**1.48**
	Cu₃(PO₄)₂·3H₂O(s)	**0.76**	-6.50	-0.34	-3.44	-5.78	-0.17	-10.4	-5.64	-0.06	**0.66**	-5.96	**0.35**	-7.96	-6.49	-0.25
	CuCO₃(s)	**0.18**	-4.11	-0.39	**0.55**	-4.13	-0.39	-0.62	-4.13	-0.39	-0.59	-4.12	-0.39	-0.16	-4.10	-0.39
	Langite	**4.15**	-7.97	**2.87**	**3.16**	-7.97	**3.03**	-3.43	-8.17	**2.85**	**2.40**	-8.03	**2.89**	-1.16	-9.08	**2.80**
	Malachite	**4.40**	-4.19	**3.26**	**5.15**	-4.21	**3.25**	**2.79**	-4.22	**3.25**	**2.85**	-4.20	**3.26**	**3.72**	-4.17	**3.26**
	Tenorite(am)	**1.76**	-2.54	**1.19**	**2.13**	-2.55	**1.19**	**1.00**	-2.55	**1.19**	**0.99**	-2.54	**1.19**	**1.42**	-2.52	**1.19**
	Tenorite(c)	**2.61**	-1.69	**2.04**	**2.98**	-1.70	**2.04**	**1.81**	-1.70	**2.04**	**1.84**	-1.69	**2.04**	**2.27**	-1.67	**2.04**

[a] natural pH = measured pH value after 120 min of kinetic experiments with individual metals (see Figs. 4.3, S4.5)

Table S4.4 Saturation indices (SI) of selected solubility-controlling phases during kinetic experiment calculated by MINTEQ 3.1 (bold = SI > 0, i.e. supersaturation of the leachates with respect to the solid phase; grey filling = -1 < SI > 1, i.e. saturation close to zero) (part 3/5).

| | | SC1 | | | SC2 | | | SC3 | | | SC4 | | | SC5 | |
	Phase	natural[a]	5	7	natural[a]	5	7	natural[a]	5	7	natural[a]	5	7	natural[a]	5	7
									pH							
Ni	Ni(OH)₂(am)	-1.71	-6.93	-2.94	-0.10	-6.95	-2.95	0.10	-6.95	-2.95	-2.39	-6.94	-2.94	**0.09**	-6.92	-2.94
	Ni(OH)₂(c)	**0.39**	-4.83	-0.84	**2.00**	-4.85	-0.85	**2.20**	-4.85	-0.85	-0.29	-4.84	-0.84	**2.19**	-4.82	-0.84
	Ni₃(PO₄)₂(s)	-0.44	-10.3	-3.20	-0.34	-9.58	-3.04	-4.05	-9.45	-2.93	-1.15	-9.77	-2.51	-3.32	-10.3	-3.12
	NiCO₃(s)	**0.81**	-4.41	-0.42	**2.42**	-4.42	-0.43	**2.62**	-4.43	-0.43	**0.14**	-4.42	-0.42	**2.61**	-4.40	-0.42

[a]natural pH = measured pH value after 120 min of kinetic experiments with individual metals (see Figs. 4.3, S4.5)

Table S4.4 Saturation indices (SI) of selected solubility-controlling phases during kinetic experiment calculated by MINTEQ 3.1 (bold = SI > 0, i.e. supersaturation of the leachates with respect to the solid phase; grey filling = -1 < SI > 1, i.e. saturation close to zero) (part 4/5).

	Phases	SC1			SC2			SC3			SC4			SC5		
		natural[a]	5	7	natural[a]	5	7	natural[a]	5	7	natural[a]	5	7	natural[a]	5	7
								pH								
Pb	Anglesite	-0.92	-0.57	-0.77	-4.08	-0.53	-0.60	-6.19	-0.73	-0.77	-0.74	-0.62	-0.75	-5.44	-1.70	-0.84
	Cerrusite	2.15	-2.42	1.45	2.24	-2.43	1.44	1.35	-2.44	1.44	1.61	-2.43	1.45	1.76	-2.40	1.45
	Hydrocerrusite	7.17	-6.53	5.07	7.44	-6.57	5.05	4.78	-6.57	5.05	5.57	-6.55	5.07	6.01	-6.48	5.07
	Hydroxyl pyromorphite	18.2	3.32	15.4	8.30	4.39	15.6	0.60	4.59	15.8	17.6	4.12	16.4	4.09	3.36	15.5
	Chloro pyromorphite(c)	16.3	15.6	25.7	4.78	5.02	14.2	-3.42	5.21	26.1	27.6	16.3	26.4	11.8	15.5	25.5
	Chloro pyromorphite (soil)	12.3	11.6	21.7	0.75	1.00	10.2	-7.45	1.18	22.0	23.6	12.3	22.4	7.74	11.5	21.5
	Larnakite	2.24	-1.98	1.69	-0.83	-1.95	1.85	-3.83	-2.15	1.68	1.89	-2.03	1.72	-2.67	-3.10	1.63
	$Pb(OH)_2(s)$	2.37	-2.20	1.67	2.46	-2.21	1.66	1.57	-2.22	1.66	1.83	-2.21	1.67	1.98	-2.19	1.67
	$Pb2(OH)3Cl(s)$	-11.3	-6.27	-0.47	-12.7	-17.9	-12.2	-15.0	-17.9	-0.51	-0.44	-6.33	-0.75	-2.49	-6.38	-0.78
	$Pb_2OCO_3(s)$	0.02	-9.11	-1.38	0.20	-9.14	-1.39	-1.57	-9.14	-1.39	-1.05	-9.12	-1.38	-0.76	-9.08	-1.38
	$Pb_3(PO_4)_2(s)$	10.3	1.90	8.64	3.67	2.62	8.79	-1.17	2.75	8.90	10.1	2.43	9.33	1.02	1.92	8.72
	$Pb_3O_2CO_3(s)$	-1.05	-14.7	-3.14	-0.77	-14.8	-3.16	-3.43	-14.8	-3.16	-2.64	-14.8	-3.14	-2.21	-14.7	-3.14
	$Pb_3O_2SO_4(s)$	1.63	-7.15	0.39	-1.34	-7.14	0.54	-5.23	-7.34	0.37	0.75	-7.20	0.41	-3.66	-8.25	0.32
	$Pb_4(OH)_6SO_4(s)$	1.73	-11.6	-0.21	-1.15	-11.6	-0.06	-5.93	-11.8	-0.24	0.32	-11.7	-0.18	-3.94	-12.7	-0.28
	$Pb_4O_3SO_4(s)$	0.95	-12.4	-1.00	-1.93	-12.4	-0.84	-6.70	-12.6	-1.02	-0.45	-12.5	-0.96	-4.72	-13.5	-1.06
	$PbHPO_4(s)$	1.92	0.02	1.45	-1.43	0.38	1.53	-3.41	0.45	1.56	2.08	0.29	1.79	-2.52	0.02	1.49
	$PbO·0.3H_2O(s)$	-2.45	-7.03	-3.16	-2.37	-7.04	-3.17	-3.261	-7.05	-3.17	-3.00	-7.04	-3.16	-2.85	-7.02	-3.17

[a]natural pH = measured pH value after 120 min of kinetic experiments with individual metals (see Figs. 4.3, S4.5)

Table S4.4 Saturation indices (SI) of selected solubility-controlling phases during kinetic experiment calculated by MINTEQ 3.1 (bold = SI > 0, i.e. supersaturation of the leachates with respect to the solid phase; grey filling = -1 < SI > 1, i.e. saturation close to zero) (part 5/5).

Phase	SC1			SC2			SC3 pH			SC4			SC5		
	natural[a]	5	7	natural[a]	5	7	natural[a]	5	7	natural[a]	5	7	natural[a]	5	7
Hydrozincite	**3.24**	-22.1	-2.11	**10.6**	-22.1	-2.15	**6.09**	-22.1	-2.25	**0.06**	-22.1	-2.11	**10.4**	-22.0	-2.12
Smithsonite	**0.35**	-4.71	-0.72	**1.81**	-4.72	-0.73	**0.92**	-4.73	-0.73	-0.29	-4.72	-0.72	**1.78**	-4.70	-0.73
Zincite	-0.22	-5.27	-1.29	**1.25**	-5.29	-1.29	**0.36**	-5.29	-1.29	-0.85	-5.28	-1.28	**1.22**	-5.26	-1.29
Zn(OH)₂ (am)	-1.46	-6.52	-2.53	**0.00**	-6.53	-2.54	-0.89	-6.53	-2.54	-2.10	-6.52	-2.53	-0.03	-6.51	-2.53
Zn(OH)₂ (β)	-0.74	-5.80	-1.81	**0.72**	-5.81	-1.82	-0.17	-5.81	-1.82	-1.38	-5.80	-1.81	**0.69**	-5.79	-1.81
Zn(OH)₂ (δ)	-0.83	-5.89	-1.90	**0.63**	-5.90	-1.91	-0.26	-5.90	-1.91	-1.47	-5.89	-1.90	**0.60**	-5.88	-1.90
Zn Zn(OH)₂ (ε)	-0.52	-5.58	-1.59	**0.94**	-5.59	-1.60	**0.05**	-5.59	-1.60	-1.16	-5.58	-1.59	**0.91**	-5.57	-1.59
Zn(OH)₂ (γ)	-0.72	-5.78	-1.79	**0.74**	-5.79	-1.80	-0.15	-5.79	-1.80	-1.36	-5.78	-1.79	**0.71**	-5.77	-1.79
Zn₃(PO₄)₂·4H₂O(s)	**3.40**	-6.19	**0.88**	**2.18**	-5.46	**1.04**	-5.17	-5.33	**1.15**	**2.74**	-5.65	**1.57**	**0.66**	-6.18	**0.96**
Zn₄(OH)₆SO₄(s)	-3.68	-18.9	-7.00	-0.45	-18.9	-6.84	-6.50	-19.1	-7.02	-5.63	-18.9	-6.96	-1.57	-20.0	-7.06
ZnCO₃(s)	**0.25**	-4.81	-0.82	**1.71**	-4.82	-0.83	**0.82**	-4.83	-0.83	-0.39	-4.82	-0.82	**1.68**	-4.80	-0.83
ZnCO₃·1H₂O(s)	-0.29	-5.35	-1.36	-8.85	-5.36	-1.37	**0.28**	-5.37	-1.37	-0.93	-5.36	-1.36	**1.14**	-5.34	-1.36

[a] natural pH = measured pH value after 120 min of kinetic experiments with individual metals (see Figs. 4.3, S4.5)
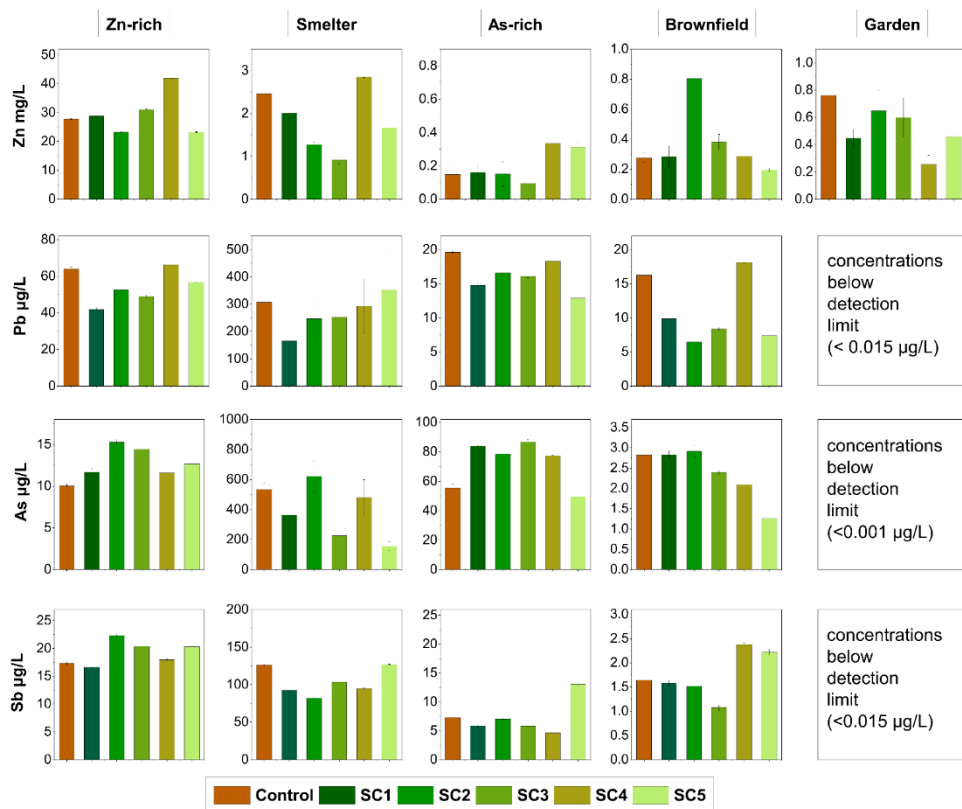
Figure S4.8 Risk elements in the soil pore water of soil samples.
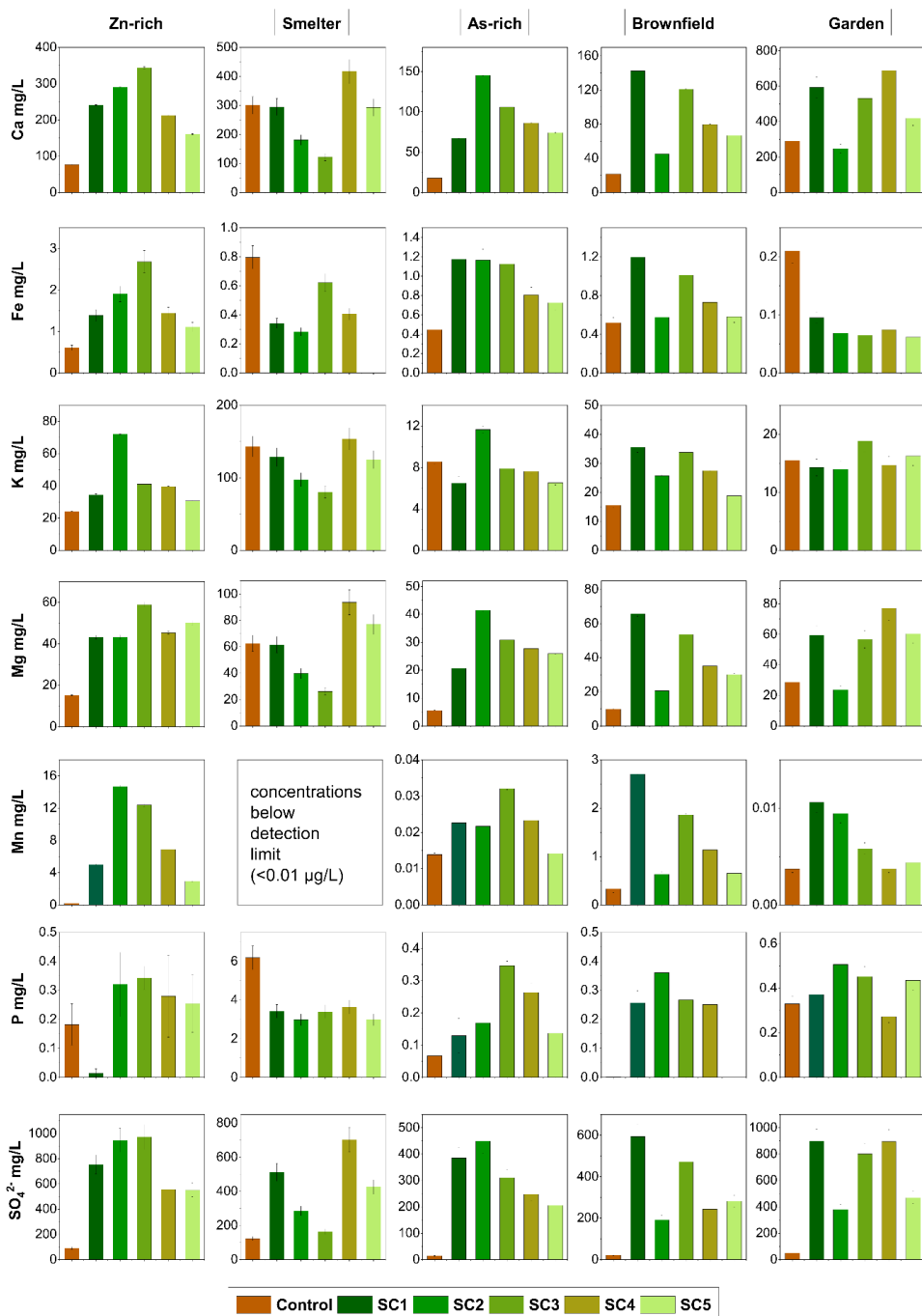
Figure S4.9 *Concentrations of nutrients in the soil pore water*

Table S4.5 *Table of the most efficient sludgechar for each risk element according to the total content of soils; high, moderate, and low.*

Risk element	Soil content	Most efficient treatment
Zn	high	SC1, SC2
	moderate	SC3
	low	SC5, SC4
Pb	high	SC1, SC3
	moderate	SC2, SC5
	low	SC2, SC5
Cd	high	SC3, SC4, SC5
	moderate	–
	low	
Cu	high	SC1, SC4
	moderate	–
	low	
As	high	SC5
	moderate	SC1
	low	SC5
Sb	high	SC2, SC5
	moderate	SC3
	low	SC4

Chapter V

Remediation of contaminated soil under dynamic redox conditions: implications for amendment efficiency in environmental relevant conditions

Aikaterini Mitzia, Martina Vítková, Xing Yang, Sabry Shaheen, Michael Komárek, Jörg Rinklebe

Content

Abstract

Immobilisation of metal(loid)s in soils is a promising remediation solution but the real environmental conditions taking place on the contaminated site need be taken into consideration. Flooding events which are likely in the field may provoke changes in the redox conditions and thus significantly affect metal(loid) mobility in soils. We employed a microcosm experiment under dynamic redox conditions to study the metal(loid) mobility and amendment efficiency under flooded conditions. A real contaminated soil with increased levels of Zn, Pb, Cd, and As was incubated for 3 months. The soil was treated with 2 wt.% of 1) a woody BC, 2) air-stable nZVI and 3) a composite of the two (nZVI-BC). The incubated soil samples were subjected to a microcosm experiment for 3 weeks during which the Eh values were automatically controlled by the inflow of N_2 and O_2. We observed that redox changes and subsequent pH changes were the primer factors influencing metal(loid) mobility and the amendment effect was secondary. The nZVI-containing treatments showed increased efficiency compared to BC. Zinc was only slightly immobilised by nZVI and nZVI-BC, Pb was significantly decreased by both nZVI and nZVI-BC, Cd yielded similar values in all treatments and As was almost completely immobilised by nZVI and secondarily by nZVI-BC. Our findings are supporting for the nZVI-containing treatments in soils experiencing flood events, but more research is recommended before field applications.

5.1 Introduction

A significant amount of metal(loid)-contaminated sites exists worldwide, and this imposes a serious threat for the environment and human health. Therefore, there is an urgent need for remediation. Among other techniques, the application of amendments for risk element immobilisation has been suggested as a promising solution (Khalid et al., 2017). Nano zero-valent iron (nZVI) is currently a popular amendment for soil remediation. The efficiency of nZVI is mainly attributed to its strong reduction ability (Jiang et al., 2018). It has been reported that nZVI is a promising stabilising agent but certain downsides such as its agglomeration tendency (Stefaniuk et al, 2016) created the demand for modifications. When modified or combined with other materials such as biochar (BC), nZVI may show improved features (Tan et al., 2015; Trakal et al., 2019); however, the studies on nZVI-BC composite products are still scarce (e.g. Su et al., 2016; Wang et al., 2019; Mitzia et al., 2023). On the contrary, the use of BC in soils is common not only for its remediation potential of risk elements but also for its ability to enhance soil properties which are in turn affecting the mobility of risk elements (Shaheen et al., 2020).

One of the most important soil properties that is improved by the application of BC and nZVI is the pH and has a great effect on the availability of metals and metalloids (Kumpiene et al., 2019). The redox potential (Eh), which expresses the oxidation-reduction potential, is another important soil property. Although not as widely studied as pH (Husson, 2013), Eh is often the driving factor which impacts pH values (El-Naggar et al., 2019; Rinklebe et al., 2016). Changes in redox conditions can affect risk element mobility directly (by changing their speciation) or indirectly (by inducing changes in pH, DOC, Fe, Mn, and S chemistry) (Frohne et al., 2014). Furthermore, as redox potential is affected by the activity of microorganisms in wet soils, contrasting results about metal(loid) availability may occur based on the actual soil water content (Young 2013). It is therefore clear, that redox potential has a crucial role in soils and is linked with changes of other variables. Since nZVI has a strongly reducing ability, special attention to Eh needs to be paid when studying nZVI-amended soils, and particularly when redox conditions change.

The efficiency of the before-mentioned amendments for the remediation of contaminated sites has been widely assessed in laboratories using aqueous solutions and/or soil (Palansooriya et al., 2020). Nevertheless, it is important

to check the impact of immobilising amendments under various environmental conditions in order to evaluate their efficiency in a realistic way. Natural events such as floods can severely affect the metal(loid) mobility in soils (Ponting et al., 2021) and -if amended- the amendment behaviour as well. For this reason, we tested nZVI, BC, and a nZVI-BC composite in saturated soil under dynamic redox conditions. Their efficiency was evaluated under changing redox conditions using a unique automated biogeochemical microcosm setup described by Yu & Rinklebe (2011). Our main hypothesis was that the amendments would have different efficiency depending on the Eh status. Additionally, intense nZVI oxidation and formation of variable Fe oxides as an effect of the induced difference in oxidation-reduction conditions was expected. The present study provides important information about risk element availability in environmental-relevant conditions in a real contaminated soil and elucidates the involved redox-originated processes. Thus, our research is not limited to the studied contaminated site, but describes phenomena possibly occurring in other industrially or otherwise contaminated sites worldwide.

5.2 Materials and Methods

5.2.1 Soil characterisation and incubation with amendments

The soil samples used in the present study were obtained from the alluvium of the Litavka River in the district of Příbram, Czech Republic. The area is known for past mining and smelting activities which have resulted in serious soil contamination by risk metal(loid)s (e.g. Ettler et al., 2001; Mitzia et al., 2020; Vítková et al., 2018). The area receives an average annual precipitation of about 650-750 mm and periodic floods (Šípek et al., 2019).

The soil was obtained from the surface layer (i.e., 0-25 cm), air-dried and sieved to particles < 2mm. Table 5.1 presents the basic soil and amendment characteristics. Although the soil was already investigated before, a new determination of the total values of risk and major elements was conducted for this study. The concentrations of major and trace elements were measured by ICP OES (Horiba Jobin Yvon, Uterhaching, DE) after microwave-assisted *aqua regia* digestion (EPA 3051A, 2007).

Table 5.1 *Basic characteristics of the studied soil and the used amendments (n = 3)*

Soil characteristics	Value		
pH			
pH$_{H2O}$[a]	5.98		
Major and risk elements in contaminated soil (*Aqua Regia* extracted)	**mg/kg**		
Zn	2487		
Pb	4064		
Cd	23.6		
As	315		
Fe	31996		
Mn	4174		
Amendment characteristics			
pH$_{H2O}$[a]	BC	nZVI	nZVI-BC
	6.7	10	11.3

[a] According to ISO10390:2005

The air-stable nZVI product (NANOFER STAR) used in this study was purchased from NANOIRON Ltd. (CZ) and the other two soil amendments (pure BC and BC-nZVI composite) were purchased by LAC Ltd. (CZ). The final composite product contained 60% of BC and 40% of nZVI. For more details on the synthesis of the studied materials refer to Mitzia et al., 2023.

The used soil amendments were sieved to particle size <0.5 mm and activated according to the manufacturer's recommendations. Briefly, the activation procedure included individual mixing and stirring of the amendments with deionised water in ratio 1:4 (S/L) and conservation in room temperature for 48 h prior to application in soils. This procedure aimed at the destruction of the protective layer of Fe oxides covering the nZVI particles so that the material becomes more reactive in the soil matrix. The same activation procedure was applied for BC particles for uniformity. The suspension of each amendment was applied to the contaminated soil samples right after the completion of the 48h activation. A soil sample without amendments (control) was also prepared. Each soil treatment was 1 kg including the amount of amendment (2 wt.%) and watered to 70% of the soil's water holding capacity (WHC). The soil samples were incubated for 3 months during which they were regularly watered

to maintain 70% of WHC. The samples were kept at room temperature and away from direct sunlight throughout the incubation period. Afterwards, the soil samples were dried in an oven at maximum 40 °C and sieved again to <2mm size particles for further manipulation.

5.2.2 Sequential extraction of incubated soil

In order to investigate the geochemical fractions of the target elements (Zn, Pb, Cd and As), 1 g of each soil treatment (*n*=3) was used for the 8-step sequential extraction by Zeien and Brümmer (1989) as modified by El-Naggar et al. (2018). Briefly, the 8 fractions were extracted as follows: 1) soluble and exchangeable fraction using 1 M $NH_4CH_3CO_2$ at pH=7, 2) fraction bound to carbonates using 1 M $NH_4CH_3CO_2$ at pH=6, 3) fraction bound to manganese oxides was extracted by 0.1 M NH_2OH-HCl+ $NH_4CH_3CO_2$ at pH=6, 4) organic matter fraction was extracted by 0.025 M NH_4EDTA at pH=4.6, 5) fraction bound to sulphides was extracted by 3 mL of 0.02 M HNO_3 + 5 mL 30% H_2O_2 (pH=2 buffered with concentrated HNO_3), then using 3 mL of 30% H_2O_2 (pH =2), and eventually 5 mL of 3.2 M $NH_4CH_3CO_2$ in 20% HNO_3 and dilution with demineralised water, 6) fraction bound to amorphous Fe oxides was extracted by 0.2 M $(NH_4)_2C_2O_4$ at pH=3.25, 7) fraction bound to crystalline oxides by 0.1 M ascorbic acid in 0.2 M $(NH_4)_2C_2O_4$ at pH=3.25, and 8) residual fraction was determined using *Aqua Regia* microwave assisted digestion according to protocol EPA 3051A (2007). The samples occurring from each step were centrifuged, filtered (0.45 μm nitrocellulose filters), and diluted for ICP OES analysis. Specific details and conditions about the 8-step sequential extraction can be found in El-Naggar et al. (2018).

5.2.3 Microcosm experiment

An automated biogeochemical microcosm (MC) system as described by Yu and Rinklebe (2011) and reported previously by other researchers (e.g. El-Naggar et al. 2019; Frohne et al. 2011; Rinklebe et al. 2016; Yang et al., 2021) was employed. This unique setup allows 1) to simulate redox cycles in soils in the laboratory scale under saturated conditions, 2) to continuously monitor the prevailing redox and pH conditions in the soil suspension and 3) to control the redox potential by setting predefined Eh windows (i.e. selected Eh ranges). For technical details see detailed description in Yu and Rinklebe (2011).

In this study, 3 replicates of each soil treatment, i.e. 1) control, 2) 2% BC-treated soil, 3) 2% nZVI-treated soil, and 4) 2% nZVI-BC-treated soil were used; making a total of 12 microcosms. The glass container of each MC was filled with 210 g of soil and 1680 mL of tap water (ratio 1:8). On the initial day of the MC experiment, 5 g of glucose and 5 g of wheat straw were added to each MC unit in one dose in order to enhance the microorganism activity and further reduce the Eh values (Frohne et al., 2011). The soil slurry was hermetically closed in the glass containers and continuously stirred by incorporated steel stirrers for the whole duration of the experiment (i.e. 585 h). Each container was equipped with a platinum (Pt) Eh electrode with a silver-silver chloride (Ag/AgCl) reference electrode (EMC 33), a pH electrode (EGA 153), and a thermometer (Meinsberger Elektroden, Ziegra-Knobeldorf, DE). The MC setup allowed us to define and induce specific Eh values in the soil slurry by controlling the inflow of N_2 (to decrease) and inflow of O_2 or synthetic air (to increase the Eh). The initial sampling of soil slurry occurred 2 h after the soil flooding without Eh control and served as a background value. Afterwards, we aimed for the lowest possible Eh by continuous purging with N_2 and later steadily increased the target Eh values. Each targeted Eh value (i.e. 1) the lowest Eh possible $\approx$ -300 mV, 2) -200 mV, 3) -100 mV, 4) 0 mV, and 5) the highest Eh possible $\approx$ 100 mV), was obtained in the form of selected Eh ranges ($\pm$ 20 mV from the target value). The actual Eh values were determined after recalculation of the measured values according to the equation of Wolkersdorfer (2008); practically adding 210 mV to each measured value. To ensure that the soil interactions under each Eh window had time to evolve, the Eh ranges were maintained for at least 48 h before each sampling. At the lowest and highest targeted Eh values (i.e. -300 mV and 100 mV) two consequent samplings were conducted. The values of Eh and pH were recorded every 10 min and the data was stored in a data logger connected to a computer. During the sampling procedure, an amount of about 80 mL of soil slurry was ejected from the glass container with the help of syringes via a specially designed opening allowing no excess of oxygen inside the MC system. The syringes were sealed right after the sampling and immediately transferred inside a glove-box without oxygen (MK3 Anaerobic Work Station, Don Whitley Scientific, Shipley, UK) for further manipulation. The samples of soil slurry were distributed to 50 mL centrifuge tubes and centrifuged for 30 min at 5000 rpm. Filtration using 0.45 μm nitrocellulose filters was conducted before the separation of the liquid and solid phase for subsequent analyses.

5.2.4 Liquid phase analyses

The liquid phase samples were subjected to ICP OES analysis (Ultima 2, Horiba Jobin Yvon, Unterhaching, Germany) analysis to determine major and trace elements, ionic chromatography (IC) (Personal IC 790, Metrohm, Filderstadt, DE) to determine the concentration of anions, and carbon analysis (C/N analyser, Analytik Jena, Jena, DE) to determine the concentrations of total and dissolved organic carbon (DOC). A UV/VIS spectrophotometer (CADAS 200, Dr. Lange, DE) was used to measure UV absorbance in the filtrates from the soil slurry using demineralised water as a blank solution. In order to calculate the specific UV absorbance (SUVA), the measured 254-nm UV absorbance was normalised to the concentration of DOC (Weishaar et al., 2003). The SUVA value can be used as an indicator of the aromatic compounds present in the soil solution (Shaheen et al., 2014; El-Naggar et al., 2018, 2019). The concentration of Fe^{2+} was determined using 2 mL of 1.10 phenanthroline and 5 mL of 2M HAc- NaAc buffer in 1 mL of acidified sample. Final dilution to 50 mL with deionised water was followed by the measurement of absorbance at 510 nm (Harvey et al., 1955).

5.2.5 Solid phase analyses

For the study of solid phase characteristics, soil suspension sampled from the MCs was placed on Lacey carbon Cu-grids and Au-grids and dried under a heating lamp in mild nitrogen flow for 30 minutes. The dried samples were then used for microscopic investigation using elemental mapping. A Cs-corrected Hitachi HD-2700 scanning transmission electron microscope (STEM) equipped with two EDAX Octane T Ultra W energy dispersive X-ray spectrometer (EDS) detectors were used. Additionally, X-ray absorption spectrometry (XAS) was employed mainly for the determination of the different forms of Fe in the solid phase. The experiments were conducted at the National Synchrotron Radiation Research Centre (NSRRC), Taiwan.

5.2.6 Data treatment

A total of 3305 measurements of Eh and pH were conducted in each MC unit during the experiment and were used as the dataset for the calculation of mean values. The Eh and pH at the time of sampling was calculated as the mean of

6 h before the sampling (Rinklebe et al., 2016). Data from ICP OES analysis with more than 5% of relative standard deviation were excluded from the calculations. The software Origin (Origin Lab 2018, version 95E) was used for the data treatment in addition to software Statistica (13.4.0.14, Tibco Software Inc.).

5.3 Results and Discussion

5.3.1 Metal(loid) mobility under dynamic redox conditions

Already after 48 h from the beginning of the MC experiment a sharp decrease in Eh values was observed as a consequence of the N_2 inflow and the microorganism activity (X. Yang, 2021) in all the treatments, and then the values gradually increased again following the inflow of O_2. The average lowest recorded Eh values were as follows: -33 mV, -43 mV, -119 mV and -70 and the highest were 511 mV, 546 mV, 497 mV, and 528 mV in control, BC, nZVI, and nZVI-BC, respectively (Fig. 5.1). The pH values followed an opposite trend than the Eh as expected and already observed in other studies (e.g. Rinklebe et al., 2016). The lowest average pH values were 4.4, 4.6, 4.5 and 4.6 and the highest were 6.8, 7, 7.1 and 7 in control, BC, nZVI, and nZVI-BC, respectively (Fig.5.1). Except for the slightly lower Eh values in nZVI-treated soil, the rest of the treatments presented similar oscillations in both Eh and pH. The lower Eh in nZVI-treated soil was already hypothesised since the reducing character of nZVI probably reinforced the reducing conditions in this soil treatment. Apparently, nZVI-BC did not exhibit such strong reducing ability which is explained by the lower total amount of Fe contained in the product (40%). Based on the alkalinity of the treatments (Table 5.1), higher pH values could be expected in the BC-containing treatments. Contrarily, all the treatments exhibited similar pH values which implies that the induced redox changes were the primary factor influencing pH in this soil. Although the pH of the control soil was only 0.2—0.3 units lower than the treated soils, the high number of observations (n=3305) makes this difference statistically significant and verifies the positive effect of the studied amendments on acidic soils.

From the first sight it occurs that the mobility trend of risk and major elements is the same regardless of the treatment implying that the induced changes in redox conditions were the governing factor. Yet, significant differences were

observed between the treatments. Overall, all target risk elements were less mobile in the nZVI-treated soil and secondarily in the nZVI-BC-treated soil (Fig. 5.1). In addition, Pb showed decreased concentrations compared to control in the BC-treated soil but only under reducing conditions (Fig. 5.1). Surprisingly, As was the only element which decreased again after the initial increase in its mobility (peak values around 250 h) in all treatments (Fig. 5.1). Nevertheless, BC yielded similar values to control whereas nZVI-containing treatments showed significantly lower to null concentrations in oxic conditions (Fig. 5.1). Iron concentrations were significantly higher (occasionally up to 2×) in the nZVI-treated soil, compared to control and BC, with the maximum amounts observed when oxic conditions were induced (Fig. 5.1). This release was expected by the nZVI treatments since the soil was loaded with extra Fe. Unlike what we observed in our previous studies (Michálková et al., 2017; Mitzia et al., 2020, 2023), nZVI did not provoke an excessive Mn release (Fig. 5.1). Instead, all the treatments showed similar values and the same trend in Mn mobility throughout the experiment with only exception the values under the lowest Eh (~80 h) in the nZVI and nZVI-BC treatments (Fig.5.1).
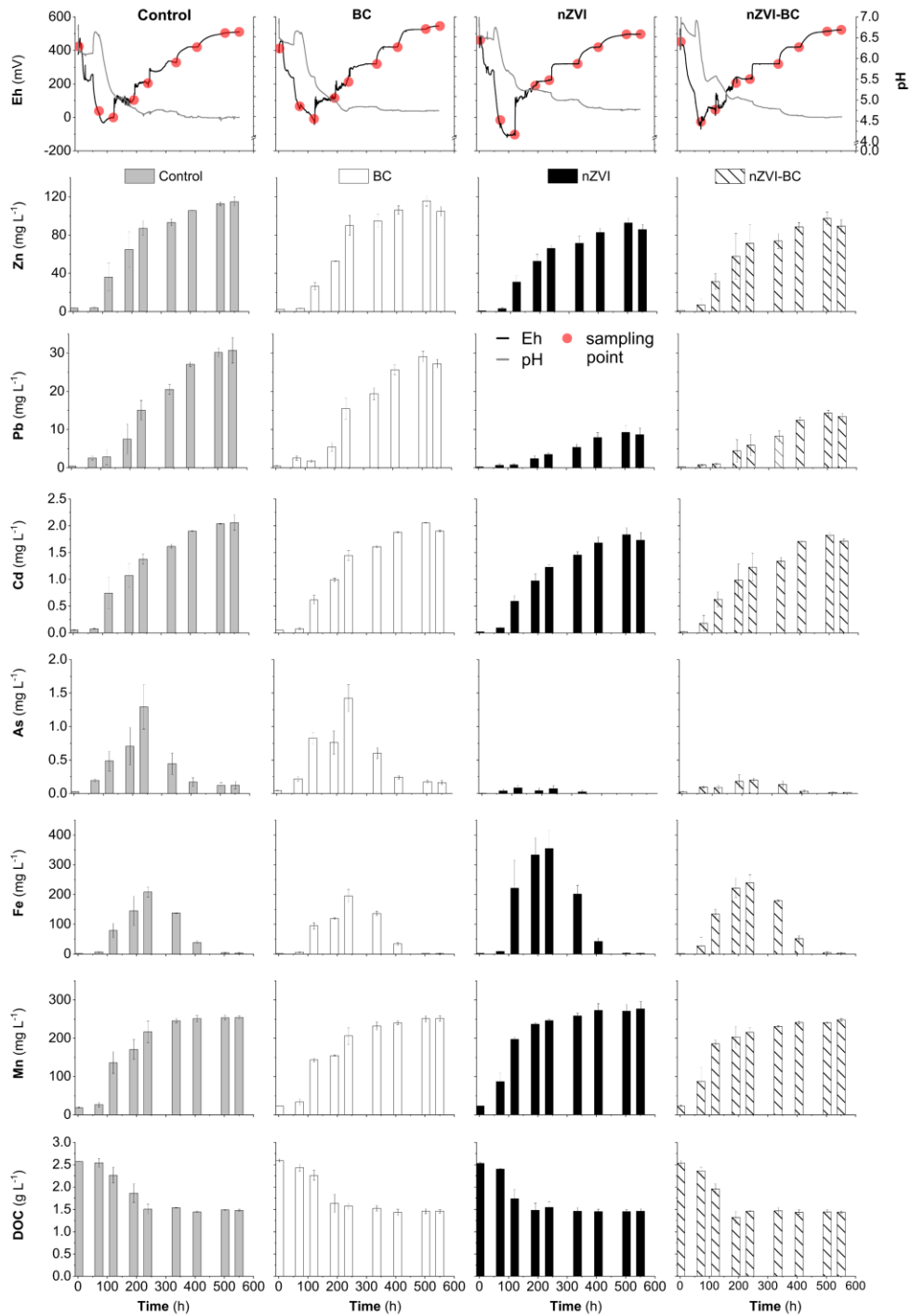
Figure 5.1: *Availability of risk metal(loid)s, Mn, Fe and DOC under the presented Eh-pH conditions.*

According to Fig. 5.1 we can classify the presented parameters into two groups based on their mobility under the defined Eh values: the first group includes Zn, Pb, Cd, and Mn and the second group includes As, Fe, and DOC. It is apparent that Zn, Pb, Cd, and Mn exhibited the same mobility trend according to the Eh values and showed significant positive correlations with Eh (Table 5.2). On the contrary, As, Fe, and DOC had the opposite trend of Eh values as verified by significant negative correlations (Table 5.2). Frohne et al. (2011, 2014) also reported an increase in Zn mobility as a consequence of Eh increase, which was attributed to the oxidation of sulphides under oxic conditions followed by Zn release in the soil solution. Grybos et al. (2007) suggested that the release of organic matter (OM) in reducing conditions is mainly owed to the pH increase and provokes a release of the risk elements (incl. Pb) bound to OM. Therefore, the role of organic matter was found to be superior than Fe (oxyhydr)oxides in metal(loid) retention (Grybos et al., 2007). In our study, although the highest DOC release was observed under reducing conditions this was not the point of the highest risk element release in the soil solution (Fig. 5.1). We assume that the increased DOC concentrations under reducing conditions were not a consequence of Eh or pH values but actually due to the loading of soil with wheat straw and glucose at the beginning of the experiment which were later consumed by the microorganisms and thus the DOC decreased. Additionally, the significant correlations between DOC and Cd ($r=-0.91$), Pb ($r=-0.61$), Zn ($r=-0.90$) (Table 5.2) were negative suggesting that increased risk element mobility is not due to OM release but rather owed to another parameter; likely Eh. However, particularly for Pb, the fraction of bound to OM by nZVI-containing treatments (Fig. 5.2) validates the importance of OM for Pb immobilisation. The Eh showed weak positive correlations with all the metals (up to $r=0.59$) while strong negative correlations between metals and pH (Cd-pH $r=-0.94$; Pb-pH $r=-0.94$; Zn-pH $r=-0.95$) (Table 5.2) were decisive for the main factor controlling metal mobility in this soil.

Based on the results from the 8-step sequential extraction procedure (Fig.5.2), nZVI treatment substantially decreased the exchangeable fraction of Zn, Pb and Cd and increased the fraction bound to amorphous Fe oxides in all metals and As. In the case of Pb, the exchangeable fraction was almost completely redistributed as bound to OM and bound to amorphous Fe oxides (Fig. 5.2). Among the target elements Cd was the most available and As the least (Fig.5.2).

Table 5.2 *Correlation matrix of the studied parameters.*

		As	Cd	Fe	Mn	Pb	Zn	DOC	Eh	pH
As	Pearson Corr.	1.00	0.07	0.31	0.03	0.13	0.14	-0.08	-0.34	-0.25
	p-value	--	0.681	0.065	0.843	0.437	0.401	0.651	0.045	0.134
Cd	Pearson Corr.	0.07	1.00	0.04	0.93	0.82	0.99	-0.91	0.58	-0.94
	p-value	0.681	--	0.835	0.000	0.000	0.000	0.000	0.000	0.000
Fe	Pearson Corr.	0.31	0.04	1.00	0.31	-0.23	0.07	-0.36	-0.42	-0.24
	p-value	0.065	0.835	--	0.069	0.174	0.675	0.029	0.011	0.157
Mn	Pearson Corr.	0.03	0.93	0.31	1.00	0.62	0.91	-0.96	0.37	-0.94
	p-value	0.843	0.000	0.069	--	0.000	0.000	0.000	0.028	0.000
Pb	Pearson Corr.	0.13	0.82	-0.23	0.62	1.00	0.86	-0.61	0.59	-0.70
	p-value	0.437	0.000	0.174	0.000	--	0.000	0.000	0.000	0.000
Zn	Pearson Corr.	0.14	0.99	0.07	0.91	0.86	1.00	-0.90	0.57	-0.95
	p-value	0.401	0.000	0.675	0.000	0.000	--	0.000	0.000	0.000
DOC	Pearson Corr.	-0.08	-0.91	-0.36	-0.96	-0.61	-0.90	1.00	-0.39	0.93
	p-value	0.651	0.000	0.029	0.000	0.000	0.000	--	0.018	0.000
Eh	Pearson Corr.	-0.34	0.58	-0.42	0.37	0.59	0.57	-0.39	1.00	-0.37
	p-value	0.045	0.000	0.011	0.028	0.000	0.000	0.018	--	0.026
pH	Pearson Corr.	-0.25	-0.94	-0.24	-0.94	-0.70	-0.95	0.93	-0.37	1.00
	p-value	0.134	0.000	0.157	0.000	0.000	0.000	0.000	0.026	--

Red *values represent* statistically significant results ($p < 0.05$).
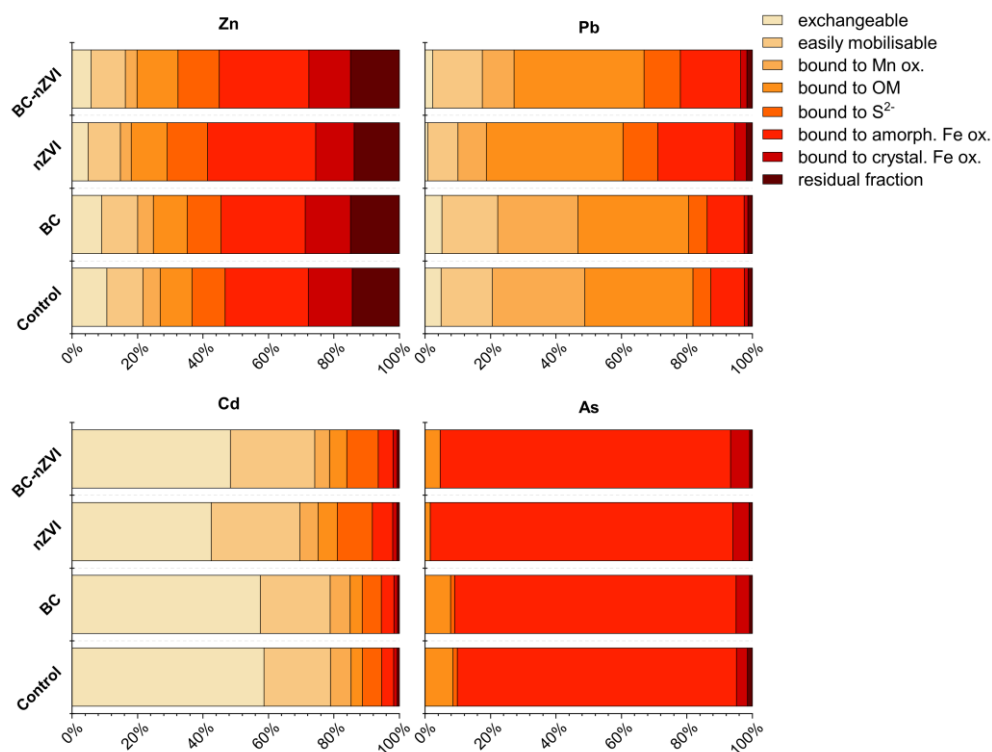
Figure 5.2: *Sequential extraction (8-step) of target metal(loid)s.*

5.3.2 Microscopic investigations

The concurrent presence of Fe, Mn, and O with target metals and As was indicative of the immobilisation mechanism in this soil as illustrated in Figs. 5.3 and 5.4. The importance of Fe and Mn oxides for the immobilisation of Zn and Pb was extensively reported previously (e.g. Mitzia et al., 2023; Vítková et al., 2018). Additionally, significant correlations between Mn and Pb (r=0.62) and Zn (r=0.91) (Table 5.2) further support the scavenging behaviour of Mn oxides in this soil. Although significant correlations between metal(loid)s and Fe were not determined (Table 5.2), based on the microscopic observations (Figs. 5.3 and 5.4) and our earlier findings, we suggest that various Fe phases were among the primary solubility-controlling phases in this soil as predicted also by geochemical modelling results in our previous study (Mitzia et., 2020).
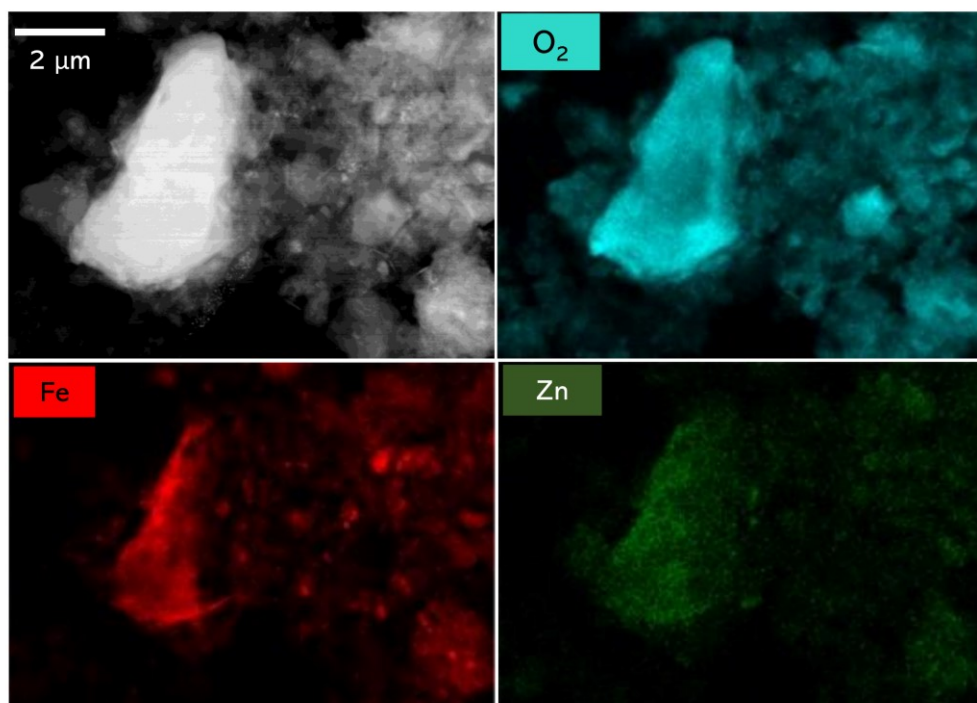
Figure 5.3: *Elemental map from dark field STEM of the nZVI-treated specimen under reduced (~-100 mV) conditions.*
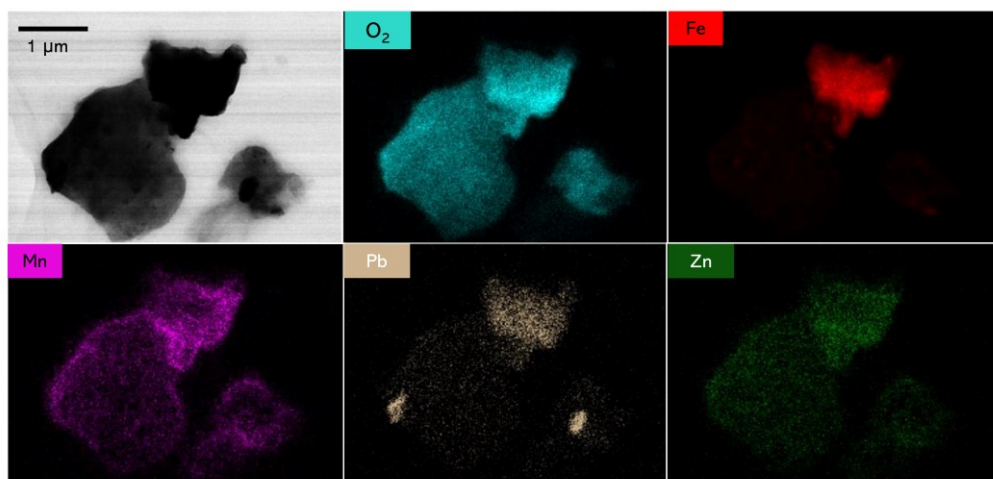
Figure 5.4: *Elemental map from bright field STEM of the nZVI-treated specimen under oxic (~500 mV) conditions.*

5.4 Conclusion

Inducing flood and redox changes in the studied soil simulated the natural flooding events that occur in the contaminated site and gave us an insight about the metal(loid) availability under these conditions. This study revealed that redox fluctuation and subsequent pH changes were the key factors affecting metal(loid) mobility. Especially pH, was significantly correlated with the mobility of Zn, Pb, and Cd. The effect of the used amendments was suggested to be inferior compared to the Eh-pH changes. Among the tested amendments (i.e. BC, nZVI, and nZVI-BC) nZVI was regarded as the most efficient for both metal and As immobilisation. This was partially attributed to the enhancement of nZVI's reducing ability under the induced negative Eh conditions. The composite of nZVI-BC was the second most efficient treatment while BC yielded in most cases similar outcome as non-amended soil. The results from the sequential extraction pointed at the role of OM and amorphous Fe oxides for metal(loid) immobilisation. Finally, the presence of Fe and Mn oxides important for metal(loid) immobilisation was confirmed by STEM/EDS investigations. The study brought a new perspective on the use of nZVI- and BC-based amendments under varying redox conditions and thus provided new insight into potential real-scale applications with occasional flooding.

Chapter VI

Summary and commentary

When searching for remediation solutions for contaminated soils, it is crucial to evaluate the behaviour of the remediating agent in a wholistic manner and take into account the potential interactions between the soil and the amendment. Changes in environmental conditions (e.g. temperature, wind, and precipitation) (Punia, 2021) and soil properties (soil type, pH, Eh, and elemental composition) (Rieuwerts et al., 1998) can significantly affect the metal(loid) mobility in soils and consequently the amendment retention efficiency. Overall, the interactions between environmental and soil properties and amendment properties have a bilateral influence on each other. Additionally, time induces changes in multiple levels which can also affect amendment functionality. To avoid costly and risky applications directly in the field, the before-mentioned parameters need to be thoroughly tested in the laboratory first.

This thesis dealt with the metal(loid) immobilisation efficiency of two main materials: BC and nZVI which were occasionally modified, combined or originated from alternative sources. In most of the cases, the used amendments were commercially available products which have known characteristics and thus guaranteed reproducibility for different experiments (up to a certain extent). The soil that was primarily used (i.e. Příbram soil, Příbram District, Czech Republic) represents an example of multi-element contamination as a consequence of past mining and smelting activities. The contaminated site is occasionally used for agriculture and pasture purposes, and it is periodically flooded during heavy rains. These characteristics were taken into consideration when studying potential remediation solutions and when deciding about the experimental design (Chapters II, III, V). Therefore, the real field conditions were taken into account although the studies were concluded in the laboratory scale. Additionally, five contrasting soils from the Czech Republic were involved during the investigation of sludge-derived BC (Chapter IV). Wide range of soil types and soil uses provided a wider assessment of the used amendment efficiency. Overall, in the present work, special attention was paid to amendment behaviour from the perspective of the following conditions: **water content, time, redox potential,** and **soil properties**. Solid phase was studied in detail and the implications of important metal(loid) scavengers were observed and suggested as possible immobilisation mechanisms in soil. The effect of natural attenuation in metal(loid) immobilisation was also observed and is discussed further in this chapter. Figure 6.1 presents the suggested process of testing the suitability of

naturally occurring amendments for soil remediation and what questions shall be answered during the efficiency assessment. The proposed approach facilitates a wholistic investigation of the amendment behaviour under various environmentally relevant conditions.
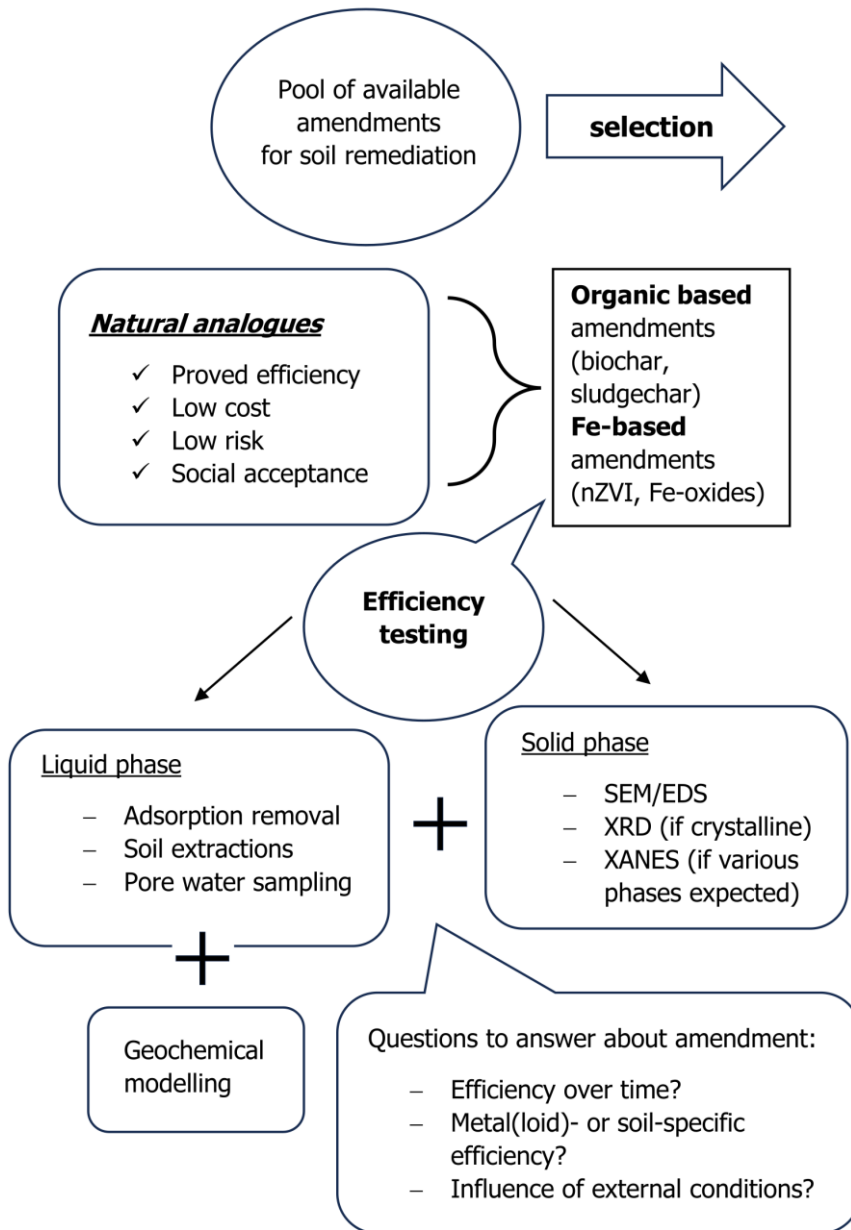
Figure 6.1: *Suggested efficiency assessment for natural-based amendments aimed for metal(loid) contaminated soil remediation.*

Biochar and nZVI can be both considered natural analogues of soil components, i.e. organic matter and Fe oxides. This fact makes them advantageous compared to other (i.e. synthesised) metal(loid) sorbents. As discussed in the first chapter of this thesis, soil components with proven ability to act as metal(loid) scavengers are the most popular candidates for immobilisation applications in soils. An interesting aspect of this scavenging behaviour is the natural attenuation process which may take place in contaminated soils without external assistance. Natural attenuation was suggested as a possible remediation mechanism in our experiments, where it was observed that the availability of risk metal(loid)s decreased with longer time even in non-amended soil (Mitzia et al., 2023). Similar results have been reported by other researchers (Clemente et al., 2006; Jurkovič et al., 2019; Vázquez et al., 2011) and highlight the intrinsic potential of contaminated soils for self-recovery. Despite the encouraging effect of natural attenuation though, in sites where the level of contamination is as high as in the case of Příbram soil, natural attenuation may only be an assisting mechanism. Such extreme concentrations or risk elements cannot be lowered to reach safety limits by natural attenuation alone, but the amendments may act synergistically or consecutively with natural attenuation for enhanced remediation outcomes. Therefore, using natural analogues as amendments for soil remediation is a viable solution which can "magnify" the natural abilities of soils. On top of that, naturally-based amendments are usually more easily approved by the public rather than fabricated materials or disruptive remediation techniques (L. Wang et al., 2021). Since products of the same composition already exist in the soil, the risk of adverse effects after application of these amendments is minimised. However, some possible side-effects of BC and nZVI application in soils may occur and were discussed in the presented studies and later in this chapter. At last, BC and nZVI can be considered relatively cost-efficient products intended for metal(loid) immobilisation. For instance, 1 kg of BC costs between 0.2 and 17 € based on the feedstock, production method, storage and transportation needs (Tareq et al., 2019; P. Zhang et al., 2022) whereas nZVI is a more costly material with 1 kg of an air-stable nZVI powder product costing from 114 € (NANOIRON, Ltd., CZ) to approximately 1200 € (MKnano) (based on market research). Considering all the aspects above, BC and nZVI were selected as suitable amendments for soil remediation of metal(loid) contaminated sites.

The first part of this thesis explored the potential of BC, nZVI, and their modifications for the immobilisation of Zn, Pb, Cd, and As in a mining-affected soil under changing moisture conditions. Our aim was to investigate temporal changes in the amendments' immobilisation efficiency under different water regimes. Although the sorbent materials were already popular when this study commenced, their efficiency in soils and particularly when environmental conditions change was, and still is, unclear up to a high extent (Sachdeva et al., 2023). A woody BC and an air-stable nZVI product were chosen to be used individually and as a combination. At first, the materials were applied in the contaminated soil and incubated at different moisture conditions based on the soil's WHC. Soil extractions and pore water sampling provided the initial results which were then coupled with geochemical modelling. Thus, suggestions regarding the solubility controlling phases in the soil solution were made. This approach enabled us to understand the effect of different moisture content on metal mobility and pH fluctuations over time. The possible immobilisation mechanisms were suggested by SEM/EDS analyses where we observed the common occurrence of Fe oxides in combination with Zn, Mn oxides with Pb, and Al oxides with Cd. Overall, BC-containing treatments were reported to be efficient for longer metal immobilisation and long-lasting pH increase while nZVI treatments were more rapid and efficient for shorter time.

Our findings were comparable to the findings of other studies dealing with BC (Table 6.1) and nZVI (Table 6.2) treatments for soil remediation. The most important factors influencing amendment efficiency are generally acknowledged to be soil pH and the application rate (X. Li & Liu, 2021; Liang et al., 2022; Palansooriya et al., 2020), therefore included in all tables. Similarly to our findings, BC was reported in the literature to be highly efficient for cationic metal immobilisation, e.g. Zn, Pb, Cd, Cu (Houben et al., 2013; Penido et al., 2019; F. Yang et al., 2021b). On the contrary, it was reported that BC was not efficient for anionic metal(loid)s (e.g. As, Cr, Sb, Mo) and particularly for As; BC was even considered responsible for its mobilisation in soils (Beesley et al., 2014; J. Wu et al., 2020). The potential mobilisation of As by BC is a certain limitation that was taken into account in our next study. The modification of BC with Fe-based products and especially nZVI has been suggested as a potential solution for the concurrent immobilisation of metals and metalloids (Mazarji et al., 2023; Sun et al., 2022; Trakal et al., 2019). Although a simple mixture of BC and nZVI was attempted in our first study, our

findings did not indicate that this material is superior than the individual products (Mitzia et al., 2020). According to Fan et al. (2020), one-pot synthesis of nZVI-BC composite resulted in a product with increased efficiency for As immobilisation in two soils compared to BC and nZVI alone and in combination. In view of limiting As mobilisation in soil, a nZVI-BC composite was used in our next study. Nano zero-valent iron, was reported by almost all studies to effectively decrease the concentrations of both metals and metalloids (Table 6.2). However, in our study (Mitzia et.al., 2020) and also in Hiller et al. (2021), Pb yielded occasionally the same or higher concentrations than untreated soil. Also, As and Sb amounts were occasionally increased or similar to control soil after nZVI application (Hiller et al., 2021; Mitzia et al., 2023; Vítková et al., 2018). Based on the previously observed affinity of Pb to Mn oxides, this mobilisation was explained by the tendency of nZVI to dissolve Mn in soils (Michálková et al., 2017). In the case of As, which has known affinity to Fe oxides, the similar concentrations to untreated soil could be owed to dissolution of nZVI particles in the acidic soil solutions (Hiller et al., 2021).

Table 6.1: *Immobilisation of Zn, Pb, Cd, and As in contaminated soils by various pristine (i.e. not modified) biochars according to literature*.

Metal(loids)	Soil pH	Total concentration in mg/kg	Mobility after application	Application rate	Incubation time	Reference
Pb	4.9	3192±45	Pb ↓	1 & 3 wt.%	90 days	Netherway et al., 2019
Pb, Cd	6.23±1.56	25.87±2.28 (Pb) 4.80±0.56 (Cd)	Pb ↓ Cd ↓	2 wt.%	45 days	Mujtaba Munir et al., 2020
Zn, Pb, Cd	7.4	22145 (Zn) 5887 (Pb) 102 (Cd)	Zn ↓ Pb↓ or similar to control Cd ↓	3 & 6 wt.%	28 days	Penido et al., 2019
Zn, Pb, Cd	5.8	530 (Zn) 1253 (Pb) 1.6 (Cd)	Zn ↓ Pb ↓ Cd ↓	3 & 6 wt.%	28 days	Penido et al., 2019
Zn, Pb, Cd	6.57	2980 (Zn) 3110 (Pb) 24 (Cd)	Zn ↓ Pb ↓ Cd ↓	1, 5, & 10 wt.%	Up to 56 days	Houben et al., 2013
Zn, Pb, Cd	5.98	3082 (Zn) 3857 (Pb) 31.6 (Cd)	Zn↓ Cd↓ Pb same as control	2 wt.%	30 days	Mitzia et al., 2020
Zn, Pb, Cd	5.90	1680 (Zn) 248 (Pb) 18.7 (Cd)	All ↓ in order Pb>Zn>Cd	1, 3, & 5 wt.%	42 days	F. Yang et al., 2021
Zn, Pb, Cd, As	n.d.	13200 (Zn) 4170 (Pb) 74 (Cd) 7490 (As)	Zn↓ Pb↓ Cd similar to control As↑	10% v/v	Up to 28 days	Beesley et al., 2014
Zn, Pb, Cd, As	5.98	3082 (Zn) 3857 (Pb) 31.6 (Cd) 385 (As)	Zn↓ Cd↓ Pb & As ↑ occasionally	2 wt.%	Up to 15 months	Mitzia et al., 2023
Cd, As	4.65	46.9 (Cd) 3.01 (As) µg/kg	Cd ↓ As same as control	1, 2, & 3 wt.%	160 days	J. Wu et al., 2020
As	5.45	96	As ↑	50 % v/v	60 days	Beesley et al., 2010

n.d.: value not defined

Table 6.2: *Immobilisation of Zn, Pb, Cd, and As in contaminated soils by various nZVI products according to literature.*

Metal(loids)	Soil pH	Total concentration in mg/kg	Mobility after application	Application rate	Incubation time	Reference
Zn, Pb, As	7.58	63—81.5 (Zn) 29—37.5 (Pb) 110—1334 (As)	As & Zn ↓ Pb similar to control	1 wt.%	84 days	Hiller et al., 2021
Sb, As, Pb, Zn	3.85—6.05	979—4430 (Sb) 84—2030 (As) 85—539 (Pb) 10-71 (Zn)	As ↓ or similar to control Sb↑ occasionally	1 wt.%	84 days	Hiller et al., 2021
Zn, Pb, Cd, As	5.95	4107±179 (Zn) 4234±429 (Pb) 42.1±2.14 (Cd) 332±20.1 (As)	Zn & Cd ↓ Pb & As ↓ or similar to control	1 wt.%	90 days	Vítková et al., 2018
Zn, Pb, Cd	5.98	3082 (Zn) 3857 (Pb) 31.6 (Cd)	Zn↓ Pb ↑ occasionally Cd ↓ or similar to control	2 wt.%	30 days	Mitzia et al., 2020
Zn, Pb, Cd, As	5.98	3082 (Zn) 3857 (Pb) 31.6 (Cd) 385 (As)	All ↓ Zn, Cd, & As ↓ or occasionally similar to control	2 wt.%	Up to 15 months	Mitzia et al., 2023
Zn, Cu, As, Cr	5.25	1221±12 (Zn) 1037±37 (Cu) 5989±61 (As) 2082±44 (Cr)	Mainly Zn & As ↓	2 wt.%	14 days	Danila et al., 2020
Pb, Zn, As	6.8	37781 (Pb) 14062 (Zn) 10926 (As)	All ↓ in order As>Pb>Zn	3 wt.%	60 days	Santos et al., 2022
As	7.14	5800±450	As ↓	~ 0.1 & 1 wt.%	33 days	Gil-Díaz et al., 2016
As	8.57	1305	As ↓ mostly when 2 wt.% applied	0.5, 2, 5, & 10 wt.%	-	Baragaño et al., 2020
As, Zn	6.09	15910±1094 (As) 193±12.2 (Zn)	As↓ Zn↓ or similar to control	1 wt. %	90 days	Vítková et al., 2018
Sb, As	4.02—4.44	1118—1273 (Sb) 855—970 (As)	As↓ Sb↓	2 wt. %	70 days	Zarzsevszkij et al., 2023

It is evident from Tables 6.1, 6.2 and 6.3 that most of the studies had a rather short life-span and the possible interactions between the sorbents and the soil in longer time (i.e. >12 months) were still undiscovered. Nevertheless, the

long-term efficiency of soil amendments is of paramount concern for remediation technologies. The interactions between soil and sorbent are continuous and can have variable effects on the actual metal(loid) availability in soil. Desorption or release of previously contained metal(loid)s from BC and nZVI is not unlikely and this aspect needs to be carefully considered before field-scale applications. It was reported that retention of Cd, Cu, and Ni in spiked soils (Vasarevičius et al., 2020) and Cu, Pb, and As in mining-contaminated soil (Danila et al., 2020) decreased over time. In particular, when nZVI gets oxidised usually ferrihydrite is the first Fe oxide to be formed which has a poorly crystalline character and a high specific surface area. Further oxidation of ferrihydrite and formation of more-crystalline phases (such as goethite or haematite) is expected to occur over time. However, as these more crystalline phases have lower specific surface area than ferrihydrite, their formation can result in metal(loid) release (Danila et al., 2020; Kumpiene et al., 2012). In addition, ageing of Fe^0 and Fe oxides can provoke changes in Fe oxides crystallinity and consequently in metal(loid) retention (Shi et al., 2021). These observations and remaining questions regarding amendment efficiency paved the way for our next study.

We tested the long-term efficiency of a woody BC, an air-stable nZVI, and an nZVI-BC composite. The nZVI oxidation process in the soil was also investigated in detail. Incubation times from 1 up to 15 months were employed to show potential differences of amendment behaviour over time. The objectives of this study were 1) to present the amendments' efficiency for metal(loid) immobilisation over time and 2) to understand the pathway of Fe^0 oxidation in soil. Soil extractions and pore water sampling were conducted to show the progress of immobilisation in the soil. Additionally, the visual changes in nZVI and potential immobilisation mechanisms were observed by SEM/EDS where the formation of new (hydr)oxides was indicated and statistically verified. Potential Fe phases that were present in the soil were initially assessed by XRD but this method lacks robustness when it comes to non-crystalline phases. Therefore, XANES was later employed to validate the presence and the amounts of specific Fe oxides in the solid phase. Geochemical modelling using the PHREEQC code proposed possible changes in metal speciation over time and the most important phases in the soil solution. It was shown that BC was efficient for long-term immobilisation of Zn and Cd, and nZVI for rather short-term immobilisation of Pb and As. These findings were similar to our first study;

yet the longer incubation experiments were key for the result validation. The pH was suggested as a crucial factor affecting metal(loid) mobility and fluctuated over time but less in the BC-treated samples compared to nZVI-treated ones. The detailed SEM/EDS analyses allowed us to statistically verify and suggest that the main immobilisation mechanism induced by the amendments was retention on Fe and Mn oxides. In fact, the amended soil samples showed at least 2× higher presence of Fe and Mn oxides in combination with risk metal(loid)s rather than untreated soil. Despite the possible heterogeneity of the soil samples, more than 6000 EDS measurements were acquired per each tested soil sample which makes this result significant. Regarding Fe^0 oxidation we observed that nZVI transformation was more rapid in the short-term and was not directly proportional to time. Eventually, the newly formed Fe oxides (ferrihydrite, lepidocrocite, magnetite) existed in the same proportions in all samples regardless of the incubation time. The results of this study were enlightening regarding the behaviour of amendments over time. It was shown again that BC might not be as rapid as nZVI but provides long-lasting metal(loid) immobilisation and mainly pH retention in the soil. Furthermore, the role of natural attenuation was highlighted by the longer incubation showing that a decrease in available metal(loid) concentrations is possible even in untreated soil. Although this is a positive outcome, natural attenuation needs to be reinforced with soil amendments -preferably natural analogues- for improved remediation results.

In Table 6.3, the existing literature about nZVI-BC composites used for remediation of real (i.e. not spiked) contaminated soils is summarised. It is apparent that the use of nZVI-BC in soils is still scarce although a few studies dealing with nZVI-BC composites for Cr remediation in soils have been excluded from this table since Cr was not a contaminant in the studied soil. Therefore, these studies were considered irrelevant in this context. In all the studies reviewed in Table 6.3., the nZVI-BC products decreased the concentrations of metals and As in soils even when applied in low concentrations (D. Yang et al., 2021). Nevertheless, based on our findings the composite material did not outweigh the efficiency of the individual products; it did immobilise the target metal(loid)s though. Similarly, Zarzsevszkij et al. 2023 used the same nZVI-BC composite in soil with increased levels of As and Sb and found it effective, yet not more effective than nZVI alone. Further studies evaluating the potential of nZVI-BC composites in soil (especially in the field) are therefore recommended.

Table 6.3: *Immobilisation of Zn, Pb, Cd, and As in contaminated soils by various nZVI-BC composite products according to literature.*

Metal(loids)	Soil pH	Total concentration in mg/kg	Mobility after application	Application rate	Incubation time	Reference
As	8.19 & 7.91	3015±20 & 1902±20	As ↓	5 wt.%	15 days	Fan et al., 2020
Cd	7.64	30.9±0.47 (in sediment)	Cd↓ mostly at 8 wt.%	2, 5, & 8 wt.%	Up to 140 days	Q. Liu et al., 2021
Pb, Cd	7.42	281±42.7 (Pb) 2.43±0.29 (Cd)	Pb↓ Cd↓	5 wt.%	30 days	Aborisade et al., 2023
Zn, Pb, Cu, Cd, As	8.47	898 (Zn) 252 (Pb) 62.1 (Cu) 1.97 (Cd) 54.9 (As)	All↓	3 wt.%	40 days	Song et al., 2022
Zn, Pb, Cd, As	5.98	3082 (Zn) 3857 (Pb) 31.6 (Cd) 385 (As)	All ↓ Pb & As ↑ occasionally	2 wt.%	Up to 15 months	Mitzia et al., 2023
Pb, Cd, As	7.93	2811 (Pb) 23.5 (Cd) 119 (As)	All ↓ max at 0.5 wt.%	0.5 wt.% and 0.05—1 wt.%	48 h and up to 120 h	D. Yang et al., 2021
Pb, Zn, As	6.8	37781 (Pb) 14062 (Zn) 10926 (As)	All ↓ in order As>Pb>Zn	3 wt.%	60 days	Santos et al., 2022
Sb, As	4.02—4.44	1118—1273 (Sb) 855—970 (As)	As↓ Sb↓	2 wt. %	70 days	Zarzsevszkij et al., 2023

Except for the direct effect of amendment application in metal(loid) immobilisation, there are other indirect effects or external factors that can influence the metal(loid) mobility in soils. The most important, as highlighted in numerous studies, is the pH, which strongly affects metal(loid) mobility in water and soils. Furthermore, the co-existence of different metal(loid)s can yield variable results in soil remediation due to the competition for sorption sites between them (Covelo et al., 2007; Sipos et al., 2019). The actual level of metal(loid)s concentrations also plays a key role in the effect of immobilisation. In this sense, soils with increased levels of contamination may show different remediation results compared to less contaminated soils even if the same amendment is used (Lwin et al., 2018). At last, the soil type and the

origin of metal(loid) contamination can significantly affect the mobility and consequently the immobilisation of metal(loid)s in soils (Palansooriya et al., 2020). The effects of geogenic contamination are usually milder compared to anthropogenic (Kabata-Pendias, 2011). In many cases, regardless of the total concentrations, soils with anthropogenic contamination exhibit higher toxicity and metal(loid) mobility than those with geogenic contamination. In these terms, investigating the soil properties seems crucial before choosing amendments for soil remediation as their efficiency can be strongly affected by those. At the same time, remediation of contaminated soils does not solely regard amendment efficiency but is interconnected with environmental sustainability and cost efficiency. Sustainability shall not be sacrificed over remediation efficiency but preferably combined. Therefore, remediation projects which take into account sustainability and material reuse (especially waste), are rightfully gaining ground in the last years (Mayilswamy et al., 2023). In this sense, waste-originated Fe-based amendments (e.g. Fe scrap; Appendix A) and organic amendments (e.g. sludge-derived biochars), can represent cost-effective and viable solutions promoting material reuse and circular economy. Based on these, and the observed long-lasting efficiency of BC for metal(loid) immobilisation, our next study dealt with waste-derived organic amendments and particularly pyrolysed sludge (sludgechar).

Our study evaluated the performance of five different pyrolysed sludges for metal(loid) removal in aqueous solutions and their efficiency for immobilisation in contrasting soils. To achieve this, the retention efficiency of sludgechars of different origin and properties was evaluated under various conditions. Sludge with variable composition was pyrolysed at final temperature of 650 °C and thus five different SCs were produced. The pyrolysis procedure led to significant or total removal of organic contaminants enhancing the SC environmental safety. Detailed characterisation of the physical, chemical, and mineralogical content of sludgechars was conducted to give an insight of their individual composition and characteristics. Solid phase investigations using XRD and SEM/EDS suggested the main mineral phases existing in the SCs and their structural and mineralogical composition. The presence of Fe phases detected by SEM/EDS was crucial for the immobilisation of metalloids. Minimal leaching of risk metal(loid)s and nutrients from the sludgechars was observed in the water solutions while their removal efficiency for 9 metal(loid)s (i.e. Cd, Co, Cu, Ni, Pb, Zn, As, Cr, and Sb) at different pH values was validated. Afterwards,

the amendments were applied in soils. Five soils with distinct properties, variable contamination levels, different pH, and different land uses were employed in this study. Soil extractions and pore water sampling were conducted to evaluate the SC immobilisation efficiency for different metal(loid)s. Visual MINTEQ geochemical modelling and solid phase analyses using XRD and SEM/EDS suggested possible immobilisation mechanisms. This comprehensive study proved that the same amendment could behave differently under different conditions. Hence, our research proposed solutions which were tailored to the contamination status of each soil based on the origin and level of contamination, soil type and soil properties (especially pH). The presence of nutrients in the sludge was suggested as a positive side-effect of SC application in soils especially in terms of P recovery.

In Table 6.4, our findings were compared with the findings from other studies employing sludge-derived biochars. It is interesting to note that SCs, unlike BCs made from other feedstock, exhibit a distinct immobilisation efficiency for metals and metalloids. In many cases, cationic metals yielded either the same (Álvarez-Rogel et al., 2018; Figueiredo et al., 2019; X. Yang et al., 2022) or higher (Méndez et al., 2012; J. Zhang et al., 2021) concentrations than the non-amended soil. This is mainly explained by the increased concentrations of risk metal(loid)s in the raw sludge and represents the main challenge of SC reuse. On the contrary, As, which is typically mobilised by conventional BCs, was immobilised as also reported by Khan et al. (2013). This behaviour was attributed to the increased levels of S and P (Khan et al., 2013) or Fe (Agrafioti et al., 2014) in the in the sewage sludge, which can lower As availability. Nevertheless, other studies reported increased As concentrations after SC application (X. Yang et al., 2022) which indicates the need for further studies on the suitability of sludge-derived BCs for As remediation in soils.

Table 6.4: *Immobilisation of Zn, Pb, Cd, and As in contaminated soils by various sludge-derived biochars according to literature (part 1/2).*

Metal(loids)	Soil pH	Total concentration in mg/kg	Mobility after application	Application rate	Incubation time	Reference
Pb, Cd	8.2	7937 (Pb) 9.92 (Cd)	All ↓ esp. With increased app. rate	2, 4, and 8 wt.%	42 days	Karimi et al., 2020
Pb, Cu, Zn	4.9	254—281 (Pb) 53.7—59 (Cu) 26.4—30.8 (Zn)	Similar to control	0.7 wt.%	1 year field trial	Figueiredo et al., 2019
Zn, Pb, Cd	4.7	13956±406 (Zn) 16758±291 (Pb) 16.7±0.44 (Cd)	All ↓	6 wt.%	20 days and up to 303 days column experiment	Álvarez-Rogel et al., 2018
Zn, Pb, Cd	7.4	11784±404 (Zn) 7354±210 (Pb) 30.9±2.21 (Cd)	All similar to control	6 wt.%	20 days and up to 303 days column experiment	Álvarez-Rogel et al., 2018
Pb, Zn, Cu	7.1	845±12.6 (Pb) 204±10.2 (Zn) 45.7±3 (Cu)	Pb ↓ Zn ↓ or occasionally similar Cu ↑, ↓ or similar to control	7.5 t/ha	60 days	Z. Wang et al., 2021
Pb, Zn, Cd	5.8	1253 (Pb) 530 (Zn) 1.6 (Cd)	Pb & Cd ↓ Zn ↓ or similar to control	3 & 6 wt.%	28 days	Penido et al., 2019
Zn, Pb, Cd	7.4	22145 (Zn) 5887 (Pb) 102 (Cd)	All ↓	3 & 6 wt.%	28 days	Penido et al., 2019
Cd, Pb, Zn, Cu	8.63	4.35 (Cd) 26.8 (Pb) 48.5 (Zn) 7.6 (Cu)	All ↑ with higher app. rate	4 & 8 wt.%	200 days	Méndez et al., 2012
Pb, Cd, Zn, Cu	5.27	9.56±0.24 (Pb) 0.20±0.01 (Cd) 54.8±5.56 (Zn) 7.30±0.46 (Cu)	All ↑ with higher app. rate Pb occasionally similar to control	7.5, 15, & 30 t/ha	Up to 1 year field experiment	J. Zhang et al., 2021
Zn, Pb, Cd, Cu, As, Cr	4.02	19 (Zn) 3.58 (Pb) 0.16 (Cd) 7.56 (Cu) 1.09 (As) 6.56 (Cr)	Pb, As, & Cr ↓ Zn, Cd, & Cu↑	5 & 10 wt.%	12 weeks	Khan et al., 2013

Table 6.4: *Immobilisation of Zn, Pb, Cd, and As in contaminated soils by various sludge-derived biochars according to literature (part 2/2).*

Zn, Pb, Cd, Cu, As, Sb	6.50	561±9 (Zn) 224±5 (Pb) 3.52±0.18 (Cd) 64.0±2.3 (Cu) 291±10 (As) 520±28 (Sb)	Cu ↓ As ↑ rest similar to control	5 wt.%	30 days	X. Yang et al., 2022
Zn, Pb, Cd, Cu, As, Sb	5.95	3082±83 (Zn) 3854±121 (Pb) 31.6±1 (Cd) 82±1 (Cu) 385±11 (As) 63.7±4.7 (Sb)	Zn & Pb ↓ (by specific SCs) Cd ↓or similar to control Cu & As ↑ Sb similar to control	3 % v/v	30 days	Mitzia et al., 2024
Zn, Pb, Cd, Cu, As, Sb	7.49	3559±207 (Zn) 8604±675 (Pb) 48±5 (Cd) 309±13 (Cu) 307±45 (As) 231±86 (Sb)	Zn ↓ (by specific SC) Pb & Cd similar to control Cu ↑ (by specific SC) As & Sb ↓	3 % v/v	30 days	Mitzia et al., 2024
Zn, Pb, Cd, Cu, As	6.09	193±12 (Zn) 73±12 (Pb) 3 (Cd) 51±5 (Cu) 17563±2798 (As)	Zn & Cd ↑ Pb similar to control Cu ↑ (by specific SC) As ↓ (by specific SC)	3 % v/v	30 days	Mitzia et al., 2024
Zn, Pb, Cu, As, Sb	5.19	86±7 (Zn) 130±16 (Pb) 13 (Cu) 7 (As) 20 (Sb)	Zn ↑ Pb ↓ (by specific SCs) Cd & Cu ↑ or similar to control	3 % v/v	30 days	Mitzia et al., 2024
Zn, Pb, Cd, Cu, As, Sb	7.38	128±10 (Zn) 79±10 (Pb) 1 (Cd) 38±2 (Cu) 15±1 (As) 2 (Sb)	Zn ↑ Cu similar to control (rest not detected)	3 % v/v	30 days	Mitzia et al., 2024

Taking into account that immobilisation is tested in the lab but intended to be applied in the field, actual environmental conditions are important to be simulated in our experiments. Redox potential is an important factor controlling metal(loid) mobility and speciation in soils (Frohne et. al., 2014). Flooding events which are likely in many contaminated sites provoke reduced conditions in the soil and raise questions regarding risk metal(loid) mobility and amendment efficiency under this scenario. When amendments are applied with the scope of remediation, their efficiency as well as other aspects (e.g. oxidation, dissolution, element release) are assumed to change. This is especially the case of redox-reactive amendments. In particular, nZVI is expected to thrive under reducing conditions which can enhance its already strong reducing ability resulting in increased immobilisation efficiency. Biochar has also been reported to facilitate redox reactions on its surface and work simultaneously as an electron donor and acceptor affecting risk metal(loid) mobility and speciation (Klüpfel et al., 2014). For these reasons, in our last study we investigated the mobility of Zn, Pb, Cd, and As in Litavka soil using the unique biogeochemical microcosm system according to Yu and Rinklebe (2011). Except for the untreated soil, samples of BC-, nZVI-, and nZVI-BC-treated soil were tested. The setup allowed us to: 1) simulate anoxic flooding conditions in soils 2) continuously monitor the existing redox and pH values in the soil and 3) control the redox potential by setting predefined Eh windows. Additionally, an 8-step sequential extraction and solid phase analyses were implemented for a complete assessment of the amendment behaviour under dynamic redox conditions. Our preliminary results were enlightening regarding the effect of redox changes and amendments towards metal(loid) mobility: redox changes were suggested to be the main factor influencing the metal(loid) mobility trend while pH was significantly correlated with metal mobility. Among the treatments, nZVI was the most efficient for both metal and metalloid immobilisation followed by nZVI-BC. The fractions of OM and Fe oxides increased in the treated samples and thus were found crucial for the decrease in metal(loid) mobility. Additional analyses are expected to reinforce our understanding about the interactions in the soil under changing redox conditions.

In view of the increasing need for viable and affordable amendments for soil remediation, an attempt to make full use of valuable waste was made. Our final experiment contains unpublished results (Appendix A) regarding the efficiency

of various Fe-based amendments including Fe scrap (metallurgical waste). This ongoing research was initiated by the criticism against nZVI for its cost-efficiency and other potential disadvantages. In particular, nZVI has been often accused for being toxic to plants and biota (Anza et al., 2019; Gómez-Sagasti et al., 2019; Kotchaplai et al., 2019) although this topic is still debateable as other authors found no toxicity risk (Teodoro et al., 2020; Vanzetto & Thomé, 2022) or even positive effects (Němeček et al., 2014) by the use of nZVI. Furthermore, the synthesis of nZVI might involve toxic chemicals; when $NaBH_4$ is used for nZVI synthesis, boron residues are generated, which present an environmental danger. On top of that, this nZVI synthesis is rather expensive and complicated (Pasinszki & Krebsz, 2020) as compared to synthesis by H_2 reduction or "green" synthesis. These reasons contributed to a general vigilant attitude towards nZVI.

Nevertheless, the research on the application of nZVI products for soil remediation is still flourishing as depicted in Figures 6.2 and 6.3 which present the publications involving nZVI and nZVI-BC in the last 15 years. It is evident that researchers are still interested in the potential of nZVI products for soil remediation. Based on the results of our first two studies, in which nZVI was not superior to BC and also exhibited short-term remediation efficiency, we decided to involve other Fe-based amendments in our experiments and make a step towards more efficient, sustainable and financially wiser applications for soil remediation (Appendix A).
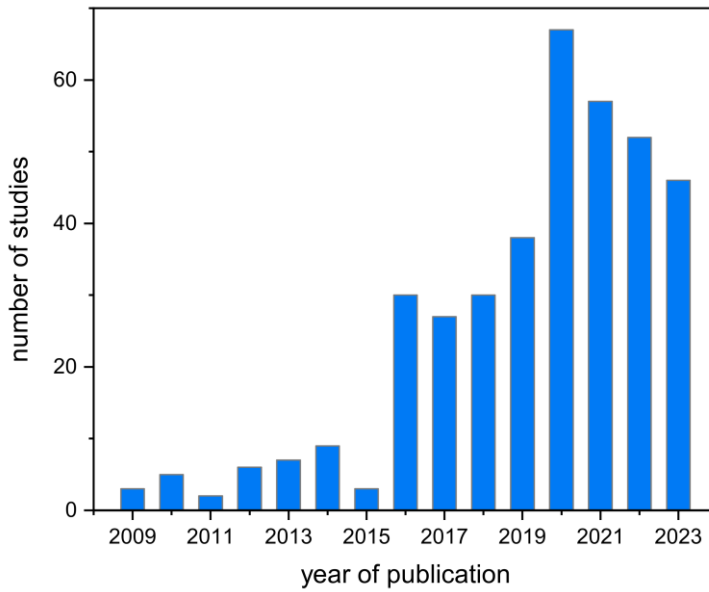
Figure 6.2: *Number of published papers per year as a result of search with the keywords: "nZVI; soil; metal; remediation" in the Web of Science database (assessed in February 2024).*
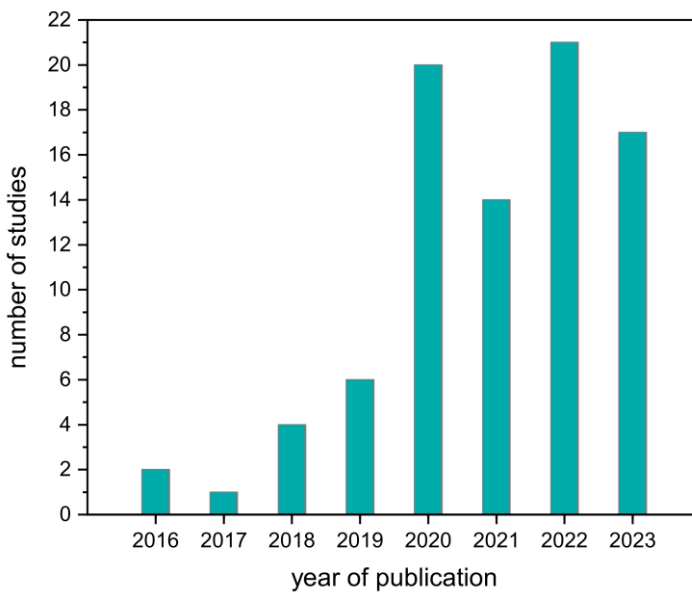
Figure 6.3: *Number of published papers per year as a result of search with the keywords: "nZVI; biochar; soil; metal; remediation" in the Web of Science database (assessed in February 2024).*

239

Our preliminary results are surprisingly promising regarding the use of Fe scrap for soil remediation which was found to be similarly or more efficient as the commercial products used in the experiment (Appendix A). With the exception of As, which seemed to be mobilised, the cationic metals were immobilised by nZVI slurry, S-nZVI slurry and Fe scrap. Occasionally, Fe scarp was the most efficient sorbent among the rest. The pH values were also increased by 1 unit in the Fe-scrap-treated soil samples after 1 month of incubation (Appendix A) although they were later decreased again (finally same as untreated soil). Therefore, more research and possible cost-effective modifications of the Fe waste product, could result in an innovative, stable, and environmentally safe material for metal and metalloid remediation. Caution is recommended when applying Fe waste products as they might contain residues of other toxic metal(loid)s which can be released in the soil.

The conclusive remark and essence of the presented thesis is that long-term and environmentally relevant studies which employ a wholistic investigation including variable conditions are necessary for the appropriate evaluation of soil amendments. More field studies are also needed to show the real potential and the real limitations of each amendment used for environmental remediation. At the same time, researchers are encouraged to keep in mind sustainability and not merely amendment efficiency in remediation projects.

References

Abbas, Z., Ali, S., Rizwan, M., Zaheer, I. E., Malik, A., Riaz, M. A., Shahid, M. R., Rehman, M. & Al-Wabel, M. I. (2018). A critical review of mechanisms involved in the adsorption of organic and inorganic contaminants through biochar. *Arabian Journal of Geosciences*, *11*(16), 448. https://doi.org/10.1007/s12517-018-3790-1

Abdelhafez, A. A., Li, J., & Abbas, M. H. H. (2014). Feasibility of biochar manufactured from organic wastes on the stabilization of heavy metals in a metal smelter contaminated soil. *Chemosphere*, 117, 66–71. https://doi.org/10.1016/j.chemosphere.2014.05.086

Aborisade, M. A., Feng, A., Oba, B. T., Kumar, A., Battamo, A. Y., Huang, M., Chen, D., Yang, Y., Sun, P., & Zhao, L. (2023). Pyrolytic synthesis and performance efficacy comparison of biochar-supported nanoscale zero-valent iron on soil polluted with toxic metals. *Archives of Agronomy and Soil Science*, *69*(12), 2249–2266. https://doi.org/10.1080/03650340.2022.2146100

Ábrego, J., Arauzo, J., Sánchez, J.L., Gonzalo, A., Cordero, T., Rodríguez-Mirasol, J., 2009. Structural changes of sewage sludge char during fixed-bed pyrolysis. *Industrial & Engineering Chemistry Research*, 48, 3211–3221. https://doi.org/10.1021/ie801366t

Adriano, D. C. (2001). *Trace elements in terrestrial environments: Biogeochemistry, bioavailability, and risks of metals* (2nd ed). Springer.

Agrafioti, E., Bouras, G., Kalderis, D., & Diamadopoulos, E. (2013). Biochar production by sewage sludge pyrolysis. *Journal of Analytical and Applied Pyrolysis*, 101, 72–78. https://doi.org/10.1016/j.jaap.2013.02.010

Agrafioti, E., Kalderis, D., & Diamadopoulos, E. (2014). Arsenic and chromium removal from water using biochars derived from rice husk, organic solid wastes and sewage sludge. *Journal of Environmental Management*, 133, 309–314. https://doi.org/10.1016/j.jenvman.2013.12.007

Ahmad, M., Lee, S. S., Lee, S. E., Al-Wabel, M. I., Tsang, D. C. W., & Ok, Y. S. (2017). Biochar-induced changes in soil properties affected immobilization/mobilization of metals/metalloids in contaminated soils. *Journal of Soils and Sediments*, *17*(3), 717–730. https://doi.org/10.1007/s11368-015-1339-4

Ahmad, M., Rajapaksha, A. U., Lim, J. E., Zhang, M., Bolan, N., Mohan, D., Vithanage, M., Lee, S. S., & Ok, Y. S. (2014). Biochar as a sorbent for contaminant management in soil and water: A review. *Chemosphere*, 99, 19–33. https://doi.org/10.1016/j.chemosphere.2013.10.071

Ahmed, N., Shah, A. R., Danish, S., Fahad, S., Ali, M. A., Zarei, T., Vranová, V., & Datta, R. (2021). Immobilization of Cd in soil by biochar and new emerging chemically produced carbon. *Journal of King Saud University - Science*, 33(5), 101472. https://doi.org/10.1016/j.jksus.2021.101472

Alazaiza, M. Y. D., Albahnasawi, A., Copty, N. K., Bashir, M. J. K., Nassani, D. E., Al Maskari, T., Abu Amr, S. S., & Abujazar, M. S. S. (2022). Nanoscale zero-valent iron application for the treatment of soil, wastewater and groundwater contaminated with heavy metals: A review. *Desalination and water treatment*, 253, 194–210. https://doi.org/10.5004/dwt.2022.28302

Alef, K., & Nannipieri, P. (1995). *Methods in applied soil microbiology and biochemistry*. Academic Press.

Alengebawy, A., Abdelkhalek, S. T., Qureshi, S. R., & Wang, M.-Q. (2021). Heavy Metals and Pesticides Toxicity in Agricultural Soil and Plants: Ecological Risks and Human Health Implications. *Toxics*, *9*(3), 42. https://doi.org/10.3390/toxics9030042

Alewell, C., Ringeval, B., Ballabio, C., Robinson, D.A., Panagos, P., Borrelli, P., 2020. Global phosphorus shortage will be aggravated by soil erosion. *Nature Communications*, 11, 4546. https://doi.org/10.1038/s41467-020-18326-7

Ali, A., Guo, D., Arockiam Jeyasundar, P.G.S., Li, Y., Xiao, R., Du, J., Li, R., Zhang, Z., 2019. Application of wood biochar in polluted soils stabilized the toxic metals and enhanced

wheat (Triticum aestivum) growth and soil enzymatic activity. *Ecotoxicology and Environmental Safety*, 184, 109635. https://doi.org/10.1016/j.ecoenv.2019.109635

Alloway, B. J. (Ed.). (2013). *Heavy metals in soils: Trace metals and metalloids in soils and their bioavailability* (3rd ed). Springer.

Álvarez-Rogel, J., Tercero Gómez, M. del C., Conesa, H. M., Párraga-Aguado, I., & González-Alcaraz, M. N. (2018). Biochar from sewage sludge and pruning trees reduced porewater Cd, Pb and Zn concentrations in acidic, but not basic, mine soils under hydric conditions. *Journal of Environmental Management*, *223*, 554–565. https://doi.org/10.1016/j.jenvman.2018.06.055

Amin, M., Ahmad, Mahtab, Farooqi, A., Hussain, Q., Ahmad, Munir, Al-Wabel, M.I., Saleem, H., 2020. Arsenic release in contaminated soil amended with unmodified and modified biochars derived from sawdust and rice husk. *Journal of Soils and Sediments*, 20, 3358–3367. https://doi.org/10.1007/s11368-020-02661-9

Amonette, J. E., & Joseph, S. (2012). *Characteristics of Biochar: Microchemical Properties.* (Lehmann, J. and Joseph, S., Eds., Biochar for Environmental Management: Science and Technology). Taylor and Francis.

Anawar, H. M., Akter, F., Solaiman, Z. M., & Strezov, V. (2015). Biochar: An Emerging Panacea for Remediation of Soil Contaminants from Mining, Industry and Sewage Wastes. *Pedosphere*, *25*(5), 654–665. https://doi.org/10.1016/S1002-0160(15)30046-1

Anza, M., Salazar, O., Epelde, L., Alkorta, I., & Garbisu, C. (2019). The Application of Nanoscale Zero-Valent Iron Promotes Soil Remediation While Negatively Affecting Soil Microbial Biomass and Activity. *Frontiers in Environmental Science*, 7, 19. https://doi.org/10.3389/fenvs.2019.00019

Bae, S., Collins, R. N., Waite, T. D., & Hanna, K. (2018). Advances in Surface Passivation of Nanoscale Zerovalent Iron: A Critical Review. *Environmental Science & Technology*, *52*(21), 12010–12025. https://doi.org/10.1021/acs.est.8b01734

Bakshi, S. (2018). Arsenic sorption on zero-valent iron-biochar complexes. *Water Research*, 11.

Bandosz, T.J., Block, K., 2006. Effect of pyrolysis temperature and time on catalytic performance of sewage sludge/industrial sludge-based composite adsorbents. *Applied Catalysis B: Environmental*, 67, 77–85. https://doi.org/10.1016/j.apcatb.2006.04.006

Baragaño, D., Alonso, J., Gallego, J. R., Lobo, M. C., & Gil-Díaz, M. (2020). Zero valent iron and goethite nanoparticles as new promising remediation techniques for As-polluted soils. *Chemosphere*, *238*, 124624. https://doi.org/10.1016/j.chemosphere.2019.124624

Beesley, L., & Marmiroli, M. (2011). The immobilisation and retention of soluble arsenic, cadmium and zinc by biochar. *Environmental Pollution*, *159*(2), 474–480. https://doi.org/10.1016/j.envpol.2010.10.016

Beesley, L., Inneh, O. S., Norton, G. J., Moreno-Jimenez, E., Pardo, T., Clemente, R., & Dawson, J. J. C. (2014). Assessing the influence of compost and biochar amendments on the mobility and toxicity of metals and arsenic in a naturally contaminated mine soil. *Environmental Pollution*, *186*, 195–202. https://doi.org/10.1016/j.envpol.2013.11.026

Beesley, L., Moreno-Jiménez, E., & Gomez-Eyles, J. L. (2010). Effects of biochar and greenwaste compost amendments on mobility, bioavailability and toxicity of inorganic and organic contaminants in a multi-element polluted soil. *Environmental Pollution*, *158*(6), 2282–2287. https://doi.org/10.1016/j.envpol.2010.02.003

Beesley, L., Moreno-Jimenez, E., Fellet, G., Melo, L., & Sizmur, T. (2015). *Biochar and heavy metals. In Biochar for environmental management (pp. 563-594). Routledge.* (J. Lehmann & S. Joseph, Eds.; Second edition). Routledge, Taylor & Francis Group.

Beiyuan, J., Awad, Y. M., Beckers, F., Wang, J., Tsang, D. C. W., Ok, Y. S., Wang, S.-L., Wang, H., & Rinklebe, J. (2020). (Im)mobilization and speciation of lead under dynamic redox conditions in a contaminated soil amended with pine sawdust biochar. *Environment International*, *135*, 105376. https://doi.org/10.1016/j.envint.2019.105376

Berry, R. F., Danyushevsky, L. V., Goemann, K., Parbhakar-Fox, A., & Rodemann, T. (2017). Micro-analytical Technologies for Mineral Mapping and Trace Element Deportment. In B. Lottermoser (Ed.), *Environmental Indicators in Metal Mining* (pp. 55–72). Springer International Publishing. https://doi.org/10.1007/978-3-319-42731-7_4

Binner, H., Sullivan, T., Jansen, M. A. K., & McNamara, M. E. (2023). Metals in urban soils of Europe: A systematic review. *Science of The Total Environment*, *854*, 158734. https://doi.org/10.1016/j.scitotenv.2022.158734

Birch, H. F. (1958). The effect of soil drying on humus decomposition and nitrogen availability. *Plant and Soil*, *10*(1), 9–31. https://doi.org/10.1007/BF01343734

Bissen, M., Frimmel, F.H., 2003. Arsenic — a Review. Part I: Occurrence, toxicity, speciation, mobility. *Acta Hydrochimica et Hydrobiologica*, 31, 9–18. https://doi.org/10.1002/aheh.200390025

Bolan, N. S., Park, J. H., Robinson, B., Naidu, R., & Huh, K. Y. (2011). *Phytostabilization: A Green Approach to Contaminant Containment*. In: Advances in Agronomy, 112, 145–204. Elsevier. https://doi.org/10.1016/B978-0-12-385538-1.00004-4

Borrajo-Pelaez, R., & Hedström, P. (2018). Recent Developments of Crystallographic Analysis Methods in the Scanning Electron Microscope for Applications in Metallurgy. *Critical Reviews in Solid State and Materials Sciences*, *43*(6), 455–474. https://doi.org/10.1080/10408436.2017.1370576

Boruvka, L., & Vacha, R. (2006). Litavka river alluvium as a model area heavily polluted with potentially risk elements. In J.-L. Morel, G. Echevarria, & N. Goncharova (Eds.), *Phytoremediation of Metal-Contaminated Soils* (Vol. 68, pp. 267–298). Kluwer Academic Publishers. https://doi.org/10.1007/1-4020-4688-X_9

Břendová, K., Tlustoš, P., & Száková, J. (2015). Biochar immobilizes cadmium and zinc and improves phytoextraction potential of willow plants on extremely contaminated soil. *Plant and Soil Environment*, 61, 303-308. DOI: 10.17221/181/2015-PSE

Brumovský, M., Filip, J., Malina, O., Oborná, J., Sracek, O., Reichenauer, T. G., Andrýsková, P., & Zbořil, R. (2020). Core–Shell Fe/FeS Nanoparticles with Controlled Shell Thickness for Enhanced Trichloroethylene Removal. *ACS Applied Materials & Interfaces*, *12*(31), 35424–35434. https://doi.org/10.1021/acsami.0c08626

Burke, M., Rakovan, J., & Krekeler, M. P. S. (2017). A study by electron microscopy of gold and associated minerals from Round Mountain, Nevada. *Ore Geology Reviews*, 91, 708–717. https://doi.org/10.1016/j.oregeorev.2017.08.026

Buss, W. (2021). Pyrolysis Solves the Issue of Organic Contaminants in Sewage Sludge while Retaining Carbon—Making the Case for Sewage Sludge Treatment via Pyrolysis. *ACS Sustainable Chemistry & Engineering*, *9*(30), 10048–10053. https://doi.org/10.1021/acssuschemeng.1c03651

Calderon, B., & Fullana, A. (2015). Heavy metal release due to aging effect during zero valent iron nanoparticles remediation. *Water Research*, 83, 1–9. https://doi.org/10.1016/j.watres.2015.06.004

Campillo-Cora, C., Conde-Cid, M., Arias-Estévez, M., Fernández-Calviño, D., & Alonso-Vega, F. (2020). Specific Adsorption of Heavy Metals in Soils: Individual and Competitive Experiments. *Agronomy*, *10*(8), 1113. https://doi.org/10.3390/agronomy10081113

Carter, M.R., Gregorich, E.G. (Eds.), 2007. Soil sampling and methods of analysis, 0 ed. CRC Press. https://doi.org/10.1201/9781420005271

Carvalho, F. P. (2017). Mining industry and sustainable development: Time for change. *Food and Energy Security*, *6*(2), 61–77. https://doi.org/10.1002/fes3.109

Castaño, A., Prosenkov, A., Baragaño, D., Otaegui, N., Sastre, H., Rodríguez-Valdés, E., Gallego, J. L. R., & Peláez, A. I. (2021). Effects of in situ Remediation With Nanoscale Zero Valence Iron on the Physicochemical Conditions and Bacterial Communities of

Groundwater Contaminated With Arsenic. *Frontiers in Microbiology*, *12*, 643589. https://doi.org/10.3389/fmicb.2021.643589

CEN ISO/TS 17892-4, 2004. Geotechnical investigation and testing – Laboratory testing of soil – Part 4: Determination of Particle Size Distribution., 2004.

Cerqueira, B., Covelo, E.F., Andrade, M.L., Vega, F.A., 2011. Retention and mobility of copper and lead in soils as influenced by soil horizon properties. *Pedosphere,* 21, 603–614. https://doi.org/10.1016/S1002-0160(11)60162-8

Chagas, J. K. M., Figueiredo, C. C. D., & Paz-Ferreiro, J. (2021). Sewage sludge biochars effects on corn response and nutrition and on soil properties in a 5-yr field experiment. *Geoderma*, *401*, 115323. https://doi.org/10.1016/j.geoderma.2021.115323

Chagas, J.K.M., Figueiredo, C.C. de, Silva, J. da, Shah, K., Paz-Ferreiro, J., 2021. Long-term effects of sewage sludge–derived biochar on the accumulation and availability of trace elements in a tropical soil. *Journal of Environmental Quality*, 50, 264–277. https://doi.org/10.1002/jeq2.20183

Chang, C., Li, F., Wang, Q., Hu, M., Du, Y., Zhang, Xiaoqing, Zhang, Xiaolu, Chen, C., Yu, H.-Y., 2022. Bioavailability of antimony and arsenic in a flowering cabbage–soil system: Controlling factors and interactive effect. *Science of The Total Environment,* 815, 152920. https://doi.org/10.1016/j.scitotenv.2022.152920

Chen, H., & Qian, L. (2024). Performance of field demonstration nanoscale zero-valent iron in groundwater remediation: A review. *Science of The Total Environment*, *912*, 169268. https://doi.org/10.1016/j.scitotenv.2023.169268

Chen, T., Zhang, Y., Wang, H., Lu, W., Zhou, Z., Zhang, Y., & Ren, L. (2014). Influence of pyrolysis temperature on characteristics and heavy metal adsorptive performance of biochar derived from municipal sewage sludge. *Bioresource Technology*, *164*, 47–54. https://doi.org/10.1016/j.biortech.2014.04.048

Chen, X., Zhang, P., Wang, Y., Peng, W., Ren, Z., Li, Y., Chu, B., & Zhu, Q. (2023). Research progress on synthesis of zeolites from coal fly ash and environmental applications. *Frontiers of Environmental Science & Engineering*, *17*(12), 149. https://doi.org/10.1007/s11783-023-1749-2

Christodoulou, A., & Stamatelatou, K. (2016). Overview of legislation on sewage sludge management in developed countries worldwide. *Water Science and Technology*, *73*(3), 453–462. https://doi.org/10.2166/wst.2015.521

Clemente, J.S., Beauchemin, S., Thibault, Y., MacKinnon, T., Smith, D., 2018. Differentiating Inorganics in Biochars Produced at Commercial Scale Using Principal Component Analysis. *ACS Omega*, 3, 6931–6944. https://doi.org/10.1021/acsomega.8b00523

Clemente, R., Almela, C., & Bernal, M. P. (2006). A remediation strategy based on active phytoremediation followed by natural attenuation in a soil contaminated by pyrite waste. *Environmental Pollution*, *143*(3), 397–406. https://doi.org/10.1016/j.envpol.2005.12.011

Cornell, R. M., & Schwertmann, U. (2003). *The iron oxides: Structure, properties, reactions, occurrences, and uses* (2nd, completely rev. and extended ed ed.). Wiley-VCH.

Costa, F. R., Nery, G. P., Carneiro, C. D. C., Kahn, H., & Ulsen, C. (2022). Mineral characterization of low-grade gold ore to support geometallurgy. *Journal of Materials Research and Technology*, *21*, 2841–2852. https://doi.org/10.1016/j.jmrt.2022.10.085

Covelo, E. F., Vega, F. A., & Andrade, M. L. (2007). Competitive sorption and desorption of heavy metals by individual soil components. *Journal of Hazardous Materials*, *140*(1–2), 308–315. https://doi.org/10.1016/j.jhazmat.2006.09.018

Craw, D., MacKenzie, D., & Lilly, K. (2016). Southland gold nuggets: sources on the southwest margin of the Otago Schist? *Proceedings of the 49th New Zealand Branch Annual Conference on exploration, mining and New Zealand's mineral resources*.

Cruz, J.R.F., Leone da Cruz Ferreira, R., Silva Conceição, S., Ugulino Lima, E., Ferreira de Oliveira Neto, C., Rodrigues Galvão, J., da Cunha Lopes, S., de Jesus Matos Viegas, I., 2022. *Copper toxicity in plants: nutritional, physiological, and biochemical aspects*, In: Ngui Kimatu, J. (Ed.), Advances in Plant Defense Mechanisms. IntechOpen. https://doi.org/10.5772/intechopen.105212

ČSN EN ISO 21656. 2021. Solid recovered fuels — Determination of ash content.

ČSN EN ISO 22167. 2021. Solid alternative fuels — Determination of volatile combustible content.

Cui, H., Yang, X., Xu, L., Fan, Y., Yi, Q., Li, R., & Zhou, J. (2017). Effects of goethite on the fractions of Cu, Cd, Pb, P and soil enzyme activity with hydroxyapatite in heavy metal-contaminated soil. *RSC Advances, 7*(72), 45869–45877. https://doi.org/10.1039/C7RA08786A

Cui, W., Li, X., Duan, W., Xie, M., & Dong, X. (2023). Heavy metal stabilization remediation in polluted soils with stabilizing materials: A review. *Environmental Geochemistry and Health*, *45*(7), 4127–4163. https://doi.org/10.1007/s10653-023-01522-x

Cui, Z., Xu, G., Ormeci, B., Liu, H., & Zhang, Z. (2022). Transformation and stabilization of heavy metals during pyrolysis of organic and inorganic-dominated sewage sludges and their mechanisms. *Waste Management*, *150*, 57–65. https://doi.org/10.1016/j.wasman.2022.06.023

Danila, V., Kumpiene, J., Kasiuliene, A., & Vasarevičius, S. (2020). Immobilisation of metal(loid)s in two contaminated soils using micro and nano zerovalent iron particles: Evaluating the long-term stability. *Chemosphere*, *248*, 126054. https://doi.org/10.1016/j.chemosphere.2020.126054

Das, S., Sultana, K. W., Ndhlala, A. R., Mondal, M., & Chandra, I. (2023). Heavy Metal Pollution in the Environment and Its Impact on Health: Exploring Green Technology for Remediation. *Environmental Health Insights*, *17*, 11786302231201259. https://doi.org/10.1177/11786302231201259

Decree No. 153/2016 Coll., on determining the details of agricultural soil quality protection for ordinary soils. Collection of Laws Czech Republic, Amount 59 (2016).

Decree No. 273/2021 Coll., on details of waste management. Collection of Laws Czech Republic, Amount 119 (2021).

Decree No. 294/2005 Coll., on the conditions of waste disposal to the landfills. Collection of Laws Czech Republic, Amount 105 (2005).

Deng, J., Dong, H., Zhang, C., Jiang, Z., Cheng, Y., Hou, K., Zhang, L. & Fan, C. (2018). Nanoscale zero-valent iron/biochar composite as an activator for Fenton-like removal of sulfamethazine. *Seperation and Purification Technology*, 202, 130-137. DOI: 10.1016/j.seppur.2018.03.048

Derakhshan Nejad, Z., Jung, M. C., & Kim, K.-H. (2018). Remediation of soils contaminated with heavy metals with an emphasis on immobilization technology. *Environmental Geochemistry and Health*, *40*(3), 927–953. https://doi.org/10.1007/s10653-017-9964-z

Dhaliwal, S. S., Singh, J., Taneja, P. K., & Mandal, A. (2020). Remediation techniques for removal of heavy metals from the soil contaminated through different sources: A review. *Environmental Science and Pollution Research*, *27*(2), 1319–1333. https://doi.org/10.1007/s11356-019-06967-1

Ding, N., Meng, X., Zhang, Z., Ma, J., Shan, Y., Zhong, Z., Yu, H., Li, M., & Jiao, W. (2024). A Review of Life Cycle Assessment of Soil Remediation Technology: Method Applications and Technological Characteristics. *Reviews of Environmental Contamination and Toxicology*, *262*(1), 4. https://doi.org/10.1007/s44169-023-00051-z

Dong, H., Deng, J., Xie, Y., Zhang, C., Jiang, Z., Cheng, Y., Hou, K., & Zeng, G. (2017). Stabilisation of nanoscale zero-valent iron (nZVI) with modified biochar for Cr (VI)

removal from aqueous solution. *Journal of Hazardous Materials* 322, 79-86. DOI: 10.1016/j.jhazmat.2017.03.002

Dong, H., Li, L., Wang, Y., Ning, Q., Wang, B., & Zeng, G. (2020). Aging of zero-valent iron-based nanoparticles in aqueous environment and the consequent effects on their reactivity and toxicity. *Water Environment Research*, *92*(5), 646–661. https://doi.org/10.1002/wer.1265

Dostál, J., Kunický, Z., & Vurm, K. (2006). *220 let olověné a stříbrné hutě Příbram 1786 – 2006 220-year Anniversary of the Silver and Lead Smelting Works in Příbram*. https://www.kovopb.cz/wp-content/uploads/kopb-historie-do-2006_publikace-220let-hute-1.pdf

Dovletyarova, E. A., Fareeva, O. S., Zhikharev, A. P., Brykova, R. A., Vorobeichik, E. L., Slukovskaya, M. V., Vítková, M., Ettler, V., Yáñez, C., & Neaman, A. (2022). Choose your amendment wisely: Zero-valent iron nanoparticles offered no advantage over microparticles in a laboratory study on metal immobilization in a contaminated soil. *Applied Geochemistry*, *143*, 105369. https://doi.org/10.1016/j.apgeochem.2022.105369

Du Laing, G., Rinklebe, J., Vandecasteele, B., Meers, E., & Tack, F. M. G. (2009). Trace metal behaviour in estuarine and riverine floodplain soils and sediments: A review. *Science of The Total Environment*, *407*(13), 3972–3985. https://doi.org/10.1016/j.scitotenv.2008.07.025

Dume, B., Hanč, A., Švehla, P., Michal, P., Pospíšil, V., Grasserová, A., Cajthaml, T., Chane, A.D., Nigussie, A., 2023. Influence of earthworms on the behaviour of organic micropollutants in sewage sludge. *Journal of Cleaner Production*, 137869.

Duwiejuah, A. B., Abubakari, A. H., Quainoo, A. K., & Amadu, Y. (2020). Review of Biochar Properties and Remediation of Metal Pollution of Water and Soil. *Journal of Health and Pollution*, *10*(27), 200902. https://doi.org/10.5696/2156-9614-10.27.200902

EEA. (2014). *European Environment Agency. Progress in the management of contaminated sites in Europe.* Publications Office. https://data.europa.eu/doi/10.2788/4658

EEA. (2022). *Progress in the management of contaminated sites in Europe*. https://www.eea.europa.eu/en/analysis/indicators/progress-in-the-management-of?activeAccordion=546a7c35-9188-4d23-94ee-005d97c26f2b

El-Naggar, A., Chen, Z., Jiang, W., Cai, Y., & Chang, S. X. (2022). Biochar effectively remediates Cd contamination in acidic or coarse- and medium-textured soils: A global meta-analysis. *Chemical Engineering Journal*, *442*, 136225. https://doi.org/10.1016/j.cej.2022.136225

El-Naggar, A., Shaheen, S. M., Ok, Y. S., & Rinklebe, J. (2018). Biochar affects the dissolved and colloidal concentrations of Cd, Cu, Ni, and Zn and their phytoavailability and potential mobility in a mining soil under dynamic redox-conditions. *Science of the Total Environment*, 624, 1059-1071. https://doi.org/10.1016/j.scitotenv.2017.12.190

EPA. (2007). Framework for Metals Risk Assessment. *EPA 120/R-07/001*, 172.

EPA. (2007). Method 3051a, Microwave Assisted Acid Digestion of Sludges, Sediments, Soils, and Oils. Washington, DC: US-EPA.

Ericsson, M., & Löf, O. (2019). Mining's contribution to national economies between 1996 and 2016. *Mineral Economics*, *32*(2), 223–250. https://doi.org/10.1007/s13563-019-00191-6

ESDAC. European Soil Data Centre. https://esdac.jrc.ec.europa.eu/themes/soil-contamination

Ettler, V. (2016). Soil contamination near non-ferrous metal smelters: A review. *Applied Geochemistry*, 64, 56–74. https://doi.org/10.1016/j.apgeochem.2015.09.020

Ettler, V., Červinka, R., & Johan, Z. (2009). Mineralogy of medieval slags from lead and silver smelting (bohutín, příbram district, czech republic): towards estimation of historical

smelting conditions*: Medieval slags from Bohutín, Czech Republic. *Archaeometry*, *51*(6), 987–1007. https://doi.org/10.1111/j.1475-4754.2008.00455.x

Ettler, V., Johan, Z., Baronnet, A., Jankovský, F., Gilles, C., Mihaljevič, M., Šebek, O., Strnad, L., & Bezdička, P. (2005). Mineralogy of Air-Pollution-Control Residues from a Secondary Lead Smelter: Environmental Implications. *Environmental Science & Technology*, *39*(23), 9309–9316. https://doi.org/10.1021/es0509174

Ettler, V., Legendre, O., Bodenan, F., & Touray, J.-C. (2001). PRIMARY PHASES AND NATURAL WEATHERING OF OLD LEAD ZINC PYROMETALLURGICAL SLAG FROM PRIBRAM, CZECH REPUBLIC. *The Canadian Mineralogist*, *39*(3), 873–888. https://doi.org/10.2113/gscanmin.39.3.873

Ettler, V., Mihaljevic, M., & Komarek, M. (2004). ICP-MS measurements of lead isotopic ratios in soils heavily contaminated by lead smelting: Tracing the sources of pollution. *Analytical and Bioanalytical Chemistry*, *378*(2), 311–317. https://doi.org/10.1007/s00216-003-2229-y

Ettler, V., Mihaljevič, M., Šebek, O., Molek, M., Grygar, T., & Zeman, J. (2006). Geochemical and Pb isotopic evidence for sources and dispersal of metal contamination in stream sediments from the mining and smelting district of Příbram, Czech Republic. *Environmental Pollution*, *142*(3), 409–417. https://doi.org/10.1016/j.envpol.2005.10.024

EU. (1986). *European Regulation 86/278/EEC.*

Fajardo, C., García-Cantalejo, J., Botías, P., Costa, G., Nande, M., & Martin, M. (2019). New insights into the impact of nZVI on soil microbial biodiversity and functionality. *Journal of Environmental Science and Health, Part A*, *54*(3), 157–167. https://doi.org/10.1080/10934529.2018.1535159

Fan, J., Chen, X., Xu, Z., Xu, X., Zhao, L., Qiu, H., & Cao, X. (2020). One-pot synthesis of nZVI-embedded biochar for remediation of two mining arsenic-contaminated soils: Arsenic immobilization associated with iron transformation. *Journal of Hazardous Materials*, *398*, 122901. https://doi.org/10.1016/j.jhazmat.2020.122901

Fan, J., Li, Y., Yu, H., Li, Y., Yuan, Q., Xiao, H., Li, F., & Pan, B. (2020). Using sewage sludge with high ash content for biochar production and Cu(II) sorption. *Science of The Total Environment*, *713*, 136663. https://doi.org/10.1016/j.scitotenv.2020.136663

FAO & ITPS. (2015). *Status of the world's soil resources: Main report*. FAO: ITPS.

FAO and UNEP. (2021). *Global assessment of soil pollution: Report*. FAO and UNEP. https://doi.org/10.4060/cb4894en

FAO. (2018). *Global Symposium on Soil Pollution Outcome document*. https://www.fao.org/about/meetings/global-symposium-on-soil-pollution/en/

Farkas, É., Feigl, V., Gruiz, K., Vaszita, E., Fekete-Kertész, I., Tolner, M., Kerekes, I., Pusztai, É., Kari, A., Uzinger, N. and Rékási, M., 2020. Long-term effects of grain husk and paper fibre sludge biochar on acidic and calcareous sandy soils–a scale-up field experiment applying a complex monitoring toolkit. *Science of the Total Environment*, 731, p.138988.

Fernández Rodríguez, M. D., García Gómez, M. C., Alonso Blazquez, N., & Tarazona, J. V. (2014). Soil Pollution Remediation. In *Encyclopedia of Toxicology* (pp. 344–355). Elsevier. https://doi.org/10.1016/B978-0-12-386454-3.00579-0

Figueiredo, C. C., Chagas, J. K. M., Da Silva, J., & Paz-Ferreiro, J. (2019). Short-term effects of a sewage sludge biochar amendment on total and available heavy metal content of a tropical soil. *Geoderma*, *344*, 31–39. https://doi.org/10.1016/j.geoderma.2019.01.052

Figueiredo, C.C., Reis, A. de S.P.J., Araujo, A.S. de, Blum, L.E.B., Shah, K., Paz-Ferreiro, J., 2021. Assessing the potential of sewage sludge-derived biochar as a novel phosphorus fertilizer: Influence of extractant solutions and pyrolysis temperatures. *Waste Managment* 124, 144–153. https://doi.org/10.1016/j.wasman.2021.01.044

Filip, J., Kolařík, J., Petala, E., Petr, M., Šráček, O., & Zbořil, R. (2019). Nanoscale Zerovalent Iron Particles for Treatment of Metalloids. In T. Phenrat & G. V. Lowry (Eds.), *Nanoscale Zerovalent Iron Particles for Environmental Restoration* (pp. 157–199). Springer International Publishing. https://doi.org/10.1007/978-3-319-95340-3_4

Frick, H., Tardif, S., Kandeler, E., Holm, P. E., & Brandt, K. K. (2019). Assessment of biochar and zero-valent iron for in-situ remediation of chromated copper arsenate contaminated soil. *Science of the Total Environment,* 655, 414-422. DOI: 10.1016/j.scitotenv.2018.11.193

Frišták, V., Pipíška, M., Soja, G., 2018. Pyrolysis treatment of sewage sludge: A promising way to produce phosphorus fertilizer. *Journal of Cleaner Production,* 172, 1772–1778. https://doi.org/10.1016/j.jclepro.2017.12.015

Frohne, T., Rinklebe, J., & Diaz-Bone, R. A. (2014). Contamination of Floodplain Soils along the Wupper River, Germany, with As, Co, Cu, Ni, Sb, and Zn and the Impact of Pre-definite Redox Variations on the Mobility of These Elements. *Soil and Sediment Contamination: An International Journal*, 23(7), 779–799. https://doi.org/10.1080/15320383.2014.872597

Frohne, T., Rinklebe, J., Diaz-Bone, R. A., & Du Laing, G. (2011). Controlled variation of redox conditions in a floodplain soil: Impact on metal mobilization and biomethylation of arsenic and antimony. *Geoderma*, 160(3–4), 414–424. https://doi.org/10.1016/j.geoderma.2010.10.012

Fu, D., Kurniawan, T.A., Wang, Y., Zhou, Z., Wei, Q., Hu, Y., Hafiz Dzarfan Othman, M., Wayne Chew, K., Hwang Goh, H., Gui, H., 2023. Applicability of magnetic biochar derived from Fe-enriched sewage sludge for chromate removal from aqueous solution. *Chemical Engineering Science* 281, 119145. https://doi.org/10.1016/j.ces.2023.119145

Fu, T., Zhang, B., Gao, X., Cui, S., Guan, C.-Y., Zhang, Y., Zhang, B., & Peng, Y. (2023). Recent progresses, challenges, and opportunities of carbon-based materials applied in heavy metal polluted soil remediation. *Science of The Total Environment*, 856, 158810. https://doi.org/10.1016/j.scitotenv.2022.158810

Galdames, A., Mendoza, A., Orueta, M., de Soto García, I. S., Sánchez, M., Virto, I., & Vilas, J. L. (2017). Development of new remediation technologies for contaminated soils based on the application of zero-valent iron nanoparticles and bioremediation with compost. *Resource-Efficient Technologies*, 3(2), 166–176. https://doi.org/10.1016/j.reffit.2017.03.008

Gale, M., Nguyen, T., Moreno, M., Gilliard-AbdulAziz, K.L., 2021. Physiochemical properties of biochar and activated carbon from biomass residue: influence of process conditions to adsorbent properties. *ACS Omega* 6, 10224–10233. https://doi.org/10.1021/acsomega.1c00530

Ganie, A. S., Bano, S., Khan, N., Sultana, S., Rehman, Z., Rahman, M. M., Sabir, S., Coulon, F., & Khan, M. Z. (2021). Nanoremediation technologies for sustainable remediation of contaminated environments: Recent advances and challenges. *Chemosphere*, 275, 130065. https://doi.org/10.1016/j.chemosphere.2021.130065

Gao, J., Zhao, T., Tsang, D.C.W., Zhao, N., Wei, H., Feng, M., Liu, K., Zhang, W., Qiu, R., 2020. Effects of Zn in sludge-derived biochar on Cd immobilization and biological uptake by lettuce. *Science of The Total Environment,* 714, 136721. https://doi.org/10.1016/j.scitotenv.2020.136721

Gao, L.-Y., Deng, J.-H., Huang, G.-F., Li, K., Cai, K.-Z., Liu, Y., Huang, F., 2019. Relative distribution of Cd2+ adsorption mechanisms on biochars derived from rice straw and sewage sludge. *Bioresource Technology,* 272, 114–122. https://doi.org/10.1016/j.biortech.2018.09.138

Gao, Y., Wu, P., Jeyakumar, P., Bolan, N., Wang, H., Gao, B., Wang, S., & Wang, B. (2022). Biochar as a potential strategy for remediation of contaminated mining soils:

Mechanisms, applications, and future perspectives. *Journal of Environmental Management*, 313, 114973. https://doi.org/10.1016/j.jenvman.2022.114973

Gee, G.W., Or, D., 2002. 2.4 *Particle-Size Analysis*, in: Dane, J.H., Clarke Topp, G. (Eds.), SSSA Book Series. Soil Science Society of America, Madison, WI, USA, pp. 255–293. https://doi.org/10.2136/sssabookser5.4.c12

Gerdelidani, A.F., Towfighi, H., Shahbazi, K., Lamb, D.T., Choppala, G., Abbasi, S., Bari, A.S.M.F., Naidu, R., Rahman, M.M., 2021. Arsenic geochemistry and mineralogy as a function of particle-size in naturally arsenic-enriched soils. *Journal of Hazardous Materials,* 403, 123931. https://doi.org/10.1016/j.jhazmat.2020.123931

Gievers, F., Loewen, A., Nelles, M., 2021. Life cycle assessment of sewage sludge pyrolysis: environmental impacts of biochar as carbon sequestrator and nutrient recycler. *Detritus,* 94–105. https://doi.org/10.31025/2611-4135/2021.15111

Gil-Díaz, M., Diez-Pascual, S., González, A., Alonso, J., Rodríguez-Valdés, E., Gallego, J. R., & Lobo, M. C. (2016). A nanoremediation strategy for the recovery of an As-polluted soil. *Chemosphere*, 149, 137–145. https://doi.org/10.1016/j.chemosphere.2016.01.106

Gil-Díaz, M., Pérez-Sanz, A., Ángeles Vicente, M., & Carmen Lobo, M. (2014). Immobilisation of Pb and Zn in Soils Using Stabilised Zero-valent Iron Nanoparticles: Effects on Soil Properties: Metal Soil Immobilisation Using Zero-valent Iron Nanoparticles. *CLEAN - Soil, Air, Water*, 42(12), 1776–1784. https://doi.org/10.1002/clen.201300730

Gil-Díaz, M., Rodríguez-Valdés, E., Alonso, J., Baragaño, D., Gallego, J. R., & Lobo, M. C. (2019). Nanoremediation and long-term monitoring of brownfield soil highly polluted with As and Hg. *Science of The Total Environment*, 675, 165–175. https://doi.org/10.1016/j.scitotenv.2019.04.183

Giwa, A.S., Maurice, N.J., Luoyan, A., Liu, X., Yunlong, Y., Hong, Z., 2023. Advances in sewage sludge application and treatment: Process integration of plasma pyrolysis and anaerobic digestion with the resource recovery. *Heliyon* 9, e19765. https://doi.org/10.1016/j.heliyon.2023.e19765

Godlewska, P., Ok, Y. S., & Oleszczuk, P. (2021). THE DARK SIDE OF BLACK GOLD: Ecotoxicological aspects of biochar and biochar-amended soils. *Journal of Hazardous Materials*, 403, 123833. https://doi.org/10.1016/j.jhazmat.2020.123833

Goldstein, J. I., Newbury, D. E., Echlin, P., Joy, D. C., Lyman, C. E., Lifshin, E., Sawyer, L., & Michael, J. R. (2003). *Scanning Electron Microscopy and X-ray Microanalysis: Third Edition*. Springer US. https://doi.org/10.1007/978-1-4615-0215-9

Gómez-Sagasti, M. T., Epelde, L., Anza, M., Urra, J., Alkorta, I., & Garbisu, C. (2019). The impact of nanoscale zero-valent iron particles on soil microbial communities is soil dependent. *Journal of Hazardous Materials*, 364, 591–599. https://doi.org/10.1016/j.jhazmat.2018.10.034

Gong, H., Zhao, L., Rui, X., Hu, J., & Zhu, N. (2022). A review of pristine and modified biochar immobilizing typical heavy metals in soil: Applications and challenges. *Journal of Hazardous Materials*, 432, 128668. https://doi.org/10.1016/j.jhazmat.2022.128668

Gopinath, A., Divyapriya, G., Srivastava, V., Laiju, A.R., Nidheesh, P.V., Kumar, M.S., 2021. Conversion of sewage sludge into biochar: A potential resource in water and wastewater treatment. *Environmental Research*, 194, 110656. https://doi.org/10.1016/j.envres.2020.110656

Grangeon, S., Bataillard, P., & Coussy, S. (2020). The Nature of Manganese Oxides in Soils and Their Role as Scavengers of Trace Elements: Implication for Soil Remediation. In E. D. Van Hullebusch, D. Huguenot, Y. Pechaud, M.-O. Simonnot, & S. Colombano (Eds.), *Environmental Soil Remediation and Rehabilitation,* 399–429. Springer International Publishing. https://doi.org/10.1007/978-3-030-40348-5_7

Grieger, K., Hjorth, R., Carpenter, A. W., Klaessig, F., Lefevre, E., Gunsch, C., Soratana, K., Landis, A. E., Wickson, F., Hristozov, D., & Linkov, I. (2019). Sustainable Environmental

Remediation Using NZVI by Managing Benefit-Risk Trade-Offs. In T. Phenrat & G. V. Lowry (Eds.), *Nanoscale Zerovalent Iron Particles for Environmental Restoration* (pp. 511–562). Springer International Publishing. https://doi.org/10.1007/978-3-319-95340-3_15

Grobelak, A., & Jaskulak, M. (2019). Sludge multifunctions in a phytobiome—Forest and plantation application including microbial aspects. In *Industrial and Municipal Sludge* (pp. 323–336). Elsevier. https://doi.org/10.1016/B978-0-12-815907-1.00014-3

Grybos, M., Davranche, M., Gruau, G., & Petitjean, P. (2007). Is trace metal release in wetland soils controlled by organic matter mobility or Fe-oxyhydroxides reduction? *Journal of Colloid and Interface Science*, *314*(2), 490–501. https://doi.org/10.1016/j.jcis.2007.04.062

Gu, W., Guo, J., Bai, J., Dong, B., Hu, J., Zhuang, X., Zhang, C., Shih, K., 2022. Co-pyrolysis of sewage sludge and Ca(H2PO4)2: heavy metal stabilization, mechanism, and toxic leaching. *Journal of Environmental Management*, 305, 114292. https://doi.org/10.1016/j.jenvman.2021.114292

Han, L., Xue, S., Zhao, S., Yan, J., Qian, L., & Chen, M. (2015). Biochar supported nanoscale iron particles for the efficient removal of methyl orange dye in aqueous solutions. *PloS One* 10, e0132067. DOI: 10.1371/journal.pone.0132067

Hartley, W., Riby, P., Waterson, J., 2016. Effects of three different biochars on aggregate stability, organic carbon mobility and micronutrient bioavailability. *Journal of Environmental Management,* 181, 770–778. https://doi.org/10.1016/j.jenvman.2016.07.023

Harvey, A. E., Smart, J. A., & Amis, E. S. (1955). Simultaneous Spectrophotometric Determination of Iron(II) and Total Iron with 1,10-Phenanthroline. *Analytical Chemistry*, *27*(1), 26–29. https://doi.org/10.1021/ac60097a009

Havlin, J. L. (2005). FERTILITY. In *Encyclopedia of Soils in the Environment,* 10–19. Elsevier. https://doi.org/10.1016/B0-12-348530-4/00228-9

He, E., Yang, Y., Xu, Z., Qiu, H., Yang, F., Peijnenburg, W.J.G.M., Zhang, W., Qiu, R., Wang, S., 2019. Two years of aging influences the distribution and lability of metal(loid)s in a contaminated soil amended with different biochars. *Science of The Total Environment,* 673, 245–253. https://doi.org/10.1016/j.scitotenv.2019.04.037

He, L., Zhong, H., Liu, G., Dai, Z., Brookes, P.C., Xu, J., 2019. Remediation of heavy metal contaminated soils by biochar: Mechanisms, potential risks and applications in China. *Environmental Pollution*, 252, 846–855. https://doi.org/10.1016/j.envpol.2019.05.151

He, Y., Fang, T., Wang, J., Liu, X., Yan, Z., Lin, H., Li, F., & Guo, G. (2022). Insight into the stabilization mechanism and long-term effect on As, Cd, and Pb in soil using zeolite-supported nanoscale zero-valent iron. *Journal of Cleaner Production*, 355, 131634. https://doi.org/10.1016/j.jclepro.2022.131634

Henderson, G. S., De Groot, F. M. F., & Moulton, B. J. A. (2014). X-ray Absorption Near-Edge Structure (XANES) Spectroscopy. *Reviews in Mineralogy and Geochemistry*, *78*(1), 75–138. https://doi.org/10.2138/rmg.2014.78.3

Hiller, E., Jurkovič, Ľ., Faragó, T., Vítková, M., Tóth, R., & Komárek, M. (2021). Contaminated soils of different natural pH and industrial origin: The role of (nano) iron- and manganese-based amendments in As, Sb, Pb, and Zn leachability. *Environmental Pollution*, 285, 117268. https://doi.org/10.1016/j.envpol.2021.117268

Houben, D., Evrard, L., & Sonnet, P. (2013). Mobility, bioavailability and pH-dependent leaching of cadmium, zinc and lead in a contaminated soil amended with biochar. *Chemosphere*, *92*(11), 1450–1457. https://doi.org/10.1016/j.chemosphere.2013.03.055

Huang, H.-H. (2016). The Eh-pH Diagram and Its Advances. *Metals*, 6(1), 23. https://doi.org/10.3390/met6010023

Hudcová B., Vítková M., Ouředníček P., Komárek M., (2019). Stability and stabilizing efficiency of Mg-Fe layered double hydroxides and mixed oxides in aqueous solutions and soils with elevated As(V), Pb (II) and Zn(II) contents. *Science of The Total Environment*, 648, 1511–1519. https://doi.org/10.1016/j.scitotenv.2018.08.277

Hudcová, B., Fein, J.B., Tsang, D.C.W., Komárek, M., 2022. Mg-Fe LDH-coated biochars for metal(loid) removal: Surface complexation modeling and structural change investigations. *Chemical Engineering Journal*, 432, 134360. https://doi.org/10.1016/j.cej.2021.134360

Hudcová, B., Osacký, M., Vítková, M., Mitzia, A., & Komárek, M. (2021). Investigation of zinc binding properties onto natural and synthetic zeolites: Implications for soil remediation. *Microporous and Mesoporous Materials*, 317, 111022. https://doi.org/10.1016/j.micromeso.2021.111022

Hudcová, B., Vítková, M., Ouředníček, P., & Komárek, M. (2019). Stability and stabilizing efficiency of Mg-Fe layered double hydroxides and mixed oxides in aqueous solutions and soils with elevated As(V), Pb(II) and Zn(II) contents. *Science of The Total Environment*, 648, 1511–1519. https://doi.org/10.1016/j.scitotenv.2018.08.277

Hušek, M., Moško, J., & Pohořelý, M. (2022). Sewage sludge treatment methods and P-recovery possibilities: Current state-of-the-art. *Journal of Environmental Management*, 315, 115090. https://doi.org/10.1016/j.jenvman.2022.115090

Husson, O. (2013). Redox potential (Eh) and pH as drivers of soil/plant/microorganism systems: A transdisciplinary overview pointing to integrative opportunities for agronomy. *Plant and Soil*, *362*(1–2), 389–417. https://doi.org/10.1007/s11104-012-1429-7

IARC (Ed.). (2012). *A review of human carcinogens*. International agency for research on cancer.

IBI. International Biochar Initiative. Retrieved 29 January 2024, from https://biochar-international.org

Innemanová, P., Grasserová, A., Cajthaml, T., 2022. Pilot-scale vermicomposting of dewatered sewage sludge from medium-sized wastewater treatment plant (WWTP). *Detritus*, 18, p.35. https://doi.org/10.31025/2611-4135/2022.15166

Ippolito, J. A., Cui, L., Kammann, C., Wrage-Mönnig, N., Estavillo, J. M., Fuertes-Mendizabal, T., Cayuela, M. L., Sigua, G., Novak, J., Spokas, K., & Borchard, N. (2020). Feedstock choice, pyrolysis temperature and type influence biochar characteristics: A comprehensive meta-data analysis review. *Biochar*, *2*(4), 421–438. https://doi.org/10.1007/s42773-020-00067-x

ISO 10390, 2005. Soil quality−Determination of pH.

ISO 12782-1:2012. Soil quality -- Parameters for geochemical modelling of leaching and speciation of constituents in soils and materials -- Part 1: Extraction of amorphous iron oxides and hydroxides with ascorbic acid.

ISO 12782-2:2012. Soil quality -- Parameters for geochemical modelling of leaching and speciation of constituents in soils and materials -- Part 2: Extraction of crystalline iron oxides and hydroxides with dithionite.

ISO 12782-3:2012. Soil quality -- Parameters for geochemical modelling of leaching and speciation of constituents in soils and materials -- Part 3: Extraction of aluminium oxides and hydroxides with ammonium oxalate/oxalic acid

Jačka, L., Trakal, L., Ouředníček, P., Pohořelý, M., & Šípek, V. (2018). Biochar presence in soil significantly decreased saturated hydraulic conductivity due to swelling. *Soil and Tillage Research*, 184, 181–185. https://doi.org/10.1016/j.still.2018.07.018

Jensen, P. E., Ottosen, L. M. & Pedersen, A. J. (2006). Speciation of Pb in industrially polluted soils. *Water Air Soil Pollution*, 170, 359-382. https://doi.org/10.1007/s11270-005-9008-7

Jien, S.-H. (2019). *Physical Characteristics of Biochars and Their Effects on Soil Physical Properties,* In: Biochar from Biomass and Waste*, 21–35. Elsevier. https://doi.org/10.1016/B978-0-12-811729-3.00002-9

Jin, J., Li, Y., Zhang, Jianyun, Wu, S., Cao, Y., Liang, P., Zhang, Jin, Wong, M.H., Wang, M., Shan, S., Christie, P., 2016. Influence of pyrolysis temperature on properties and environmental safety of heavy metals in biochars derived from municipal sewage sludge. *Journal of Hazardous Materials*, 320, 417–426. https://doi.org/10.1016/j.jhazmat.2016.08.050

Jurkovič, Ľ., Majzlan, J., Hiller, E., Klimko, T., Voleková-Lalinská, B., Méres, Š., Göttlicher, J., & Steininger, R. (2019). Natural attenuation of antimony and arsenic in soils at the abandoned Sb-deposit Poproč, Slovakia. *Environmental Earth Sciences*, *78*(24), 672. https://doi.org/10.1007/s12665-019-8701-6

Kabata-Pendias, A. (2011). *Trace elements in soils and plants* (4th ed). CRC press.

Kacprzak, M., Neczaj, E., Fijałkowski, K., Grobelak, A., Grosser, A., Worwag, M., Rorat, A., Brattebo, H., Almås, Å., & Singh, B. R. (2017). Sewage sludge disposal strategies for sustainable development. *Environmental Research*, 156, 39–46. https://doi.org/10.1016/j.envres.2017.03.010

Kakade, A., Sharma, M., Salama, E.-S., Zhang, P., Zhang, L., Xing, X., Yue, J., Song, Z., Nan, L., Yujun, S., & Li, X. (2023). Heavy metals (HMs) pollution in the aquatic environment: Role of probiotics and gut microbiota in HMs remediation. *Environmental Research*, 223, 115186. https://doi.org/10.1016/j.envres.2022.115186

Kaljunen, J.U., Yazdani, R., Al-Juboori, R.A., Zborowski, C., Meinander, K., Mikola, A., 2022. Adsorptive behavior of phosphorus onto recycled waste biosolids after being acid leached from wastewater sludge. *Chemical Engineering Journal Advances,* 11, 100329. https://doi.org/10.1016/j.ceja.2022.100329

Karimi, F., Rahimi, G., Kolahchi, Z., & Nezhad, A. K. J. (2020). Using Industrial Sewage Sludge-Derived Biochar to Immobilize Selected Heavy Metals in a Contaminated Calcareous Soil. *Waste and Biomass Valorization*, *11*(6), 2825–2836. https://doi.org/10.1007/s12649-018-00563-z

Kašlík, J., Kolařík, J., Filip, J., Medřík, I., Tomanec, O., Petr, M., Malina, O., Zbořil, R., & Tratnyek, P. G. (2018). Nanoarchitecture of advanced core-shell zero-valent iron particles with controlled reactivity for contaminant removal. *Chemical Engineering Journal*, 354, 335–345. https://doi.org/10.1016/j.cej.2018.08.015

Ken, D. S., & Sinha, A. (2020). Recent developments in surface modification of nano zero-valent iron (nZVI): Remediation, toxicity and environmental impacts. *Environmental Nanotechnology, Monitoring & Management*, *14*, 100344. https://doi.org/10.1016/j.enmm.2020.100344

Kennou, B., El Meray, M., Romane, A., & Arjouni, Y. (2015). Assessment of heavy metal availability (Pb, Cu, Cr, Cd, Zn) and speciation in contaminated soils and sediment of discharge by sequential extraction. *Environmental and Earth Sciences*, 74, 5849-5858. https://doi.org/10.1007/s12665-015-4609-y

Khalid, S., Shahid, M., Niazi, N. K., Murtaza, B., Bibi, I., & Dumat, C. (2017). A comparison of technologies for remediation of heavy metal contaminated soils. *Journal of Geochemical Exploration*, 182, 247–268. https://doi.org/10.1016/j.gexplo.2016.11.021

Khan, R., Shukla, S., Kumar, M., Zuorro, A., & Pandey, A. (2023). Sewage sludge derived biochar and its potential for sustainable environment in circular economy: Advantages and challenges. *Chemical Engineering Journal*, 471, 144495. https://doi.org/10.1016/j.cej.2023.144495

Khan, S., Chao, C., Waqas, M., Arp, H. P. H., & Zhu, Y.-G. (2013). Sewage Sludge Biochar Influence upon Rice (*Oryza sativa* L) Yield, Metal Bioaccumulation and Greenhouse Gas

Emissions from Acidic Paddy Soil. *Environmental Science & Technology*, *47*(15), 8624–8632. https://doi.org/10.1021/es400554x

Klüpfel, L., Keiluweit, M., Kleber, M., & Sander, M. (2014). Redox Properties of Plant Biomass-Derived Black Carbon (Biochar). *Environmental Science & Technology*, *48*(10), 5601–5611. https://doi.org/10.1021/es500906d

Komárek, M., Antelo, J., Králová, M., Veselská, V., Číhalová, S., Chrastný, V., Ettler, V., Filip, J., Yu, Q., Fein, J. B., & Koretsky, C. M. (2018). Revisiting models of Cd, Cu, Pb and Zn adsorption onto Fe(III) oxides. *Chemical Geology*, *493*, 189–198. https://doi.org/10.1016/j.chemgeo.2018.05.036

Komárek, M., Vaněk, A., & Ettler, V. (2013). Chemical stabilization of metals and arsenic in contaminated soils using oxides – A review. *Environmental Pollution*, *172*, 9–22. https://doi.org/10.1016/j.envpol.2012.07.045

Kotchaplai, P., Khan, E., & Vangnai, A. S. (2019). Microbial Perspective of NZVI Applications. In T. Phenrat & G. V. Lowry (Eds.), *Nanoscale Zerovalent Iron Particles for Environmental Restoration,* 387–413. Springer International Publishing. https://doi.org/10.1007/978-3-319-95340-3_10

Kumar, A., & Bhattacharya, T. (2022). Removal of Arsenic by Wheat Straw Biochar from Soil. *Bulletin of Environmental Contamination and Toxicology*, *108*(3), 415–422. https://doi.org/10.1007/s00128-020-03095-2

Kumar, A., Joseph, S., Tsechansky, L., Privat, K., Schreiter, I. J., Schüth, C., & Graber, E. R. (2018). Biochar aging in contaminated soil promotes Zn immobilization due to changes in biochar surface structural and chemical properties. *Science of The Total Environment,* 626, 953-961. https://doi.org/10.1016/j.scitotenv.2018.01.157

Kumarathilaka, P., Seneweera, S., Meharg, A., & Bundschuh, J. (2018). Arsenic speciation dynamics in paddy rice soil-water environment: Sources, physico-chemical, and biological factors - A review. *Water Research*, 140, 403–414. https://doi.org/10.1016/j.watres.2018.04.034

Kumpiene, J., Antelo, J., Brännvall, E., Carabante, I., Ek, K., Komárek, M., Söderberg, C., & Wårell, L. (2019a). In situ chemical stabilization of trace element-contaminated soil – Field demonstrations and barriers to transition from laboratory to the field – A review. *Applied Geochemistry*, *100*, 335–351. https://doi.org/10.1016/j.apgeochem.2018.12.003

Kumpiene, J., Carabante, I., Kasiuliene, A., Austruy, A., & Mench, M. (2021). LONG-TERM stability of arsenic in iron amended contaminated soil. *Environmental Pollution*, *269*, 116017. https://doi.org/10.1016/j.envpol.2020.116017

Kumpiene, J., Fitts, J. P., & Mench, M. (2012). Arsenic fractionation in mine spoils 10 years after aided phytostabilization. *Environmental Pollution*, 166, 82–88. https://doi.org/10.1016/j.envpol.2012.02.016

Kumpiene, J., Lagerkvist, A., & Maurice, C. (2008). Stabilization of As, Cr, Cu, Pb and Zn in soil using amendments – A review. *Waste Management*, *28*(1), 215–225. https://doi.org/10.1016/j.wasman.2006.12.012

Kwiatkowska-Malina, J. (2018). Functions of organic matter in polluted soils: the effect of organic amendments on phytoavailability of heavy metals. *Applied Soil Ecology*, 123, 542-545. DOI: 10.1016/j.apsoil.2017.06.021

Lacalle, R. G., Gómez-Sagasti, M. T., Artetxe, U., Garbisu, C., & Becerril, J. M. (2018). Brassica napus has a key role in the recovery of the health of soils contaminated with metals and diesel by rhizoremediation. *Science of The Total Environment,* 618, 347-356. DOI: 10.1016/j.scitotenv.2017.10.334

Latini, A., Bacci, G., Teodoro, M., Gattia, D. M., Bevivino, A., & Trakal, L. (2019). The Impact of Soil-Applied Biochars From Different Vegetal Feedstocks on Durum Wheat Plant

Performance and Rhizospheric Bacterial Microbiota in Low Metal-Contaminated Soil. *Frontiers in Microbiology*, *10*, 2694. https://doi.org/10.3389/fmicb.2019.02694

Lee, J., Sarmah, A. K., & Kwon, E. E. (2019). *Production and Formation of Biochar*. In Biochar from Biomass and Waste*,* 3–18. Elsevier. https://doi.org/10.1016/B978-0-12-811729-3.00001-7

Lefevre, E., Bossa, N., Wiesner, M. R., & Gunsch, C. K. (2016). A review of the environmental implications of in situ remediation by nanoscale zero valent iron (nZVI): Behavior, transport and impacts on microbial communities. *Science of The Total Environment*, *565*, 889–901. https://doi.org/10.1016/j.scitotenv.2016.02.003

Lehmann, J. (2009). *Terra Preta Nova – Where to from Here?* In: W. I. Woods, W. G. Teixeira, J. Lehmann, C. Steiner, A. WinklerPrins, & L. Rebellato (Eds.), Amazonian Dark Earths: Wim Sombroek's Vision, 473–486. Springer Netherlands. https://doi.org/10.1007/978-1-4020-9031-8_28

Lehmann, J., & Joseph, S. (Eds.). (2015). *Biochar for environmental management: Science, technology and implementation* (Second edition). Routledge, Taylor & Francis Group.

Li, D., Shan, R., Jiang, L., Gu, J., Zhang, Y., Yuan, H., & Chen, Y. (2022). A review on the migration and transformation of heavy metals in the process of sludge pyrolysis. *Resources, Conservation and Recycling*, 185, 106452. https://doi.org/10.1016/j.resconrec.2022.106452

Li, H., Dong, X., da Silva, E. B., de Oliveira, L. M., Chen, Y., & Ma, L. Q. (2017). Mechanisms of metal sorption by biochars: Biochar characteristics and modifications. *Chemosphere*, *178*, 466–478. https://doi.org/10.1016/j.chemosphere.2017.03.072

Li, J., Li, S., Dong, H., Yang, S., Li, Y., Zhong, J., 2015. Role of alumina and montmorillonite in changing the sorption of herbicides to biochars. *Journal of Agriculture and Food Chemistry*, 63, 5740–5746. https://doi.org/10.1021/acs.jafc.5b01654

Li, J., Yu, G., Xie, S., Pan, L., Li, C., You, F., Wang, Y., 2018. Immobilization of heavy metals in ceramsite produced from sewage sludge biochar. *Science of The Total Environment,* 628–629, 131–140. https://doi.org/10.1016/j.scitotenv.2018.02.036

Li, K., Li, J., Qin, F., Dong, H., Wang, W., Luo, H., Qin, D., Zhang, C., & Tan, H. (2023). Nano zero valent iron in the 21st century: A data-driven visualization and analysis of research topics and trends. *Journal of Cleaner Production*, 415, 137812. https://doi.org/10.1016/j.jclepro.2023.137812

Li, S., Wang, W., Liu, Y., & Zhang, W. (2014). Zero-valent iron nanoparticles (nZVI) for the treatment of smelting wastewater: A pilot-scale demonstration. *Chemical Engineering Journal*, 254, 115–123. https://doi.org/10.1016/j.cej.2014.05.111

Li, X., & Liu, L. (2021). Recent advances in nanoscale zero-valent iron/oxidant system as a treatment for contaminated water and soil. *Journal of Environmental Chemical Engineering*, *9*(5), 106276. https://doi.org/10.1016/j.jece.2021.106276

Lian, F., Xing, B., 2017. Black carbon (biochar) in water/soil environments: molecular structure, sorption, stability, and potential risk. *Environmental Science & Technology,* 51, 13517–13532. https://doi.org/10.1021/acs.est.7b02528

Liang, W., Wang, G., Peng, C., Tan, J., Wan, J., Sun, P., Li, Q., Ji, X., Zhang, Q., Wu, Y., & Zhang, W. (2022). Recent advances of carbon-based nano zero valent iron for heavy metals remediation in soil and water: A critical review. *Journal of Hazardous Materials*, 426, 127993. https://doi.org/10.1016/j.jhazmat.2021.127993

Lima, A. T., Hofmann, A., Reynolds, D., Ptacek, C. J., Van Cappellen, P., Ottosen, L. M., Pamukcu, S., Alshawabekh, A., O'Carroll, D. M., Riis, C., Cox, E., Gent, D. B., Landis, R., Wang, J., Chowdhury, A. I. A., Secord, E. L., & Sanchez-Hachair, A. (2017). Environmental Electrokinetics for a sustainable subsurface. *Chemosphere*, 181, 122–133. https://doi.org/10.1016/j.chemosphere.2017.03.143

Lin, H., Wang, Z., Liu, C., & Dong, Y. (2022). Technologies for removing heavy metal from contaminated soils on farmland: A review. *Chemosphere*, 305, 135457. https://doi.org/10.1016/j.chemosphere.2022.135457

Lin, J., Lin, X., Qiu, J., You, X., & Xu, J. (2023). Association between heavy metals exposure and infertility among American women aged 20–44 years: A cross-sectional analysis from 2013 to 2018 NHANES data. *Frontiers in Public Health*, 11, 1122183. https://doi.org/10.3389/fpubh.2023.1122183

Lindsay, W. L. (1991). Iron oxide solubilization by organic matter and its effect on iron availability. In: Y. Chen and Y. Hadar (eds.), *Plant and Soil*, 130, 27-34. Kluwer Academic Publishers. DOI: 10.1007/978-94-011-3294-7_2

Liu, A., Liu, J., Han, J., & Zhang, W. (2017). Evolution of nanoscale zero-valent iron (nZVI) in water: Microscopic and spectroscopic evidence on the formation of nano- and micro-structured iron oxides. *Journal of Hazardous Materials*, 322, 129–135. https://doi.org/10.1016/j.jhazmat.2015.12.070

Liu, A., Liu, J., Pan, B., & Zhang, W. (2014). Formation of lepidocrocite (γ-FeOOH) from oxidation of nanoscale zero-valent iron (nZVI) in oxygenated water. *RSC Advances, 4*(101), 57377–57382. https://doi.org/10.1039/C4RA08988J

Liu, L., Li, W., Song, W., & Guo, M. (2018). Remediation techniques for heavy metal-contaminated soils: Principles and applicability. *Science of The Total Environment*, 633, 206–219. https://doi.org/10.1016/j.scitotenv.2018.03.161

Liu, M., Almatrafi, E., Zhang, Y., Xu, P., Song, B., Zhou, C., Zeng, G., & Zhu, Y. (2022). A critical review of biochar-based materials for the remediation of heavy metal contaminated environment: Applications and practical evaluations. *Science of The Total Environment*, 806, 150531. https://doi.org/10.1016/j.scitotenv.2021.150531

Liu, M., Wang, J., Xu, M., Tang, S., Zhou, J., Pan, W., Ma, Q., & Wu, L. (2022). Nano zero-valent iron-induced changes in soil iron species and soil bacterial communities contribute to the fate of Cd. *Journal of Hazardous Materials*, 424, 127343. https://doi.org/10.1016/j.jhazmat.2021.127343

Liu, M., Xu, M., Zhang, X., Zhou, J., Ma, Q., & Wu, L. (2021). Poorly crystalline Fe(II) mineral phases induced by nano zero-valent iron are responsible for Cd stabilization with different soil moisture conditions and soil types. *Ecotoxicology and Environmental Safety*, 223, 112616. https://doi.org/10.1016/j.ecoenv.2021.112616

Liu, Q., Sheng, Y., Wang, W., & Liu, X. (2021). Efficacy and microbial responses of biochar-nanoscale zero-valent during in-situ remediation of Cd-contaminated sediment. *Journal of Cleaner Production*, 287, 125076. https://doi.org/10.1016/j.jclepro.2020.125076

Liu, T., Liu, B., & Zhang, W. (2014). Nutrients and Heavy Metals in Biochar Produced by Sewage Sludge Pyrolysis: Its Application in Soil Amendment. *Polish Journal of Environmental Studies*, 23(1), 271–275.

Lock K. & Janssen C.R. (2003). Influence of Aging on Metal Availability in Soils. In: Ware G.W. (eds), *Reviews of Environmental Contamination and Toxicology*, 178, 1-21. Springer, New York, NY. DOI: 10.1007/0-387-21728-2_1

Lomaglio, T., Hattab-Hambli, N., Bret, A., Miard, F., Trupiano, D., Scippa, G.S., Motelica-Heino, M., Bourgerie, S., Morabito, D., 2017. Effect of biochar amendments on the mobility and (bio) availability of As, Sb and Pb in a contaminated mine technosol. *Journal of Geochemical Exploration*, 182, 138–148. https://doi.org/10.1016/j.gexplo.2016.08.007

Lottermoser, B. (Ed.). (2017). *Environmental Indicators in Metal Mining*. Springer International Publishing. https://doi.org/10.1007/978-3-319-42731-7

Lu, H., Zhang, W., Wang, S., Zhuang, L., Yang, Y., Qiu, R., 2013. Characterization of sewage sludge-derived biochars from different feedstocks and pyrolysis temperatures. *Journal of Analytical and Applied Pyrolysis*, 102, 137–143. https://doi.org/10.1016/j.jaap.2013.03.004

Lund, C., & Lamberg, P. (2014). *Geometallurgy – A tool for better resource efficiency*.

Lwin, C. S., Seo, B.-H., Kim, H.-U., Owens, G., & Kim, K.-R. (2018). Application of soil amendments to contaminated soils for heavy metal immobilization and improved soil quality—A critical review. *Soil Science and Plant Nutrition*, *64*(2), 156–167. https://doi.org/10.1080/00380768.2018.1440938

Mackenzie, K., & Georgi, A. (2019). *NZVI Synthesis and Characterization*. In: T. Phenrat & G. V. Lowry (Eds.), Nanoscale Zerovalent Iron Particles for Environmental Restoration, 45–95. Springer International Publishing. https://doi.org/10.1007/978-3-319-95340-3_2

Mahieux, P.-Y., Aubert, J.-E., Cyr, M., Coutand, M., Husson, B., 2010. Quantitative mineralogical composition of complex mineral wastes – Contribution of the Rietveld method. *Waste Management*, 30, 378–388. https://doi.org/10.1016/j.wasman.2009.10.023

Mandal, S., Pu, S., Shangguan, L., Liu, S., Ma, H., Adhikari, S., & Hou, D. (2020). Synergistic construction of green tea biochar supported nZVI for immobilization of lead in soil: A mechanistic investigation. *Environment International*, 135, 105374. https://doi.org/10.1016/j.envint.2019.105374

Mayilswamy, N., Nighojkar, A., Edirisinghe, M., Sundaram, S., & Kandasubramanian, B. (2023). Sludge-derived biochar: Physicochemical characteristics for environmental remediation. *Applied Physics Reviews*, *10*(3), 031308. https://doi.org/10.1063/5.0137651

Mazarji, M., Bayero, M. T., Minkina, T., Sushkova, S., Mandzhieva, S., Bauer, T. V., Soldatov, A., Sillanpää, M., & Wong, M. H. (2023). Nanomaterials in biochar: Review of their effectiveness in remediating heavy metal-contaminated soils. *Science of The Total Environment*, 880, 163330. https://doi.org/10.1016/j.scitotenv.2023.163330

Méndez, A., Gascó, G., Freitas, M.M.A., Siebielec, G., Stuczynski, T., Figueiredo, J.L., 2005. Preparation of carbon-based adsorbents from pyrolysis and air activation of sewage sludges. *Chemical Engineering Journal*, 108, 169–177. https://doi.org/10.1016/j.cej.2005.01.015

Méndez, A., Gómez, A., Paz-Ferreiro, J., & Gascó, G. (2012). Effects of sewage sludge biochar on plant metal availability after application to a Mediterranean soil. *Chemosphere*, *89*(11), 1354–1359. https://doi.org/10.1016/j.chemosphere.2012.05.092

Meng, Z., Huang, S., Lin, Z., Mu, W., Ge, H., Huang, D., 2022. Cadmium long-term immobilization by biochar and potential risks in soils with different pH under combined aging. *Science of The Total Environment,* 825, 154018. https://doi.org/10.1016/j.scitotenv.2022.154018

Mercl, F., Košnář, Z., Pierdonà, L., Ulloa-Murillo, L.M., Száková, J., Tlustoš, P., 2020. Changes in availability of Ca, K, Mg, P and S in sewage sludge as affected by pyrolysis temperature. *Plant Soil Environment*, 66, 143–148. https://doi.org/10.17221/605/2019-PSE

Michálková Z., Komárek M., Vítková M., Řečínská M. & Ettler V., (2016). Stability, transformations and stabilizing potential of an amorphous manganese oxide and its surface-modified form in contaminated soils. *Applied Geochemistry*, 75, 125-136. https://doi.org/10.1016/j.apgeochem.2016.10.020.

Michálková, Z., Komárek, M., Šillerová, H., Della Puppa, L., Joussein, E., Bordas, F., Vaněk, A., Vaněk, O., & Ettler, V. (2014). Evaluating the potential of three Fe- and Mn-(nano)oxides for the stabilization of Cd, Cu and Pb in contaminated soils. *Journal of Environmental Management*, 146, 226–234. https://doi.org/10.1016/j.jenvman.2014.08.004

Michálková, Z., Komárek, M., Veselská, V., & Číhalová, S. (2016). Selected Fe and Mn (nano)oxides as perspective amendments for the stabilization of As in contaminated soils. *Environmental Science and Pollution Research*, *23*(11), 10841–10854. https://doi.org/10.1007/s11356-016-6200-9

Michálková, Z., Komárek, M., Vítková, M., Řečínská, M., & Ettler, V. (2016). Stability, transformations and stabilizing potential of an amorphous manganese oxide and its

surface-modified form in contaminated soils. *Applied Geochemistry*, 75, 125–136. https://doi.org/10.1016/j.apgeochem.2016.10.020

Michálková, Z., Martínez-Fernández, D., & Komárek, M. (2017). Interactions of two novel stabilizing amendments with sunflower plants grown in a contaminated soil. *Chemosphere*, *186*, 374–380. https://doi.org/10.1016/j.chemosphere.2017.08.009

USGS. (2022). *Mineral commodity summaries 2022.* https://doi.org/10.3133/mcs2022

Mineralogical Society of America. http://www.minsocam.org/msa/collectors_corner/article/oremin.htmhttp://www.minsocam.org/msa/collectors_corner/article/oremin.htm. Assessed on 29.11.2023

Mitzia, A., Böserle Hudcová, B., Vítková, M., Kunteová, B., Casadiego Hernandez, D., Moško, J., Pohořelý, M., Grasserová, A., Cajthaml, T., & Komárek, M. (2024). Pyrolysed sewage sludge for metal(loid) removal and immobilisation in contrasting soils: Exploring variety of risk elements across contamination levels. *Science of The Total Environment*, 918, 170572. https://doi.org/10.1016/j.scitotenv.2024.170572

Mitzia, A., Vítková, M., & Komárek, M. (2020). Assessment of biochar and/or nano zero-valent iron for the stabilisation of Zn, Pb and Cd: A temporal study of solid phase geochemistry under changing soil conditions. *Chemosphere*, 242, 125248. https://doi.org/10.1016/j.chemosphere.2019.125248

Mitzia, A., Vítková, M., Ratié, G., Chotěborský, R., Vantelon, D., Neaman, A., & Komárek, M. (2023). Revealing the long-term behaviour of nZVI and biochar in metal(loid)-contaminated soil: Focus on Fe transformations. *Environmental Science: Nano*, 10, 2861–2879. https://doi.org/10.1039/D3EN00429E

MKnano. https://www.mknano.com/Nanoparticles/Elements/Iron-Nanopowder/Zero-Valent-Iron-Nanopowder-25-nm

Moreno-Jiménez, E., Beesley, L., Lepp, N. W., Dickinson, N. M., Hartley, W., & Clemente, R. (2011). Field sampling of soil pore water to evaluate trace element mobility and associated environmental risk. *Environmental Pollution*, 159, 3078-3085. https://doi.org/10.1016/j.envpol.2011.04.004

Moreno-Jiménez, E., Esteban, E., & Peñalosa, J. M. (2012). The Fate of Arsenic in Soil-Plant Systems. In D. M. Whitacre (Ed.), *Reviews of Environmental Contamination and Toxicology,* 215, 1–37. Springer New York. https://doi.org/10.1007/978-1-4614-1463-6_1

Moško, J., Pohořelý, M., Cajthaml, T., Jeremiáš, M., Robles-Aguilar, A.A., Skoblia, S., Beňo, Z., Innemanová, P., Linhartová, L., Michalíková, K., Meers, E., 2021a. Effect of pyrolysis temperature on removal of organic pollutants present in anaerobically stabilized sewage sludge. *Chemosphere*, 265, 129082. https://doi.org/10.1016/j.chemosphere.2020.129082

Moško, J., Pohořelý, M., Skoblia, S., Fajgar, R., Straka, P., Soukup, K., Beňo, Z., Farták, J., Bičáková, O., Jeremiáš, M., Šyc, M., Meers, E., 2021b. Structural and chemical changes of sludge derived pyrolysis char prepared under different process temperatures. *Journal of Analytical and Applied Pyrolysis*, 156, 105085. https://doi.org/10.1016/j.jaap.2021.105085

Moura, H. M., & Unterlass, M. M. (2020). Biogenic Metal Oxides. *Biomimetics*, *5*(2), 29. https://doi.org/10.3390/biomimetics5020029

Mueller, N. C., Braun, J., Bruns, J., Černík, M., Rissing, P., Rickerby, D., & Nowack, B. (2012). Application of nanoscale zero valent iron (NZVI) for groundwater remediation in Europe. *Environmental Science and Pollution Research*, *19*(2), 550–558. https://doi.org/10.1007/s11356-011-0576-3

Mujtaba Munir, M. A., Liu, G., Yousaf, B., Ali, M. U., Cheema, A. I., Rashid, M. S., & Rehman, A. (2020). Bamboo-biochar and hydrothermally treated-coal mediated geochemical speciation, transformation and uptake of Cd, Cr, and Pb in a polymetal(iod)s-

contaminated mine soil. *Environmental Pollution*, 265, 114816. https://doi.org/10.1016/j.envpol.2020.114816

Mukhopadhyay, R., Sarkar, B., Khan, E., Alessi, D. S., Biswas, J. K., Manjaiah, K. M., Eguchi, M., Wu, K. C. W., Yamauchi, Y., & Ok, Y. S. (2021). Nanomaterials for sustainable remediation of chemical contaminants in water and soil. *Critical Reviews in Environmental Science and Technology*, 1–50. https://doi.org/10.1080/10643389.2021.1886891

Mulligan, C. N., & Yong, R. N. (2004). Natural attenuation of contaminated soils. *Environment International*, *30*(4), 587–601. https://doi.org/10.1016/j.envint.2003.11.001

Murr, L. E. (2015). *Handbook of Materials Structures, Properties, Processing and Performance*. Springer International Publishing. https://doi.org/10.1007/978-3-319-01815-7

Nakato, T., & Miyamoto, N. (2009). Liquid Crystalline Behavior and Related Properties of Colloidal Systems of Inorganic Oxide Nanosheets. *Materials*, 2(4), 1734–1761. https://doi.org/10.3390/ma2041734

NANOIRON, Ltd. (CZ). https://nanoiron.cz/en/ Assessed 16.02.2024

NANOREM. (2013, 2017). *Taking Nanotechnological Remediation Processes from Lab Scale to End User Applications for the Restoration of a Clean Environment*. https://cordis.europa.eu/project/id/309517/reporting

Negra, C., Ross, D. S., & Lanzirotti, A. (2005). Soil Manganese Oxides and Trace Metals: Competitive Sorption and Microfocused Synchrotron X-ray Fluorescence Mapping. *Soil Science Society of America Journal*, *69*(2), 353–361. https://doi.org/10.2136/sssaj2005.0353

Nelson Y.M., Lion L.W., Ghiorse W.C., Shuler M.L. (1999). Production of biogenic Mn oxides by Leptothrix discophora SS-1 in a chemically defined growth medium and evaluation of their Pb adsorption characteristics. *Applied Environmental Microbiology*, 65, 175-80.

Neubauer, U., Furrer, G., & Schulin, R. (2002). Heavy metal sorption on soil minerals affected by the siderophore desferrioxamine B: the role of Fe (III) (hydr) oxides and dissolved Fe (III). Eur. J. Soil Sci. 53, 45-55. https://doi.org/10.1046/j.1365-2389.2002.00425.x

Němeček, J., Lhotský, O., & Cajthaml, T. (2014). Nanoscale zero-valent iron application for in situ reduction of hexavalent chromium and its effects on indigenous microorganism populations. *Science of The Total Environment*, 485–486, 739–747. https://doi.org/10.1016/j.scitotenv.2013.11.105

Netherway, P., Reichman, S. M., Laidlaw, M., Scheckel, K., Pingitore, N., Gascó, G., Méndez, A., Surapaneni, A., & Paz-Ferreiro, J. (2019). Phosphorus-Rich Biochars Can Transform Lead in an Urban Contaminated Soil. *Journal of Environmental Quality*, *48*(4), 1091–1099. https://doi.org/10.2134/jeq2018.09.0324

O'Carroll, D., Sleep, B., Krol, M., Boparai, H., & Kocur, C. (2013). Nanoscale zero valent iron and bimetallic particles for contaminated site remediation. *Advances in Water Resources*, *51*, 104–122. https://doi.org/10.1016/j.advwatres.2012.02.005

O'Connor, D., Peng, T., Zhang, J., Tsang, D. C. W., Alessi, D. S., Shen, Z., Bolan, N. S., & Hou, D. (2018). Biochar application for the remediation of heavy metal polluted land: A review of in situ field trials. *Science of The Total Environment*, 619–620, 815–826. https://doi.org/10.1016/j.scitotenv.2017.11.132

Ok, Y.-S., Tsang, D. C. W., Bolan, N., & Novak, J. M. (Eds.). (2019). *Biochar from biomass and waste: Fundamentals and applications*. ELSEVIER.

Okereafor, U., Makhatha, M., Mekuto, L., Uche-Okereafor, N., Sebola, T., & Mavumengwana, V. (2020). Toxic Metal Implications on Agricultural Soils, Plants, Animals, Aquatic life and Human Health. *International Journal of Environmental Research and Public Health*, *17*(7), 2204. https://doi.org/10.3390/ijerph17072204

Oldeman, L. R. (1991). Global Extent of Soil Degradation. *Annual Report*.

Oleszczuk, P., & Kołtowski, M. (2017). Effect of co-application of nano-zero valent iron and biochar on the total and freely dissolved polycyclic aromatic hydrocarbons removal and toxicity of contaminated soils. *Chemosphere*, 168, 1467–1476. https://doi.org/10.1016/j.chemosphere.2016.11.100

Osuna, F.J., Pavón, E., Alba, M.D., 2019. Design swelling micas: Insights on heavy metals cation exchange reaction. *Applied Clay Science*, 182, 105298. https://doi.org/10.1016/j.clay.2019.105298

Otunola, B. O., & Ololade, O. O. (2020). A review on the application of clay minerals as heavy metal adsorbents for remediation purposes. *Environmental Technology & Innovation*, 18, 100692. https://doi.org/10.1016/j.eti.2020.100692

Ouředníček, P., Hudcová, B., Trakal, L., Pohořelý, M., & Komárek, M. (2019). Synthesis of modified amorphous manganese oxide using low-cost sugars and biochars: Material characterization and metal(loid) sorption properties. *Science of The Total Environment*, 670, 1159–1169. https://doi.org/10.1016/j.scitotenv.2019.03.300

Palansooriya, K. N., Shaheen, S. M., Chen, S. S., Tsang, D. C. W., Hashimoto, Y., Hou, D., Bolan, N. S., Rinklebe, J., & Ok, Y. S. (2020a). Soil amendments for immobilization of potentially toxic elements in contaminated soils: A critical review. *Environment International*, 134, 105046. https://doi.org/10.1016/j.envint.2019.105046

Pansu, M., & Gautheyrou, J. (2006). *Handbook of soil analysis: Mineralogical, organic and inorganic methods*. Springer.

Paranaíba, J. R., Quadra, G., Josué, I. I. P., Almeida, R. M., Mendonça, R., Cardoso, S. J., Silva, J., Kosten, S., Campos, J. M., Almeida, J., Araújo, R. L., Roland, F., & Barros, N. (2020). Sediment drying-rewetting cycles enhance greenhouse gas emissions, nutrient and trace element release, and promote water cytogenotoxicity. *PLOS ONE*, 15(4), e0231082. https://doi.org/10.1371/journal.pone.0231082

Parida, L., & Patel, T. N. (2023). Systemic impact of heavy metals and their role in cancer development: A review. *Environmental Monitoring and Assessment*, 195(6), 766. https://doi.org/10.1007/s10661-023-11399-z

Parkhurst, D. L., & Appelo, C. A. J. (2013). Description of input and examples for PHREEQC version 3: a computer program for speciation, batch-reaction, one-dimensional transport, and inverse geochemical calculations (No. 6-A43). US Geological Survey. https://pubs.usgs.gov/tm/06/a43/

Pasinszki, T., & Krebsz, M. (2020). Synthesis and Application of Zero-Valent Iron Nanoparticles in Water Treatment, Environmental Remediation, Catalysis, and Their Biological Effects. *Nanomaterials*, 10(5), 917. https://doi.org/10.3390/nano10050917

Payá Pérez, A., & Rodríguez Eugenio, N. (2018). *Status of local soil contamination in Europe revision of the indicator 'Progress in the management contaminated sites in Europe'*. Publications Office.

Penido, E. S., Martins, G. C., Mendes, T. B. M., Melo, L. C. A., do Rosário Guimarães, I., & Guilherme, L. R. G. (2019). Combining biochar and sewage sludge for immobilization of heavy metals in mining soils. *Ecotoxicology and Environmental Safety*, 172, 326–333. https://doi.org/10.1016/j.ecoenv.2019.01.110

Pérez-Esteban, J., Escolástico, C., Masaguer, A., Vargas, C., & Moliner, A. (2014). Soluble organic carbon and pH of organic amendments affect metal mobility and chemical speciation in mine soils. *Chemosphere* 103, 164-171. https://doi.org/10.1016/j.chemosphere.2013.11.055

Petala, E., Pradhan, A. C., & Filip, J. (2022). *Surface modification of nano-based catalytic materials for enhanced water treatment applications*. In Surface Modified Nanomaterials for Applications in Catalysis, 73–101. Elsevier. https://doi.org/10.1016/B978-0-12-823386-3.00014-3

Phenrat, T., & Lowry, G. V. (Eds.). (2019). *Nanoscale Zerovalent Iron Particles for Environmental Restoration: From Fundamental Science to Field Scale Engineering Applications*. Springer International Publishing. https://doi.org/10.1007/978-3-319-95340-3

Phenrat, T., Lowry, G. V., & Babakhani, P. (2019). *Colloidal and Surface Science and Engineering for Bare and Polymer-Modified NZVI Applications: Dispersion Stability, Mobility in Porous Media, and Contaminant Specificity*. In: T. Phenrat & G. V. Lowry (Eds.), Nanoscale Zerovalent Iron Particles for Environmental Restoration, 201–233. Springer International Publishing. https://doi.org/10.1007/978-3-319-95340-3_5

Pohořelý, M., Moško, J., Hušek, M., Komárek, M., Vítková, M., Cajthaml, T., Čechmánková, J., Vácha, R., 2023. Proven technology for the removal of organic pollutants from sewage sludge by pyrolysis. Proven technology, March 2023 (in Czech). Accessed on 17.11.2023 from website: https://hdl.handle.net/11104/0342851

Ponting, J., Kelly, T. J., Verhoef, A., Watts, M. J., & Sizmur, T. (2021). The impact of increased flooding occurrence on the mobility of potentially toxic elements in floodplain soil – A review. *Science of The Total Environment*, 754, 142040. https://doi.org/10.1016/j.scitotenv.2020.142040

Pownceby, M. I., MacRae, C. M., & Wilson, N. C. (2007). Mineral characterisation by EPMA mapping. *Minerals Engineering*, *20*(5), 444–451. https://doi.org/10.1016/j.mineng.2006.10.014

Pračke, K., Száková, J., & Tlustoš, P. (2022). Biochar applications enhance the phytoextraction potential of Salix smithiana [Willd.] (willow) in heavily contaminated soil: Potential for a sustainable remediation method? *Journal of Soils and Sediments*, *22*(3), 905–915. https://doi.org/10.1007/s11368-021-03104-9

Punia, A. (2021). Role of temperature, wind, and precipitation in heavy metal contamination at copper mines: A review. *Environmental Science and Pollution Research*, *28*(4), 4056–4072. https://doi.org/10.1007/s11356-020-11580-8

Punia, A., & Bharti, R. (2023). Impact of decades long mining on weathering. *Arabian Journal of Geosciences*, *16*(5), 292. https://doi.org/10.1007/s12517-023-11388-z

Quevauviller, P., 1998. Operationally defined extraction procedures for soil and sediment analysis I. Standardization. *Trends in Analytical Chemistry*, 17, 289–298. https://doi.org/10.1016/S0165-9936(97)00119-2

Raj, A., Yadav, A., Rawat, A.P., Singh, A.K., Kumar, S., Pandey, A.K., Sirohi, R., Pandey, A., 2021. Kinetic and thermodynamic investigations of sewage sludge biochar in removal of Remazol Brilliant Blue R dye from aqueous solution and evaluation of residual dyes cytotoxicity. *Environmental Technology and Innovation*, 23, 101556. https://doi.org/10.1016/j.eti.2021.101556

Rajendran, S., Priya, T. A. K., Khoo, K. S., Hoang, T. K. A., Ng, H.-S., Munawaroh, H. S. H., Karaman, C., Orooji, Y., & Show, P. L. (2022). A critical review on various remediation approaches for heavy metal contaminants removal from contaminated soils. *Chemosphere*, *287*, 132369. https://doi.org/10.1016/j.chemosphere.2021.132369

Rangabhashiyam, S., Lins, P. V. dos S., Oliveira, L. M. T. de M., Sepulveda, P., Ighalo, J. O., Rajapaksha, A. U., & Meili, L. (2022). Sewage sludge-derived biochar for the adsorptive removal of wastewater pollutants: A critical review. *Environmental Pollution*, *293*, 118581. https://doi.org/10.1016/j.envpol.2021.118581

Rashid, M.S., Liu, G., Yousaf, B., Hamid, Y., Rehman, A., Munir, M.A.M., Arif, M., Ahmed, R., Song, Y., 2022. Assessing the influence of sewage sludge and derived-biochar in immobilization and transformation of heavy metals in polluted soil: Impact on intracellular free radical formation in maize. *Environmental Pollution*, 309, 119768. https://doi.org/10.1016/j.envpol.2022.119768

Rauret, G., Lopez-Sanchez, J.F., Sahuquillo, A., Barahona, E., Lachica, M., Ure, A.M., Davidson, C.M., Gomez, A., Luck, D., Bacon, J., Yli-Halla, M., Muntau, H. & Quevauviller, P.,

(2000). Application of a modified BCR sequential extraction (three-step) procedure for the determination of extractable trace metal contents in a sewage sludge amended soil reference material (CRM 483), complemented by a three-year stability study of acetic acid and EDTA extractable metal content. *Journal of Environmental Monitoring*, 2, 228-233. DOI: 10.1039/B001496F

Ravel, B., & Newville, M. (2005). *ATHENA, ARTEMIS, HEPHAESTUS*: Data analysis for X-ray absorption spectroscopy using *IFEFFIT. Journal of Synchrotron Radiation*, *12*(4), 537–541. https://doi.org/10.1107/S0909049505012719

Rehman, Z. U., Junaid, M. F., Ijaz, N., Khalid, U., & Ijaz, Z. (2023). Remediation methods of heavy metal contaminated soils from environmental and geotechnical standpoints. *Science of The Total Environment*, *867*, 161468. https://doi.org/10.1016/j.scitotenv.2023.161468

Rhizosphere Research Products. https://www.rhizosphere.com/

Ribas, D., Černík, M., Benito, J. A., Filip, J., & Marti, V. (2017). Activation process of air stable nanoscale zero-valent iron particles. *Chemical Engineering Journal*, 320, 290–299. https://doi.org/10.1016/j.cej.2017.03.056

Rieuwerts, J. S., Thornton, I., Farago, M. E., & Ashmore, M. R. (1998). Factors influencing metal bioavailability in soils: Preliminary investigations for the development of a critical loads approach for metals. *Chemical Speciation & Bioavailability*, *10*(2), 61–75. https://doi.org/10.3184/095422998782775835

Ringeval, B., Augusto, L., Monod, H., Van Apeldoorn, D., Bouwman, L., Yang, X., Achat, D.L., Chini, L.P., Van Oost, K., Guenet, B., Wang, R., Decharme, B., Nesme, T., Pellerin, S., 2017. Phosphorus in agricultural soils: drivers of its distribution at the global scale. *Global Change Biology*, 23, 3418–3432. https://doi.org/10.1111/gcb.13618

Rinklebe, J. (2020). Redox-induced mobilization of Ag, Sb, Sn, and Tl in the dissolved, colloidal and solid phase of a biochar-treated and un-treated mining soil. *Environment International*, 140, 105754. https://doi.org/10.1016/j.envint.2020.105754

Rinklebe, J., Shaheen, S. M., & Frohne, T. (2016). Amendment of biochar reduces the release of toxic elements under dynamic redox conditions in a contaminated floodplain soil. *Chemosphere*, 142, 41–47. https://doi.org/10.1016/j.chemosphere.2015.03.067

Rinklebe, J., Shaheen, S. M., & Yu, K. (2016b). Release of As, Ba, Cd, Cu, Pb, and Sr under pre-definite redox conditions in different rice paddy soils originating from the USA and Asia. *Geoderma* 270, 21-32. DOI: 10.1016/j.geoderma.2015.10.011

Roberts, D., M. Nachtegaal, D. L. Sparks (2005). Speciation of Metals in Soils. In: M.A. Tabatabai, D.L. Sparks (eds): *Chemical Processes in Soils*, SSSA Book Series 8. SSSA, Madison, WI, 619-654. https://doi.org/10.2136/sssabookser8.c13

Rodríguez Eugenio, N., McLaughlin, M. J., & Pennock, D. J. (2018). *Soil pollution: A hidden reality*. Food and Agriculture Organization of the United Nations.

Sachdeva, S., Kumar, R., Sahoo, P. K., & Nadda, A. K. (2023). Recent advances in biochar amendments for immobilization of heavy metals in an agricultural ecosystem: A systematic review. *Environmental Pollution*, 319, 120937. https://doi.org/10.1016/j.envpol.2022.120937

Salam, A., Shaheen, S. M., Bashir, S., Khan, I., Wang, J., Rinklebe, J., Rehman, F.U., & Hu, H. (2019). Rice straw-and rapeseed residue-derived biochars affect the geochemical fractions and phytoavailability of Cu and Pb to maize in a contaminated soil under different moisture content. *Journal of Environmental Management,* 237, 5-14. https://doi.org/10.1016/j.jenvman.2019.02.047g

Sall, M. L., Diaw, A. K. D., Gningue-Sall, D., Efremova Aaron, S., & Aaron, J.-J. (2020). Toxic heavy metals: Impact on the environment and human health, and treatment with conducting organic polymers, a review. *Environmental Science and Pollution Research*, *27*(24), 29927–29942. https://doi.org/10.1007/s11356-020-09354-3

Santos, F. H. dos, Soares, M. B., & Alleoni, L. R. F. (2022). Pristine and biochar-supported nano zero-valent iron to immobilize As, Zn and Pb in soil contaminated by smelting activities. *Journal of Environmental Management*, 321, 116017. https://doi.org/10.1016/j.jenvman.2022.116017

Schlegel, M. L., Bataillon, C., Benhamida, K., Blanc, C., Menut, D., & Lacour, J.-L. (2008). Metal corrosion and argillite transformation at the water-saturated, high-temperature iron–clay interface: A microscopic-scale study. *Applied Geochemistry*, 23(9), 2619–2633. https://doi.org/10.1016/j.apgeochem.2008.05.019

Schmitt, R. (2014). Scanning Electron Microscope. In The International Academy for Production Engineering, L. Laperrière, & G. Reinhart (Eds.), *CIRP Encyclopedia of Production Engineering,* 1085–1089. Springer Berlin Heidelberg. https://doi.org/10.1007/978-3-642-20617-7_6595

Semerád, J., Hatasová, N., Grasserová, A., Černá, T., Filipová, A., Hanč, A., Innemanová, P., Pivokonský, M., Cajthaml, T., 2020. Screening for 32 per- and polyfluoroalkyl substances (PFAS) including GenX in sludges from 43 WWTPs located in the Czech Republic - Evaluation of potential accumulation in vegetables after application of biosolids. *Chemosphere* 261, 128018. https://doi.org/10.1016/j.chemosphere.2020.128018

Semerád, J., Ševců, A., Nguyen, N. H. A., Hrabák, P., Špánek, R., Bobčíková, K., Pospíšková, K., Filip, J., Medřík, I., Kašlík, J., Šafařík, I., Filipová, A., Nosek, J., Pivokonský, M., & Cajthaml, T. (2021). Discovering the potential of an nZVI-biochar composite as a material for the nanobioremediation of chlorinated solvents in groundwater: Degradation efficiency and effect on resident microorganisms. *Chemosphere*, 281, 130915. https://doi.org/10.1016/j.chemosphere.2021.130915

Seyedsadr, S., Šípek, V., Jačka, L., Sněhota, M., Beesley, L., Pohořelý, M., Kovář, M., & Trakal, L. (2022). Biochar considerably increases the easily available water and nutrient content in low-organic soils amended with compost and manure. *Chemosphere*, 293, 133586. https://doi.org/10.1016/j.chemosphere.2022.133586

Shaheen, S. M., El-Naggar, A., Wang, J., Hassan, N. E. E., Niazi, N. K., Wang, H., Tsang, D. C. W., Ok, Y. S., Bolan, N., & Rinklebe, J. (2019). *Biochar as an (Im)mobilizing Agent for the Potentially Toxic Elements in Contaminated Soils*. In Biochar from Biomass and Waste, 255–274. Elsevier. https://doi.org/10.1016/B978-0-12-811729-3.00014-5

Shaheen, S.M., Kwon, E.E., Biswas, J.K., Tack, F.M.G., Ok, Y.S., Rinklebe, J., 2017. Arsenic, chromium, molybdenum, and selenium: Geochemical fractions and potential mobilization in riverine soil profiles originating from Germany and Egypt. *Chemosphere* 180, 553–563. https://doi.org/10.1016/j.chemosphere.2017.04.054

Shen, T., Tang, Y., Lu, X.-Y., & Meng, Z. (2018). Mechanisms of copper stabilization by mineral constituents in sewage sludge biochar. *Journal of Cleaner Production*, 193, 185–193. https://doi.org/10.1016/j.jclepro.2018.05.071

Shi, M., Min, X., Ke, Y., Lin, Z., Yang, Z., Wang, S., Peng, N., Yan, X., Luo, S., Wu, J., & Wei, Y. (2021). Recent progress in understanding the mechanism of heavy metals retention by iron (oxyhydr)oxides. *Science of The Total Environment*, 752, 141930. https://doi.org/10.1016/j.scitotenv.2020.141930

Shi, Z., Nurmi, J. T., & Tratnyek, P. G. (2011). Effects of nano zero-valent iron on oxidation–reduction potential. *Environmental Science and Technology*, 45, 1586-1592. https://doi.org/10.1021/es/103185t

Simón, M., García, I., Diez-Ortiz, M., González, V., 2018. Biochar from different carbonaceous waste materials: ecotoxity and effectiveness in the sorption of metal(loid)s. *Water Air Soil Pollution*, 229, 224. https://doi.org/10.1007/s11270-018-3860-8

Singh, S., Kumar, V., Dhanjal, D. S., Datta, S., Bhatia, D., Dhiman, J., Samuel, J., Prasad, R., & Singh, J. (2020). A sustainable paradigm of sewage sludge biochar: Valorization,

opportunities, challenges and future prospects. *Journal of Cleaner Production*, *269*, 122259. https://doi.org/10.1016/j.jclepro.2020.122259

Singh, S.B., Srivastava, P.K., 2020. Bioavailability of arsenic in agricultural soils under the influence of different soil properties. *SN Applied Sciences*, 2, 153. https://doi.org/10.1007/s42452-019-1932-z

Šípek, V., Jačka, L., Seyedsadr, S., & Trakal, L. (2019). Manifestation of spatial and temporal variability of soil hydraulic properties in the uncultivated Fluvisol and performance of hydrological model. *CATENA*, 182, 104119. https://doi.org/10.1016/j.catena.2019.104119

Sipos, P., Kis, V. K., Balázs, R., Tóth, A., Kovács, I., & Németh, T. (2018). Contribution of individual pure or mixed-phase mineral particles to metal sorption in soils. *Geoderma*, 324, 1-8. https://doi.org/10.1016/j.geoderma.2018.03.008

Sipos, P., Tóth, A., Kis, V. K., Balázs, R., Kovács, I., & Németh, T. (2019). Partition of Cd, Cu, Pb and Zn among mineral particles during their sorption in soils. *Journal of Soils and Sediments*, *19*(4), 1775–1787. https://doi.org/10.1007/s11368-018-2184-z

Skála, J., Vácha, R., Čechmánková, J., 2011. Evaluation of arsenic occurrence in agricultural soils of the Bohemian Forest region.

Skousen, J. G., Ziemkiewicz, P. F., & McDonald, L. M. (2019). Acid mine drainage formation, control and treatment: Approaches and strategies. *The Extractive Industries and Society*, *6*(1), 241–249. https://doi.org/10.1016/j.exis.2018.09.008

Song, P., Ma, W., Gao, X., Ai, S., Wang, J., & Liu, W. (2022). Remediation mechanism of Cu, Zn, As, Cd, and Pb contaminated soil by biochar-supported nanoscale zero-valent iron and its impact on soil enzyme activity. *Journal of Cleaner Production*, *378*, 134510. https://doi.org/10.1016/j.jclepro.2022.134510

Song, P., Xu, D., Yue, J., Ma, Y., Dong, S., & Feng, J. (2022). Recent advances in soil remediation technology for heavy metal contaminated sites: A critical review. *Science of The Total Environment*, *838*, 156417. https://doi.org/10.1016/j.scitotenv.2022.156417

Soria, R. I., Rolfe, S. A., Betancourth, M. P., & Thornton, S. F. (2020). The relationship between properties of plant-based biochars and sorption of Cd(II), Pb(II) and Zn(II) in soil model systems. *Heliyon*, *6*(11), e05388. https://doi.org/10.1016/j.heliyon.2020.e05388

Sposito, G. (2008). *The chemistry of soils* (second edition). Oxford university press.

Stefaniuk, M., Oleszczuk, P., & Ok, Y. S. (2016). Review on nano zerovalent iron (nZVI): From synthesis to environmental applications. *Chemical Engineering Journal*, 287, 618–632. https://doi.org/10.1016/j.cej.2015.11.046

Su, H., Fang, Z., Tsang, P. E., Zheng, L., Cheng, W., Fang, J., & Zhao, D. (2016). Remediation of hexavalent chromium contaminated soil by biochar-supported zero-valent iron nanoparticles. *Journal of Hazardous Materials*, 318, 533–540. https://doi.org/10.1016/j.jhazmat.2016.07.039

Sun, Y., Wang, T., Bai, L., Han, C., & Sun, X. (2022). Application of biochar-based materials for remediation of arsenic contaminated soil and water: Preparation, modification, and mechanisms. *Journal of Environmental Chemical Engineering*, *10*(5), 108292. https://doi.org/10.1016/j.jece.2022.108292

Sun, Y., Xiong, X., He, M., Xu, Z., Hou, D., Zhang, W., Ok, Y. S., Rinklebe, J., Wang, L., & Tsang, D. C. W. (2021). Roles of biochar-derived dissolved organic matter in soil amendment and environmental remediation: A critical review. *Chemical Engineering Journal*, **424**, 130387. https://doi.org/10.1016/j.cej.2021.130387

Sverjensky, D.A., 2005. Prediction of surface charge on oxides in salt solutions: Revisions for 1:1 (M+L−) electrolytes. *Geochimica et Cosmochimica Acta*, 69, 225–257. https://doi.org/10.1016/j.gca.2004.05.040

Tack, F. M. G., & Egene, C. E. (2019a). *Potential of Biochar for Managing Metal Contaminated Areas, in Synergy With Phytomanagement or Other Management Options*. In Biochar

from Biomass and Waste, 91–111. Elsevier. https://doi.org/10.1016/B978-0-12-811729-3.00006-6

Tan, X. F., Liu, Y. G., Gu, Y. L., Xu, Y., Zeng, G. M., Hu, X. J., Liu, S., Wang, X., Liu, S.M., & Li, J. (2016). Biochar-based nano-composites for the decontamination of wastewater: a review. *Bioresource Technology*, 212, 318-333. https://doi.org/10.1016/j.biortech.2016.04.093

Tang, H., Wang, J., Zhang, S., Pang, H., Wang, X., Chen, Z., Li, M., Song, G., Qiu, M., & Yu, S. (2021). Recent advances in nanoscale zero-valent iron-based materials: Characteristics, environmental remediation and challenges. *Journal of Cleaner Production*, 319, 128641. https://doi.org/10.1016/j.jclepro.2021.128641

Taraqqi-A-Kamal, A., Atkinson, C. J., Khan, A., Zhang, K., Sun, P., Akther, S., & Zhang, Y. (2021). Biochar remediation of soil: Linking biochar production with function in heavy metal contaminated soils. *Plant, Soil and Environment*, *67*(No. 4), 183–201. https://doi.org/10.17221/544/2020-PSE

Tareq, R., Akter, N., & Azam, Md. S. (2019). *Biochars and Biochar Composites.* In Biochar from Biomass and Waste, 169–209. Elsevier. https://doi.org/10.1016/B978-0-12-811729-3.00010-8

Tauqeer, H. M., Fatima, M., Rashid, A., Shahbaz, A. K., Ramzani, P. M. A., Farhad, M., Basharat, Z., Turan, V., & Iqbal, M. (2021). *The Current Scenario and Prospects of Immobilization Remediation Technique for the Management of Heavy Metals Contaminated Soils*. In M. Hasanuzzaman (Ed.), Approaches to the Remediation of Inorganic Pollutants, 155–185. Springer Singapore. https://doi.org/10.1007/978-981-15-6221-1_8

Tchounwou, P. B., Yedjou, C. G., Patlolla, A. K., & Sutton, D. J. (2012). *Heavy Metal Toxicity and the Environment*. In A. Luch (Ed.), Molecular, Clinical and Environmental Toxicology 101, 133–164. Springer Basel. https://doi.org/10.1007/978-3-7643-8340-4_6

Teodoro, M., Clemente, R., Ferrer-Bustins, E., Martínez-Fernández, D., Pilar Bernal, M., Vítková, M., Vítek, P., & Komárek, M. (2020). Nanoscale Zero-Valent Iron Has Minimum Toxicological Risk on the Germination and Early Growth of Two Grass Species with Potential for Phytostabilization. *Nanomaterials*, *10*(8), 1537. https://doi.org/10.3390/nano10081537

Teodoro, M., Hejcman, M., Vítková, M., Wu, S., & Komárek, M. (2020). Seasonal fluctuations of Zn, Pb, As and Cd contents in the biomass of selected grass species growing on contaminated soils: Implications for in situ phytostabilization. *Science of The Total Environment*, 703, 134710. https://doi.org/10.1016/j.scitotenv.2019.134710

Teodoro, M., Trakal, L., Gallagher, B. N., Šimek, P., Soudek, P., Pohořelý, M., Beesley, L., Jačka, L., Kovář, M., Seyedsadr, S., & Mohan, D. (2020). Application of co-composted biochar significantly improved plant-growth relevant physical/chemical properties of a metal contaminated soil. *Chemosphere*, 242, 125255. https://doi.org/10.1016/j.chemosphere.2019.125255

Tessier, A., Campbell, P. G. C., & Bisson, M. (1979). Sequential extraction procedure for the speciation of particulate trace metals. *Analytical Chemistry*, *51*(7), 844–851. https://doi.org/10.1021/ac50043a017

Tomczyk, A., Sokołowska, Z., & Boguta, P. (2020). Biochar physicochemical properties: Pyrolysis temperature and feedstock kind effects. *Reviews in Environmental Science and Bio/Technology*, *19*(1), 191–215. https://doi.org/10.1007/s11157-020-09523-3

Trakal, L., Bingöl, D., Pohořelý, M., Hruška, M., Komárek, M., 2014. Geochemical and spectroscopic investigations of Cd and Pb sorption mechanisms on contrasting biochars: Engineering implications. *Bioresource Technology*, 171, 442–451. https://doi.org/10.1016/j.biortech.2014.08.108

Trakal, L., Komárek, M., Száková, J., Zemanová, V., & Tlustoš, P. (2011). Biochar application to metal-contaminated soil: Evaluating of Cd, Cu, Pb and Zn sorption behavior using

single- and multi-element sorption experiment. *Plant, Soil and Environment*, *57*(No. 8), 372–380. https://doi.org/10.17221/155/2011-PSE

Trakal, L., Veselská, V., Šafařík, I., Vítková, M., Číhalová, S., & Komárek, M. (2016a). Lead and cadmium sorption mechanisms on magnetically modified biochars. *Bioresource Technology*, 203, 318–324. https://doi.org/10.1016/j.biortech.2015.12.056

Trakal, L., Vítková, M., Hudcová, B., Beesley, L., & Komárek, M. (2019). *Biochar and Its Composites for Metal(loid) Removal From Aqueous Solutions*. In: Biochar from Biomass and Waste, 113–141. Elsevier. https://doi.org/10.1016/B978-0-12-811729-3.00007-8

Tye, A. M., Young, S. D., Crout, N. M. J., Zhang, H., Preston, S., Barbosa-Jefferson, V. L., Davison, W., McGrath, S.P., Paton, G.I., Kilham, K., & Resende, L. (2003). Predicting the activity of Cd2+ and Zn2+in soil pore water from the radio-labile metal fraction. *Geochimica et Cosmochimica Acta*, 67, 375-385. https://doi.org/10.1016/S0016-7037(02)01138-9

U.S. EPA. (2007). Method 3051A (SW-846): Microwave assisted acid digestion of sediments, sludges, and oils (Revision 1). Washington, DC.

Uddin, M. K. (2017). A review on the adsorption of heavy metals by clay minerals, with special focus on the past decade. *Chemical Engineering Journal*, 308, 438–462. https://doi.org/10.1016/j.cej.2016.09.029

Unger, S., Máguas, C., Pereira, J. S., David, T. S., & Werner, C. (2010). The influence of precipitation pulses on soil respiration – Assessing the "Birch effect" by stable carbon isotopes. *Soil Biology and Biochemistry*, *42*(10), 1800–1810. https://doi.org/10.1016/j.soilbio.2010.06.019

Urra, Alkorta, & Garbisu. (2019). Potential Benefits and Risks for Soil Health Derived From the Use of Organic Amendments in Agriculture. *Agronomy*, *9*(9), 542. https://doi.org/10.3390/agronomy9090542

Van Damme, A., Degryse, F., Smolders, E., Sarret, G., Dewit, J., Swennen, R., & Manceau, A. (2010). Zinc speciation in mining and smelter contaminated overbank sediments by EXAFS spectroscopy. *Geochimica et Cosmochimica Acta,* 74, 3707-3720. https://doi.org/10.1016/j.gca.2010.03.032

Vaněk, A., Ettler, V., Grygar, T., Borůvka, L., Šebek, O., & Drábek, O. (2008). Combined Chemical and Mineralogical Evidence for Heavy Metal Binding in Mining- and Smelting-Affected Alluvial Soils. *Pedosphere*, *18*(4), 464–478. https://doi.org/10.1016/S1002-0160(08)60037-5

Vantelon, D., Trcera, N., Roy, D., Moreno, T., Mailly, D., Guilet, S., Metchalkov, E., Delmotte, F., Lassalle, B., Lagarde, P., & Flank, A.-M. (2016). The LUCIA beamline at SOLEIL. *Journal of Synchrotron Radiation*, *23*(2), 635–640. https://doi.org/10.1107/S1600577516000746

Vanzetto, G. V., & Thomé, A. (2022). Toxicity of nZVI in the growth of bacteria present in contaminated soil. *Chemosphere*, 135002. https://doi.org/10.1016/j.chemosphere.2022.135002

Vasarevičius, S., Danila, V., & Januševičius, T. (2020). Immobilisation of Cadmium, Copper, Lead, and Nickel in Soil Using Nano Zerovalent Iron Particles: Ageing Effect on Heavy Metal Retention. *Water, Air, & Soil Pollution*, *231*(10), 496. https://doi.org/10.1007/s11270-020-04864-9

Vázquez, S., Hevia, A., Moreno, E., Esteban, E., Peñalosa, J. M., & Carpena, R. O. (2011). Natural attenuation of residual heavy metal contamination in soils affected by the Aznalcóllar mine spill, SW Spain. *Journal of Environmental Management*, *92*(8), 2069–2075. https://doi.org/10.1016/j.jenvman.2011.03.030

Venegas, A., Rigol, A., & Vidal, M. (2016). Effect of ageing on the availability of heavy metals in soils amended with compost and biochar: evaluation of changes in soil and amendment

properties. *Environmental Science and Pollution Research*, 23, 20619-20627. https://doi.org/10.1007/s11356-016-7250-8

Vidya, C.S.-N., Shetty, R., Vaculíková, M., Vaculík, M., 2022. Antimony toxicity in soils and plants, and mechanisms of its alleviation. *Environmental and Experimental Botany*, 202, 104996. https://doi.org/10.1016/j.envexpbot.2022.104996

Vithanage, M., Herath, I., Joseph, S., Bundschuh, J., Bolan, N., Ok, Y. S., Kirkham, M. B., & Rinklebe, J. (2017). Interaction of arsenic with biochar in soil and water: A critical review. *Carbon*, *113*, 219–230. https://doi.org/10.1016/j.carbon.2016.11.032

Vítková, M., Puschenreiter, M., & Komárek, M. (2018). Effect of nano zero-valent iron application on As, Cd, Pb, and Zn availability in the rhizosphere of metal(loid) contaminated soils. *Chemosphere*, *200*, 217–226. https://doi.org/10.1016/j.chemosphere.2018.02.118

Vítková, M., Rákosová, S., Michálková, Z., & Komárek, M. (2017). Metal(loid)s behaviour in soils amended with nano zero-valent iron as a function of pH and time. *Journal of Environmental Management*, 186, 268–276. https://doi.org/10.1016/j.jenvman.2016.06.003

Vodyanitskii, Y. N. (2014). Natural and technogenic compounds of heavy metals in soils. *Eurasian Soil Science*, 47, 255-265. https://doi.org/10.1134/S1064229314040103

Wainwright, M. (1978). Microbial sulphur oxidation in soil. *Science Progress*, 65(260), 459–475. http://www.jstor.org/stable/43423736

Wang, H., Feng, M., Zhou, F., Huang, X., Tsang, D.C.W., Zhang, W., 2017. Effects of atmospheric ageing under different temperatures on surface properties of sludge-derived biochar and metal/metalloid stabilization. *Chemosphere*, 184, 176–184. https://doi.org/10.1016/j.chemosphere.2017.05.175

Wang, J., Fang, Z., Cheng, W., Yan, X., Tsang, P. E., & Zhao, D. (2016). Higher concentrations of nanoscale zero-valent iron (nZVI) in soil induced rice chlorosis due to inhibited active iron transportation. *Environmental Pollution*, *210*, 338–345. https://doi.org/10.1016/j.envpol.2016.01.028

Wang, J., Shi, L., Zhai, L., Zhang, H., Wang, S., Zou, J., Shen, Z., Lian, C., & Chen, Y. (2021a). Analysis of the long-term effectiveness of biochar immobilization remediation on heavy metal contaminated soil and the potential environmental factors weakening the remediation effect: A review. *Ecotoxicology and Environmental Safety*, 207, 111261. https://doi.org/10.1016/j.ecoenv.2020.111261

Wang, L., Ok, Y. S., Tsang, D. C. W., Alessi, D. S., Rinklebe, J., Wang, H., Mašek, O., Hou, R., O'Connor, D., & Hou, D. (2020). New trends in biochar pyrolysis and modification strategies: Feedstock, pyrolysis conditions, sustainability concerns and implications for soil amendment. *Soil Use and Management*, *36*(3), 358–386. https://doi.org/10.1111/sum.12592

Wang, L., Rinklebe, J., Tack, F. M. G., & Hou, D. (2021). A review of green remediation strategies for heavy metal contaminated soil. *Soil Use and Management*, *37*(4), 936–963. https://doi.org/10.1111/sum.12717

Wang, S., Zhao, M., Zhou, M., Li, Y. C., Wang, J., Gao, B., Sato, S., Feng, K., Yin, W., Igalavithana, A. D., Oleszczuk, P., Wang, X., & Ok, Y. S. (2019a). Biochar-supported nZVI (nZVI/BC) for contaminant removal from soil and water: A critical review. *Journal of Hazardous Materials*, 373, 820–834. https://doi.org/10.1016/j.jhazmat.2019.03.080

Wang, Y., Liu, Y., Su, G., Yang, K., & Lin, D. (2021). Transformation and implication of nanoparticulate zero valent iron in soils. *Journal of Hazardous Materials*, *412*, 125207. https://doi.org/10.1016/j.jhazmat.2021.125207

Wang, Y., Wang, H.-S., Tang, C.-S., Gu, K., & Shi, B. (2020). Remediation of heavy-metal-contaminated soils by biochar: A review. *Environmental Geotechnics*, 1–14. https://doi.org/10.1680/jenge.18.00091

References

Wang, Z., Shen, R., Ji, S., Xie, L., & Zhang, H. (2021). Effects of biochar derived from sewage sludge and sewage sludge/cotton stalks on the immobilization and phytoavailability of Pb, Cu, and Zn in sandy loam soil. *Journal of Hazardous Materials*, *419*, 126468. https://doi.org/10.1016/j.jhazmat.2021.126468

Wolkersdorfer C. (2008). *Water Management at Abandoned Flooded Underground Mines*. Springer Berlin Heidelberg. https://doi.org/10.1007/978-3-540-77331-3

Weishaar, J. L., Aiken, G. R., Bergamaschi, B. A., Fram, M. S., Fujii, R., & Mopper, K. (2003). Evaluation of Specific Ultraviolet Absorbance as an Indicator of the Chemical Composition and Reactivity of Dissolved Organic Carbon. *Environmental Science & Technology*, *37*(20), 4702–4708. https://doi.org/10.1021/es030360x

Wenzel, W.W., Kirchbaumer, N., Prohaska, T., Stingeder, G., Lombi, E., Adriano, D.C., 2001. Arsenic fractionation in soils using an improved sequential extraction procedure. *Analytica Chimica Acta*, 436, 309–323. https://doi.org/10.1016/S0003-2670(01)00924-2

WHO. (2022). Guidelines for drinking-water quality (Fourth edition incorporating the first and second addenda). World Health Organization

Wijesekara, H., Bolan, N. S., Kumarathilaka, P., Geekiyanage, N., Kunhikrishnan, A., Seshadri, B., Saint, C., Surapaneni, A., & Vithanage, M. (2016). *Biosolids Enhance Mine Site Rehabilitation and Revegetation*. In: Environmental Materials and Waste, 45–71. Elsevier. https://doi.org/10.1016/B978-0-12-803837-6.00003-2

Wu, J., Li, Z., Huang, D., Liu, X., Tang, C., Parikh, S. J., & Xu, J. (2020). A novel calcium-based magnetic biochar is effective in stabilization of arsenic and cadmium co-contamination in aerobic soils. *Journal of Hazardous Materials*, 387, 122010. https://doi.org/10.1016/j.jhazmat.2019.122010

Wu, P., Singh, B. P., Wang, H., Jia, Z., Wang, Y., & Chen, W. (2023). Bibliometric analysis of biochar research in 2021: A critical review for development, hotspots and trend directions. *Biochar*, *5*(1), 6. https://doi.org/10.1007/s42773-023-00204-2

Wu, S., Cajthaml, T., Semerád, J., Filipová, A., Klementová, M., Skála, R., Vítková, M., Michálková, Z., Teodoro, M., Wu, Z., Martínez-Fernández, D., & Komárek, M. (2019). Nano zero-valent iron aging interacts with the soil microbial community: A microcosm study. *Environmental Science: Nano*, *6*(4), 1189–1206. https://doi.org/10.1039/C8EN01328D

Wu, S., Vosátka, M., Vogel-Mikus, K., Kavčič, A., Kelemen, M., Šepec, L., Pelicon, P., Skála, R., Valero-Powter, A.R., Teodoro, M., Michálková, Z. & Komárek M. (2018). Nano zero-valent iron mediated metal (loid) uptake and translocation by arbuscular mycorrhizal symbioses. *Environmental Science and Technology*, 52, 7640-7651. https://doi.org/10.1021/acs.est.7b05516

Wu, Y., Yan, Y., Wang, Z., Tan, Z., & Zhou, T. (2024). Biochar application for the remediation of soil contaminated with potentially toxic elements: Current situation and challenges. *Journal of Environmental Management*, 351, 119775. https://doi.org/10.1016/j.jenvman.2023.119775

Xie, Y., Dong, H., Zeng, G., Tang, L., Jiang, Z., Zhang, C., Deng, J., Zhang, L., & Zhang, Y. (2017). The interactions between nanoscale zero-valent iron and microbes in the subsurface environment: A review. *Journal of Hazardous Materials*, 321, 390–407. https://doi.org/10.1016/j.jhazmat.2016.09.028

Xin, D., Xian, M., & Chiu, P. C. (2019). New methods for assessing electron storage capacity and redox reversibility of biochar. *Chemosphere*, 215, 827–834. https://doi.org/10.1016/j.chemosphere.2018.10.080

Xing, J., Xu, G., Li, G., 2021. Comparison of pyrolysis process, various fractions and potential soil applications between sewage sludge-based biochars and lignocellulose-based biochars.

Ecotoxicology and Environmental Safety, 208, 111756. https://doi.org/10.1016/j.ecoenv.2020.111756

Xu, D.-M., Fu, R.-B., Liu, H.-Q., & Guo, X.-P. (2021). Current knowledge from heavy metal pollution in Chinese smelter contaminated soils, health risk implications and associated remediation progress in recent decades: A critical review. *Journal of Cleaner Production*, 286, 124989. https://doi.org/10.1016/j.jclepro.2020.124989

Xu, X., Zhao, Y., Sima, J., Zhao, L., Mašek, O., Cao, X., 2017. Indispensable role of biochar-inherent mineral constituents in its environmental applications: A review. *Bioresource Technology*, 241, 887–899. https://doi.org/10.1016/j.biortech.2017.06.023

Xue, W., Huang, D., Zeng, G., Wan, J., Cheng, M., Zhang, C., Hu, C., & Li, J. (2018). The interactions between nanoscale zero-valent iron and microbes in the subsurface environment: A review. *Chemosphere*, 210, 1145–1156. https://doi.org/10.1016/j.chemosphere.2018.07.118

Yang, B., Cao, Y., Ren, J., Wang, M., Luo, H., & Li, F. (2019). Water incubation-induced fluctuating release of heavy metals in two smelter-contaminated soils. *Journal of Environmental Science*, 82, 14-23. https://doi.org/10.1016/j.jes.2019.02.026

Yang, D., Yang, S., Yuan, H., Wang, F., Wang, H., Xu, J., & Liu, X. (2021). Co-benefits of biochar-supported nanoscale zero-valent iron in simultaneously stabilizing soil heavy metals and reducing their bioaccessibility. *Journal of Hazardous Materials*, 418, 126292. https://doi.org/10.1016/j.jhazmat.2021.126292

Yang, F., Wang, B., Shi, Z., Li, L., Li, Y., Mao, Z., Liao, L., Zhang, H., & Wu, Y. (2021b). Immobilization of heavy metals (Cd, Zn, and Pb) in different contaminated soils with swine manure biochar. *Environmental Pollutants and Bioavailability*, 33(1), 55–65. https://doi.org/10.1080/26395940.2021.1916407

Yang, J. E., Lee, S. J., Kim, D. K., Oh, S. E., Yoon, S. H., & Ok, Y. S. (2008). Effect of Organic Matter and Moisture Content on Reduction of Cr (VI) in Soils by Zerovalent Iron. *Korean Journal of Environmental Agriculture*, 27, 60-65. https://doi.org/10.5338/KJEA.2008.27.1.060

Yang, X. (2021). Immobilization of cadmium and lead using phosphorus-rich animal-derived and iron-modified plant-derived biochars under dynamic redox conditions in a paddy soil. *Environment International*, 156, 106628. https://doi.org/10.1016/j.envint.2021.106628

Yang, X., Wan, Y., Zheng, Y., He, F., Yu, Z., Huang, J., Wang, H., Ok, Y.S., Jiang, Y., Gao, B., 2019. Surface functional groups of carbon-based adsorbents and their roles in the removal of heavy metals from aqueous solutions: A critical review. *Chemical Engineering Journal*, 366, 608–621. https://doi.org/10.1016/j.cej.2019.02.119

Yang, X., Wang, L., Guo, J., Wang, H., Mašek, O., Wang, H., Bolan, N. S., Alessi, D. S., & Hou, D. (2022). Aging features of metal(loid)s in biochar-amended soil: Effects of biochar type and aging method. *Science of The Total Environment*, 815, 152922. https://doi.org/10.1016/j.scitotenv.2022.152922

Yano, J., & Yachandra, V. K. (2009). X-ray absorption spectroscopy. *Photosynthesis Research*, 102(2–3), 241–254. https://doi.org/10.1007/s11120-009-9473-8

Ying, S., Guan, Z., Ofoegbu, P. C., Clubb, P., Rico, C., He, F., & Hong, J. (2022). Green synthesis of nanoparticles: Current developments and limitations. *Environmental Technology & Innovation*, 26, 102336. https://doi.org/10.1016/j.eti.2022.102336

Yirsaw, B. D., Megharaj, M., Chen, Z., & Naidu, R. (2016). Environmental application and ecological significance of nano-zero valent iron. *Journal of Environmental Science*, 44, 88-98. https://doi.org/10.1016/j.jes.2015.07.016

Young, S. D. (2013). *Chemistry of Heavy Metals and Metalloids in Soils*. In: B. J. Alloway (Ed.), Heavy Metals in Soils, 22, 51–95. Springer Netherlands. https://doi.org/10.1007/978-94-007-4470-7_3

Yu, Y., Xu, Z., Xu, X., Zhao, L., Qiu, H., Cao, X., 2021. Synergistic role of bulk carbon and iron minerals inherent in the sludge-derived biochar for As(V) immobilization. *Chemical Engineering Journal*, 417, 129183. https://doi.org/10.1016/j.cej.2021.129183

Yuan, C., Gao, B., Peng, Y., Gao, X., Fan, B., & Chen, Q. (2021). A meta-analysis of heavy metal bioavailability response to biochar aging: Importance of soil and biochar properties. *Science of The Total Environment*, 756, 144058. https://doi.org/10.1016/j.scitotenv.2020.144058

Yuan, H., Lu, T., Huang, H., Zhao, D., Kobayashi, N., Chen, Y., 2015. Influence of pyrolysis temperature on physical and chemical properties of biochar made from sewage sludge. *Journal of Analytical and Applied Pyrolysis*, 112, 284–289. https://doi.org/10.1016/j.jaap.2015.01.010

Yuan, J., Wen, Y., Dionysiou, D. D., Sharma, V. K., & Ma, X. (2022). Biochar as a novel carbon-negative electron source and mediator: Electron exchange capacity (EEC) and environmentally persistent free radicals (EPFRs): a review. *Chemical Engineering Journal*, 429, 132313. https://doi.org/10.1016/j.cej.2021.132313

Yuan, Y., Bolan, N., Prévoteau, A., Vithanage, M., Biswas, J. K., Ok, Y. S., & Wang, H. (2017). Applications of biochar in redox-mediated reactions. *Bioresource Technology*, 246, 271-281. https://doi.org/10.1016/j.biortech.2017.06.154

Zarzsevszkij, S., Vítková, M., Zelená Pospíšková, K., Kolařík, J., Böserle Hudcová, B., & Jurkovič, Ľ. (2023). Management of a contaminated mine soil: Effect of soil water content on antimony and arsenic immobilisation by iron-based amendments and biochar composites. *Soil Use and Management*, sum.12968. https://doi.org/10.1111/sum.12968

Zhang, J., Hu, H., Wang, M., Li, Y., Wu, S., Cao, Y., Liang, P., Zhang, J., Naidu, R., Liu, Y., Man, Y. B., Wong, M. H., Zhang, C., & Shan, S. (2021). Land application of sewage sludge biochar: Assessments of soil-plant-human health risks from potentially toxic metals. *Science of The Total Environment*, 756, 144137. https://doi.org/10.1016/j.scitotenv.2020.144137

Zhang, N., Fang, Z., & Zhang, R. (2017). Comparison of Several Amendments for In-Site Remediating Chromium-Contaminated Farmland Soil. *Water, Air, & Soil Pollution*, *228*(10), 400. https://doi.org/10.1007/s11270-017-3571-6

Zhang, P., Duan, W., Peng, H., Pan, B., & Xing, B. (2022). Functional Biochar and Its Balanced Design. *ACS Environmental Au*, *2*(2), 115–127. https://doi.org/10.1021/acsenvironau.1c00032

Zhang, R., Zhang, N., & Fang, Z. (2018). In situ remediation of hexavalent chromium contaminated soil by CMC-stabilized nanoscale zero-valent iron composited with biochar. *Water Science and Technology*, *77*(6), 1622–1631. https://doi.org/10.2166/wst.2018.039

Zhang, W., Zhang, Q., Liang, Y., 2022. Ineffectiveness of ultrasound at low frequency for treating per- and polyfluoroalkyl substances in sewage sludge. *Chemosphere*, 286, 131748. https://doi.org/10.1016/j.chemosphere.2021.131748

Zhang, X., Zhao, B., Liu, H., Zhao, Y., & Li, L. (2022). Effects of pyrolysis temperature on biochar's characteristics and speciation and environmental risks of heavy metals in sewage sludge biochars. *Environmental Technology & Innovation*, 26, 102288. https://doi.org/10.1016/j.eti.2022.102288

Zhang, Y., Ren, M., Tang, Y., Cui, X., Cui, J., Xu, C., Qie, H., Tan, X., Liu, D., Zhao, J., Wang, S., & Lin, A. (2022). Immobilization on anionic metal(loid)s in soil by biochar: A meta-analysis assisted by machine learning. *Journal of Hazardous Materials*, 438, 129442. https://doi.org/10.1016/j.jhazmat.2022.129442

Zhang, Y., Wang, J., & Feng, Y. (2021). The effects of biochar addition on soil physicochemical properties: A review. *CATENA*, 202, 105284. https://doi.org/10.1016/j.catena.2021.105284

Zhao, J., Shen, X.-J., Domene, X., Alcañiz, J.-M., Liao, X., Palet, C., 2019. Comparison of biochars derived from different types of feedstock and their potential for heavy metal removal in multiple-metal solutions. *Scientific Reports*, 9, 9869. https://doi.org/10.1038/s41598-019-46234-4

Zhao, L., Cao, X., Mašek, O., & Zimmerman, A. (2013). Heterogeneity of biochar properties as a function of feedstock sources and production temperatures. *Journal of Hazardous Materials*, 256–257, 1–9. https://doi.org/10.1016/j.jhazmat.2013.04.015

Zhao, L., Sun, Z.-F., Pan, X.-W., Tan, J.-Y., Yang, S.-S., Wu, J.-T., Chen, C., Yuan, Y., & Ren, N.-Q. (2023). Sewage sludge derived biochar for environmental improvement: Advances, challenges, and solutions. *Water Research X*, 18, 100167. https://doi.org/10.1016/j.wroa.2023.100167

Zhao, Y., Zhao, L., Mei, Y., Li, F., Cao, X., 2018. Release of nutrients and heavy metals from biochar-amended soil under environmentally relevant conditions. *Environmental Science and Pollution Research*, 25, 2517–2527. https://doi.org/10.1007/s11356-017-0668-9

Zhong, D., Jiang, Y., Zhao, Z., Wang, L., Chen, J., Ren, S., Liu, Z., Zhang, Y., Tsang, D. C. W., & Crittenden, J. C. (2019). pH Dependence of Arsenic Oxidation by Rice-Husk-Derived Biochar: Roles of Redox-Active Moieties. *Environmental Science & Technology*, 53(15), 9034–9044. https://doi.org/10.1021/acs.est.9b00756

Zhu, Y.N., Zhang, X.H., Xie, Q.L., Wang, D.Q., Cheng, G.W., 2006. Solubility and stability of calcium arsenates at 25∘C. *Water Air Soil Pollution*, 169, 221–238. https://doi.org/10.1007/s11270-006-2099-y

Zulfiqar, F., Moosa, A., Nazir, M. M., Ferrante, A., Ashraf, M., Nafees, M., Chen, J., Darras, A., & Siddique, K. H. M. (2022). Biochar: An emerging recipe for designing sustainable horticulture under climate change scenarios. *Frontiers in Plant Science*, 13, 1018646. https://doi.org/10.3389/fpls.2022.1018646

Zimmermann, P., Peredkov, S., Abdala, P. M., DeBeer, S., Tromp, M., Müller, C., & Van Bokhoven, J. A. (2020). Modern X-ray spectroscopy: XAS and XES in the laboratory. *Coordination Chemistry Reviews*, 423, 213466. https://doi.org/10.1016/j.ccr.2020.213466
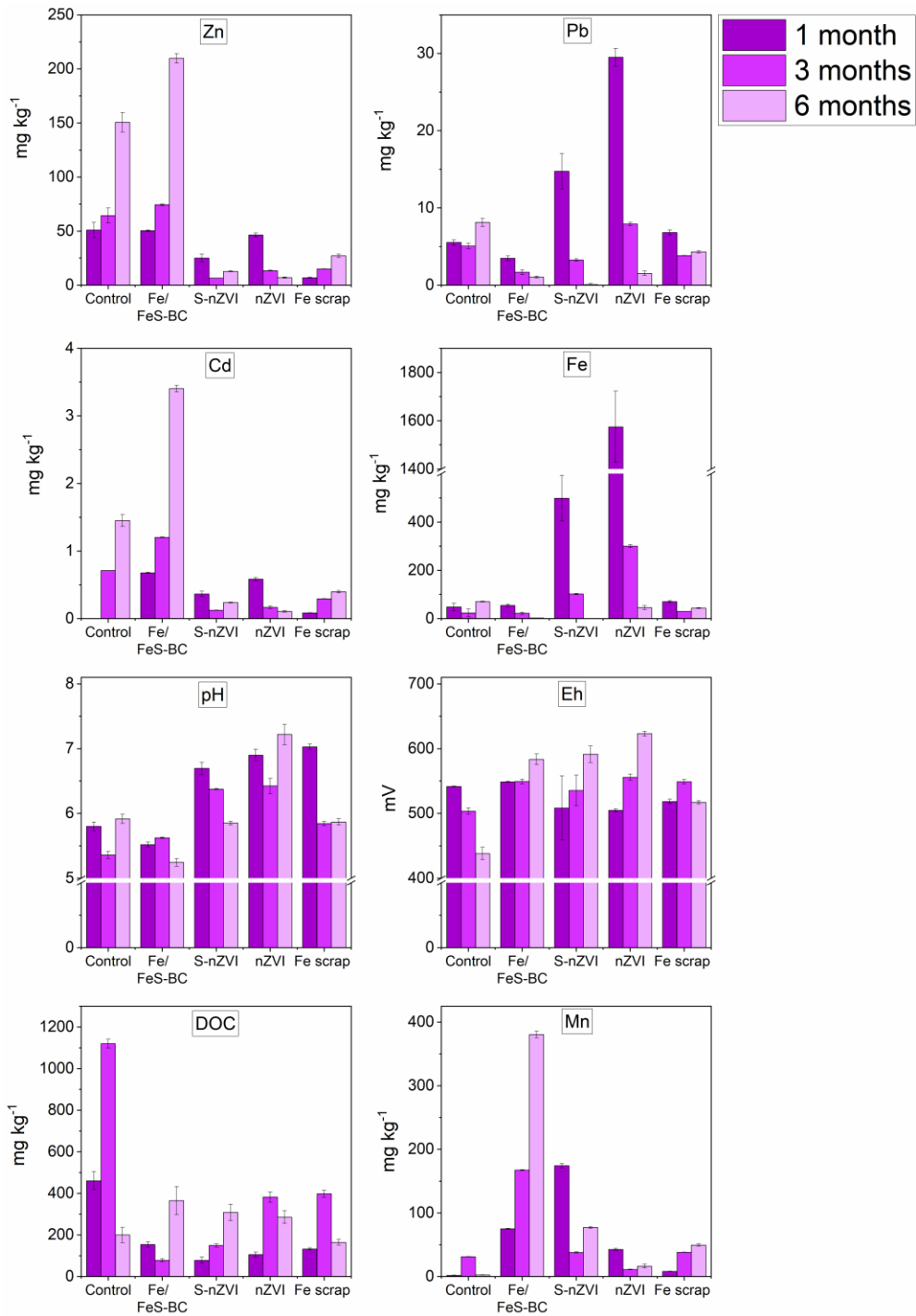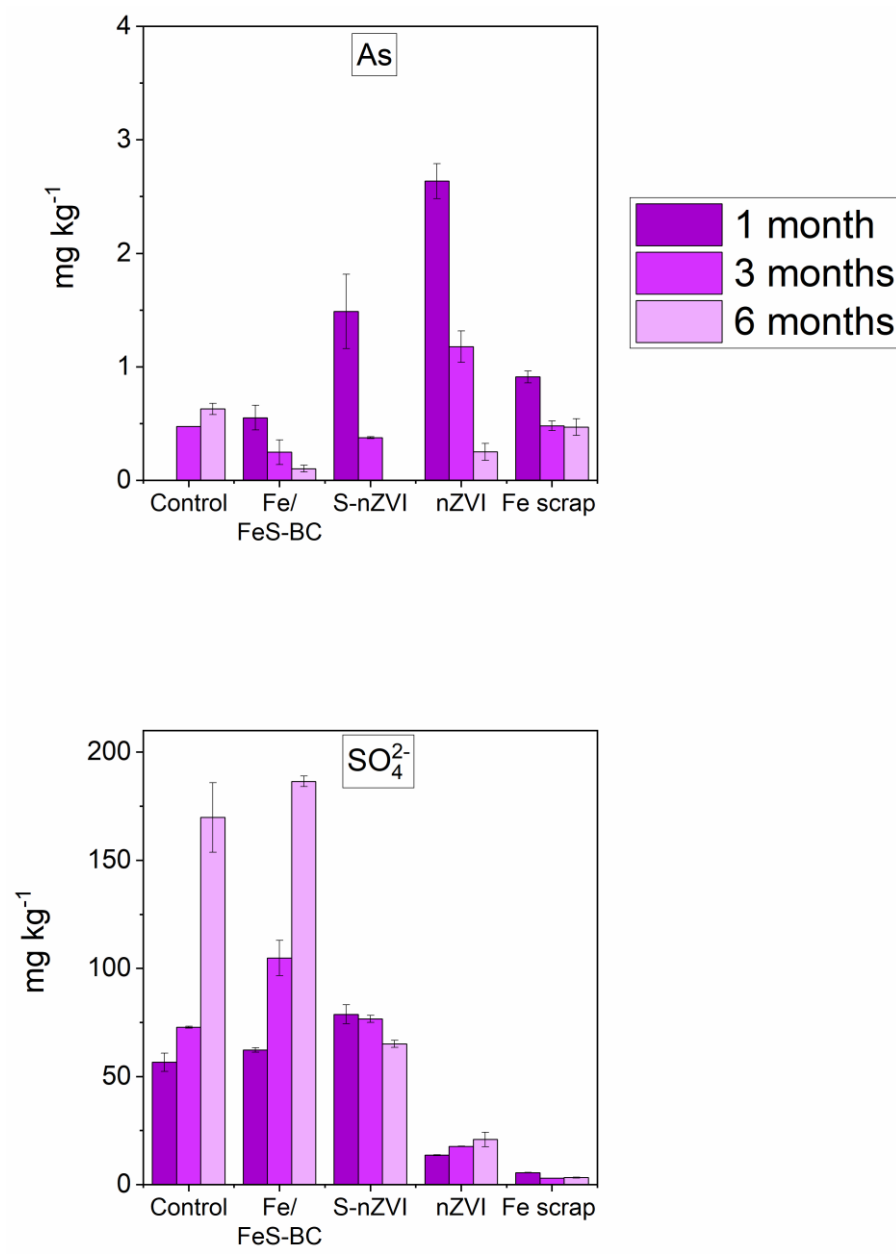
Appendix A

Unpublished results
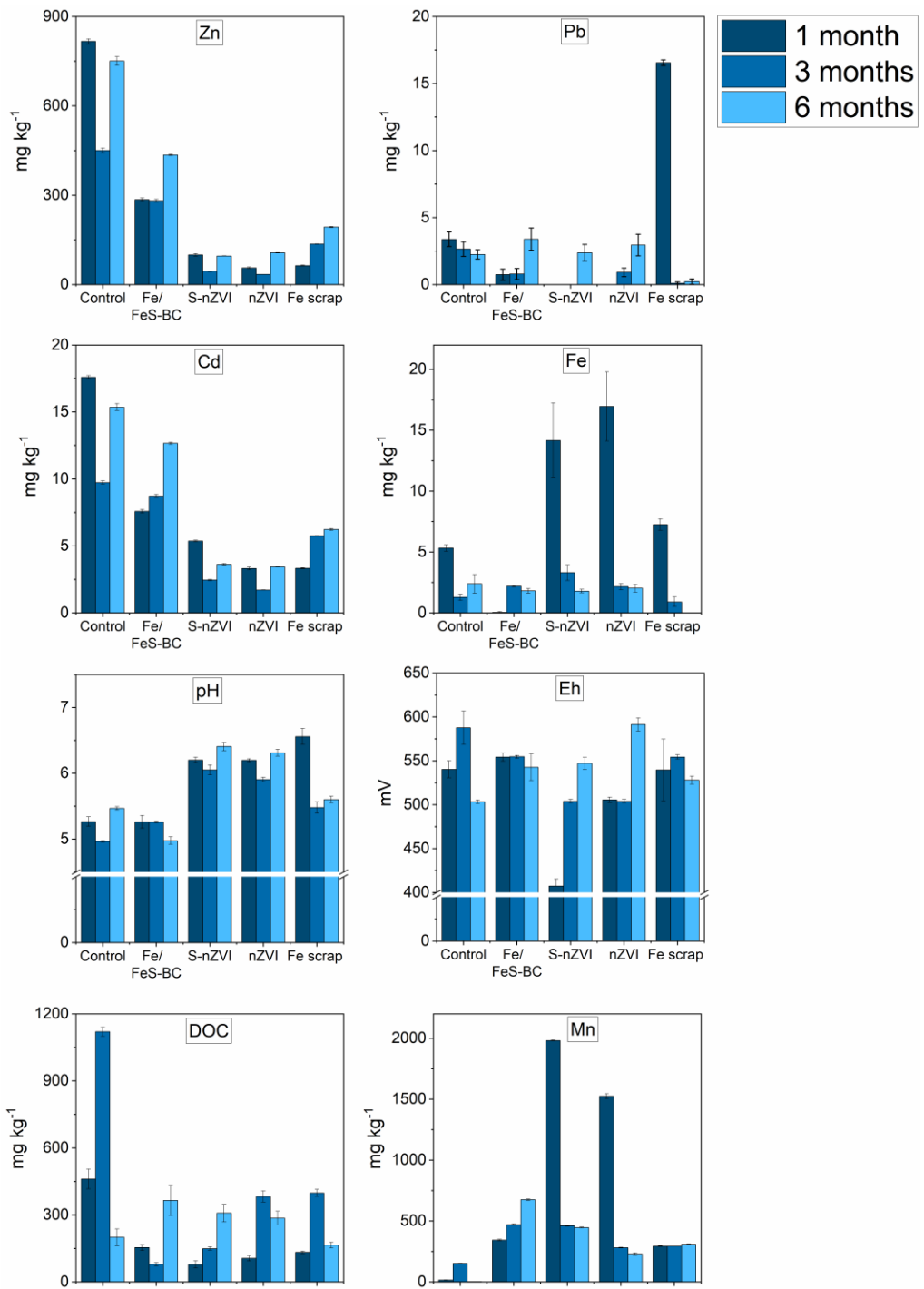
Availability of risk metals, Fe, Mn, DOC and pH, Eh values in 0.01 M CaCl$_2$ extracts in soil incubated with various Fe-based amendments.

Availability of risk metals, Fe, Mn, DOC and pH, Eh values in H₂O extracts of soil incubated with various Fe-based amendments.

Availability of As and SO₄²⁻ in H₂O extracts of soil incubated with various Fe-based amendments.

Appendix B

Curriculum Vitae & List of publications

Aikaterini Mitzia

Born: 20.04.1993, Thessaloniki, Greece

Contact:

mitzia@fzp.czu.cz

ORCiD: 0000-0003-4911-4036

Education

(2017 – present)	**PhD studies** in Applied and Lanscape Ecology, Faculty of Environmental Sciences, Department of Environmental Geochemistry Czech University of Life Sciences Prague (CZU)
	Thesis topic: Characterisation and use of innovative sorbents for metal/metalloid stabilisation in contaminated soils
(2011 – 2017)	**Integrated Master** in Forestry and Natural Environment, Aristoteles University of Thessaloniki (AUTH)
	Specialisation: Forest Genetics and Tree Improvement Diploma thesis title: Cross matching between Pinus nigra Arn. clones under xerothermic conditions

Fellowships

(2021)	Research visit to the SOLEIL synchrotron (Paris, France) at LUCIA beamtime.
(2019-2020)	Research fellowship at the laboratory of Soils and Groundwater Management, University of Wuppertal (Germany).
(2017)	Erasmus internship at the laboratories of the Department of Environmental Geochemistry, Czech University of Life Sciences Prague (CZU).

Publications

Mitzia, A., Böserle–Hudcová, B., Vítková, M. Kunteová, B., Casadiego–Hernandez, D., Moško, J., Pohořelý, M., Grasserová, A., Cajthaml, T., & Komárek, M. (2024). Pyrolysed Sewage Sludge for Metal(loid) Removal and Immobilisation: Exploring Variety of Risk Elements Across Contamination Levels, Science of the Total Environment, 918, 170572, DOI: 10.1016/j.scitotenv.2024.170572

Mitzia, A., Vítková, M., Ratié, G., Chotěborský, R., Vantelon, D., Neaman, A., & Komárek, M. (2023). Revealing the long-term behaviour of nZVI and biochar in metal(loid)-contaminated soil: focus on Fe transformations. Environmental Science: Nano, 10, 2861-2879, DOI: 10.1039/D3EN00429E

Hudcová, B., Osacký, M., Vítková, M., **Mitzia, A**., & Komárek, M. (2021) Investigation of zinc binding properties onto natural and synthetic zeolites: Implications for soil remediation. Microporous and Mesoporous Materials 317,111022, DOI: 10.1016/j.micromeso.2021.111022

Mitzia, A., Vítková, M., & Komárek, M. (2020). Assessment of biochar and/or nano zero-valent iron for the stabilisation of Zn, Pb and Cd: A temporal study of solid phase geochemistry under changing soil conditions. Chemosphere, 242, 125248. DOI: 10.1016/j.chemosphere.2019.125248

Participation in conferences

Mitzia, A., Vítková, M., Yang, X., Shaheen, S., & Rinklebe, J. The effect of dynamic redox conditions on metal(loid) immobilisation using nZVI and biochar: new insight into soil remediation efficiency. 1st joint conference: International Conference on Biochemistry of Trace Elements & International Conference on Heavy Metals (ICOBTE/ICHMET; Wuppertal, 2023).

Mitzia, A., Vítková, M. Efficiency of different Fe-based treatments for metal(loid) stabilisation in a contaminated soil. International conference: Interfaces Against Pollution: Chemical and Biological Perspectives (Antwerp, 2022).

Mitzia, A., Vítková, M., & Zarzsevszkij, S. Laboratory application of un/treated sewage sludge for soil remediation; focus on sewage sludge mineralogy. International symposium on waste management and sustainable landfilling, SARDINIA (Sardinia, 2021).

Mitzia, A., & Vítková, M. Long-term Application of Novel Materials in Contaminated Soil: laboratory Testing for Metal (loid) Stabilisation Efficiency. 6th World Congress on New Technologies (online, 2020).

Mitzia A, Vítková M & Komárek M. Assessment of nano zero-valent iron and biochar towards risk metal stabilisation in soil: a temporal study. International conference: Goldsmidt (Barcelona, 2019).

Mitzia, A., Vítková, M., & Komárek, M. Laboratory testing of biochar and/or nano zero-valent iron for remediation of metal-contaminated soil. International Conference Contaminated Sites (Banská Bystrica, 2018).

Manuscripts in preparation

Mitzia, A., Vítková, M., Yang, X., Shaheen, S., Komárek, M., Rinklebe, J. Remediation of contaminated soil under dynamic redox conditions: implications for amendment efficiency in environmental relevant conditions.

Grants & project co-operation

Team member in project: Nanoremediation of contaminated soils: Technology implementation with respect to ecotoxicological aspects Project No: TO01000170, Technology Agency of the Czech Republic (2021–2024).

Team member in project: Performance comparison of innovative metal(loid) nanosorbents in smelter-polluted soils: Geochemical and ecotoxicological benchmarks. Project no: 21-23794J, Czech Science Foundation (2021–2023).

Principal investigator in project: Sewage sludge for sustainable brownfield reclamation: exploring the mineralogy behind the sludge UGC, CZU, Ministry of Education of the Czech Republic (2021–2022).

Team member in project: Environmental aspects of soil amendments derived from organic waste: implications for sustainable soil remediation. GA FZP, (2020-2021).

Team member in project: Innovative use of nanoiron-modified biochar: advanced geochemical testing for metal(loid) stabilisation in soils. Project no: 18-24782Y, Czech Science Foundation (2018–2020).

Principal investigator in project: Characterisation and testing of novel composites for metal/metalloid stabilisation in contaminated soils. GA FZP (2018 – 2020).

Team member in project: Phytoremediation of contaminated soils using nanoparticles: implications for rhizosphere. Project no: 17-25536Y, Czech Science Foundation (2017–2019).

Workshops

European funding opportunities for junior scientists (tutor: Nikolaos Floratos, 2023).

MINTEQ geochemical modelling (tutor: Juan Antelo, 2022).

Interactive workshop on Marie Skłodowska-Curie Actions, feedback from successful candidates and project evaluators (CZU, Prague, 2022).

Recent developments and applications in Earth sciences of electron probe microanalysis (Agricultural University of Athens, 2021).

Geochemical modelling using PHREEQC code (tutor: Rémi Marsac, 2019).

Awards

Nominated for the Award of the Minister of Agriculture for Young Scientists for the publication "Pyrolysed sewage sludge for metal(loid) removal and immobilisation in contrasting soils: exploring variety of risk elements across contamination levels" (2024).

Rektor's prize for the best PhD students' publications (2020; 2023).

Teaching activities

Waste Geochemistry and Management

Environmental Soil Chemistry

Seminar for Environmental Geochemistry Studies I and II

Field practice for Environmental Geochemistry Studies

Laboratory training of Bachelor and Master students

Co-supervisor of one Master diploma thesis

Others

Member of the organising team of the 1st joint conference ICOBTE/ICHMET (Wuppertal, 2023).